

Controlling the Functionality of Amphiphilic Block Copolymers Self-assembled into Bicontinuous Nanospheres

Matthew Alexander Everden



A thesis submitted to the University of Kent in partial
fulfilment of the requirements for the degree of

Doctor of Philosophy

University of Kent
Canterbury
Kent
CT2 7NZ

28th May 2021

I dedicate this thesis to the loving memory of my
Grandad.

Dudley Charles Low

18th April 1947-25th January 2013



The man that never stopped believing in me, not for a
second.

“How can I soar amongst the eagles when I’m surrounded
by turkeys?”

Acknowledgements

Firstly, I would like to express my sincerest gratitude to Dr Simon Holder, for giving me the opportunity to do this PhD, and also for the guidance and support throughout. Without his help none of the work presented in this thesis would have been possible. He has been an excellent supervisor and it has been a great pleasure to work with him.

Thanks also goes to Ian Brown for his help and guidance with using the TEM and also the technical staff in SPS for their valuable input throughout the past four years. Special thanks to my fellow PhD students in Lab 308 and 310, who have enhanced my experience when completing my thesis.

My biggest thank you goes to my family; Mum, Nan, Katie and Richard for all of their love and support. In particular Mum and Nan who have been brilliant from day one. It has always been an aspiration of mine to complete a PhD in Chemistry and I am grateful for their interest, reassurance and unfailing support. They have both provided me with the dedication to carry on when times get tough and I love them dearly.

My passion for Chemistry was ignited from my Uncle Russell. I have always admired everything he has achieved and he has been a brilliant role model to look up too. I would like to thank him for helping me to pursue a career in this field as I have thoroughly enjoyed completing this PhD.

My acknowledgements would not be complete without thanking my fiancé, Rachel Haines. She has always been there for me and it is now exciting for the next chapter of our lives. I couldn't ask for someone better to spend my life with.

And lastly, special thanks go to my Grandad who I have dedicated this thesis too. He always believed in me and would be immensely proud for the submission of this PhD. I love him and miss him dearly.

Declaration

I declare that this thesis is my own work and effort, and has been written in my own words. Due care has been taken to properly reference the work of others wherever necessary.

Matthew Everden

28th May 2021

Abstract

Amphiphilic block copolymers (BCPs) can self-assemble into a variety of different aggregates in solution. Simple morphologies include spherical micelles, cylindrical micelles and vesicles (polymersomes). More complex aggregate structures include bicontinuous nanospheres which this thesis will focus on. The work in this thesis looks at thermoresponsive bicontinuous nanospheres which has an application for drug delivery.

Previously, research has demonstrated that bicontinuous nanospheres can be made from PEO-*b*-PODMA (poly(ethylene oxide)-block-poly(octadecyl methacrylate)) & PEO-*b*-PDSMA (poly(ethylene oxide)-block-poly(docosyl methacrylate)). The bicontinuous nanospheres formed are semi-crystalline due to the methacrylate block which gives a melting transition temperature (T_m). PEO-*b*-PODMA has a T_m of 21.8°C and PEO-*b*-PDSMA has a T_m of 41.3°C. This previous work showed that by copolymerising and varying wt% ratios of PODMA:DSMA that there was manipulation of the T_m which was conducted using differential scanning calorimetry (DSC). The work outlined in this thesis repeated this work but instead of copolymerising, blending block copolymers in the same varied wt% ratios of PODMA:DSMA was carried out. This was to assess whether blending polymers could manipulate the T_m in the same way. DSC analysis suggested partial mixing occurred when PEO-*b*-PODMA & PEO-*b*-PDSMA were blended.

In the hopes to achieve full blending, a series of nucleobase monomers were made which contained adenine and thymine. Adenine and thymine are base pairs where hydrogen bonding occurs between the two bases. These nucleobase monomers were then added in ATRP reactions to make random copolymers of PODMA-*co*-PVBT and PDSMA-*co*-PVBA and block copolymers of PEO-*b*-PODMA-*co*-PVBT and PEO-*b*-PDSMA-*co*-PVBA. It was the hope of the strong hydrogen bonding affect that occurs between adenine and thymine, would be enough to encourage full mixing of the polymer blends. The block copolymers were lastly self-assembled to see if bicontinuous nanospheres still formed after the nucleobases had been incorporated into the random and block copolymers.

Abbreviations

AGET-ATRP	Activator Generated by Electron Transfer-Atom Transfer Radical
AIBN	Azobisisobutyronitrile
ATRP	Atom Transfer Radical Polymerisation
BCP	Block copolymer
BIBB	2-bromoisobutryl bromide
BN	Bicontinuous Nanospheres
BPNs	Bicontinuous polymeric nanospheres
BzCl	Benzyl chloride
CDCl ₃	Deuterated chloroform
CFRP	Controlled Free Radical polymerisation
CMC	Critical Micelle Concentration
C-NMR	Carbon- Nuclear Magnetic Resonance
CRP	Controlled Radical polymerisation
CryoTEM	Cryogenic transmission electron microscopy
CSIRO	Commonwealth Scientific and Industrial Research Organisation
Cu	Copper
Cu(I)Br	Copper (I) Bromide
Cu(I)Cl	Copper (I) Chloride
D ₂ O	Deuterated water
D _c	Degree of crystallinity
DCM	Dichloromethane
D _H	Hydrodynamic diameter
DLS	Dynamic light scattering
DMAP	4-dimethylamino pyridine
DMF	Dimethylformamide
DMSO	Dimethyl Sulfoxide
DP	Degree of Polymerisation
DSC	Differential scanning calorimetry
DSMA	Docosyl methacrylate
EPR	Enhanced permeability and retention effect
EtOH	Ethanol
FRP	Free radical polymerisations
FTIR	Fourier Transform-Infrared Spectroscopy
GPC	Gel Permeation Chromatography
HCl	Hydrochloric acid
H-NMR	Proton Nuclear Magnetic Resonance
IPA	Isopropyl alcohol
LCST	Lower critical solution temperature
MeOH	Methanol
M _n	Number average molecular weight
M _w	Weight average molecular weight

NMP	Nitroxide-mediated polymerisation
NMR	Nuclear magnetic resonance
NMRP	Nitroxide mediated radical polymerisation
ODMA	Octadecyl methacrylate
OEGME	Oligo(ethylene glycol) methyl ether
P2VP	Poly(2-vinylpyridine)
PAA- <i>b</i> -PMA- <i>b</i> -PS	Poly(acrylic acid)- <i>block</i> -poly(methyl acrylate)- <i>block</i> -polystyrene
PB- <i>b</i> -PEO	Polybutadiene- <i>block</i> -poly(ethylene oxide)
PBMA	Poly(butyl methacrylate)
PD	Polydispersity
PDMAAm	Poly(N-dimethylacrylamide)
PEG	Poly(ethylene glycol)
PEGME	Poly(ethylene glycol)methyl ether
PEO	Poly(ethylene oxide)
PEO- <i>b</i> -PBMA	PEO-poly(nbutyl methacrylate)
PEO- <i>b</i> -PDSMA	Poly(ethylene oxide)- <i>block</i> -poly(docosyl methacrylate)
PEO- <i>b</i> -PODMA	Poly(ethylene oxide)- <i>block</i> -poly(octadecyl methacrylate)
PMDETA	N,N,N'N'-pentamethyldiethylenetriamine
PMMA	Poly(methyl acrylate)
PNIPAM	Poly(N-isopropylacrylamide)
PS	Poly(styrene)
PS- <i>b</i> -PAA	Poly(styrene)- <i>block</i> -poly(acrylic acid)
PS- <i>b</i> -PE	Polystyrene- <i>block</i> -polyethylene
PS- <i>b</i> -PI	Poly(styrene- <i>b</i> -isoprene)
RAFT	Radical Addition-Fragmentation Chain Transfer
RMM	Relative Molar Mass
SARA ATRP	Supplemental activator and reducing agents ATRP
SEC	Size-exclusion chromatography
SET-LRP	Single Electron Transfer-Living Radical Polymerisation
TEA	Triethylamine
TEM	Transmission electron microscopy
T _g	Glass Transition Temperature
THF	Tetrahydrofuran
T _m	Melting transition temperature
Đ	Dispersity index

Chapter 1 Introduction to Polymers and Polymer Synthesis

Table of Contents

Introduction.....	10
1.1 Polymerisation Techniques.....	10
1.1.1 Complex Architectures.....	10
Copolymers	11
Block Copolymers.....	12
Random Copolymers.....	12
1.1.2 Free radical polymerisations (FRP)	12
1.1.3 Controlled free radical polymerisations (CFRP)	14
Nitroxide mediated radical polymerisation (NMRP)	15
Atom Transfer radical polymerisation (ATRP).....	17
Reversible addition fragmentation chain transfer (RAFT).....	25
1.2 Self-assembly of polymers	26
1.2.1 Nanoparticles	27
Simple morphologies	27
Lipid based systems	29
Liposomes and Polymersomes	30
More complex architectures.....	32
Complex morphologies of vesicles.....	32
Complex morphologies of micelles.....	33
1.2.2 Polymer Aggregate Preparation.....	37
Principles of block copolymer self-assembly.....	39
1.2.3 Block copolymer in solid state (Microphase separation)	42
Free energy contributions to micellisation.....	42
1.3 Polymer blends	42
1.3.1 Immiscible polymer blends.....	44
1.4 Aims and objectives	45
References	47

Introduction

It has been demonstrated that when amphiphilic block copolymers self-assembled in aqueous solutions, they can form a variety of different morphologies. Simple examples include spherical and cylindrical micelles¹ as well as vesicles.² More complex examples include morphologies such as toroids, multi-lamellar vesicles, disk-like micelles and internally-structured (bicontinuous) nanospheres.³

Microscopy is used to observe these structures made from the self-assembly of block copolymers. Transmission electron microscopy (TEM) where the sample can be negatively stained, requires the removal of water. This means that images recorded will not reflect an in situ view of the particle and can cause soft matter to collapse which will affect the structure seen. The staining process uses a heavy metal which allows the contrast of aggregates to be enhanced. CryoTEM is different to traditional TEM and allows the aqueous environment to be undisturbed when aggregate species are observed. This means that images produced will be aggregates in their hydrated state. Both techniques can be seen when studying the aggregates of block copolymers.

The most widely used and studied amphiphilic block copolymers are the Pluronics^{4,5} which include poly(ethylene oxide) (PEO) and poly(propylene oxide) (PPO) blocks. Block copolymers that contain a hydrophobic block such as polystyrene or poly(methyl methacrylate), can be self-assembled when the block copolymer is first dissolved in an organic solvent, followed by slow addition of water. The interest in block copolymers has been driven by their potential as surfactants⁵, drug carriers on the nano and micro scale for controlled release of encapsulated compounds⁶ and inorganic materials templating.³ The demand by these applications has allowed block copolymers to be heavily studied. Research has focused on manipulating the properties of different aggregate species. This is done through the control of the chemistry of the polymer blocks as well as studying the external and internal morphology of different aggregate species. The control on the chemistry has allowed more monomers to be used in polymerisations which offer alternative blocks in the resulting block copolymer. The last two decades have seen dramatic advances in the chemistry when controlled radical polymerisations came about.^{7,8,9} This allowed block copolymers to be made with more precise molecular weights.

1.1 Polymerisation Techniques

1.1.1 Complex Architectures

There are two major classes of polymers. These are naturally occurring polymers as well as synthetic ones, which can be prepared by different polymerisation pathways. Examples of polymers that occur naturally¹⁰ are protein,¹¹ cellulose¹¹ and one of the most complex polymers DNA. Examples of synthetic polymers are polyamides¹² (commonly known as nylon), poly(vinyl chloride)¹³ and polymethacrylates,¹⁴ which this thesis focuses on. Polymers in general can be described as having a particular topology. Examples are given in Figure 1 and include linear, comb-like, star, brush, graft or branched structure.

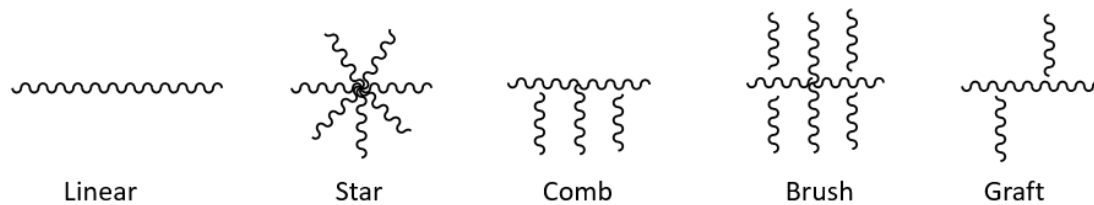


Figure 1. Representation of the different polymers topologies.

Copolymers

One of the main uses that make copolymers so attractive is that they can be synthesised with desired functionality.¹⁵ A polymer that has two monomers in the polymerisation step is known as a copolymer and is categorised by the ordering of the two monomers. For example, in random copolymers,¹⁶ the monomers units are arranged randomly along the polymer chain. When a copolymer is made up of monomer units in a regular repeating chain, this is known as alternating copolymers.¹⁷ Block copolymers¹⁸ are polymers made up of two or more different monomers that are polymerised in blocks. Graft copolymers¹⁹ are synthesised with a block of one monomer along the polymer backbone and from this the second monomer is grafted or grown from the backbone. The last type of copolymer is known as gradient copolymers.²⁰ This is where the ratio of one monomer goes up against the second monomer (1:2:3: etc). Examples of different types of copolymers are shown in Figure 2.

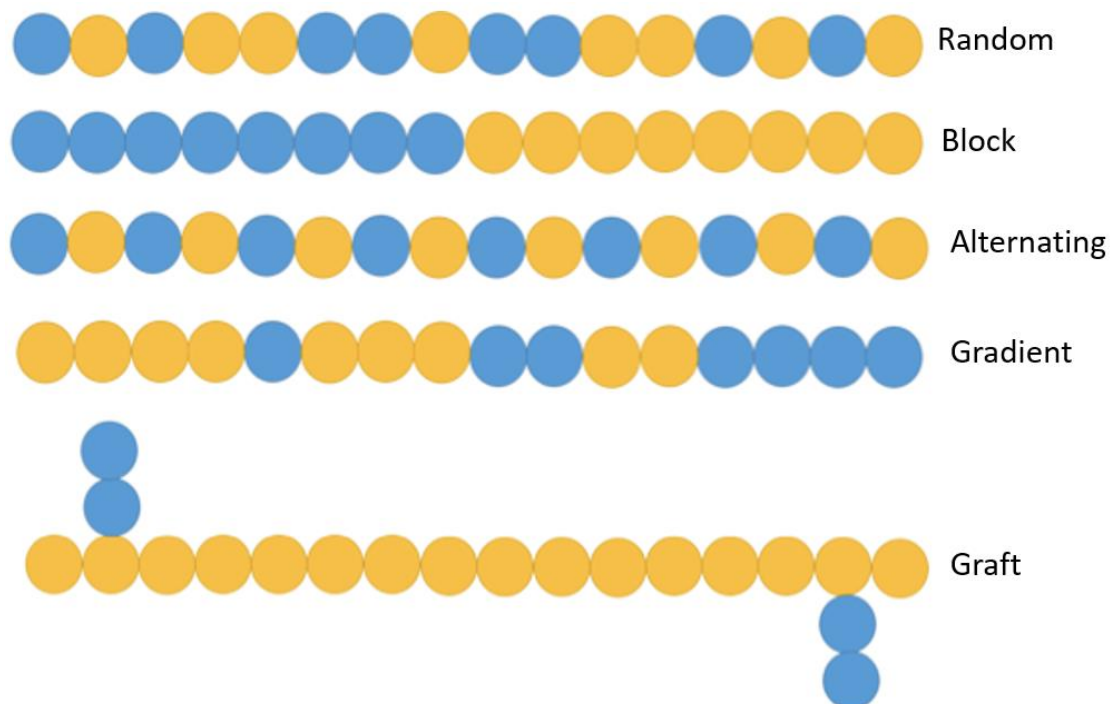


Figure 2. Representation of the different types of copolymers using two monomer units.

Block and graft copolymers behave similarly where the properties of these polymers tend to come from the composite monomers. Alternating and random polymers tend to exhibit properties that are a compromise of the two monomers. The ordering of the two monomer units in the polymer is hugely dependent upon the reactive sites present on the macroinitiator at the point the monomers are added to it.

Block Copolymers

A typical way to synthesise a block copolymer is by using an initiator that has a reactive end group. The first block (A) is polymerised and the reaction is then purified. The polymer is then polymerised with the second monomer using the reactive end of the first block (A). At this point other blocks can be added to form triblocks if desired. Block copolymers can be made through ionic polymerisations and controlled living radical polymerisations²² and as there is control on certain parameters such as molecular weight these polymer systems very desirable.

Block copolymers are of great interest due to the properties they can exhibit from each block. Different blocks can be added such as a hydrophilic block for (Block A) and a hydrophobic block for (Block B). This has been studied before²³ and allows the block copolymer to self-assemble in aqueous conditions to form well-defined structures.

Random Copolymers

Probably the most common type of copolymer that can be made by polymerisation of two monomer species, are random copolymers. The way random copolymers are synthesised is that the two or more different monomer units are added to the chain randomly. The ratio between the two monomer units can be varied to achieve the desired properties wanted in the random polymer.²⁴ However the drawback with this approach if full conversion of monomer is not achieved is that chains can grow unevenly and the ratio of the monomer units are different with each synthesis. The solution to this problem is using controlled radical polymerisation techniques where high monomer conversions are achieved and this makes sure that the copolymer composition is consistent each time the reaction is completed.

1.1.2 Free radical polymerisations (FRP)

Nanoparticles show real potential and can be readily made using polymeric systems. This occurs by the self-assembly of the polymeric structure in aqueous solutions. These polymeric systems offer good chemical versatility.²⁵ By tuning the monomer composition used in the polymerisation allows for chemical functionality, charge, stimuli-responsivity and degradability. It has been well documented how different nanoparticle architectures can be formed by self-assembly such as micelles,²⁶ nanoworms/cylindrical micelles,²⁷ vesicles,²⁸ polymersomes, branched polymers²⁹ and dendrimers³⁰ with straight forward synthesis routes. These examples can be made by controlled free radical polymerisation (CFRP) but this would not be possible if scientists did not persevere with the limitations of free radical polymerisation (FRP).

Free radical polymerisation has gained interest commercially, as polymers can still be made when reaction mixtures contain high level of impurities, reactions can be performed over a range of different temperatures and a variety of different solvents can be used to perform the reaction in. This main advantage is that plants which produce these polymers on a large scale are not governed by strict reaction temperatures which differs from more recent techniques. On average around 100 million tonnes of polymer is made each year from a variety of different monomers using FRP.³¹

Radical polymerisation³² involves taking vinyl monomers and by exposing them to a catalyst which in turn can make high molecular weight polymers. Typically, these polymerisations are very easy to perform. The polymerisation reactions that occur in FRP are either described at 'step-growth' or 'chain growth'. The distinction between the two was best described by Flory in 1953.³³ The main difference between the two is that with step-growth polymerisation the reaction proceeds through monomers containing functional groups whilst with chain-growth the polymerisation proceeds through ions or radical species. The principle behind step and chain growth polymerisations sometimes gets confused with the terms 'addition' and 'condensation' polymerisation reactions.³⁴ These terms refer to the products formed rather than the mechanism which the reaction proceeds through. In addition polymerisation, the only product formed at the end of the reaction is the polymer. In a condensation polymerisation there is more than one product formed, one being the polymer and the other being a leaving group which usually is water.

Free radical polymerisation is best described as a three-step process which includes initiation, propagation and termination. The first step (initiation) involves making a reactive species (radicals) with an unpaired electron which is able to attack the vinyl carbon-carbon bond on monomers. This happens through homolytic fission of the initiator through thermal decomposition, photoinitiation or chemical reaction. The second step (propagation) involves the monomer acquiring an unpaired electron once the vinyl bond has been broken. This causes the initiator-monomer molecule to become the reactive species at this point in the reaction. This initiator-monomer radical molecule will then react with other monomer units growing the chain. The last step of FRP is the termination step which occurs when two reactive sites on two growing chains come into contact. This is known as bimolecular termination. When this occurs, there is a loss of reactive sites in the polymerisation reaction and other chains cannot join onto the terminated molecule. The other termination process that occurs is known as disproportionation and this happens when a reactive site interacts with a hydrogen atom present on another chain. The mechanism for FRP is shown in Figure 3.

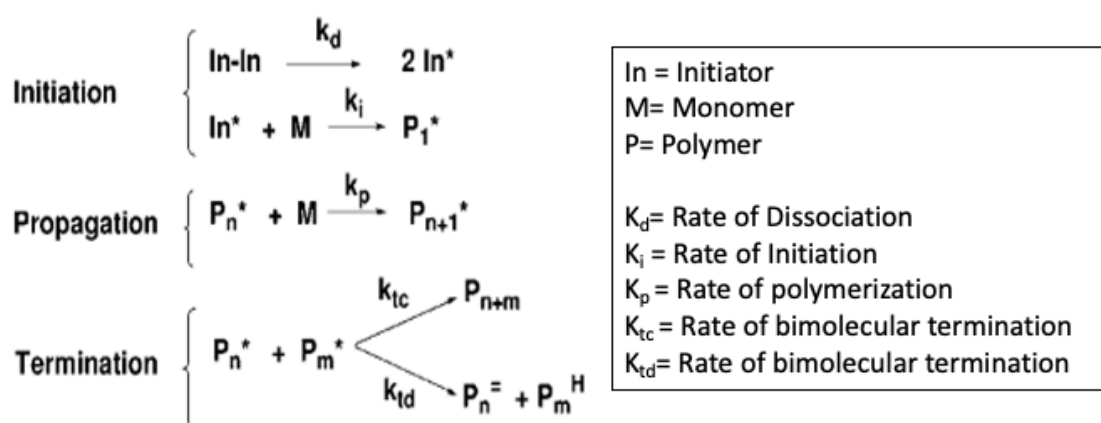


Figure 3. Mechanisms involved in the three stages of free radical polymerisation.

However, the problem with free radical polymerisation is that it can be difficult to get uniform polymers chains due to the termination steps involved. Figure 3 shows that as high number of radicals are present, then bimolecular termination is favoured. This means that polymers will be terminated before they have chance to grow. Additionally, if propagation is slower than rate of initiation then there will always be more reactive sites present meaning termination will be favoured. This means that you cannot easily

make block copolymers which in turn means that it is difficult to incorporate well-defined hydrophilic and hydrophobic components which allows for self-assembly.

1.1.3 Controlled free radical polymerisations (CFRP)

To overcome the problems with free radical polymerisation, controlled polymerisation was developed which allowed well-defined polymer architectures. The development of controlled free radical polymerisation (CRFP) produced uniform polymers which only left a small amount of monomer in the reaction mixture. The control comes from the CRFP method used which is discussed in more detail below, but the main principle behind these methods is that they limit and control the number of radicals reacting at a particular time. Monomers will keep being added to the active chain end until most of the monomer is used up.

Controlled free radical polymerisation or sometimes referred to as living radical polymerisation, limited the termination reactions as previously seen with FRP allowing polymers to be made with a much narrower dispersity. The criteria for a living polymerisation was suggested in 1992 by Quirk.³⁵ For a polymerisation to be considered as living the following must be met:

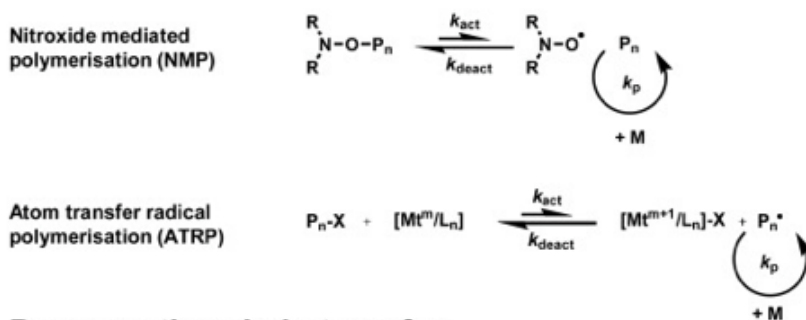
1. The relationship of molecular weight with conversion must be linear.
2. The propagation stage must continue until all the monomer has been converted to polymer.
3. The concentration of active radical species in the reaction mixture must be constant.
4. Polymers made must have a narrow polydispersity ($M_w/M_n < 1.5$).
5. The end of the polymer must retain its functionality.

For CFRP polymerisation³⁶ to give well defined polymers, initiation should occur from all of initiating molecules quickly and uniformly. This occurs due to the dynamic equilibrium between propagating radicals and the dormant chains. There are two ways this can be achieved:

- 1) Radicals are reversibly changed from activated (propagating) and deactivated (terminated) states via mediating species. This is known as reversible deactivation.
- 2) Direct exchange of an active site between the propagating and dormant chains. This is known as chain transfer.

This means that there are reversible deactivation techniques available, a few examples include atom transfer radical polymerisation (ATRP), nitroxide mediated polymerisation (NMP) and single electron transfer-living radical polymerisation (SET-LRP) and degenerative chain transfer techniques, an example being reversible addition fragmentation chain transfer (RAFT). Figure 4 shows the mechanism for NMP, ATRP and RAFT polymerisations.

Reversible deactivation



Degenerative chain transfer

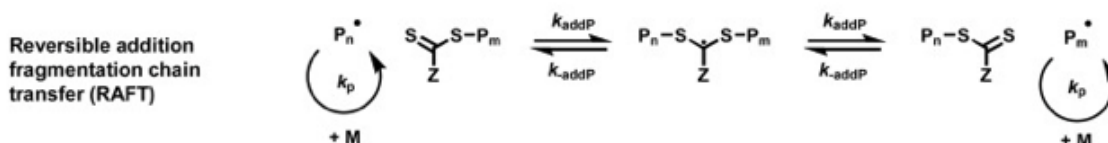


Figure 4. Mechanisms involved in reversible deactivation and degenerative chain transfer.³⁷

These types of polymerisations allow control over the reaction and polymers can be made with narrow molecular weight distributions³⁸ with polydispersities (M_w/M_n) < 1.5.⁷ These polymers can also have functional end-groups³⁹ as well as versatility in block architecture. By having control over molecular weight and the hydrophilic:hydrophobic ratios, allows for certain morphologies to be targeted in the self-assembly of these block polymers.

Nitroxide mediated radical polymerisation (NMRP)

One of the earliest examples of CFRP is nitroxide mediated radical polymerisation (NMRP) and in the last few decades has been used in research.⁴⁰ The initial work on NMRP was undertaken by Commonwealth Scientific and Industrial Research Organisation (CSIRO) and demonstrated the potential NMRP had in the synthesis of block and graft copolymers in the 1980s. However, despite this promising potential as a new type of polymerisation to use, the polymer community did not pay close attention until publications from Georges, Hawker and others were submitted between 1993-1995.^{41,42,43} This was approximately 10 years after the initial work was carried out by the CSIRO. During 1993-2000^{44,45,46} there were many publications which explained the mechanism and kinetics behind NMRP, along with examples of polystyrene, polyacrylates, polymethacrylates, polyvinylpyridine and derivatives copolymers being made from this technique. Despite promising work surrounding NMRP, the control on NMRP reaction is not as good as other CFRP methods.⁴⁷ The choice of monomers is limited in NMRP and polymers are also made with higher polydispersities, which led other research groups to explore alternative polymerisation reactions such as ATRP and RAFT.

The reaction mechanism of NMRP involves trapping of propagating polymer chains by stable nitroxide radicals which provides the formation of dormant species.⁴⁰ Figure 5 shows the mechanism for NMRP.

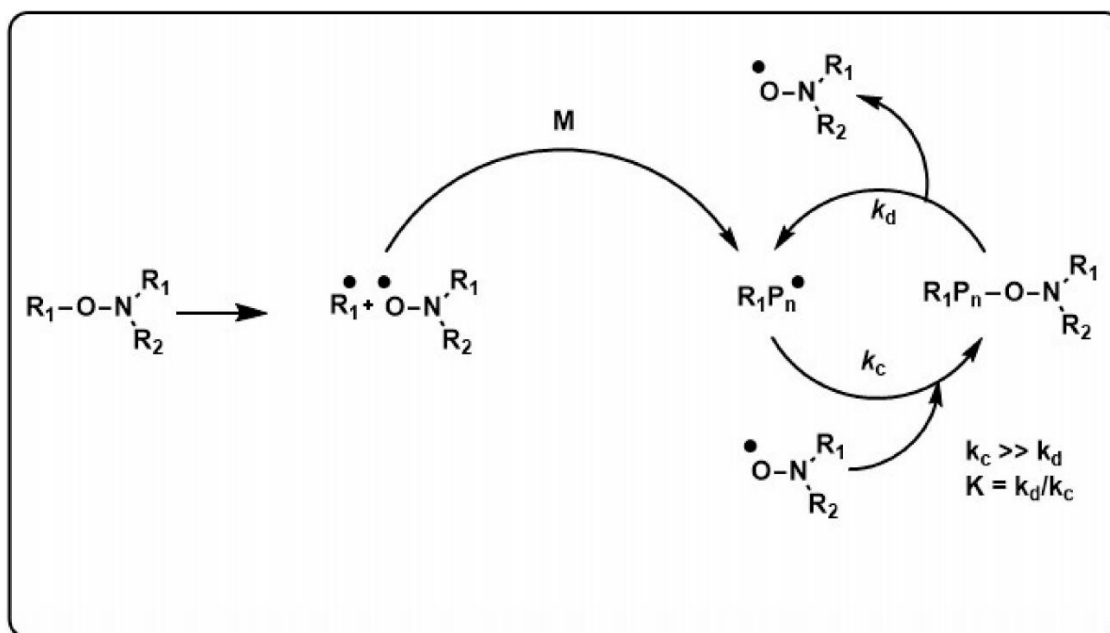


Figure 5. Mechanism involved in nitroxide mediated radical polymerisation.⁴⁰

Where k_d is the rate constant of homolytic cleavage of the C-O bond and k_c is the rate constant of coupling of propagating radical and free nitroxide (deactivation step). When the equilibrium is $k_c \gg k_d$ there is an excess of nitroxide which means that the concentration of the active chains is relatively low. This means that irreversible chain termination is low.

The polymerisation reaction can be started by using thermal initiators such as 2,2'-azobis(2-methylpropionitrile) (AIBN)⁴⁸ or benzoylperoxide (BPO)⁴⁹ when nitroxide radicals are present. Nitroxide radicals can also be produced in a unimolecular reaction through chemical, thermal or photochemical cleavage of an alkoxyamine. This is shown in Figure 6.

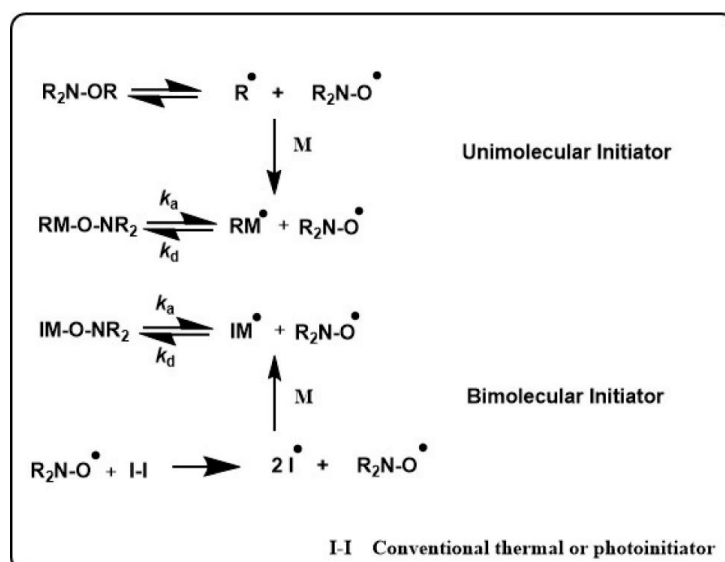


Figure 6. The formation of nitroxide radicals from unimolecular and bimolecular reactions.⁴⁰

At the end of the reaction, the nitroxide reforms with the propagating active chain to give a nitroxide terminated radical as a dormant species. NMRP is a very good example of living polymerisations as it demonstrates key features.⁵⁰ Fine-tuning the alkyl and

nitroxide fragments allows functionalised polymers to be made. Block copolymers are useful as blocks can be selected due to the characteristics of the polymer desired. This has led NMRP to use different block copolymers,⁵¹ as they are easily accessible to make many useful polymer structures.

Atom Transfer radical polymerisation (ATRP)

This technique was first discovered by Matyjaszewski⁵² and Sawamoto⁵² independently in 1995 and has gained much interest over the years. The reason for this is that polymers can be synthesised from a very large range of vinyl monomers such as styrene, acrylates/methacrylates, poly(ethylene glycol) derivatives and N-isopropyl acrylamide. Many publications are submitted each year on this topic, which demonstrates how useful this controlled/living polymerisation technique is and the wide uses it has in polymer chemistry.

Atom transfer radical polymerisation is one type of reversible-deactivation radical polymerisation that will be discussed here. The way this polymerisation works is through initiation and reversible termination of propagating radicals ($R-P_n^*$), through a reversible homolytic halogen transfer between dormant species ($R-X$ or $R-P_n-X$).⁵³ A transition metal catalyst is used with the most common one being copper in a low oxidation state. Iron⁵⁴ and rubidium⁵⁵ have also been used as effective catalysts and nickel was first used by Sawamoto in 1995. Figure 7 Shows a general mechanism for ATRP. Deactivation of radical species is favoured by the equilibrium of the reversible process. This means that this type of polymerisation can minimise bimolecular termination and chain transfer, meaning that chains can continue to grow.⁵⁶ There is fast exchange of the halide between the catalyst and the dormant species which means that only a few monomer units are added at each exchange. This all helps to offer control on polymer molecular weights and keeps the chain growth uniform.

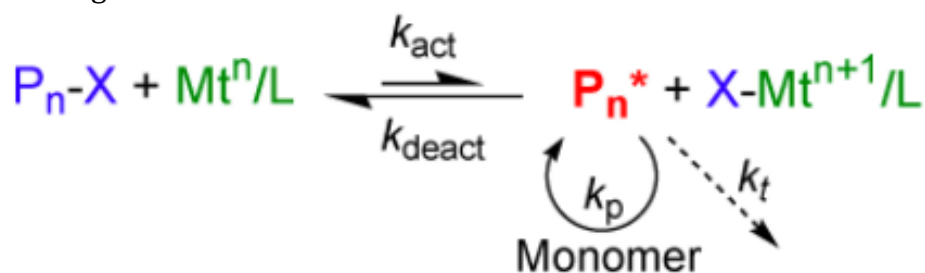


Figure 7. General mechanism for ATRP.⁵⁷

The main concepts of the mechanism of ATRP involves the homolytic bond cleavage of a carbon-halogen bond and the radical species which is formed from this attack. This radical species will then attack vinyl monomers. The propagation step occurs through a stepwise addition of monomer units. Termination occurs to produce the desired polymer. A more detail explanation of the mechanism can be seen in Figure 8.

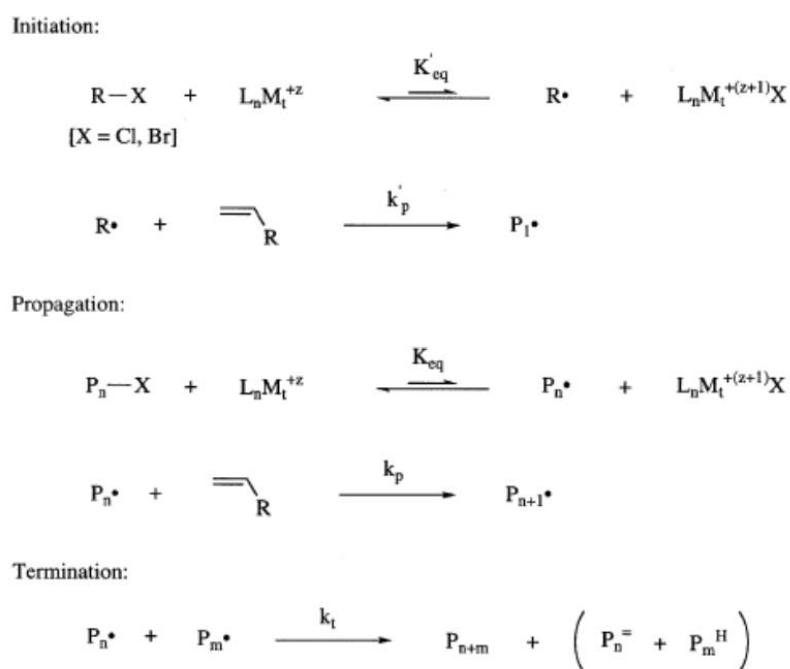


Figure 8. Mechanism of ATRP for a vinyl monomer. (X = halogen).⁵⁸

There are limitations in using ATRP that have led to other polymerisations being used instead. The first is that it can take a few hours for the desired polymer to be made. The second is that ATRP is sensitive to oxygen and if oxygen can get into the reaction, it can stop or slow down the reaction. Oxygen will react to form peroxy radicals which will react with the propagating radicals and stabilise them made in the ATRP reaction. Oxygen also poisons ATRP activators and for this reason inert gases such as nitrogen or argon should be used.⁵³

ATRP kinetics

The ATRP equilibrium constant (K_{ATRP}) is best described as by the following equation.⁵⁹

Equation 1.1 Determination of K_{ATRP} .

$$K_{\text{ATRP}} = \frac{k_{\text{ACT}}}{k_{\text{DEACT}}} = \frac{[P^*][Cu^{II}X]}{[Cu^I][PX]}$$

Where k_{ACT} and k_{DEACT} are the rate constants of activation and deactivation, P^* is the polymer radical species, X is the halide and Cu is the copper catalyst switching between oxidation states.

When the situation of $k_{\text{ACT}} < k_{\text{DEACT}}$ occurs, K_{ATRP} is small and the process is very slow or the polymerisation will not proceed. If $k_{\text{ACT}} > k_{\text{DEACT}}$ situation occurs, then K_{ATRP} is large and there is a high radical concentration and control is lost on the reaction. Termination process will overrule the propagation of the chain. This means polymers are synthesised with large polydisperties and degree of polymerisations (DP) are much larger than originally wanted. A solution to this second scenario is that it can be overcome by introducing deactivating species. The easiest way is by using a mixture of copper in the Cu^I and Cu^{II} oxidation states as the catalyst.⁶⁰ Another alternative would be to use CuCl

instead of CuBr as the chlorine group is a worse leaving group than bromine so this slows the reaction down.

ATRP is affected by the overall equilibrium constant but expanding on this, it is determined by four sub-equilibria and these are displayed in Figure 9.⁶¹ These are:

- 1) Electron transfer (K_{ET})- involves oxidation of the copper complex;
- 2) Electron affinity (K_{EA})- involves the reduction of the halide atom to an ion;
- 3) Alkyl halide bond homolysis (K_{BH})- involves the homolytic bond fission of the alkyl halide bond to form two radicals (Propagating radical and halide radical);
- 4) Halogenophilicity (K_X)- defines the interaction the halide has to the metal complex.

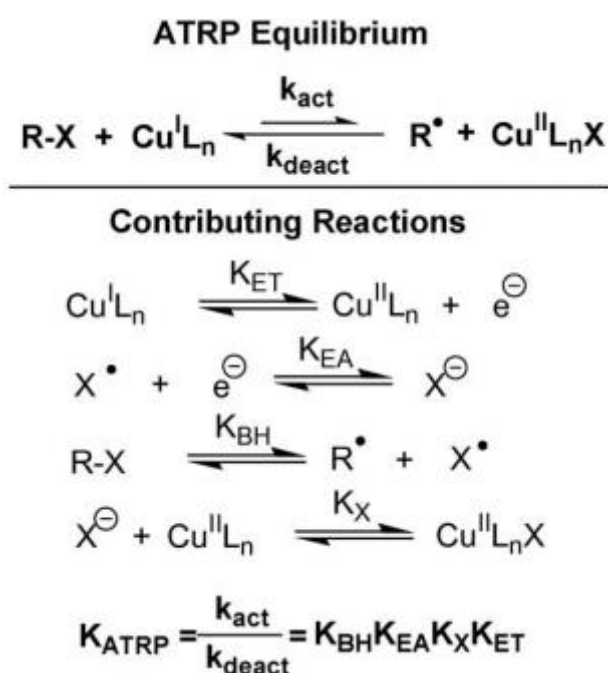


Figure 9. The sub-equilibria involved in determining the ATRP rate constant K_{ATRP} .⁶¹

All these sub-equilibria constants are highly dependent on solvents. For example in protic solvents such as water and methanol, the value of K_{EA} is expected to be large as the halide anion is stabilised.⁶²

ATRP Components

There are 4 main chemical components of ATRP, which are the initiator, monomer, catalyst and the ligand. The reaction solvent and the temperature at which the polymerisation proceeds at also play a role.⁶³

The monomers that can be used in ATRP contain vinyl groups, which can be broken by radical attack. It is when these double bonds break; it allows the monomer to join onto the polymer backbone. Monomers that are used all have a K_{ATRP} , which is dependent on the radical structure that forms. These structures are stabilised by electron withdrawing groups such as acrylates, methacrylates, amides and arenes. Less reactive monomers

such as ethylene, vinyl chloride and vinyl acetate cannot be polymerised by ATRP. This is because the radical species formed are very unstable. The rate that propagation occurs is also different depending on which monomer is selected. This means that the reaction conditions must then be carefully selected which helps to shift the equilibrium accordingly.⁵³

Initiators are used in ATRP to start the polymerisation reaction but they also influence the degree of polymerisation (DP) and the molecular weight of the resulting polymer made. This is because they are used to make the resulting polymer. The DP is determined from:

Equation 1.2 The calculation of degree of polymerisation (DP)

$$DP = \frac{[M]}{[I]}$$

Where M and I represent the monomer and initiator. It is important to understand the above equation and make sure that the correct conditions are selected. This ensures that there is a steady state of living transfer and chain termination is constant. If there is not a steady state of living transfer, then the reaction will proceed to slowly or not at all or termination will happen too quickly. If this happens then the degree of polymerisation wanted will not be met. What is desired is a linear increase in molecular weight as a function of monomer conversion into polymer.

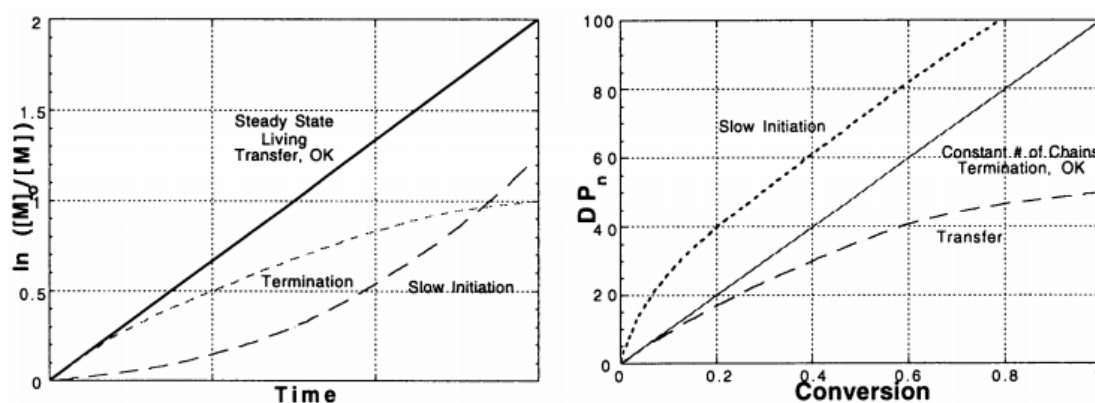


Figure 10. Schematic effects of slow initiation, transfer, termination and exchange on kinetic (left) and molecular weight (right).⁶⁴

Initiators used in ATRP usually contain an alkyl halide group (R-X). For this polymerisation to proceed, it must be activated by the presence of an electron-withdrawing group. Examples are carbonyl or a benzyl groups on the α carbon as this helps to enhance polarisation of the carbon-halide bond. This also offers stability to the radical species formed.⁶⁵

Matyjaszewski *et. al.*⁶⁵ carried out ATRP reactions using methyl methacrylate (MMA) using different initiators, which are shown along with relative reactivities in Figure 11. It is reported that initiators that are very reactive produced low monomer conversions over an 18-hour time period (10% conversion). For example, benzyl chloride (BzCl) gave a high initiation rate compared with a slower MMA propagation that meant that benzyl radicals recombined and did not initiate chain growth. This led to low M_n observed suggesting the reaction did not grow the chain as planned. In contrast ethyl 2-

bromoisobutyrate (EtBriB) which is much less reactive, gave a much faster rate of polymerisation and produced polymers with low polydispersities and M_n close to the theoretical.

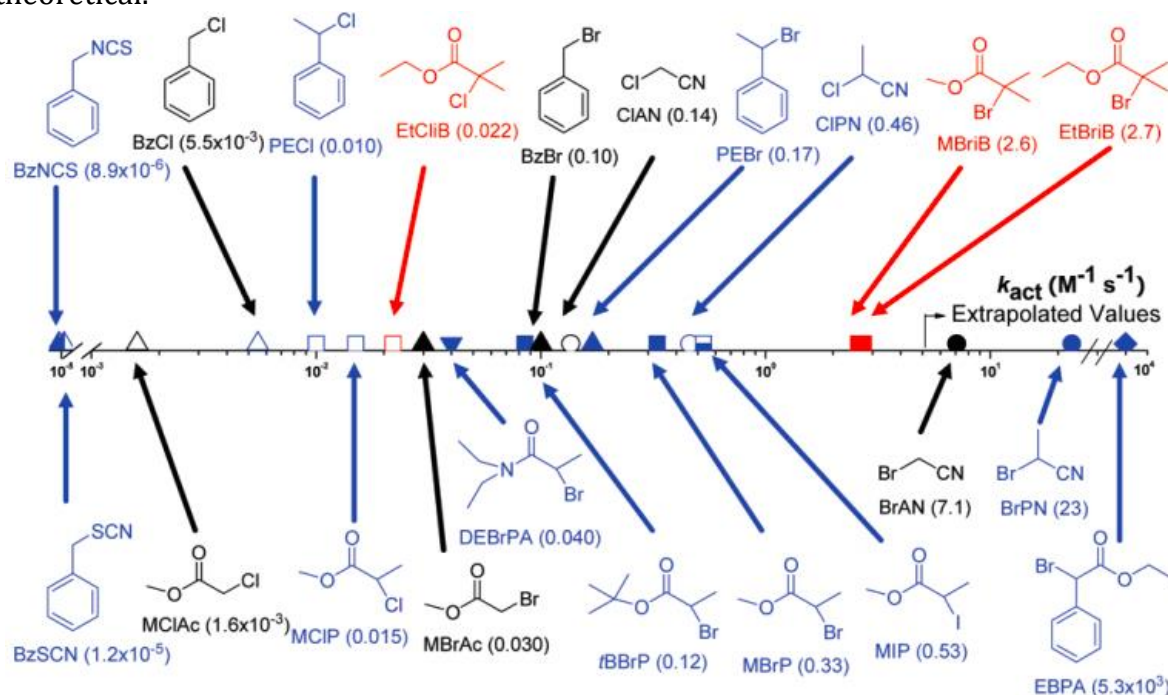


Figure 11. ATRP activation rate constants (K_{ATRP}) for various initiators.⁵⁹ ATRP reaction used PMDETA (ligand) and either CuBr or CuCl (catalyst).

The most popular choices for the halide atom are chlorine (Cl) or bromine (Br). Fluorine (F) is not used as it is very electronegative, meaning it is too strong to allow efficient exchange. Iodine (I) can be used but require specific reaction conditions due to alkyl iodides being light sensitive. For this reason, most reactions will use Cl or Br. The choice of halide will also affect how quickly the reaction proceeds. Br is a better leaving group than Cl and will allow polymerisation to occur faster. Cl has an advantage as it can slow the reaction down allowing polymers to be made with lower polydispersities as there is better control.⁶⁵

In addition to molecular initiators, macromolecules can be used and are commonly referred to as macroinitiators. These are very important in the formation of block copolymers as macroinitiators will form one of the 'blocks' and can be selected due to particular characteristics.

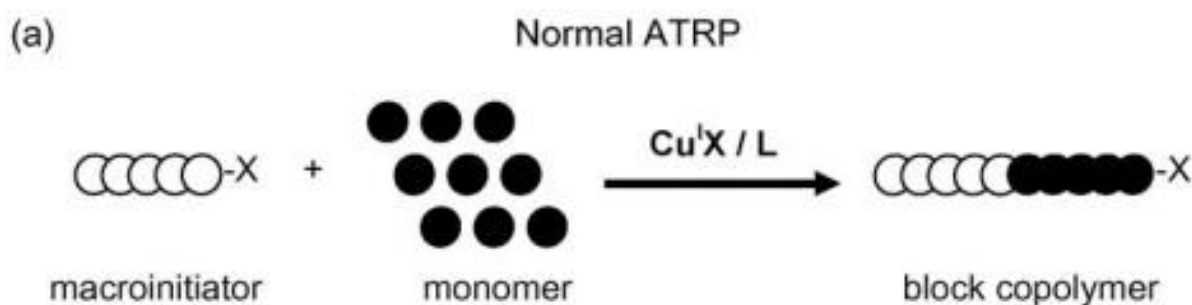


Figure 12. Formation of a block copolymer made from a macroinitiator.⁶¹

There are two main ways which block copolymers can be made. These are:

- 1) One block can be polymerised by ATRP with a low molecular weight initiator and a second block is then added after this by a second polymerisation.
- 2) The second way is to end-functionalise the macromolecule containing the desired block with the halide group. Common examples of this uses poly(ethylene glycol) (PEG) derivatives as the macroinitiator to form the block copolymers.

Most ATRP reactions will use a transition metal bound to a ligand and that metal is usually copper. The metal will undergo redox reactions where its oxidation will swap between states. When the transition metal accepts the halide from the initiator it undergoes oxidation. When the halide-metal complex dissociates due to termination of the chain, reduction takes place. It has been reported that nickel,⁶⁶ ruthenium⁶⁷ and iron⁶⁸ can also be used instead of copper for ATRP reactions.

Copper seems to be the most common choice for ATRP as it normally is cheaper to purchase and when compared to nickel, ruthenium and iron. When copper is used along with a ligand, it changes from oxidation state of +1 to a state of +2. The main role of the ligand in ATRP is to form a complex with the catalyst to stabilise the transition metal in the polymerisation. The Cu^I oxidation state prefers a tetrahedral or square planar configuration. This is achieved by coordination with a bidentate or tetradentate ligand.⁶⁹ Figure 13 shows the proposed complex of copper with a bidentate ligand (2,2'-bipyridine bpy)

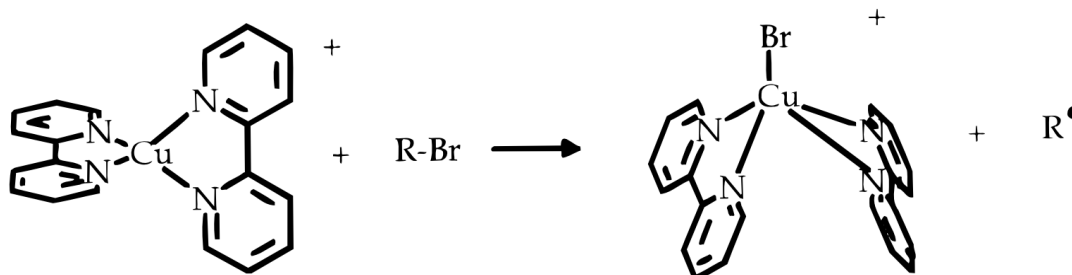


Figure 13. The proposed complex of copper with a bidentate ligand (2,2'-bipyridine bpy).⁶⁹

Reverse ATRP

In summary, normal ATRP involves the initiation of radical species, which are generated by an alkyl halide when exposed to a transition metal catalyst and ligand. The ligand and transition metal forms a complex, which means the transition metal is in a low oxidation state. An alternative method of ATRP, which is known as reverse ATRP, is where radical initiators are used instead along with the transition metal and ligand.⁵³ An example of a radical initiator that can be used in reverse ATRP is azobisisobutyronitrile (AIBN). Figure 14 shows the formation of a homopolymers through reverse ATRP using AIBN as the radical initiator.

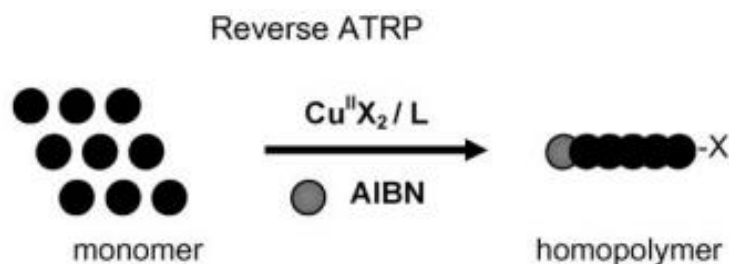


Figure 14. Formation of homopolymer from reverse ATRP

Reverse ATRP has been successfully carried out in copper based systems⁷⁰ as well as using iron complexes.⁷¹ The mechanism for reverse ATRP is shown in Figure 15.

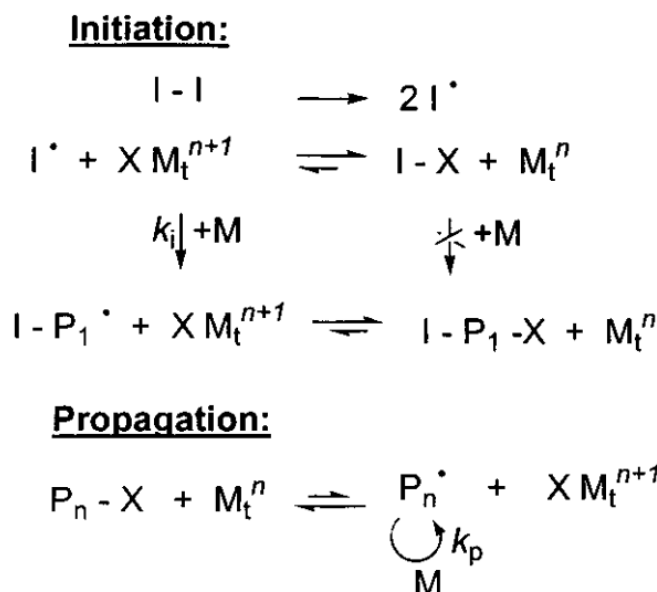


Figure 15. Mechanism for reverse ATRP demonstrating that initiation begins with a radical initiator.⁵³

Initiation in reverse ATRP is driven by the radical species ($2I^{\bullet}$) when they have been made. This causes the active catalyst-ligand complex (higher oxidation state) to be reduced to a lower oxidation state. After this the bulk of the polymer chains are initiated by normal ATRP initiation mechanism.

Activators regenerated by electron transfer (ARGET) ATRP

Through electron transfer, many reducing agents can be employed to help regenerate activators from deactivators. ARGET ATRP is when electron transfer regenerates activators, which allow the catalyst concentration to decrease to 10-100 ppm without losing control of the ATRP polymerisation.⁷² The use of using these reducing agents in excess does not just help regenerate activators but due to ATRP being sensitive to oxygen, these reducing agents offer tolerance to the air and help the reaction to proceed.⁷³ Examples of organic reducing agents which can be used in ARGET ATRP include ascorbic acid,⁷⁴ sugars⁷⁵ and phenol.⁷⁶ Inorganic reducing agents can also be used such as tin(II) complexes.⁷⁷ Ligands are also capable as acting as good reducing agents for ARGET ATRP.⁷⁸ ARGET ATRP allows polymerisations to proceed with low catalyst concentration, allowing the synthesis of polymers to be made with control and helps to prevent air from interfering with the reaction.

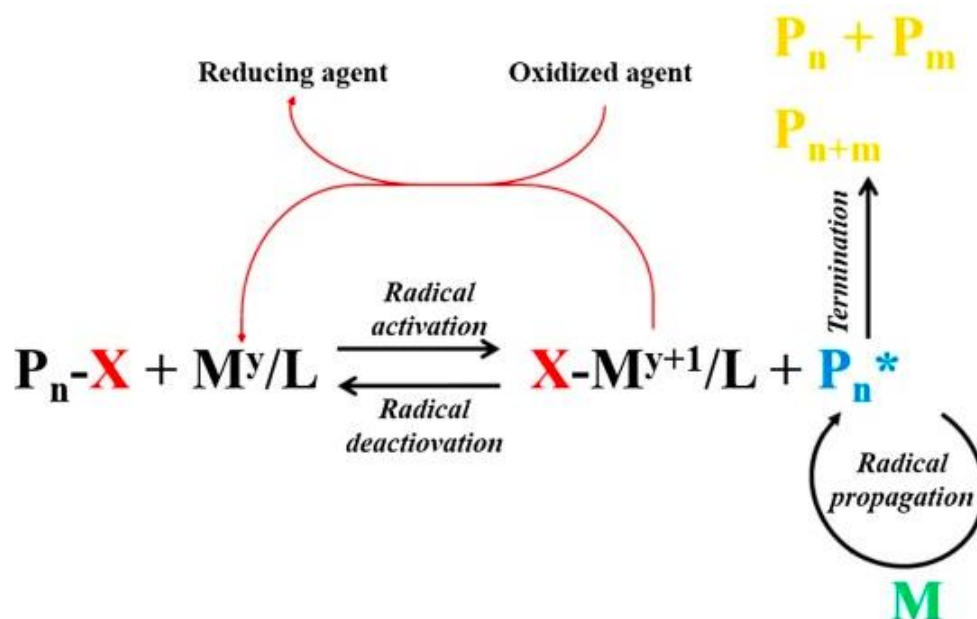


Figure 16. AGRET ATRP mechanism demonstrating how a polymer is synthesised. ⁷⁹

Figure 16 shows the mechanism of AGRET ATRP. Where M^y/L is the transition metal and ligand complex, P_n-X is macroinitiator alkyl halide, M is the monomer, P_n^* is the living polymer and P_{n+m} is the inactive polymer.

Supplemental activator and reducing agents (SARA) ATRP

With this type of ATRP, a zerovalent metal (M^0) is used and examples include Cu^0 , Zn^0 , Mg^0 and Fe^0 . Normal ATRP will use catalysts such as $CuBr$. Copper is in the oxidation of (+1) and will activate the polymerisation in this oxidation state and deactivate the reaction when in the (+2) state. With SARA ATRP, copper is in the oxidation state of (0) (oxidation state which activates the alkyl halides). The deactivation reaction occurs with copper in the oxidation state (+2).

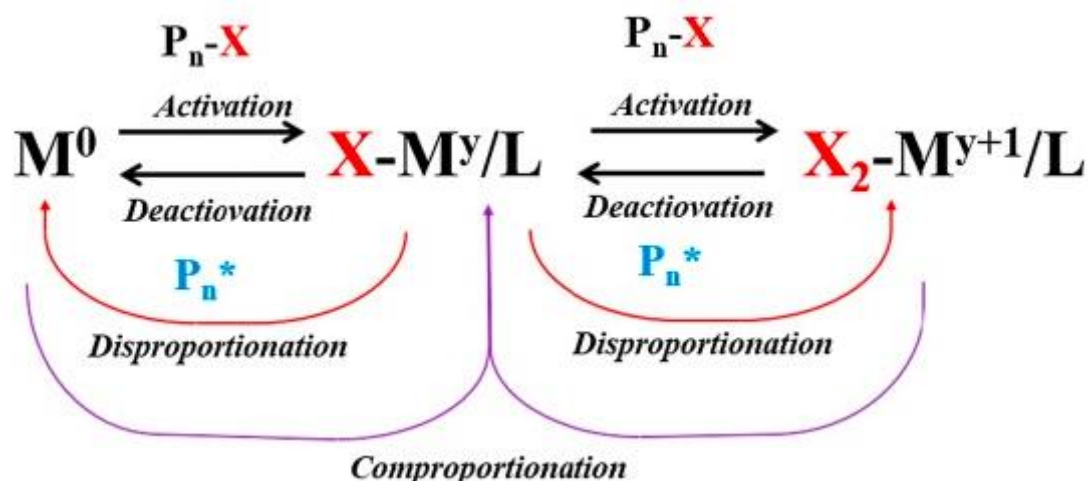


Figure 17. Mechanism of supplemental activator and reducing agents (SARA ATRP).⁷⁹

Single-electron transfer living radical polymerisation (SET-LRP)

In 2006 it was reported by Percec *et al.*⁸⁰ that single-electron transfer was able to polymerise acrylates, methacrylates and vinyl chloride monomers at 25°C. SET-LRP uses polar solvents such as water, alcohols, dipolar aprotic solvents, ethylene and propylene carbonate which causes instantaneous disproportionation of Cu(I)X into Cu⁰ and Cu(II)X₂ species when exposed to nitrogen containing ligands. This polymerisation occurs very quickly and the ability to have balance and control on the reaction comes from the fact that the instantaneous disproportionation is facilitated by the ultrafast living radical polymerisation. This means that activation occurs through the free radicals and extremely reactive Cu(0) species while deactivation is controlled by the Cu(II)X₂ species.

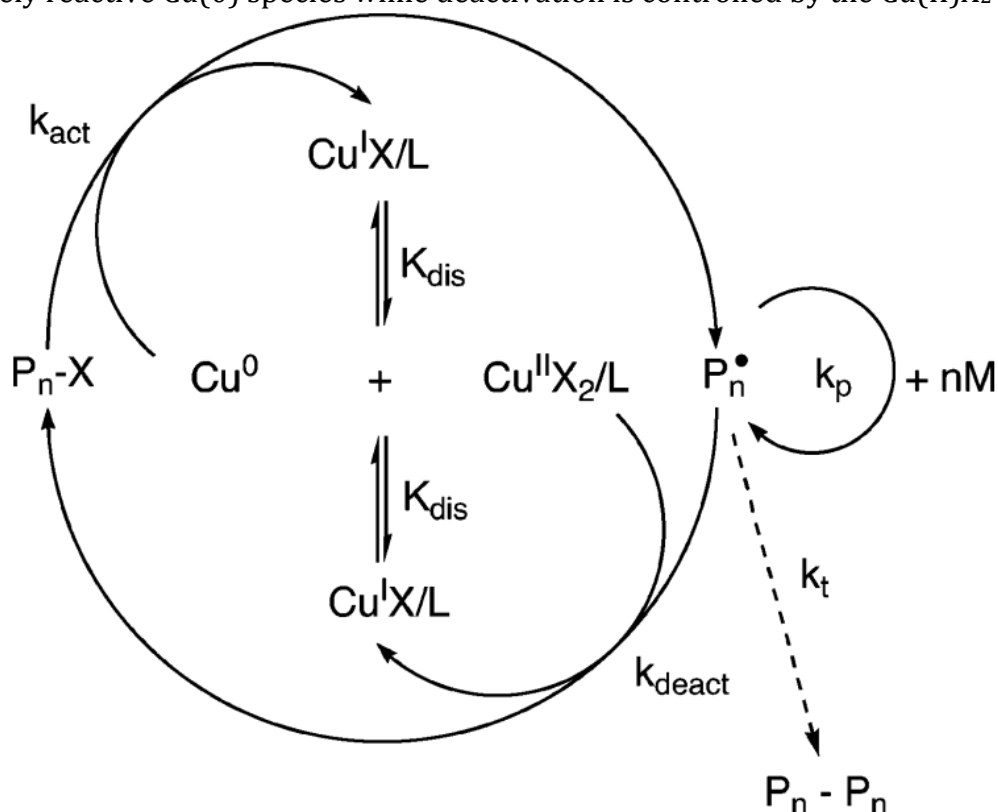


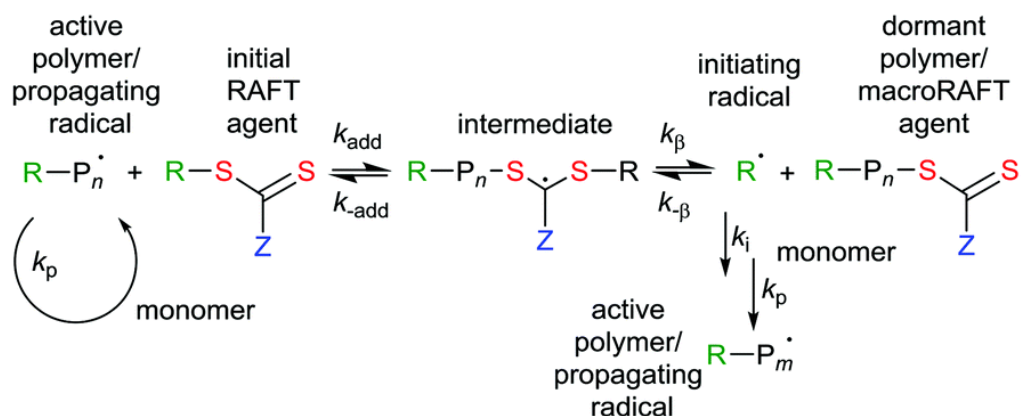
Figure 18. Mechanism for single-electron transfer living radical polymerisation (SET-LRP).

Reversible addition fragmentation chain transfer (RAFT)

The main difference between ATRP and RAFT is that RAFT is a degenerative chain transfer process, which normally does not require a catalyst. Instead a chain transfer agent (usually thiocarbonylthio based compounds) and an external radical source are used.³⁷ RAFT does come with its advantages over ATRP. Generally the synthetic process is simpler and copper complexes are not used whilst many catalysts used in ATRP are copper based.⁸¹ RAFT has been used to polymerise a broad range of vinyl monomers⁶¹ including styrene⁸², methacrylates,⁸³ vinyl esters⁸⁴ and methacrylamides.⁸⁵

Polymers made from RAFT will be able to self-assemble into nanocompounds (a particle between 1 and 100nm) and even thermoresponsive polymers such as PNIPAM have been used.⁸⁶ RAFT polymerisation can be useful as low dispersity polymers can be made through living and controlled radical techniques. The mechanism for this polymerisation is shown in Figure 19.

Initialization



Main equilibria

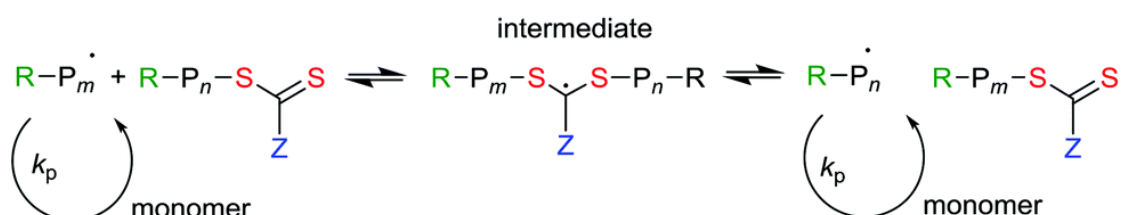


Figure 19. RAFT mechanism to synthesise polymers.⁸⁷

An important step in the RAFT mechanism is the chain transfer step. This involves the propagating radicals and dormant polymer chains that are referred to as macroRAFT agents.⁸⁷ The only difference between the two species on both sides of the equilibria is the degree of polymerisation, which is shown as n and m.

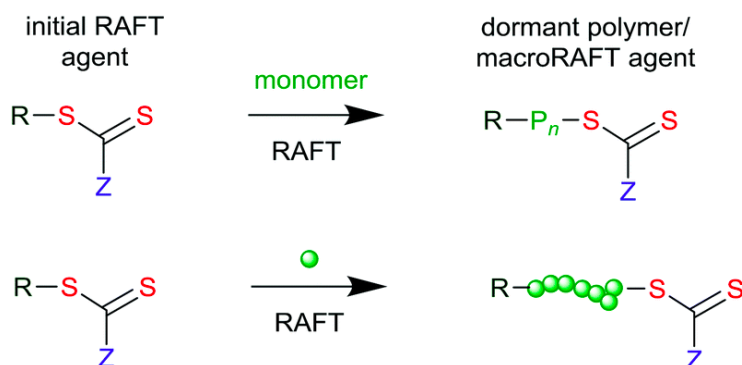


Figure 20. Two schematics of the overall RAFT process.⁸⁷

RAFT polymerisation is capable of making block copolymers. It does this by extending the chain of a polymer with one monomer and then again with a second monomer to form a block copolymer. For this to work, the RAFT agent used for the first monomer must also be suitable for the second monomer otherwise it is a synthetic nightmare.

1.2 Self-assembly of polymers

Polymers have a wide potential range of applications in therapeutic development. They can be self-assembled into drug nanocarriers which can be used in drug delivery and could have important roles in transporting drugs in and around the body.⁶ The sizes of these structures range from 1 to 1000nm. Currently there are just two approved drugs

which use polymers commercially available and these polymeric drugs aid in the treatment of hypolemia (blood loss) and relapsing multiple sclerosis. There are a further three drugs which have now passed Phase 2 trials and are now ready to commence into Phase 3 testing. These drugs look to treat bacterial vaginosis, cystic fibrosis and celiac disease. A further two polymeric drugs have failed Phase 3 testing and alterations will need to be made.⁸⁸

Many polymers which are tested only offer a potential application for delivering drugs in the future. Certain parameters can be altered such as size, morphology, charge and surface chemistry, which makes them suitable as potential drug carriers in drug delivery.⁸⁹ Nanocarriers can be defined into two main types; hard/solid core nanocarriers and soft nanocarriers. Examples of hard nanocarriers are metallic nanoparticles and quantum dots where loading takes place on the surface through passive adsorption or chemical conjugation.⁹⁰ Soft nanocarriers which this thesis will be focusing on, include lipid and polymer based systems where drugs can be added to the centre of these structures.⁹¹ Nano carriers are important as they improve pharmacokinetic properties. Many drugs are not soluble in water and have poor membrane permeability. It is the role of the drug carrier that overcomes these problems and gets the drug to the target molecule. This has led many drug carrier systems to be studied and a small amount to be developed.

1.2.1 Nanoparticles

Simple morphologies

The simplest of these nanostructures is the micelle, which can be self-assembled in aqueous solutions from amphiphilic polymers. The micelle is an amphiphilic aggregate meaning it contains both a hydrophilic region (polar head) and hydrophobic region (hydrophobic tail). Other simple morphologies also include cylindrical micelles where packing occurs differently to produce a rod like or cylindrical micelle as well as vesicles (polymersomes) that consist of liquid enclosed by a lipid bilayer. These fall into the category of soft nanocarriers and have been previously studied with hundreds of block copolymers including polybutadiene-*block*-poly(ethylene oxide) (PB-*b*-PEO) and poly(styrene)-*block*-poly(acrylic acid) (PS-*b*-PAA).⁹² These amphiphilic block copolymers that self-assembled into the simple morphologies described, allow for a hydrophobic core with a hydrophilic exterior.⁹³ Figure 21 shows examples of what these simple structures look like in the hydrated state using cryo-TEM.

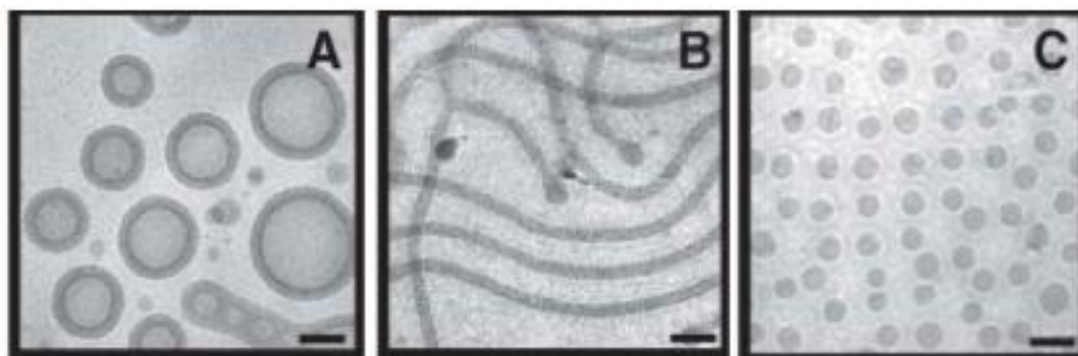


Figure 21. Cryo TEM Images of PB-*b*-PEO aggregates; (A= Vesicles), (B=Cylindrical Micelles)(C= Spherical Micelles).⁹²

Micellar aggregates offer many advantages in drug delivery with the main one being that diameters are less than 100nm usually.⁹⁴ This allows these particles to accumulate within tumor vessels through enhance permeability and retention (EPR) effect. The characteristics of different hydrophilic blocks also allow for increase circulation time when injected into the body.⁹⁵ Subsequently, hydrophobic drugs can be loaded to the centre of the micelle and the hydrophilic corona offers protection when transporting the hydrophobic drug to the tumor site.

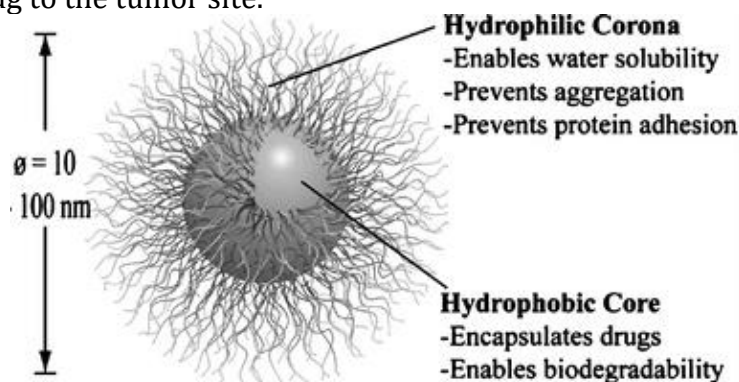


Figure 22. Diagram of a micelle with key components illustrated.⁹⁴

An example of a micellar system that is currently used as carrier of drugs in chemotherapy, is Pluronic® P105.⁹⁶ This is the most common copolymer used in micellar drug delivery although other examples have been studied.⁹⁷ The structure of this copolymer is PEO₃₇-*b*-PPO₅₆-*b*-PEO₃₇ where there are two poly(ethylene) (PEO) blocks and a polyphenylene oxide (PPO) in the middle of the polymeric structure. A known concentration of the copolymer is made in a phosphate buffered saline solution and the chemotherapy drug is then added. This micellar drug is shown in Figure 23 and would then be administrated at 1 wt%.

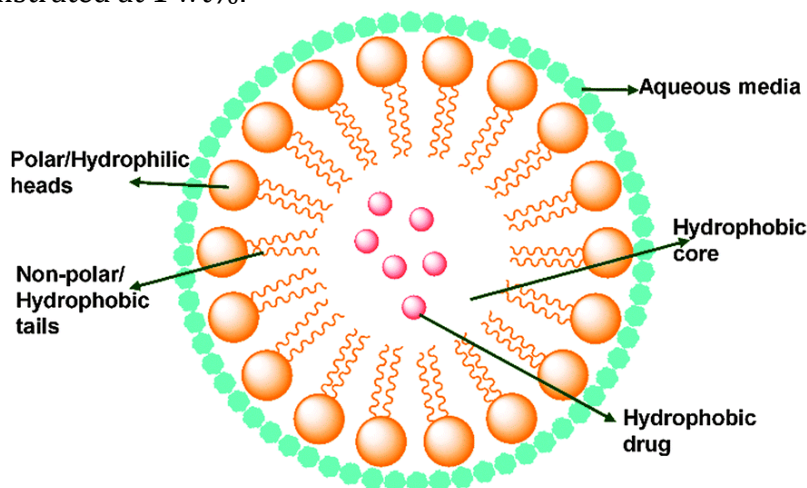


Figure 23. The structure of a micelle that has been encapsulated with a hydrophobic drug.⁹⁷

Hundreds of micellar systems have been development in laboratories around the world but only a few have become commercially available. Many believe these micellar systems do not make good delivery systems for hydrophilic guests due to their inability to load hydrophilic drugs without surface conjugation.⁹⁸ They are however still effective at delivering hydrophobic drugs and micellar drug systems are still being used on the market.⁹⁸

Lipid based systems

An alternative to micelles is self-assembled nanocarriers such as liposomes and polymersomes. Lipids are molecules that are made up of hydrocarbons and are the building blocks used in the structure of living cells.⁹⁹ Examples of lipids are waxes, oils, fats and cell membranes that do not consist of protein. Lipids are not water soluble and are non-polar in nature. This means that they are not able to self-assemble into some of the aggregate species already discussed. This has led to amphiphilic lipids such as phospholipids to be studied¹⁰⁰ as these lipids can self-assemble into liposomes.

Having said this, lipids have still been studied for drug delivery. One way to get around the issue of self-assembly is to incorporate the lipid with polymers. Lipid-based nanocarriers are hindered due to many stability problems. These systems can aggregate *in vitro* and normally need other compounds added to help overcome these stability issues.¹⁰¹ A way to overcome these stability issues is that lipid nanocarriers have been incorporated with polymers.¹⁰² An example of a lipid polymeric system (Figure 24) can be seen with 1,2-distearoyl-sn-glycero-3-phosphoethanolamine-poly(ethylene glycol) DSPE-PEG as an outer surface, with a middle polymer layer and a cationic lipid hollow core that trapped siRNA.¹⁰³

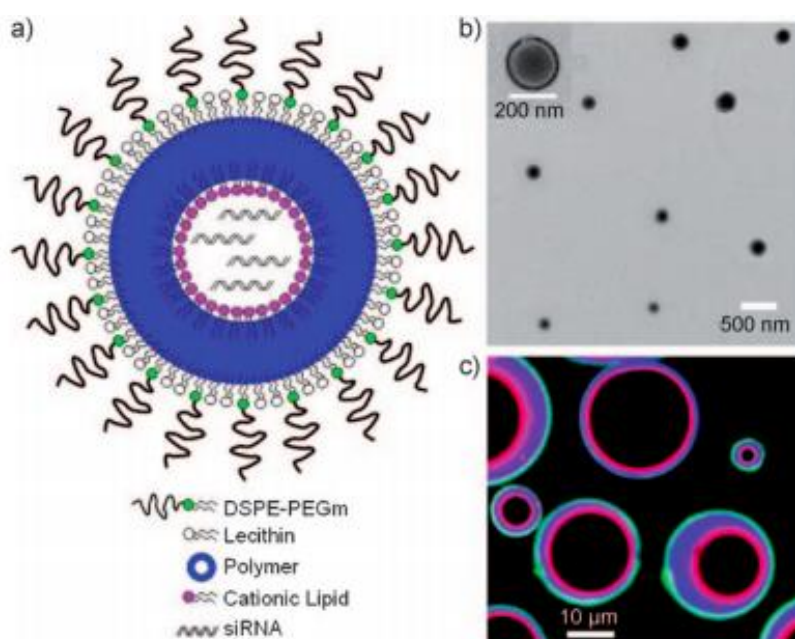


Figure 24. A) Schematic representation of lipid-polymer-lipid nanostructure. B) TEM image of the lipid-polymer-lipid nanostructure. C) Confocal laser scanning fluorescence to show each distinct layer of lipid-polymer-lipid nanostructure.¹⁰³

A second example of a lipid-polymer systems uses D-fructose modified with poly(ethylene glycol) (Fru-PEG) and fructose modified with poly(ethylene glycol)-*block*-poly(ethyl hexyl glycidyl ether) (Fru-PEG-*b*-PEHG) to form nanoparticles.¹⁰⁴ The block copolymers were self-assembled into spherical micelles, cylindrical micelles and vesicles with cryo-TEM and dynamic light scattering were carried out on these structures. These were stained with a fluorescent marker to allow for initial uptake tests with breast cancer cells.

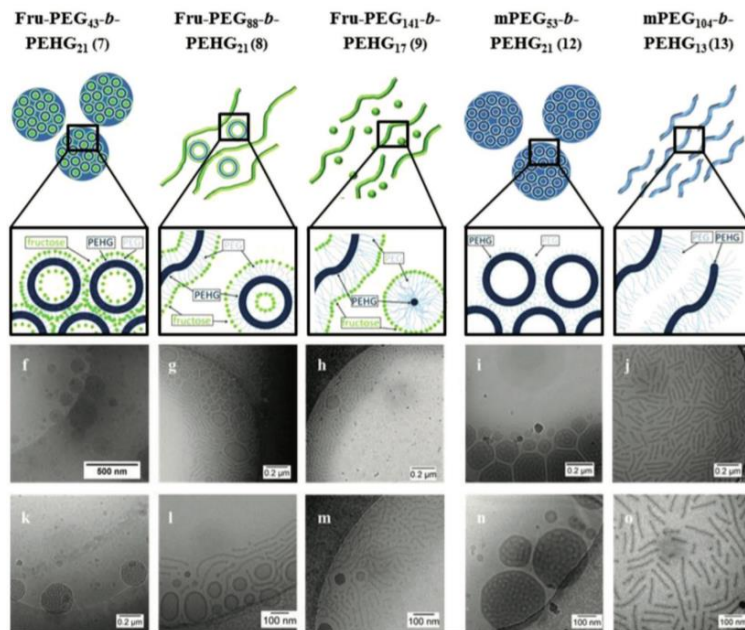


Figure 25. cyro-TEM images of lipid-polymer system using Fructose, PEG and PEHG.

These experiments demonstrated a range of different morphologies made from a lipid and polymer-based system.

Liposomes and Polymersomes

A liposome is much larger than a micelle but is still spherical shaped. It is made up of one or more phospholipids, which are molecules that normally consist of two hydrophobic fatty acids tails and one hydrophilic head that contains a phosphate group. Multilamellar liposomes can form when a second lipid bilayer forms around the first lipid bilayer. Figure 26 shows the structures of a liposome and a multilamellar liposome and also show how the phospholipids rearrange in these structures.

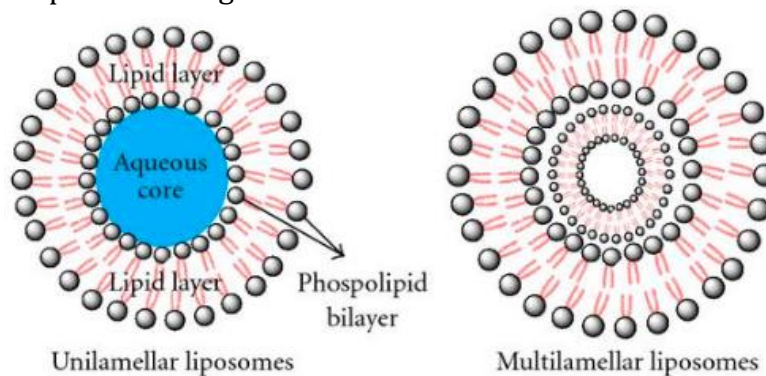


Figure 26. Structures of a liposome and multilamellar liposomes.¹⁰⁵

The middle of a liposome consists of an aqueous solution core and is surrounded by a hydrophobic membrane. The advantage these structures have is that hydrophilic and hydrophobic drugs can be loaded inside the core and bilayer membrane and this is demonstrated in Figure 27. After loading, these liposomes can then be used to transport compounds and drugs around the body.

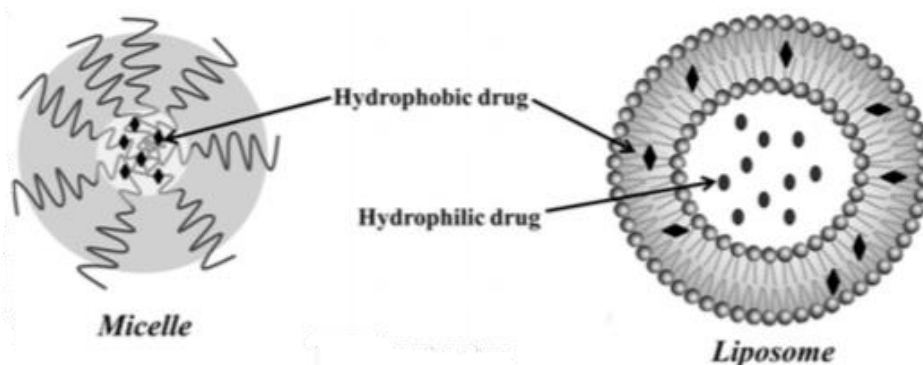


Figure 27. Structure of a micelle and liposome and how they are able to encapsulate drugs.⁹⁷

The aggregate structures discussed above can be made many ways. What this thesis will be focusing on is preparing these aggregates from synthetic routes using polymers, where previously these structures have been made from naturally occurring compounds such as fats and oils. Polymer chemistry has built on the subject of liposomes and used the same concept but with block copolymers to form polymersomes. When amphiphilic block copolymers are self-assembled in aqueous solution, polymersomes can be made. Polymersomes are very similar to liposomes but as they are usually prepared from block polymers, this means that they are artificial vesicles. They are hollow spheres with a liquid core allowing for both hydrophobic and hydrophilic drugs to be encapsulated within the polymersomes. The difference between polysomes and liposomes can be seen in Figure 28.

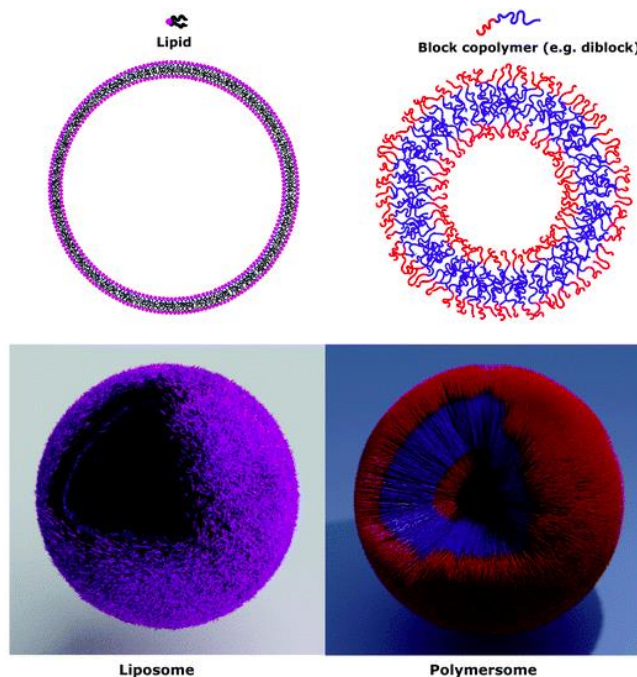


Figure 28. 2D and 3D images of liposomes and polymersomes.¹⁰⁶

Liposomes and polymersomes have many advantages for the application of drug delivery.¹⁰⁷ Due to these structures being amphiphilic, both polar and non-polar compounds can be encapsulated within these structures. These structures can be made from nontoxic and biodegradable amphiphilic molecules which is useful when it comes to the application of drug delivery. The surface of these structures can be modified with ligands for active targeting. An example of this was where a pegylated biodegradable liposome with doxorubicin encapsulated within the structure was used as a liposome-

based treatment for cancer.¹⁰⁸ The major drawback with these structures, in particular liposomes is that on their own tend to be slightly sterically unstable and will be removed from the bloodstream.⁹³

More complex architectures

The research on liposomes and polymersomes has paved the way for studying alternative nanocarriers, which contain a cubic and hexagonal internal phase. Lipid-based liquid crystalline nanocarriers that contain an internal bicontinuous cubic phase are known as cubosomes and nanocarriers with a reversed hexagonal phase are known as hexosomes. In more detail, cubosomes are nanostructured particles and the term 'bicontinuous' refers to the two distinct hydrophilic regions that are separated by the bilayer. At controlled temperatures the lipid bilayer is twisted in three dimensions to form a tight packed structure between the water and lipid. There are three phases in which the cubic structure can be within and these are:

- P-Surface (Primitive)
- G-Surface (Gyroid)
- D-Surface (Diamond)

Both cubosomes and hexosomes have been investigated as drug and vaccine delivery structures.¹⁰⁹ Figure 29 shows the internal arrangement of both examples. Cubosomes are best described as having inverse bicontinuous cubic system made from a three-dimensional folding of lipid bilayers to make non-intersecting continuous aqueous channels,¹¹⁰ whereas hexosomes are best described as having hexagonal packed arrangements of rod-shaped inverse micelles with closed aqueous channels.¹¹¹

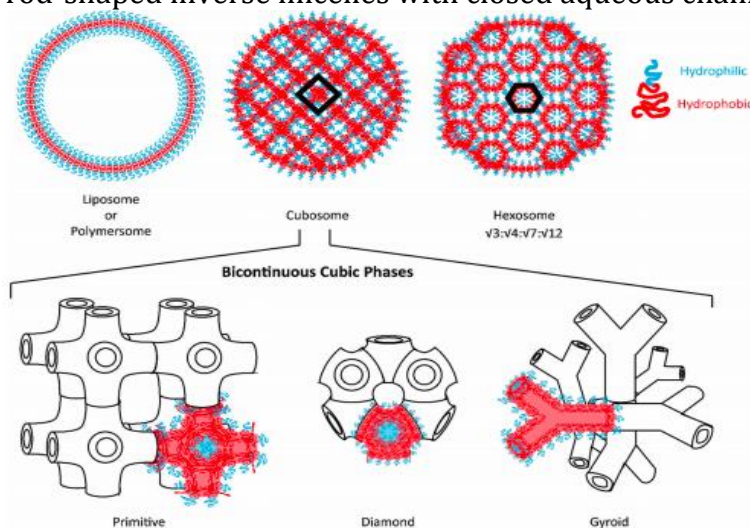


Figure 29. The internal arrangement cubosomes and hexosomes.⁹⁸

Complex morphologies of vesicles

As a greater understating on self-assembly has been built upon over the years, this has allowed an increase in different types of morphology observed. It has been recognised that by varying the degree of hydrophobic:hydrophilic, new and more complex structures have been discovered when compared to spherical micelles, cylindrical micelles and vesicles. This has been observed when the block copolymer composition is changed and different methods for the preparation of aggregate dispersions are used. This has

allowed other advancements such as vaccine formulations where they rely on the delivery of hydrophilic protein antigen structures as well as hydrophilic and hydrophobic adjuvants which could be in the form of lipids, nucleic acids and other smaller molecules.¹¹²

Self-assembled polymeric nanocarriers can be made up of block copolymers (BCPs) that contain hydrophilic and hydrophobic regions. It has been observed that as the molecular weight of the BCP increases, the more stable the aggregate is when formed. As the molecular weight increases in these polymer systems so does the thickness of nanocarriers membrane which changes the mechanisms through which neighbouring amphiphiles interact.¹¹³ The biggest advantage of using BCPs is that they can be easily tuned and altered for specific applications as they are synthesised from a large class of established monomers. This is done through changing the molecular weight as well as the weight fraction of each block. This allows for well-defined polymer structures with desired properties.

Complex morphologies involving vesicles have been seen when aqueous solutions and organic solvent-water mixes have been used. Unilamellar vesicles has been discussed previously but multilamellar or sometimes referred to as 'onion' vesicles and concentric vesicles have also been observed and are shown in Figure 30. Concentric vesicles is where there are aqueous volumes between each layer.¹¹⁴ In addition to these, large compound vesicles (LCVs) is another class where many vesicles merge together to form a flower-like arrangement.^{114,115} Zhang *et al* ¹¹⁶ witnessed the formation of vesicles with internal morphology which were made from di and triblock copolymers in a water-DMF solvent mix.

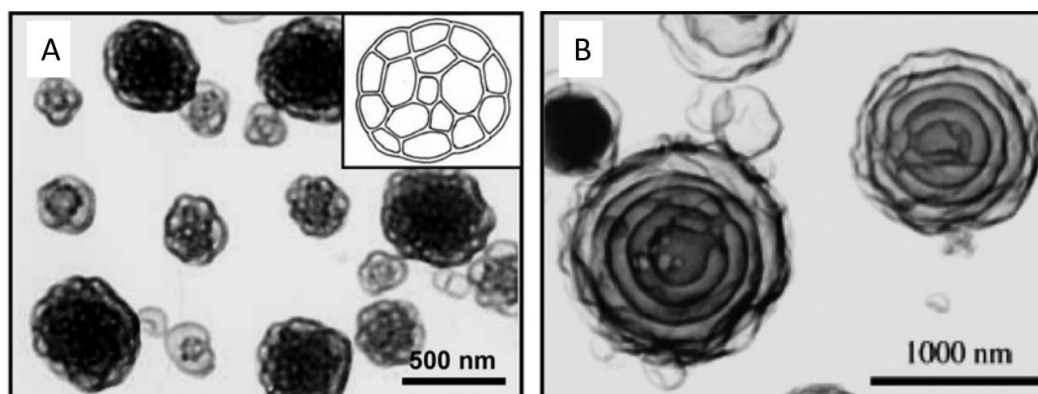


Figure 30. A) Large compound vesicles (LCVs) B) Multilamellar/ onion vesicles.¹¹⁷

Complex morphologies of micelles

Complex morphologies of micelles have been discovered and over time the research surrounding them has been built upon. The first type that will be discussed is multi-compartment micelles.¹¹⁸ These are usually made from triblock copolymer where the three blocks used are all different (ABC triblock) although diblock copolymers can be used. Multi-compartment micelles made from a diblock of PEO₄₅-b-PTMSPMA₅₉ is shown in Figure 31. When self-assembled, a phase-separation of the blocks form so that there is segregated regions within the aggregate core.¹¹⁹ This happens as there is three different interactions happening (A with B, B with C and A with C). This differs from diblock copolymers where there is just one interaction that takes place. If the architecture is

changed for example, linear to graft or linear to star, then further complexity arises. This can be useful as it allows incorporation of two or more chemically incompatible particles in the compartments of the micelles which offer advantages with delivering drugs.¹²⁰

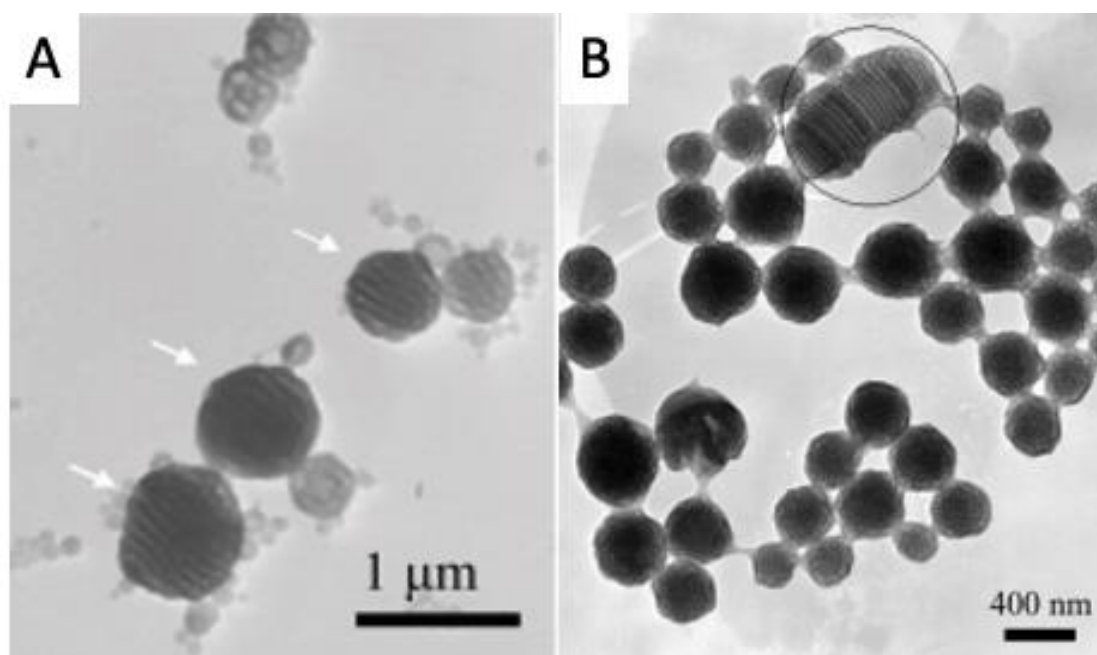


Figure 31. Two examples of multi-compartment micelles made from $PEO_{45}\text{-}b\text{-}PTMSPMA_{59}$.

When further work was conducted on more complex morphologies of block copolymers, it discovered that diblock and triblock copolymers could form helical aggregates, disk-like and toroidal micelles.¹²¹ It was discovered that disk-like or sometimes referred to as oblate spherical micelles could be made from ABC triblock copolymers with non-ionic¹²² and ionic¹²³ hydrophilic blocks. The structure of disk-like micelles is shown in Figure 32.

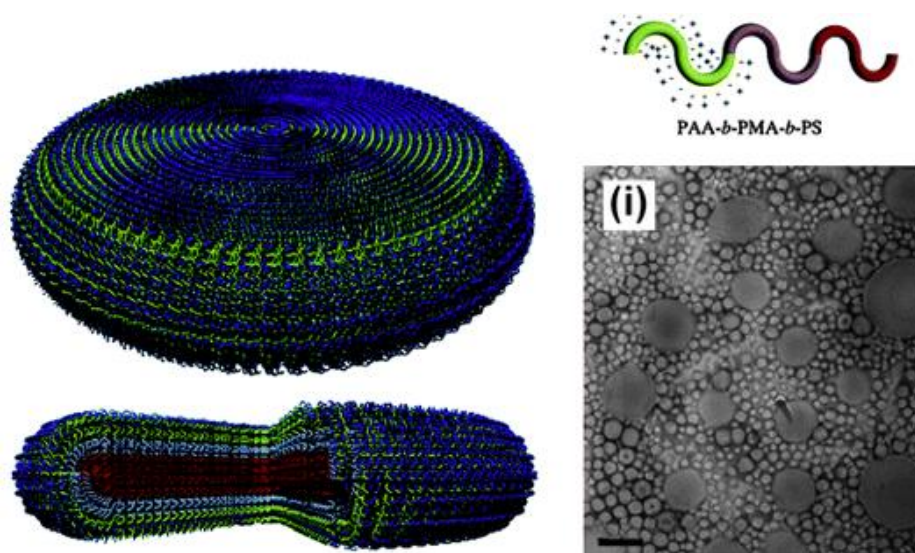


Figure 32. Disk-like micelles made from the self-assembly of $PAA\text{-}b\text{-}PMA\text{-}b\text{-}PS$.¹²⁴

Disk-like micelles were seen when poly(acrylic acid)-*block*-poly(methyl acrylate)-*block*-polystyrene ($PAA\text{-}b\text{-}PMA\text{-}b\text{-}PS$) was self-assembled. It was the strong electrostatic repulsion between the PAA corona-forming blocks which allows for a high curvature, making disk-like micelles possible.

Toroidal micelles were also observed and are a result when there is an end-to-end looping of cylindrical micelles. The formation of toroids is driven by the energetically unfavourable end-caps on cylinders.¹²³ Figure 33 shows what toroids look like under TEM.

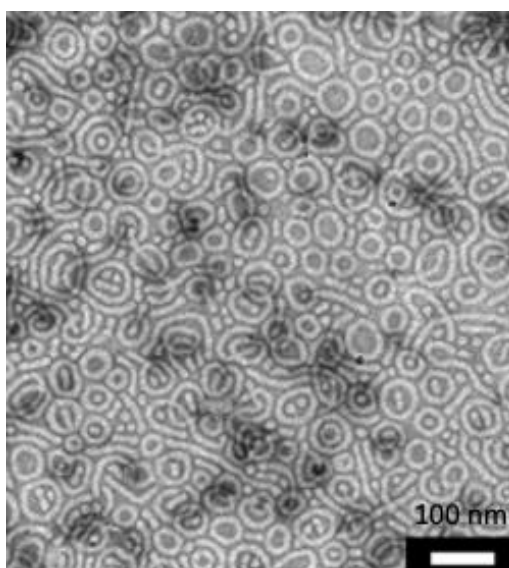


Figure 33. TEM image of toroids aggregate made from PAA-*b*-PMA-*b*-PS triblock.¹²⁴

Micelles that have internal complexity have also been seen and are known as bicontinuous nanospheres. The term 'bicontinuous' relates to the complex network of the hydrophobic block with pores made up of the hydrated hydrophilic block. The advantage bicontinuous nanospheres have over other aggregate species is that both hydrophobic and hydrophilic drugs can be loaded into the centre of the sphere. This type of aggregate was first presented by Eisenberg *et al*¹²⁵ where a block copolymer of polystyrene and poly (acrylic acid) (PS₁₉₀-*b*-PAA₂₀) was used. The solvent system was a mixture of DMSO-water with NaCl being present. TEM was performed on the sample and showed that the aggregate structure consisted of a network of interconnected rods and shown in Figure 34.

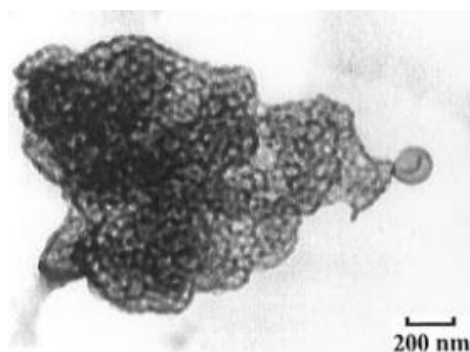


Figure 34. Bicontinuous structure of interconnected rods made from PS₁₉₀-*b*-PAA₂₀¹²⁵

A triblock copolymer of PAA-PMA-PS was self-assembled by Wooley *et al*¹²⁶ where THF-water was used as the solvent system in the present of EDDA and is shown in Figure 35. This produced aggregate structures with an internal structure which was tuneable by varying the ratio of THF:water. Aggregate structures seemed to possess a more bicontinuous structure as the water content was lowered.

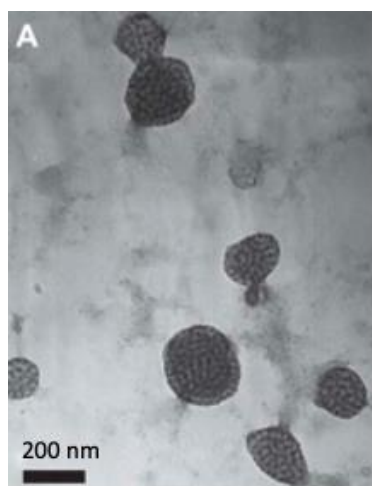


Figure 35. TEM micrograph of bicontinuous micelles made from PAA-PMA-PS.

The examples given above all required additives in order to produce bicontinuous aggregates. The first example of polymers giving a bicontinuous aggregate without using an additive was a amphiphilic polynorbonene-based block copolymer with oligo(ethylene glycol) methyl ether (OEGME) and tri-peptide glycineleucine-phenylalanine segments.¹²⁷ The self-assembly involved dissolving the polymer in DMSO and then adding water slowly by using dialysis.

The structure was classed as a branched network of worm-like hydrophobic peptide-containing segments segregated from aqueous channels containing the hydrated hydrophilic OEG moieties.¹²⁷ The structure of this aggregate is shown in Figure 36.

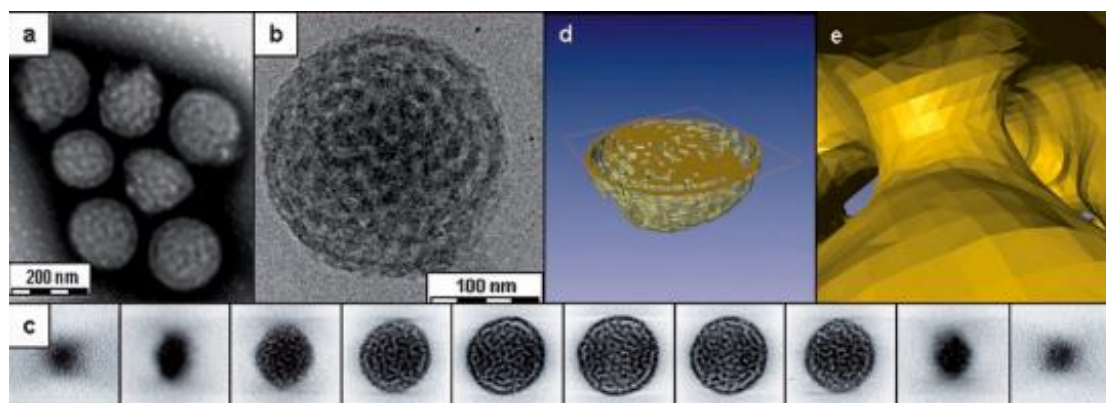


Figure 36. TEM images of amphiphilic polynorbonene-based block copolymer. A) Conventional TEM using negative staining. B) cryoTEM image of aggregate C) gallery of z slices showing different cross sections of a 3D SIRT (simultaneous iterative reconstruction technique) D) 3D cross section of aggregate E) a view of the hydrated channels within the aggregate.¹²⁷

Since these publications, block copolymer involving poly(ethylene oxide)-*block*-poly(octadecyl methacrylate) PEO-*b*-PODMA¹²⁸ have been successfully self-assembled in THF:water using dialysis to form bicontinuous nanospheres. Figure 37 shows the bicontinuous nanospheres self-assembled from PEO-*b*-PODMA. The ODMA block has thermoresponsive properties due to it being semi-crystalline. This means when it is in the aggregate form and it experiences a temperature of 21.5°C (which is the melting transition of the ODMA block) it will start to release a drug at and above this temperature effectively. This was carried out using pyrene as the drug encapsulated within the bicontinuous nanosphere.¹²⁸

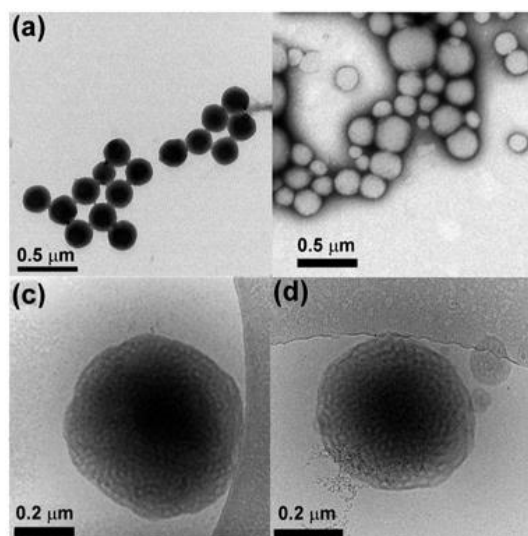


Figure 37. TEM micrographs of PEO-*b*-PODMA A) bicontinuous nanospheres with no pyrene and no negative staining, B) with pyrene encapsulated and aggregates being negative stained, C) negative staining without pyrene and D) with pyrene and negative stained.¹²⁸

1.2.2 Polymer Aggregate Preparation

The factors that affect the formation of block copolymer aggregates include preparation method, polymer composition & concentration of polymer. Self-assembly can be carried out through a number of different ways; micro-fluidic techniques, layer-by-layer assembly, electroformation and formation of aggregates during synthesis of BCPs in solution. Having said this, there are two main methods used for the formation of BCP aggregates, which are direct dissolution¹²⁹ and dialysis.¹³⁰ Depending on the degree of hydrophilicity of the block copolymer, will depend on the route taken. With direct dissolution, the polymer is dissolved directly in the solvent and works better when the BCP is more hydrophilic. Dialysis is useful to use when block copolymers contain a hydrophobic block. The common way for this to happen is that the BCP is first dissolved in a common organic solvent which dissolves the BCP fully and dialysis is then carried out to exchange the solvent molecules with water molecules. For this to work, the solvent and water must be miscible.

Dialysis is a self-assembly method that allows for the size and morphology of the resultant polymer to be controlled depending on what organic solvent is used. Previously Eisenberg¹³¹ and co have used dioxane as the organic solvent when PAA-*b*-PS was self-assembled by dialysis. The wt % of polymer was altered to see what effect this had on the aggregates that formed. Results showed that on a decrease of wt% PAA-*b*-PS in dioxane the morphology changed from spheres to rods and then to vesicles. It was shown that by changing common organic solvents not only changes the dimensions of the core of the aggregates (due to increase degree of swelling) but also increased the repulsion between the corona chains due to solvent-polymer interactions. This led to self-assembly using DMF as the common solvent where PAA-*b*-PS formed spherical micelles and then testing with THF where the degree of swelling of the core increased further. This allowed for larger aggregates to form such as spheres, vesicles and large compound micelles. The solubility of the core and the corona forming blocks in common organic solvents affect resultant morphologies and was established by Holder *et al.*¹³² This was where a block

copolymer of PEO-*b*-PBMA (17wt% PEO) was self-assembled by dialysis in THF as the common solvent to form bicontinuous nanospheres.

Block copolymers have been observed to self-assemble into many aggregate species. Dialysis has allowed crew-cut aggregates to form where the core of the forming polymer is bigger than the corona forming block.¹³³ An organic solvent is used to dissolve the polymer and distilled water is added slowly to avoid precipitation. Dialysis then allows crew-cut aggregates to form by removing the organic solvent over time. A second example was seen with Jun Fu¹³⁴ and co where a range of different morphologies were observed when PEO-*b*-PS was self-assembled using dialysis. PEO-*b*-PS was first dissolved in DMF where distilled water was added slowly to give a cloudy solution. This was then dialysed for 2 days in distilled water producing a vast range of morphologies as shown in Figure 38.

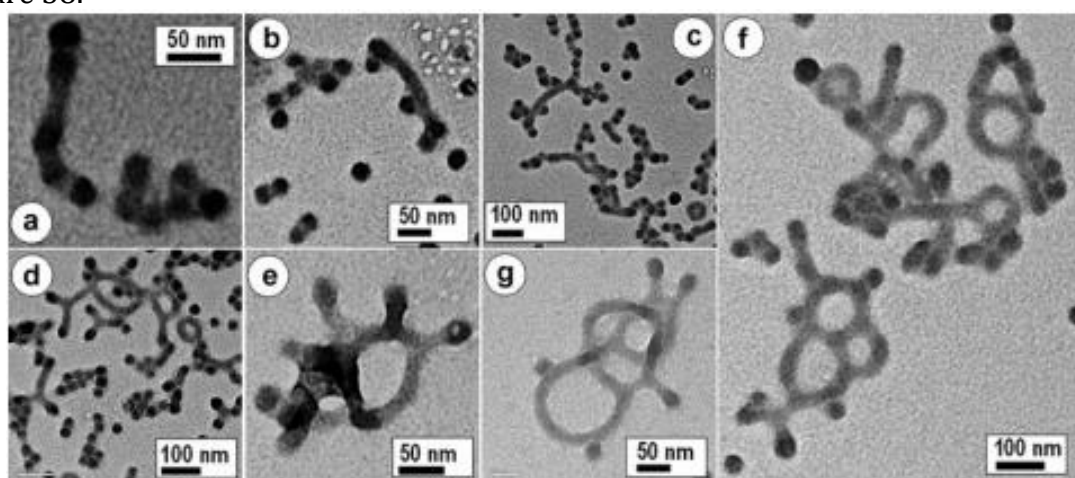


Figure 38. TEM images of PEO-*b*-PS self-assembled by dialysis. A-C shows cylinders and spherical micelles, D shows cylinders, gyoids and toroids. E-G) 2D and 3D toroids.¹³⁴

The way the direct dissolution is used is that the solution containing polymer is heated up and then allowed too cool as shown in Figure 39. This allows the self-assembly to take place and this process can take a few days. This has been carried out with a number of polymer systems,¹³⁵ an example being poly(styrene-*b*-isoprene) (PS-*b*-PI) by Yabu *et al*¹³⁵ who managed to speed up this process significantly. They used microwave annealing which meant block copolymers that contained a hydrophobic block could form stable nanoparticles in a few minutes.

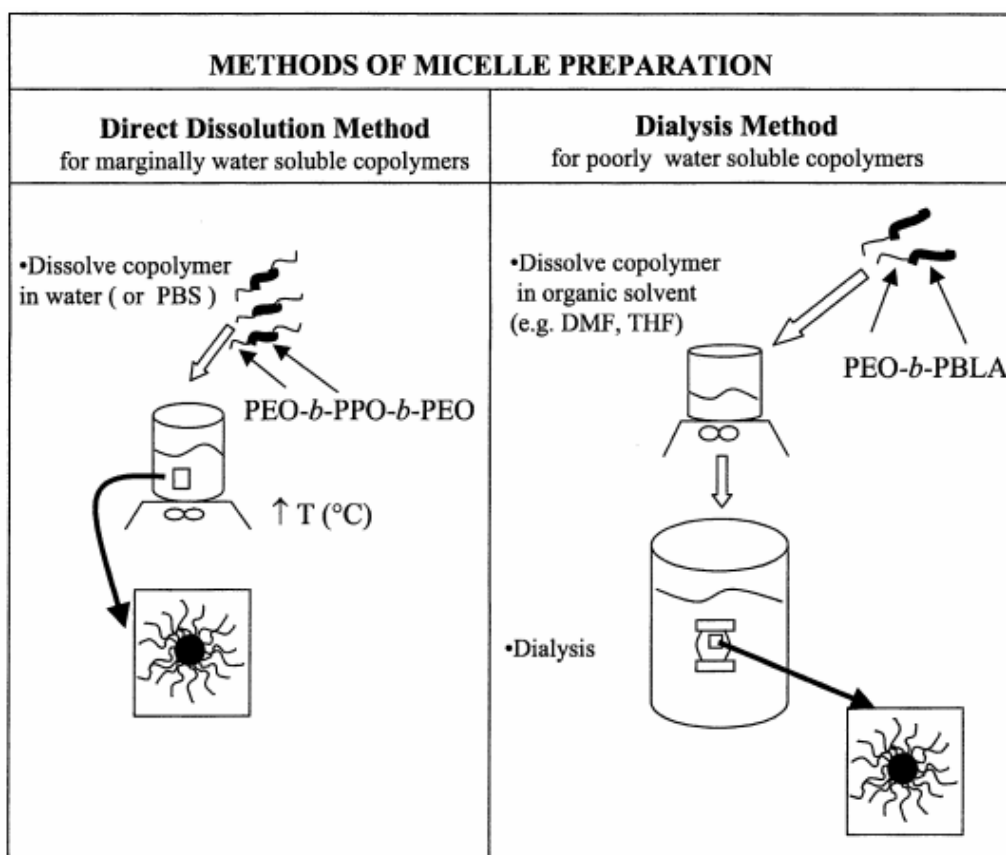


Figure 39. Direct dissolution and dialysis methods used for copolymer self-assembly.

Principles of block copolymer self-assembly

Block copolymers that contain both a hydrophilic and hydrophobic block are constrained by the covalent bonds that bond them. There are many factors which affect the self-assembly of block copolymers. This sections emphasis what those factors are. For potential applications it is important that the aggregates of BCPs are thermodynamically stable otherwise they would not be ideal as drug carriers for drugs. There are three contributing factors to the free energy of the system.

1. The degree of stretching of the core forming block (usually hydrophobic block).
2. Interfacial tension between the core and self-assembly solvent (Usually hydrophobic- water interaction).
3. Repulsive interactions between the corona forming chains.¹³⁹

Different morphologies will form depending upon these 3 factors. This means that polymer compositions, preparation techniques and concentration of polymer are vital when targeting a specific type of aggregate.

When a block copolymer is self-assembled in solution, segregated nano-compartments form with the hydrophilic region in contract with the water molecules. At the same time, the hydrophobic region has an inverse effect where the hydrophilic component pack in a particular way to minimise the exposure the hydrophobic region has with the water molecules. This effect can be seen with other self-assembled polymers in different solutions where one block of the polymer is solubilised, which allows for well-defined simple and complex aggregate structures.

Ordered morphologies can be formed when block copolymers are self-assembled in aqueous solutions. The factors which influence what is self-assembled, is the interaction between blocks, the interaction between each block and the solvent and the concentration of the block copolymer. There are many different morphologies that can result from block copolymers can be explained by the concept of packing factors and is displayed in Figure 40.¹⁴⁰

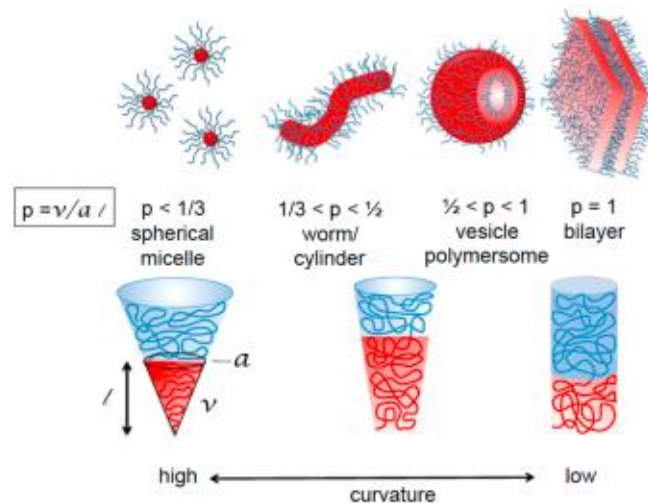


Figure 40. Block copolymer morphologies self-assembled in solution, where P is packing parameter, v is the volume of hydrophobic block, l is the length and a is the contact area.

The morphologies that can form for block copolymers in solution is dependent on the packing parameter p which is calculated from parameters where v is the volume of hydrophobic block, l is the length and a is the contact area. The relationship of these parameters is best described in Equation 1.3.

Equation 1.3 Calculation of the packing parameter (p)

$$p = \frac{v}{al}$$

The most common morphologies formed are micelles, cylindrical micelles and vesicles. The concept of packing parameters has been successful in predicting and explaining why micelles ($p \approx 1/3$), cylindrical micelles ($p \approx 1/2$) and vesicles ($p \approx 1$) form depending on the volume fractions of the copolymer used in the self-assembly process.¹⁴¹ Most block copolymers that are self-assembled will contain a hydrophobic block with a glass transition temperature (T_g) much lower than the ambient temperature used in the self-assembly process. This means the aggregate will exist in dynamic equilibrium with solvent molecules.

When block copolymers contain blocks that has a glass transition temperature greater than ambient temperature such as poly(methyl methacrylate) (PMMA) and polystyrene,¹⁴¹ aggregates can still form if a slow addition of water is added before self-assembly. To do this an organic solvent which the polymer is miscible in is used. When the packaging parameter is ($p < 1/3$) micelles are favoured. When it is between ($1/3 < p < 1/2$) cylindrical micelles or worm like structures will form and when it's between ($1/2 < p < 1$) then vesicles and polymersomes are favoured.

Packing parameters was first used by Israelachyili *et al*^{113,142} and can be a useful tool in predicting morphology of aggregates. The packing parameter calculated really can offer some insight into whether spherical micelles, cylindrical micelles and vesicles will form. However, Equation 1.3 is a general rule and not absolute³ as there are now a wider range of complex morphologies which include bicontinuous nanospheres, disk-like and toroidal micelles.

Other factors also affect which aggregate species forms and these factors are either physical or chemical. Changing the chemical structure of the block polymer will have an effect on the morphology of the aggregate. Changing the ratio of hydrophilic:hydrophobic will have a big effect on the structures formed. In addition to this, preparation techniques previously mentioned above also play a vital role. Preparation techniques include the solvent used, the concentration of polymer and how the aggregates were self-assembled in the first place.¹⁴³

The relative ratio of hydrophilic:hydrophobic in the block copolymer is extremely important to the self-assembly of aggregates. In general, when the hydrophilic:hydrophobic ratio is 1:1 then micelles are most likely to form. A ratio of 1:2 will most likely see vesicles being produced and a ratio of 1:3 will see vesicles formed along with inverted microstructures and other complex aggregates such as bicontinuous nanospheres.¹⁴⁴

Other research that outlines the self-assembly process has shown that the hydrophilic block is the driving force.^{117,145} This work showed that a polymer with a hydrophilic weight of 35% is most likely to form vesicles, <50% the formation of cylindrical micelles are favoured, >45% micelles may form and at 25% inverted micelles will be present after self-assembly of the block copolymer. Again this is not exact and exceptions to this work have been observed due to the other factors which affect the self-assembly process.^{116,146}

Critical Micelle Concentration

It has been mentioned previously that the concentration of the polymer can affect what aggregates are present after self-assembly.¹⁴⁷ This was shown when a block copolymer PS₁₉₀-*b*-PAA₂₀ changed from spherical micelles to cylindrical micelles and then to vesicles when there was an increase in polymer concentration. The solvent system used for self-assembly was a mix of DMF-water. This was not the first time where a change in morphology was seen when the polymer concentration was altered.¹⁴⁸

In order to make stable nanoparticles in solution will be dependent upon the critical micelle concentration (CMC). This is the minimum concentration of polymer needed for aggregates to form. Below this minimum concentration, the number of polymer chains present is not enough to allow self-assembly to happen. The polymer chains are spread throughout the aqueous solution and adsorbed at both the air-water interface and solvent-water interface. As the concentration of polymer is increased, the interface and bulk solution become saturated which allows the self-assembly process to proceed allowing the formation of aggregate species. Formation of aggregates form to reduce the interfacial free energy. This takes place as the hydrophobic-water interactions are unfavourable and this is known as the 'hydrophobic effect'.¹⁴⁹

1.2.3 Block copolymer in solid state (Microphase separation)

Free energy contributions to micellisation

The blocks of block copolymers would like to remain demixed, is governed by entropic effects which creates a microphase separation.¹³⁶ Many factors affect the phase behaviour of the amphiphilic block copolymer in bulk, such as the degree of polymerisation (N), Flory-Huggins Interaction parameter (χ) which is the interaction between each block in the copolymer and the volume fraction of each block (f). For a diblock copolymer, the volume fraction is determined by Equation 1.4, where A and B are two different blocks.

Equation 1.4 Determination of volume fraction

$$f_A = \frac{V_A}{V_A + V_B}$$

Where V_A and V_B are volumes of blocks A and B.

Bates and coworkers¹³⁷ have published research on block copolymers in the solid state where the Flory-Huggins thermodynamic interaction parameter (χ_{AB}), the degree of polymerisation (N) and the size of each block ($f_A = N_A/N$) were studied.¹³⁸ This work outlined that for an ordered arrangement such as spheres, cylinders, gyroids or lamellae, a minimum value of $\chi_{AB}N < 10.5$ is needed and is displayed in Figure 41.¹³⁷

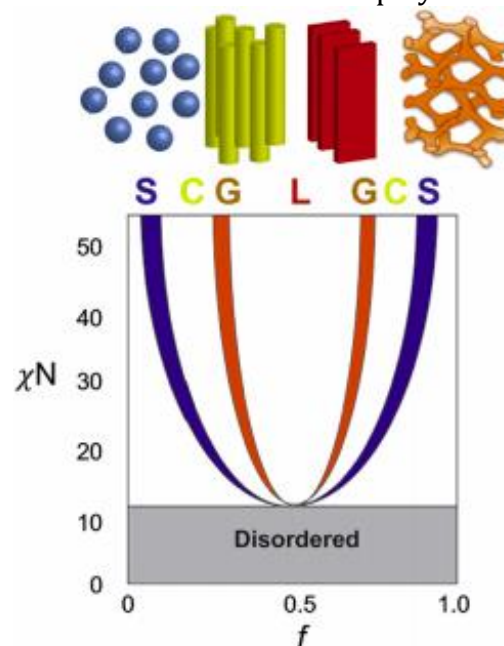


Figure 41. Block copolymer morphologies: spheres, cylinders, lamella and gyroids.

1.3 Polymer blends

Polymer blends have been studied since polymers were invented.¹⁵⁰ It can be challenging as most blends will not mix completely and will separate. Polymers that are blended can either be a mixture of homopolymers¹⁵¹ or copolymers.¹⁵² The advantage that blending two miscible polymers together would allow properties to be tuned and tailored as

desired. Such properties include strength, mechanical properties and stability to conditions such as temperature and solvent moisture.¹⁵⁰ The ability to manipulate polymers in this way has industrial uses. A few examples being in plastics,¹⁵⁰ resins,¹⁵³ automotive¹⁵⁴ and aircrafts.¹⁵⁵

In order for blends of polymers to be used for these applications, stable mixtures need to form. If two polymers are not compatible then a phase-separation will result causing properties not to be fine-tuned and two separate layers of each polymer. Generally, blends are affected by two criteria:

1. The degree of mixing of the components and the interactions that occur between these components.
2. The individual properties of each component.

Blends of polymers are classed as miscible if full blending is achieved, immiscible if blending is not achieved and partly miscible if some blending is achieved. It is rare for polymers that are blended to remain as a single miscible mixture and most will not due to the difference in properties of each polymer.¹⁵⁴ An example of polymers that are immiscible when blended is polyethylene & polypropylene and polymers that are miscible is poly(phenylene oxide) and polystyrene or polymethyl methacrylate and polystyrene.

Currently when models for polymer blending are studied, they look at random coil mixing. When this is studied the free energy of mixing is described.¹⁵⁶ For the mixing of rigid rods with random coils to be miscible, it is influenced mainly by the enthalpy part of the free energy. This means that phase separation can easily occur and therefore means that separation is largely based on entropic effects.

The second law of thermodynamics states that in all energy exchanges, if no energy enters or leaves the system, the potential energy of state will always be less than that of the initial state. This is referred to as entropy. In terms of entropy, it is very easy to move from an ordered system to a more disordered system, but it requires a lot more energy to move back the other way. An amorphous polymer has its chains tangled up randomly and chaotically. This example is best described as having high entropy due to the disorder. The reason for two polymer blends to mix completely, is down to that when blended together there is much more disorder which favours the second law of thermodynamics. Having said this, an amorphous polymer is already very disordered and so on mixing with another polymer, the system does not become any more disordered and will not gain much entropy. This means mixing is disfavoured.

The preparation of polymer blends can be made in two ways. The first way is best suited for a laboratory set up where the two polymers are dissolved in the same solvent and the solvent is allowed to evaporate off. What is left in the glass vial is a blend of those two polymers. This procedure works well in practice but when it comes to industry this would not work. Scaling this process up would mean evaporating off a large amount of solvent which is very expensive. There would be many environmental issues associated too. Releasing toxic solvents into the air would be very damaging to the environment. It is also costly in trying to recapture the solvent after evaporation to reuse for future blends. What

happens instead in industry is that both polymers are heated above the glass transition temperature and then mixed. At the point above the glass transition point, the polymers flow easily and are best described as 'gooey' which allows for easy blending. On cooling this leaves a blend of the two polymers.

1.3.1 Immiscible polymer blends

To encourage a blend of two polymers that are immiscible can be achieved by doing the following with copolymers. Polystyrene which is immiscible with most polymers can be blended when a copolymer of styrene and p-(hexafluoro2-hydroxyisopropyl)styrene is used.¹⁵⁷ The fluorine atom is very electronegative and will assert a large pulling power on nearby electrons. This means that the alcohol group becomes 'lacking' in electrons and leaves this group with a partial positive charge. This means that strong hydrogen bonds are now able to be formed upon blending. This copolymer of styrene and p-(hexafluoro2-hydroxyisopropyl)styrene is now able to form blends with polycarbonates and poly(methyl methacrylate). The mixing of two block copolymers have been studied before.¹⁵⁸ Here, polystyrene-*block*-polyethylene (PS-*b*-PE) was blended with PS-*b*-PE of varying molecular weights.

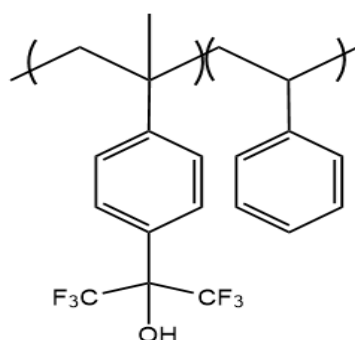


Figure 42. Chemical structure copolymer of styrene and p-(hexafluoro2-hydroxyisopropyl)styrene.

1.3.2 Thermodynamics of polymer mixing

When a blend of two polymers are miscible, the properties that blend has is somewhere between those of the two unblended polymers. If polymer 1 is blended with polymer 2, the overall T_g of the blend will depend on the ratio of polymer 1 to polymer 2. If the ratio of polymer 2 increases compared to polymer 1 then the T_g of the blend will increase. This relationship between the two polymers is generally linear. There are situations where the two polymers can bind more strongly than expected which causes the T_g to be higher than expected.

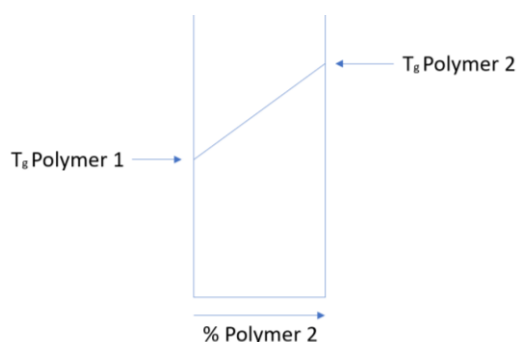


Figure 43. Schematic of a blend of two miscible polymers.¹⁵⁹

When two miscible polymers are blended together, this will form a single-phased material. There have been models that have tried to describe this relationship between the blend composition and glass transition temperature.¹⁶⁰ For two polymers to be completely miscible when blended is governed by Equation 1.5.

Equation 1.5 Thermodynamic equation for polymer blends.

$$\Delta G_{\text{mix}} = \Delta H_{\text{mix}} - T\Delta S_{\text{mix}}$$

Where ΔG_{mix} is the free energy of mixing, ΔH_{mix} is the enthalpy of mixing, T is the temperature and ΔS_{mix} is the entropy of mixing. For a miscible blend to be made then the ΔG_{mix} should be less than zero. The easiest way for the free energy of mixing to be less than zero is if the enthalpy of mixing is negative. For ΔH_{mix} to be negative is dependent on the dipole-dipole or hydrogen bonding present (intermolecular interactions).¹⁶¹ Having said this, by having a negative ΔH_{mix} does not ensure a miscible blend. When a blend X at a fixed temperature and pressure is also reliant on the second derivative of free energy ΔS_{mix} and this needs to be greater than zero.

Equation 1.6 Thermodynamic equation for a miscible polymer blend.

$$\frac{\partial^2 \Delta G_{\text{mix}}}{\partial x^2} > 0$$

Equation 1.6 must be satisfied otherwise the blend will be thermodynamically unstable and a phase separation will occur.

When two polymers that are blended are not miscible, a phase separation results.¹⁶² The entropy of mixing is always positive for polymer blends and this leads to a negative contribution for the mixing free energy.¹⁵⁴ This contribution is negligible for long chain polymers and for blends to be miscible relies on favourable enthalpic interactions.¹⁶³ Blending of two polymers allow enthalpic contributions to the mixing free energy which are positive and dominate the negative entropic contributions which means a phase separation results. It is no surprise that a phase separation occurs as properties of polymers are affected by non-covalent chemistry between the chains and polymer backbones differ from one polymer to another.¹⁶¹

1.4 Aims and objectives

Previous work has shown the thermo-responsive effect of PEO-*b*-PODMA, where pyrene was encapsulated within the centre of the bicontinuous polymer nanosphere (BPN).¹⁶⁴ The long alkyl side chains give the block copolymer a melting transition due to crystallisation of these side chains. It was recorded that the T_m of the ODMA block affected the rate of release of pyrene.¹⁶⁴ When the temperature was above the T_m of ODMA block (>21.5°C), the rate of pyrene being released increased significantly. The area of

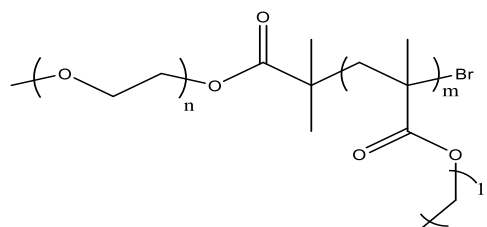


Figure 44. Structure of PEO-*b*-PODMA.

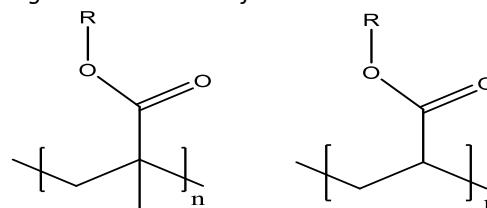


Figure 45. Structures of poly(*n*-alkyl acrylate) and poly(*n*-alkyl methacrylate).

poly(*n*-alkyl acrylate) and poly(*n*-alkyl methacrylate) side chains and the ability to crystallise has been studied before.¹⁶⁵ This work has showed that it was only the outer methylene units in the alky side chain that contributed to crystal lattice.¹⁶⁵ The methylene units closest to the polymer backbone do not contribute to side chain crystallinity. This means that the longer the side chain, the higher the T_m of the polymethacrylate is. It was shown that copolymerisation of two different methacrylate monomers allowed for manipulation of the T_m .¹⁶⁶ The melting transition temperature fell into a given range, which was between the T_m values of the two homopolymers. What this thesis will focus on is whether the same manipulation can be achieved using polymeric blends of ODMA & DSMA. Many methacrylate polymer blends have been studied before but what is novel about the approach taken in this thesis is that ODMA & DSMA are much longer than the current methacrylate monomers published in literature. The longest found was dodecyl methacrylate (DMA)²² which is 12 carbon atoms opposed to ODMA 18 and DSMA 22 carbon atoms.

Most research has focused on the hydrophilic part of block copolymers. What is less known is the hydrophobic part of block copolymers. The work outlined here will focus on polymers where the hydrophilic content is around 10-20%. This is because at this hydrophilic content bicontinuous nanospheres can form. This is a complex aggregate structure which is still new. The T_m and degree of crystallinity of the bulk block copolymers; PEO-*b*-PODMA, PEO-*b*-PDSMA & blends will be investigated by the use of DSC to demonstrate if there was any thermo-responsive effect of the alkyl side chains. If the blends form a phase separation, then alternative methods will be studied to try and encourage mixing and form thermodynamic stable aggregates. If a fully miscible sample is achieved, then this could lead to blending of thermo-responsive bicontinuous nanospheres which is a novel approach.

References

- 1 T. Smart, H. Lomas, M. Massignani, M. V. Flores-Merino, L. R. Perez and G. Battaglia, *Nano Today*, 2008, 3, 38–46.
- 2 A. Blanazs, S. P. Armes and A. J. Ryan, *Macromol. Rapid Commun.*, 2009, 30, 267–277.
- 3 S. J. Holder and N. A. J. M. Sommerdijk, *Polym. Chem.*, 2011, 2, 1018–1028.
- 4 E. V. Batrakova and A. V. Kabanov, *J. Control. Release*, 2008, 130, 98–106.
- 5 I. R. Schmolka, *J. Am. Oil Chem. Soc.*, 1977, 54, 110–116.
- 6 V. Wagner, A. Dullaart, A. K. Bock and A. Zweck, *Nat. Biotechnol.*, 2006, 24, 1211–1217.
- 7 W. A. Braunecker and K. Matyjaszewski, *Prog. Polym. Sci.*, 2007, 32, 93–146.
- 8 C. L. McCormick, S. E. Kirkland and A. W. York, *Polym. Rev.*, 2006, 46, 421–443.
- 9 M. Ouchi, T. Terashima and M. Sawamoto, *Chem. Rev.*, 2009, 109, 4963–5050.
- 10 M. Naseri-Nosar and Z. M. Ziora, *Carbohydr. Polym.*, 2018, 189, 379–398.
- 11 C. J. Buchko, L. C. Chen, Y. Shen and D. C. Martin, *Polymer (Guildf.)*, 1999, 40, 7397–7407.
- 12 F. Ide and A. Hasegawa, *J. Appl. Polym. Sci.*, 1974, 18, 963–974.
- 13 K. Endo, in *Progress in Polymer Science (Oxford)*, Pergamon, 2002, vol. 27, pp. 2021–2054.
- 14 C. D. Borman, A. T. Jackson, A. Bunn, A. L. Cutter and D. J. Irvine, *Polymer (Guildf.)*, 2000, 41, 6015–6020.
- 15 Y. Zhang, M. Cao, G. Han, T. Guo, T. Ying and W. Zhang, *Macromolecules*, 2018, 51, 5440–5449.
- 16 B. Zhao, M. A. C. Serrano, J. Gao, J. Zhuang, R. W. Vachet and S. Thayumanavan, *Polym. Chem.*, 2018, 9, 1066–1071.
- 17 W. Zhu, Z. Li, Y. Zhao and K. Zhang, *Macromol. Rapid Commun.*, 2015, 36, 1987–1993.
- 18 V. Abetz and P. F. W. Simon, *Adv. Polym. Sci.*, 2005, 189, 125–212.
- 19 Y. Deng, S. Zhang, G. Lu and X. Huang, *Polym. Chem.*, 2013, 4, 1289–1299.
- 20 K. Matyjaszewski, M. J. Ziegler, S. V. Arehart, D. Greszta and T. Pakula, *J. Phys. Org. Chem.*, 2000, 13, 775–786.
- 21 K. Letchford and H. Burt, *Eur. J. Pharm. Biopharm.*, 2007, 65, 259–269.
- 22 Y.-C. Tseng and S. B. Darling, *Polymers (Basel)*, 2010, 2, 470–489.
- 23 G. S. Kwon and K. Kataoka, *Adv. Drug Deliv. Rev.*, 1995, 16, 295–309.
- 24 C. Tsitsilianis, G. Gotzamanis and Z. Iatridi, in *European Polymer Journal*, Pergamon, 2011, vol. 47, pp. 497–510.
- 25 H. Maeda, J. Wu, T. Sawa, Y. Matsumura and K. Hori, *J. Control. Release*, 2000, 65, 271–284.
- 26 S. Croy and G. Kwon, *Curr. Pharm. Des.*, 2006, 12, 4669–4684.
- 27 N. P. Truong, J. F. Quinn, M. R. Whittaker and T. P. Davis, *Polym. Chem.*, 2016, 7, 4295–4312.
- 28 R. P. Brinkhuis, F. P. J. T. Rutjes and J. C. M. Van Hest, *Polym. Chem.*, 2011, 2, 1449–1462.
- 29 C. Gao and D. Yan, *Prog. Polym. Sci.*, 2004, 29, 183–275.
- 30 F. Aulenta, W. Hayes and S. Rannard, *Eur. Polym. J.*, 2003, 39, 1741–1771.
- 31 D. Braun, *Int. J. Polym. Sci.*, 2009, 2009.
- 32 M. K. Georges, R. P. N. Veregin, P. M. Kazmaier and G. K. Hamer, *Macromolecules*, 1993, 26, 2987–2988.

- 33 Principles of Polymer Chemistry - Paul J. Flory - Google Books, [https://books.google.co.uk/books?hl=en&lr=&id=CQ0EbEkT5R0C&oi=fnd&pg=PA3&dq=flory+principles+of+polymer+chemistry&ots=17sVdQCthw&sig=y11uE3IIqJEgRRH5izdKeBqIRmY&redir_esc=y#v=onepage&q=flory principles of polymer chemistry&f=false](https://books.google.co.uk/books?hl=en&lr=&id=CQ0EbEkT5R0C&oi=fnd&pg=PA3&dq=flory+principles+of+polymer+chemistry&ots=17sVdQCthw&sig=y11uE3IIqJEgRRH5izdKeBqIRmY&redir_esc=y#v=onepage&q=flory+principles+of+polymer+chemistry&f=false), (accessed 27 January 2021).
- 34 J. C. Patrick, *Rubber Chem. Technol.*, 1936, **9**, 373–382.
- 35 R. P. Quirk and B. Lee, *Polym. Int.*, 1992, **27**, 359–367.
- 36 R. K. O'Reilly, *Polym. Int.*, 2010, **59**, n/a-n/a.
- 37 P. Gurnani and S. Perrier, *Prog. Polym. Sci.*, 2020, **102**, 101209.
- 38 K. Matyjaszewski and J. Spanswick, *Mater. Today*, 2005, **8**, 26–33.
- 39 U. Mansfeld, C. Pietsch, R. Hoogenboom, C. R. Becer and U. S. Schubert, *Polym. Chem.*, 2010, **1**, 1560–1598.
- 40 J. Kreutzer and Y. Yagci, *Polymers (Basel)*, 2017, **10**, 35.
- 41 G. Moad and E. Rizzardo, in *RSC Polymer Chemistry Series*, Royal Society of Chemistry, 2016, vol. 2016-January, pp. 1–44.
- 42 Y. Zhu, I. Q. Li, B. A. Howell and D. B. Priddy, *ACS Symp. Ser.*, 1998, **685**, 214–224.
- 43 M. K. Georges, R. P. N. Veregin, P. M. Kazmaier, G. K. Hamer and M. Saban, *Macromolecules*, 1994, **27**, 7228–7229.
- 44 R. Jérôme, D. Mecerreyes, D. Tian, P. Dubois, C. J. Hawker, M. Trollsas and J. L. Hedrick, *Macromol. Symp.*, 1998, **132**, 385–403.
- 45 T. Fukuda, T. Terauchi, A. Goto, K. Ohno, Y. Tsujii, T. Miyamoto, S. Kobatake and B. Yamada, *Macromolecules*, 1996, **29**, 6393–6398.
- 46 R. P. N. Veregin, P. G. Odell, L. M. Michalak and M. K. Georges, *Macromolecules*, 1996, **29**, 3346–3352.
- 47 R. B. Grubbs, *Polym. Rev.*, 2011, **51**, 104–137.
- 48 D. Li and W. J. Brittain, *Macromolecules*, 1998, **31**, 3852–3855.
- 49 D. Greszta and K. Matyjaszewski, *RAPID COMMUNICATION TEMPO-Mediated Polymerization of Styrene: Rate Enhancement with Dicumyl Peroxide*, .
- 50 H. R. Lamontagne and B. H. Lessard, *ACS Appl. Polym. Mater.*, 2020.
- 51 G. J. M. Habraken, M. Peeters, P. D. Thornton, C. E. Koning and A. Heise, *Biomacromolecules*, 2011, **12**, 3761–3769.
- 52 J. S. Wang and K. Matyjaszewski, *J. Am. Chem. Soc.*, 1995, **117**, 5614–5615.
- 53 K. Matyjaszewski and J. Xia, *Chem. Rev.*, 2001, **101**, 2921–2990.
- 54 Y. Wang, Y. Zhang, B. Parker and K. Matyjaszewski, *Macromolecules*, 2011, **44**, 4022–4025.
- 55 L. Delaude, S. Delfosse, A. Richel, A. Demonceau and A. F. Noels, *Chem. Commun.*, 2003, **3**, 1526–1527.
- 56 X. Lou, M. S. Lewis, C. B. Gorman and L. He, *Anal. Chem.*, 2005, **77**, 4698–4705.
- 57 S. Kim and H. D. Sikes, *Polym. Chem*, 2020, **11**, 1424.
- 58 T. E. Patten and K. Matyjaszewski, *Adv. Mater.*, 1998, **10**, 901–915.
- 59 W. Tang and K. Matyjaszewski, *Macromolecules*, 2007, **40**, 1858–1863.
- 60 K. Matyjaszewski, A. K. Nanda and W. Tang, *Macromolecules*, 2005, **38**, 2015–2018.
- 61 W. A. Braunecker and K. Matyjaszewski, *J. Mol. Catal. A Chem.*, 2006, **254**, 155–164.
- 62 M. Arshadi, R. Yamdagni and P. Kebarle, *J. Phys. Chem.*, 1970, **74**, 1475–1482.
- 63 T. Pintauer and K. Matyjaszewski, in *Encyclopedia of Radicals in Chemistry, Biology and Materials*, John Wiley & Sons, Ltd, Chichester, UK, 2012.
- 64 SID.ir | RECENT ADVANCES IN SYNTHESIS OF NEW POLYMERS BY LIVING FREE RADICAL POLYMERIZATION, <https://www.sid.ir/en/Journal/ViewPaper.aspx?ID=48011>, (accessed 2 July

- 2020).
- 65 K. Matyjaszewski, D. A. Shipp, J. L. Wang, T. Grimaud and T. E. Patten, *Macromolecules*, 1998, **31**, 6836–6840.
 - 66 H. Uegaki, Y. Kotani, M. Kamigaito and M. Sawamoto, *Macromolecules*, 1997, **30**, 2249–2253.
 - 67 F. Simal, A. Demonceau and A. F. Noels, *Angew. Chemie Int. Ed.*, 1999, **38**, 538–540.
 - 68 T. Ando, M. Kamigaito and M. Sawamoto, *Macromolecules*, 1997, **30**, 4507–4510.
 - 69 D. M. Haddleton, C. B. Jasieczek, M. J. Hannon and A. J. Shooter, *Macromolecules*, 1997, **30**, 2190–2193.
 - 70 J. S. Wang and K. Matyjaszewski, *Macromolecules*, 1995, **28**, 7572–7573.
 - 71 Z. Xue, D. He and X. Xie, *Polym. Chem.*, 2015, **6**, 1660–1687.
 - 72 Y. Kwak, A. J. D. Magenau and K. Matyjaszewski, *Macromolecules*, 2011, **44**, 811–819.
 - 73 K. Matyjaszewski, D. Hongchen, W. Jakubowski, J. Pietrasik and A. Kusumo, *Langmuir*, 2007, **23**, 4528–4531.
 - 74 K. Min, H. Gao and K. Matyjaszewski, *Macromolecules*, 2007, **40**, 1789–1791.
 - 75 W. Jakubowski, K. Min and K. Matyjaszewski, *Macromolecules*, 2006, **39**, 39–45.
 - 76 N. Chan, M. F. Cunningham and R. A. Hutchinson, *Macromol. Chem. Phys.*, 2008, **209**, 1797–1805.
 - 77 H. Dong, W. Tang and K. Matyjaszewski, *Macromolecules*, 2007, **40**, 2974–2977.
 - 78 H. Dong and K. Matyjaszewski, *Macromolecules*, 2008, **41**, 6868–6870.
 - 79 P. R. Rodrigues and R. P. Vieira, *Eur. Polym. J.*, 2019, **115**, 45–58.
 - 80 V. Percec, T. Gulashvili, J. S. Ladislaw, A. Wistrand, A. Stjerndahl, M. J. Sienkowska, M. J. Monteiro and S. Sahoo, *J. Am. Chem. Soc.*, 2006, **128**, 14156–14165.
 - 81 B. Cao, Y. Zheng, T. Xi, C. Zhang, W. Song, K. Burugapalli, H. Yang and Y. Ma, *Biomed. Microdevices*, 2012, **14**, 709–720.
 - 82 A. Goto, K. Sato, Y. Tsujii, T. Fukuda, G. Moad, E. Rizzardo and S. H. Thang, *Macromolecules*, 2001, **34**, 402–408.
 - 83 M. Eberhardt and P. Théato, *Macromol. Rapid Commun.*, 2005, **26**, 1488–1493.
 - 84 S. Harriison, X. Liu, J.-N. Ollagnier, O. Coutelier, J.-D. Marty and M. Destarac, *Polymers (Basel)*, 2014, **6**, 1437–1488.
 - 85 Y. A. Vasilieva, C. W. Scales, D. B. Thomas, R. G. Ezell, A. B. Lowe, N. Ayres and C. L. McCormick, *J. Polym. Sci. Part A Polym. Chem.*, 2005, **43**, 3141–3152.
 - 86 N. Sanson and J. Rieger, *Polym. Chem.*, 2010, **1**, 965–977.
 - 87 G. Moad, *Polym. Chem.*, 2017, **8**, 177–219.
 - 88 E. F. Connor, I. Lees and D. Maclean, *J. Polym. Sci. Part A Polym. Chem.*, 2017, **55**, 3146–3157.
 - 89 E. A. Scott, N. B. Karabin and P. Augsornworawat, *Annu. Rev. Biomed. Eng.*, 2017, **19**, 57–84.
 - 90 A. Sangtani, O. K. Nag, L. D. Field, J. C. Breger and J. B. Delehanty, *Wiley Interdiscip. Rev. Nanomedicine Nanobiotechnology*, 2017, **9**, e1466.
 - 91 M. J. Sailor and J.-H. Park, *Adv. Mater.*, 2012, **24**, 3779–3802.
 - 92 S. J. Holder and N. A. J. M. Sommerdijk, DOI:10.1039/c0py00379d.
 - 93 S. D. Steichen, M. Caldorera-Moore and N. A. Peppas, *Eur. J. Pharm. Sci.*, 2013, **48**, 416–427.
 - 94 D. Sutton, N. Nasongkla, E. Blanco and J. Gao, *Pharm. Res.*, 2007, **24**, 1029–1046.
 - 95 A. Lavasanifar, J. Samuel and G. S. Kwon, *Adv. Drug Deliv. Rev.*, 2002, **54**, 169–190.
 - 96 P. Alexandridis, V. Athanassiou and T. A. Hatton, *Langmuir*, 1995, **11**, 2442–2450.
 - 97 R. Tanbour, A. M. Martins, W. G. Pitt and G. A. Hussein, *Curr. Pharm. Des.*, 2016, **22**,

- 2796–2807.
- 98 S. D. Allen, S. Bobbala, N. B. Karabin and E. A. Scott, *Nanoscale Horizons*, 2019, 4, 321–338.
- 99 R. H. Müller, K. Mäder and S. Gohla, *Eur. J. Pharm. Biopharm.*, 2000, 50, 161–177.
- 100 T. Lian and R. J. Y. Ho, *J. Pharm. Sci.*, 2001, 90, 667–680.
- 101 S. Bobbala, B. Gibson, A. B. Gamble, A. McDowell and S. Hook, *Immunol. Cell Biol.*, 2018, **96**, 656–665.
- 102 T. Date, V. Nimbalkar, J. Kamat, A. Mittal, R. I. Mahato and D. Chitkara, *J. Control. Release*, 2018, 271, 60–73.
- 103 J. Shi, Z. Xiao, A. R. Votruba, C. Vilos and O. C. Farokhzad, *Angew. Chemie Int. Ed.*, 2011, **50**, 7027–7031.
- 104 T. C. Majdanski, D. Pretzel, J. A. Czaplewska, J. Vitz, P. Sungur, S. Höppener, S. Schubert, F. H. Schacher, U. S. Schubert and M. Gottschaldt, *Macromol. Biosci.*, 2018, **18**, 1700396.
- 105 and A. Z. * B. S. P. M. C. B. G. I. M. T. Antônio T. A. Gomes, *Int J Biomed Imaging*, 2011, **2011**, 621905.
- 106 E. Rideau, R. Dimova, P. Schwille, F. R. Wurm and K. Landfester, *Chem. Soc. Rev.*, 2018, **47**, 8572–8610.
- 107 D. D. Lasic, *Trends Biotechnol.*, 1998, 16, 307–321.
- 108 B. Haley and E. Frenkel, *Urol. Oncol. Semin. Orig. Investig.*, 2008, 26, 57–64.
- 109 J. Ramos, A. Imaz, J. Callejas-Fernández, L. Barbosa-Barros, J. Estelrich, M. Quesada-Pérez and J. Forcada, *Soft Matter*, 2011, 7, 5067–5082.
- 110 G. Zhao, S. Chandrudu, M. Skwarczynski and I. Toth, *Eur. Polym. J.*, 2017, 93, 670–681.
- 111 P. Parhi, C. Mohanty and S. K. Sahoo, *Drug Discov. Today*, 2012, 17, 1044–1052.
- 112 N. T. K. Thanh and L. A. W. Green, *Nano Today*, 2010, 5, 213–230.
- 113 A. Blanz, S. P. Armes and A. J. Ryan, *Macromol. Rapid Commun.*, 2009, **30**, 267–277.
- 114 K. Yu and A. Eisenberg, *Macromolecules*, 1998, **31**, 3509–3518.
- 115 L. Zhang, K. Yu and A. Eisenberg, *Science (80-.)*, 1996, **272**, 1777–1779.
- 116 Y. Yu, L. Zhang and A. Eisenberg, *Macromolecules*, 1998, **31**, 1144–1154.
- 117 Y. Mai and A. Eisenberg, *Chem. Soc. Rev.*, 2012, **41**, 5969–5985.
- 118 L. Zhang, C. Bartels, Y. Yu, H. Shen and A. Eisenberg, *Phys. Rev. Lett.*, 1997, **79**, 5034–5037.
- 119 K. YU, C. BARTELS and A. EISENBERG, *Macromolecules*.
- 120 S. Kubowicz, J.-F. Baussard, J.-F. Lutz, A. F. Thünemann, H. von Berlepsch and A. Laschewsky, *Angew. Chemie Int. Ed.*, 2005, **44**, 5262–5265.
- 121 J. J. L. M. Cornelissen, M. Fischer, N. A. J. M. Sommerdijk and R. J. M. Nolte, *Science (80-.)*, 1998, **280**, 1427–1430.
- 122 W. F. Edmonds, Z. Li, M. A. Hillmyer and T. P. Lodge, *Macromolecules*, 2006, **39**, 4526–4530.
- 123 H. Cui, Z. Chen, K. L. Wooley and D. J. Pochan, *Macromolecules*, 2006, **39**, 6599–6607.
- 124 S. J. Holder and N. A. J. M. Sommerdijk, *Polym. Chem.*, 2011, 2, 1018–1028.
- 125 K. Yu, L. Zhang and A. Eisenberg, *Langmuir*, 1996, **12**, 5980–5984.
- 126 K. Hales, Z. Clen, K. L. Wooley and D. J. Pochan, *Nano Lett.*, 2008, **8**, 2023–2026.
- 127 A. L. Parry, P. H. H. Bomans, S. J. Holder, N. A. J. M. Sommerdijk and S. C. G. Biagini, *Angew. Chemie*, 2008, **120**, 8991–8994.
- 128 S. J. Holder, G. Woodward, B. McKenzie and N. A. J. M. Sommerdijk, *RSC Adv.*, 2014,

- 4, 26354–26358.
- 129 J. Du and S. P. Armes, *Soft Matter*, 2010, **6**, 4851–4857.
- 130 N. J. Warren and S. P. Armes, *J. Am. Chem. Soc.*, 2014, **136**, 10174–10185.
- 131 H. Shen and A. Eisenberg, *J. Phys. Chem. B*, 1999, **103**, 9473–9487.
- 132 B. E. McKenzie, J. F. De Visser, H. Friedrich, M. J. M. Wirix, P. H. H. Bomans, G. De With, S. J. Holder and N. A. J. M. Sommerdijk, *Macromolecules*, 2013, **46**, 9845–9848.
- 133 Z. Gao, S. K. Varshney, S. Wong and A. Eisenberg, *Macromolecules*, 1994, **27**, 7923–7927.
- 134 J. Fu, D. H. Kim and W. Knoll, *ChemPhysChem*, 2009, **10**, 1190–1194.
- 135 T. Higuchi, M. Shimomura and H. Yabu, *Macromolecules*, 2013, **46**, 4064–4068.
- 136 F. S. BATES, *Science (80-.)*, 1991, **251**, 898–905.
- 137 S. P. Nunes, in *Sustainable Nanoscale Engineering: From Materials Design to Chemical Processing*, Elsevier, 2019, pp. 297–316.
- 138 C. M. Bates and F. S. Bates, *Macromolecules*, 2017, **50**, 3–22.
- 139 Y. Mai and A. Eisenberg, *Chem. Soc. Rev.*, 2012, **41**, 5969–5985.
- 140 S. P. Nunes, *Macromolecules*, 2016, **49**, 2905–2916.
- 141 S. J. Holder and N. A. J. M. Sommerdijk, *Polym. Chem.*, 2011, **2**, 1018–1028.
- 142 J. N. Israelachvili, D. J. Mitchell and B. W. Ninham, *J. Chem. Soc. Faraday Trans. 2 Mol. Chem. Phys.*, 1976, **72**, 1525–1568.
- 143 Progress in controlled/living polymerization in aqueous media. Part I. Principles and methods, <https://www.infona.pl/resource/bwmeta1.element.baztech-article-BPL7-0004-0052>, (accessed 6 February 2021).
- 144 J. Du and R. K. O'Reilly, *Soft Matter*, 2009, **5**, 3544–3561.
- 145 D. E. Discher and A. Eisenberg, *Science (80-.)*, 2002, **297**, 967–973.
- 146 P. Lim Soo and A. Eisenberg, *J. Polym. Sci. Part B Polym. Phys.*, 2004, **42**, 923–938.
- 147 L. Zhang and A. Eisenberg, *Macromolecules*, 1999, **32**, 2239–2249.
- 148 C. Feng, G. Lu, Y. Li and X. Huang, *Langmuir*, 2013, **29**, 10922–10931.
- 149 J. H. Jordan and B. C. Gibb, *Chem. Soc. Rev.*, 2015, **44**, 547–585.
- 150 D. R. Paul and J. W. Barlow, *J. Macromol. Sci. Part C*, 1980, **18**, 109–168.
- 151 K. R. Shull and K. I. Winey, *Macromolecules*, 1992, **25**, 2637–2644.
- 152 M. W. Matsen, *Macromolecules*, 1995, **28**, 5765–5773.
- 153 D. J. Hourston and J. M. Lane, *The toughening of epoxy resins with thermoplastics: 1. Trifunctional epoxy resin-polyetherimide blends*, 1992.
- 154 H. M. Coubrough, M. Reynolds, J. A. Goodchild, S. D. A. Connell, J. Mattsson and A. J. Wilson, *Polym. Chem.*, DOI:10.1039/C9PY01913H.
- 155 L. A. Goettler and J. J. Scobbo, in *Polymer Blends Handbook*, Springer Netherlands, 2014, pp. 1433–1458.
- 156 Principles of Polymer Chemistry - Paul J. Flory - Google Books.
- 157 S. Chen, L. Tan, F. Qiu, X. Jiang, M. Wang and H. Zhang, *Polymer (Guildf.)*, 2004, **45**, 3045–3053.
- 158 J. A. Galloway, H. K. Jeon, J. R. Bell and C. W. MacOsco, *Polymer (Guildf.)*, 2005, **46**, 183–191.
- 159 X. Lu and R. A. Weiss, *Relationship between the Glass Transition Temperature and the Interaction Parameter of Miscible Binary Polymer Blends*, 1992, vol. 25.
- 160 L. A. Wood, *J. Polym. Sci.*, 1958, **28**, 319–330.
- 161 M. T. Demeuse, in *High Temperature Polymer Blends*, Elsevier Inc., 2014, pp. 1–13.
- 162 K. Dalnoki-Veress, J. A. Forrest and J. R. Dutcher, *Phys. Rev. E - Stat. Physics, Plasmas, Fluids, Relat. Interdiscip. Top.*, 1998, **57**, 5811–5817.
- 163 S. W. Kuo, *J. Polym. Res.*, 2008, **15**, 459–486.

- 164 S. J. Holder, G. Woodward, B. M. Ab and N. A. J. M. Sommerdijk, 2014, **4**, 29.
- 165 C. E. Rehberg and C. H. Fisher, *Ind. Eng. Chem.*, 2005, **40**, 1429–1433.
- 166 O. R. Monaghan, P. H. H. Bomans, N. A. J. M. Sommerdijk and S. J. Holder, *Polym. Chem.*, 2017, **8**, 5303–5316.

Chapter 2. Synthesis and Self-assemble of Poly(ethylene oxide)-*block*-Poly(octadecyl methacrylate) and Poly(ethylene oxide)-*block*-Poly(docosyl methacrylate) and the mixing of polymer blends

Contents

2.1 Introduction	55
2.2 Experimental	58
2.2.1 Materials.....	58
2.2.2 Apparatus.....	58
Self-assembly procedures.....	58
Dynamic light Scattering (DLS).....	58
Differential scanning calorimetry (DSC).....	59
Transmission electron microscopy (TEM).....	59
Self-assembly equipment.....	59
2.2.3 Syntheses.....	59
Synthesis of poly(ethylene oxide) macroinitiator.....	59
Synthesis of PEO- <i>b</i> -PODMA via ATRP.....	60
Synthesis of PEO- <i>b</i> -PDSMA via ATRP.....	60
Synthesis of PODMA via ATRP.....	61
Synthesis of PDSMA via ATRP.....	61
2.2.4 Self-assembly of PEO- <i>b</i> -PODMA & PEO- <i>b</i> -PDSMA.....	62
2.3 Results and discussion	62
2.3.1 Characterisation of PEO macroinitiator.....	63
2.3.2 Characterisation of block copolymers; PEO- <i>b</i> -PODMA and PEO- <i>b</i> -PDSMA & homopolymers; PODMA and PDSMA.....	65
2.3.3 Self-Assembly of PEO- <i>b</i> -PODMA & PEO- <i>b</i> -PDSMA and blends.....	70
2.3.4 Thermal analysis of bulk block copolymers and polymer blends.....	80
2.3.5 Thermal analysis of bulk block copolymers blends & copolymerisation species.....	85
2.3.6 Thermal analysis of bulk homopolymers and polymer blends.....	87
2.3.7 Thermal analysis of block copolymers aggregate solutions and polymer blends.....	89
Conclusion	93
References	94

2.1 Introduction

The self-assembly of block copolymer into polymeric aggregates which could be used as nanocarriers for controlled drug delivery has been extensively studied.¹⁻² This has led to the studying of thermo-responsive aggregates,³⁻⁴ aggregates that release or accelerate the rate of release of encapsulated compounds due to changes in temperature. The polymers used in such aggregates are classed as 'thermo-responsive' and have application of delivering drugs which appeal to the pharmaceutical industry.⁵

Research has mainly concentrated on the thermo-responsive hydrophilic component of a block copolymer. Examples of thermo-responsive hydrophilic polymers include poly(N-isopropylacrylamide) (PNIPAM)⁵⁻⁶, poly[oligo(ethyleneglycol) methacrylate]⁷ (POEGMA) and poly(N-dimethylacrylamide)⁷ (PDMAAm). Chung⁵ and co self-assembled a block copolymer of poly(N-isopropylacrylamide)-*block*-polybutyl methacrylate (PNIPAM-*b*-PBMA) to form thermo-responsive micelles. This is not the only example of using PNIPAM for drug delivery and there are many publications^{8,9} on this polymer. Another example was using methoxy poly(ethylene oxide)-*b*-poly(caprolactone)-*b*-poly(N-isopropylacrylamide).¹⁰

The key aspect that all publications have in common is that the approach of releasing drugs using a PNIPAM block copolymer is the same. The PNIPAM block has a lower critical solution temperature (LCST ~ 31 °C)¹⁰ and when below this temperature, the copolymer forms stable micelles with the drug encapsulated within the centre. Above the LCST, the release of the drug was accelerated when the micelles were exposed to a change in temperature and is shown in Figure 45.

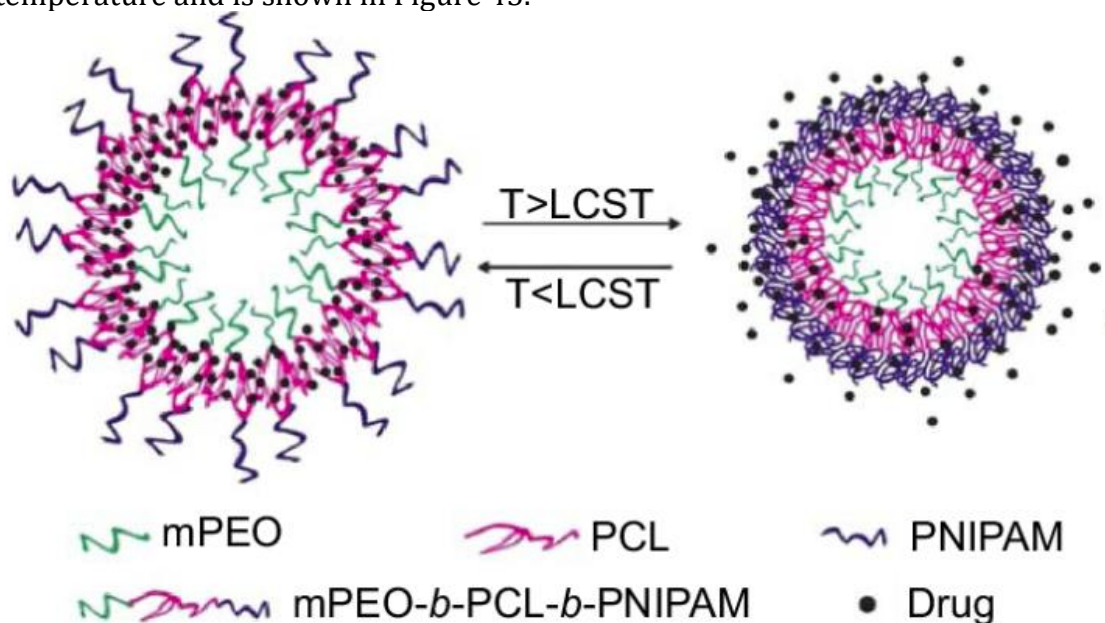


Figure 45. Block copolymer micelles of mPEO-*b*-PCL-*b*-PNIPAM when exposed to changes in temperature above and below the LCST.¹⁰

In fact, what happens to the PNIPAM block is that it undergoes a transition from hydrophilic to a hydrophobic state over a lower critical solution temperature. This contributes to a change in the size and structure of the aggregate. The examples provided involve the thermo-responsive hydrophilic component of the polymer. The research

described in this chapter aims to concentrate on the thermo-responsive hydrophobic component of the block copolymer as this is the area less understood.

One area which has started to attract interest, are bicontinuous polymer nanospheres (BPNs) which is a complex aggregate formed when block copolymer self-assembles.¹¹ The reason for the interest in BPNs is the potential advantage that comes with them unlike other aggregates. Bicontinuous polymer nanospheres are generally found to be in the size range of 100-500 nm in diameter, which makes them much larger than block copolymer micelles, which are found in the size range of 2-10 nm. They also tend to have a high hydrophobic polymer content. The size of BPNs can be controlled which make them of interest to therapies that rely upon the enhanced permeability and retention effect (EPR) in tumour treatment.¹² EPR is a phenomenon that occurs where macromolecules such as polymers and proteins showed selective accumulation in tumor cells. It was found that using nanoparticles, that tumor cells contained 10-50 times more of these polymeric molecules than normal tissues.¹³ The biggest factor that determines what can be used in EPR is particle size. This should be between 100-200 nm otherwise there is risk of the liver removing the nanocarrier as it would be too large to do the desired function. This chapter aims to make thermo-responsive nanospheres and as there is control on particle, this would make them ideal for roles involving EPR.

Controlled radical polymerisation has seen many developments over the years, which allows for the synthesis of amphiphilic block copolymers whose composition and molecular weights can be accurately targeted. These block copolymers form very stable aggregates and complex morphologies such as bicontinuous nanospheres can be made. The self-assembly of bicontinuous nanospheres has been studied before by Holder *et al.*¹¹ It was discovered that there are two important components that led to the formation of bicontinuous nanospheres, which were the weight fraction of the hydrophilic block and the molecular weight.

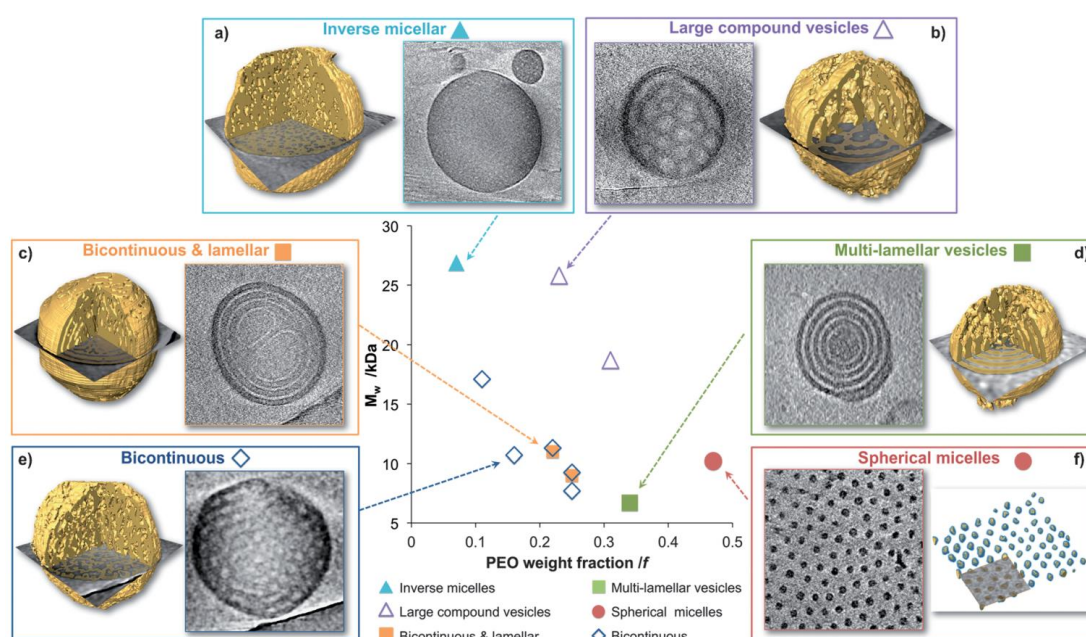


Figure 46. Phase diagram of the self-assembly of PEO-*b*-PODMA block copolymers with corresponding slices through 3D reconstructions.¹¹

The results of this work was used to construct a phase diagram (Figure 46) for the block copolymer PEO-*b*-PODMA which shows the range in which bicontinuous nanospheres form.¹⁴ Figure 46 shows that bicontinuous nanospheres are present when the hydrophilic weight fraction is <0.3 and the molecular weight is <17 kDa.¹⁵ Previously bicontinuous nanospheres of PEO-*b*-PODMA, PEO-*b*-PDSMA & PEO-*b*-P(ODMA-*co*-DMSA) have only been observed up to 5 wt % in solution.

Aims

Previous work has shown the thermo-responsive effect of PEO-*b*-PODMA, where pyrene was encapsulated within the centre of the BPN.¹⁶ The long alkyl side chains give the block copolymer a melting transition due to crystallisation of these side chains. It was recorded that the T_m of the ODMA block affected the rate of release of pyrene.¹⁶ When the temperature was above the T_m of ODMA block (>21.5°C), the rate of pyrene being released increased significantly. The area of poly(*n*-alkyl acrylate) and poly(*n*-alkyl methacrylate) side chains and the ability to crystallise has been studied before.^{17,18,19} This work has showed that it was only the outer methylene units in the alky side chain that contributed to crystal lattice.²⁰⁻²¹ The methylene units closest to the polymer backbone do not contribute to side chain crystallinity. This means that the longer the side chain, the higher the T_m of the poly(alkyl methacrylate) is. It was shown that copolymerisation of two different methacrylate monomers octadecyl methacrylate ($T_m = 21.5^\circ\text{C}$) and docosyl methacrylate ($T_m = 41.1^\circ\text{C}$) allowed for manipulation of the T_m .²² The melting transition temperature fell into a given range, which was between the T_m values of the two block copolymers.

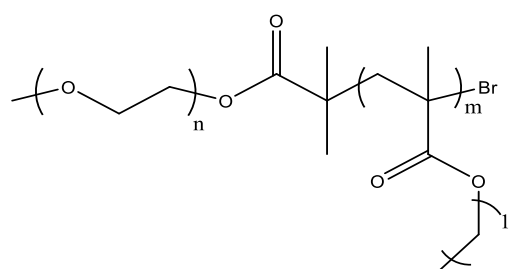


Figure 47. Structure of PEO-*b*-PODMA.

The main aims of this chapter are to repeat the previous work and add more data points to the phase diagram (Figure 46) assessing where BPNs form, fine tune the melting temperature of block copolymer nanospheres, control the temperature of two different polymer blends by mixing and assess whether polymers can be blended in these spheres. When copolymerised block copolymers are made, a series of polymers are needed to be made. With blends of block copolymers, only two polymers need to be made and are then taken and blended accordingly. This is also a straightforward approach and if blends allow for thermo-responsive aggregates to be blended, it would offer an advantage on their copolymerised counterparts. The T_m and degree of crystallinity of the bulk homopolymers PODMA, PDSMA & blends as well as block copolymers PEO-*b*-PODMA, PEO-*b*-PDSMA & blends were investigated in this chapter by the use of differential scanning calorimetry (DSC). This allowed determination of whether the copolymer blends allowed bicontinuous nanospheres to be made with thermo-responsive properties.

2.2 Experimental

2.2.1 Materials

2-bromoisobutryl bromide (BIBB) (98%), 4-dimethylamino pyridine (DMAP) (99%), copper(I) bromide (98%), N,N,N',N'-pentamethyldiethylenetriamine (PMDETA) (99%), octadecyl methacrylate (ODMA) docosyl methacrylate (DSMA), Poly(ethylene glycol)methyl ether (M_n 2000 g/mol) (PEGME) and Triethylamine (TEA) (99%) were all purchased from Sigma-Aldrich and used as received. A later sample of docosyl methacrylate (DSMA) was purchased from BASF and used as received. Aluminium oxide for column chromatography and sodium bicarbonate was purchased from Acros Organics. A saturated sample of sodium bicarbonate was used for testing. Ethanol (EtOH), isopropyl alcohol (IPA), tetrahydrofuran (THF), dichloromethane (DCM) & acetonitrile (analytical reagent grade) and hydrochloric acid (HCl)(36%) were purchased from Fisher Scientific and used as received apart from the hydrochloric acid, which was turned into a 2M solution. The deuterated chloroform ($CDCl_3$) used in 1H -NMR and ^{13}C -NMR was purchased from Cambridge Isotope Laboratories. Xylene was purchased from BDH Lab Supplies.

2.2.2 Apparatus

All reactions were performed under inert atmosphere (nitrogen) using Schlenk techniques.

Self-assembly procedures

A typical procedure used block copolymer (10 mg) or block copolymer blend (10 mg, varied weight ratios 25:75, 50:50 & 75:25) was dissolved in THF (6 mL) and stirred in an oil bath at 45°C. Deionised water (4mL) was added dropwise (at 5.15 mL h⁻¹) using a syringe pump. After addition of water, the solution was transferred to the dialysis cassette. This was sealed with dialysis membrane (12-14.0 kDa) and dialysis was carried out in 4 L of deionised water at 45°C for 24 hours. In this time the water was changed twice. The aggregates formed were analysed using dynamic light scattering (DLS) and transmission electron microscopy (TEM) to calculate the size and shape of the aggregates.

Dynamic Light Scattering (DLS)

All dynamic light scattering measurements were performed on a Malvern High Performance Particle Sizer (Nano Zetasizer HPPS HPP5001). This instrument contains a laser with a wavelength of 633 nm. The measurements were carried out using a clean quartz cuvette, which holds 1 mL of sample. Samples was first filtered using a 1.2 μ m filter and then measurements were carried out at a temperature of 25°C for the BCP aggregates. 11 measurements were recorded with the first measurement being discarded and an average then taken of the remaining 10. The size averages recorded from DLS are calculated from the hydrodynamic diameter (D_H). This is an estimate of a diameter of a hard sphere which would scatter light to the same degree as the measured particle.²³ CONTIN analysis will be carried out on bimodal distributions. This allows two particle populations to be taken separately.

Differential scanning calorimetry (DSC)

Differential scanning calorimetry was carried out on bulk samples using a Netzsch DSC 200 Phox. This instrument has a heating range of -150 - 600°C. Thermal analyses were conducted on a range of -20 to 70°C. Each sample was heated at a rate of 10°C min⁻¹. Each sample was heated and cooled twice with the transition values being taken from the second run. Each sample was measured against an empty aluminium pan as a reference.

DSC was also performed on the aqueous self-assembled samples which were tested on the Netzsch DSC 200 Phox. Thermal analysis was conducted on a range of -20 to 70°C. Each sample was heated at a rate of 10°C min⁻¹. Each sample was heated and cooled twice with the transition values being taken from the second run. Each sample (20mg) was measured against an aluminium pan containing distilled water (20 mg) as a reference.

Transmission Electron Microscopy (TEM)

The self-assembled block copolymer aggregates had transmission electron microscopy carried out on them using a JEOL JEM (200-FX) TEM instrument (120 kV). Samples of 5µl were pipetted onto a carbon coated copper grid (200 mesh) and allowed to evaporate off for 10 minutes. Any excess sample was removed using suction. 5 µl of uranyl acetate (5%) was put onto the grid to stain the sample and any excess was removed by suction.

Self-Assembly Equipment

The following equipment was used for the self-assembly of the polymers used in this thesis. A syringe pump (220 Voltz, 0.1 Amps, 50 Hz) brought from Semat Technical Limited at 0.075 mL per minute, a 10 mL dialysis cassette and dialysis membrane (MW 12-14 kDa) brought from MEDICELL international Ltd. Distilled water was used as obtained.

2.2.3 Syntheses

Synthesis of poly(ethylene oxide) macroinitiator.

A literature method¹¹ was followed for the synthesis of the PEO macroinitiator. 2-bromoisobutryl bromide (11.50 g, 50 mmol), triethylamine (5.06 g, 50 mmol) and 4-dimethylamino pyridine (6.11 g, 50 mmol) was dissolved in anhydrous dichloromethane and added to a round bottom flask. PEGME (m_n 2000) (50 g, 25mmol) was dissolved in 100 mL of anhydrous dichloromethane and added dropwise to the reaction mixture at 0°C for 1 hour.¹¹ The reaction mixture was then left stirring for 18 hours at room temperature. The mixture was then filtered and half the solvent was evaporated off. Using a separating funnel, the mixture was washed twice with saturated sodium bicarbonate solution and then twice with hydrochloric acid (10%, 2M). The organic layer was collected and dried with anhydrous magnesium sulphate for 1 hour. The solution was filtered and solvent evaporated off. Product dried in vacuum oven overnight. The compound was characterised using ¹H-NMR, ¹³C-NMR and SEC. The product was collected as a yellow solid. Percentage Yield 57%

¹H-NMR (400 Hz, CDCl₃, ppm)δ: 1.93 (Singlet, 6H, (CH₃)₂C-), 3.38 (Singlet, 3H -OCH₃), 3.64 (Broad peak, 4H, -OCH₂CH₂), 3.73 (triplet, 2H,(-OCH₂CH₂), 4.32(triplet, 2H ,(-OCH₂CH₂). **¹³C-NMR (CDCl₃, ppm)δ:** 31.0 (Br-C(CH₃)₂-), 55.7 (Br-C-), 59.2 (CH₃-O-), 65.1 (-COO-CH₂-CH₂), 70.8 (-COO-CH₂-CH₂), 171.6 (Br-C(CH₃)₂-COO). **SEC** M_w 3200, M_n 3100, Đ 1.04 **FTIR** (cm⁻¹) 2882 C-Hs, 1734 C=O stretch, 1465 C-H bend, 1098 C-O stretch, 530 C-Br stretch.

Synthesis of PEO-*b*-PODMA via ATRP

A literature method was followed for the synthesis of PEO-*b*-PODMA block copolymers.¹¹ The synthesis was carried out for PEO₄₄-*b*-PODMA₂₆. Cu(I)Br (34.4 mg, 0.24 mmol) was put into a Schlenk tube with a magnetic stirrer. The PEO macroinitiator (1.00 g, 0.48 mmol) was dissolved in xylene:IPA mixture (9:1) (4 mL) and added to a Schlenk tube. PMDETA (83 mg, 0.48 mmol) and ODMA (2.78 g, 8.2 mmol) was added to Schlenk tube which was then sealed and degassed (N₂) for 1 hour. The mixture was then stirred at 95°C for 24 hours under nitrogen. After 24 hours, the reaction was run through alumina column to remove the catalyst and ligand, then half of solvent was evaporated off. The polymer was precipitated out into acetonitrile dropwise at 0°C. The block copolymer was characterised by ¹HNMR, ¹³CNMR & SEC. The product (PEO₄₄-*b*-PODMA₂₆) was collected as a white solid; Percentage Yield 62%. The synthesis of PEO₄₄-*b*-PODMA₅₀ used (8.13g, 0.024 mol) of ODMA monomer. The product (PEO₄₄-*b*-PODMA₅₀) was collected as a white solid; Percentage Yield 61%.

¹H-NMR (400 Hz, CDCl₃, ppm)δ: 0.88 (triplet, 3H, -(CH₂)₁₇-CH₃), 1.00 (broad peak, 3H, -CH₂-C-CH₃), 1.29 (broad peak, 30H, -(CH₂)₁₄-), 1.60 (broad peak, CH₂(CH₂)₁₄-), 3.38 (Singlet, 3H, CH₃O-), 3.65 (triplet, 4H, -O-CH₂CH₂-O), 3.91(broad peak, 2H, -COO-CH₂-). **¹³C-NMR (CDCl₃, ppm)δ:** 14.22 (-CH₂CH₂CH₃), 22.77 (-CH₂CH₂CH₃), 29.38 (-CH₂(CH₂)₁₆CH₂), 29.80 (-CH₂(CH₂)₁₆CH₂), 31.92 (-CH₂CH₂CH₃), 70.59 (-OCH₂CH₂O-). **SEC** M_w 15000, M_n 12000, Đ 1.26 **FTIR** (cm⁻¹) 2917 C-H stretch, 2850 C-H stretch, 1730 stretch, 1465 C-H stretch, 1241 C-C stretch, 1145 C-O stretch.

Synthesis of PEO-*b*-PDSMA via ATRP

The synthesis of PEO₄₄-*b*-PDSMA₂₄ was as follows. Cu(I)Br (34.4 mg, 0.24 mmol) was put into a Schlenk tube with a magnetic stirrer. The PEO macroinitiator (1.00 g, 0.48 mmol) was dissolved in xylene:IPA mixture (9:1) (4 mL) and added to Schlenk tube. PMDETA (83 mg, 0.42 mmol) and DSMA (4.55 g, 12.0 mmol) was added to Schlenk tube which was then sealed and degassed (N₂) for 1 hour. The mixture was then stirred at 95°C for 24 hours under nitrogen. After 24 hours, the reaction was run through alumina column to remove the catalyst and ligand, then half of solvent was evaporated off. The polymer was precipitated out into acetonitrile dropwise at 0°C. The block copolymer was characterised by ¹HNMR, ¹³CNMR & SEC. The product (PEO₄₄-*b*-PDSMA₂₄) was collected as a white solid; Percentage Yield 28%. The synthesis of PEO₄₄-*b*-PDSMA₅₄ used (9.47g, 0.024 mol) of DSMA monomer. The product (PEO₄₄-*b*-PDSMA₅₄) was collected as a white solid; Percentage Yield 34%.

¹H-NMR (400 Hz, CDCl₃, ppm)δ: 0.89 (triplet, 3H, -(CH₂)₁₇-CH₃), 1.01 (broad peak, 3H, -CH₂-C-CH₃), 1.26 (broad peak, 30H, -(CH₂)₁₄-), 1.61 (broad peak, CH₂(CH₂)₁₄-), 3.38 (Singlet, 3H, CH₃O-), 3.65 (triplet, 4H, -O-CH₂CH₂-O), 3.91 (broad peak, 2H, -COO-CH₂-). **¹³C-NMR (CDCl₃, ppm)δ:** 14.24 (-CH₂CH₂CH₃), 22.77 (-CH₂CH₂CH₃), 29.48 (-CH₂(CH₂)₁₆CH₂), 29.81 (-CH₂(CH₂)₁₆CH₂), 32.02 (-CH₂CH₂CH₃), 70.70 (-OCH₂CH₂O-). **SEC** M_w 14500, M_n 12100, Đ 1.20 **FTIR** (cm⁻¹) 2918 C-H stretch, 2850 C-H stretch, 1730 stretch, 1464 C-H stretch, 1241 C-C stretch, 1145 C-O stretch.

Synthesis of PODMA via ATRP

A literature method was followed for the synthesis of PODMA₈₀ homopolymer. Cu(I)Br (0.017 g, 0.12 mmol) was put into a Schlenk tube with a magnetic stirrer. Ethyl α-bromoisobutyrate (0.023 g, 0.12 mmol) was dissolved in xylene:IPA mixture (9:1) (4 mL) and added to Schlenk tube. PMDETA (0.02 g, 0.12 mmol) and ODMA (2.0 g, 0.006 mol) was added to Schlenk tube which was then sealed and degassed (N₂) for 1 hour. The mixture was then stirred at 95°C for 24 hours under nitrogen. After 24 hours, the reaction was run through alumina column to remove the catalyst and ligand, then half of solvent was evaporated off. The polymer was precipitated out into acetonitrile dropwise at 0°C. The polymer was characterised by ¹HNMR, ¹³CNMR & SEC. The product (PODMA₈₀) was collected as a white solid; Percentage Yield 57%.

¹H-NMR (400 Hz, CDCl₃, ppm)δ: 0.80 (triplet, 3H, -(CH₂)₁₇-CH₃), 0.95 (broad peak, 3H, -CH₂-C-CH₃), 1.23 (broad peak, 30H, -(CH₂)₁₄-), 1.72 (broad peak, CH₂(CH₂)₁₄-), 3.85 (broad peak, 2H, -COO-CH₂-). **¹³C NMR (CDCl₃, ppm) δ:** 14.05 (-CH₂CH₂CH₃), 22.80 (-CH₂CH₂CH₃), 26.08 (-COO-CH₂CH₂CH₂-), 28.09 (Br-C(CH₃)-), 28.23 (-COOCH₂CH₂CH₂-), 29.44 (-CH₂(CH₂)₁₅CH₂-), 29.86 (-CH₂(CH₂)₁₅CH₂-), 31.96 (-CH₂CH₂CH₃), 44.7 (Br-C-), 65.0 (Br-C(CH₃)-CH₂-), 168.73 (-COOCH₂CH₂CH₂-), 176.2 (-COO-(CH₂)₁₇CH₃).

Synthesis of PDSMA via ATRP

A literature method was followed for the synthesis of PDSMA₈₃ homopolymer. Cu(I)Br (0.014 g, 0.10 mmol) was put into a Schlenk tube with a magnetic stirrer. Ethyl α-bromoisobutyrate (0.020 g, 0.10 mmol) was dissolved in xylene:IPA mixture (9:1) (4 mL) and added to Schlenk tube. PMDETA (0.017 g, 0.10 mmol) and DSMA (2.0 g, 0.005 mol) was added to Schlenk tube which was then sealed and degassed (N₂) for 1 hour. The mixture was then stirred at 95°C for 24 hours under nitrogen. After 24 hours, the reaction was run through alumina column to remove the catalyst and ligand, then half of solvent was evaporated off. The polymer was precipitated out into acetonitrile dropwise at 0°C. The polymer was characterised by ¹HNMR, ¹³CNMR & SEC. The product (PDSMA₈₃) was collected as a white solid; Percentage Yield 59%.

¹H-NMR (400 Hz, CDCl₃, ppm)δ: 0.88 (triplet, 3H, -(CH₂)₁₇-CH₃), 1.01 (broad peak, 3H, -CH₂-C-CH₃), 1.28 (broad peak, 30H, -(CH₂)₁₄-), 1.61 (broad peak, CH₂(CH₂)₁₄-), 3.92 (broad peak, 2H, -COO-CH₂-). **¹³C NMR (CDCl₃, ppm) δ:** 14.05 (-CH₂CH₂CH₃), 22.80 (-CH₂CH₂CH₃), 26.08 (-COO-CH₂CH₂CH₂-), 28.09 (Br-C(CH₃)-), 28.23 (-COOCH₂CH₂CH₂-), 29.44 (-CH₂(CH₂)₁₅CH₂-), 29.86 (-CH₂(CH₂)₁₅CH₂-), 31.96 (-CH₂CH₂CH₃), 44.7 (Br-C-), 65.0 (Br-C(CH₃)-CH₂-), 168.73 (-COOCH₂CH₂CH₂-), 176.2 (-COO-(CH₂)₁₇CH₃).

2.2.4 Self-assembly of poly(ethylene oxide)-*block*-poly(octadecyl methacrylate) and poly(ethylene oxide)-*block*-poly(docosyl methacrylate)

Self-Assembly of PEO-*b*-PODMA & PEO-*b*-PDSMA

A previously published procedure for the self-assembly of block copolymers was followed.¹⁴ Table 1 shows the quantity of THF and distilled water used for the self-assembly of each block copolymer.

Table 1. The volume of THF and water used in the dialysis of each block copolymer at self-assembled solutions of 0.1 & 1.0 wt%. PEO wt% is defined as the total hydrophilic quantity present in each block copolymer.

Structure	PEO wt %	THF Volume (mL)	Water Volume (mL)	Total Volume (mL)
PEO ₄₄ - <i>b</i> -PODMA ₂₆	18	4	6	10
PEO ₄₄ - <i>b</i> -PODMA ₅₀	10	6	4	10
PEO ₄₄ - <i>b</i> -PDSMA ₂₄	18	4	6	10
PEO ₄₄ - <i>b</i> -PDSMA ₅₄	10	6	4	10

All block copolymer blends (PEO₄₄-*b*-PODMA₂₆ with PEO₄₄-*b*-PDSMA₂₄) & (PEO₄₄-*b*-PODMA₅₀ with PEO₄₄-*b*-PDSMA₅₄) used 6 mL THF with 4 mL distilled water.

2.3 Results and Discussion

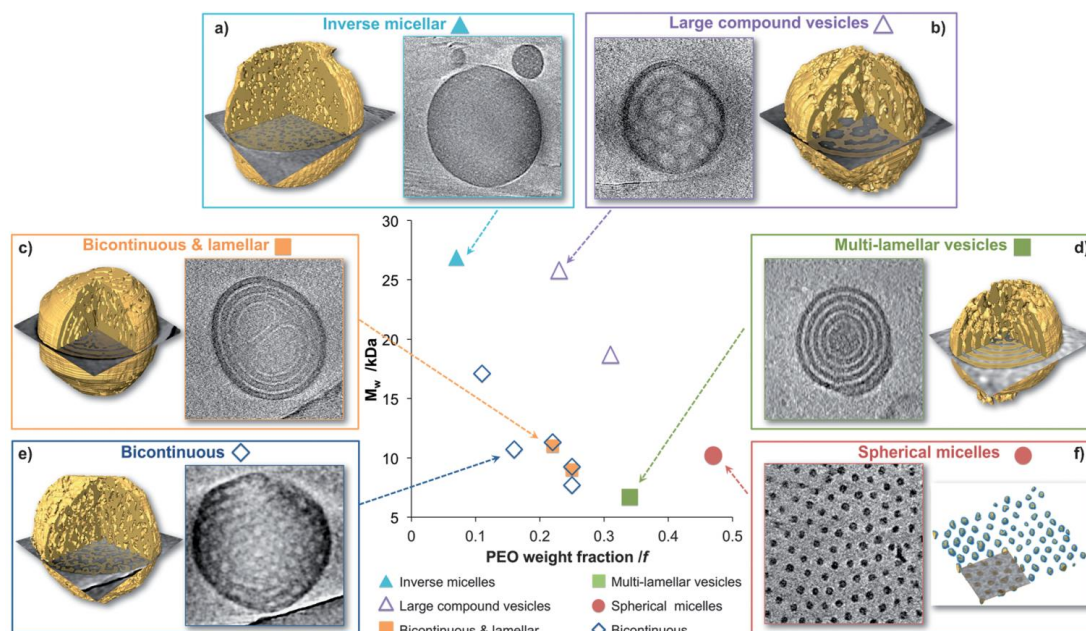


Figure 46. Phase diagram of the self-assembly behaviour of block copolymers with corresponding 3D reconstructions.²⁴

The work outlined in this chapter builds upon the earlier work involving PEO-*b*-PODMA where the phase diagram in Figure 46 was constructed.²⁴ When block copolymers are self-assembled in aqueous solution, a range of different aggregates can form. Previous work on PEO-*b*-PODMA shows that the weight fraction of the hydrophilic block and the chain length of the polymer are important when wanting bicontinuous nanospheres to

form.²⁴ For the block copolymers synthesised in this chapter, the PEO weight fractions selected were 0.18 and 0.10. This was with the intention of to produce bicontinuous nanospheres in aqueous solutions in line with what had been published previously.

2.3.1 Characterisation of PEO macroinitiator

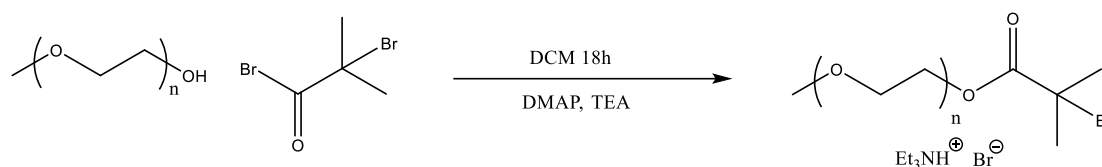


Figure 48. Reaction scheme for the synthesis of PEO macroinitiator.

Poly(ethylene glycol) methyl ether (PEGME) was reacted with 2-bromoisobutryl bromide under standard esterification procedures to give the PEO macroinitiator as shown in Figure 48. The product was washed twice with saturated bicarbonate solution (5mL) and hydrochloric acid (2M) (10mL) to remove any impurities. The PEO macroinitiator was characterised using ^1H NMR, ^{13}C NMR, SEC & FTIR.

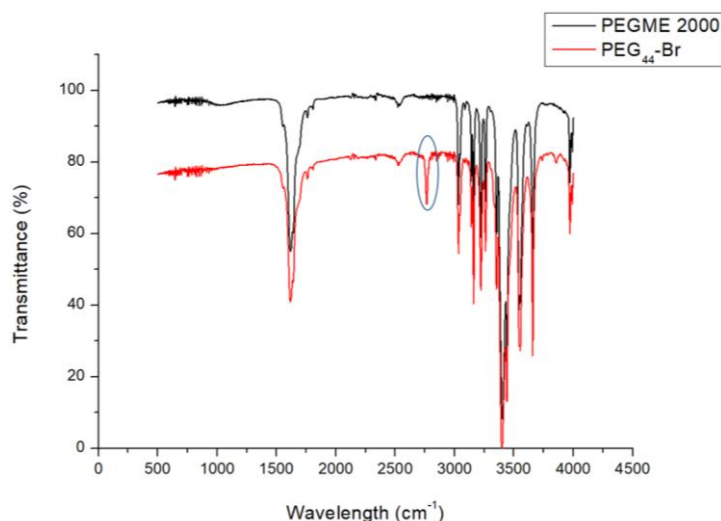


Figure 49. FTIR spectra of PEGME 2000 overlaid with macroinitiator (PEO-Br). (The absorption due to the carbonyl of the ester group is circled)

The FTIR spectrum (Figure 49) confirmed the presence of a $\text{C}=\text{O}$ stretch at 1735 cm^{-1} due to the presence of an ester group. This is the key difference between the PEGME 2000 and the macroinitiator made from the reaction.

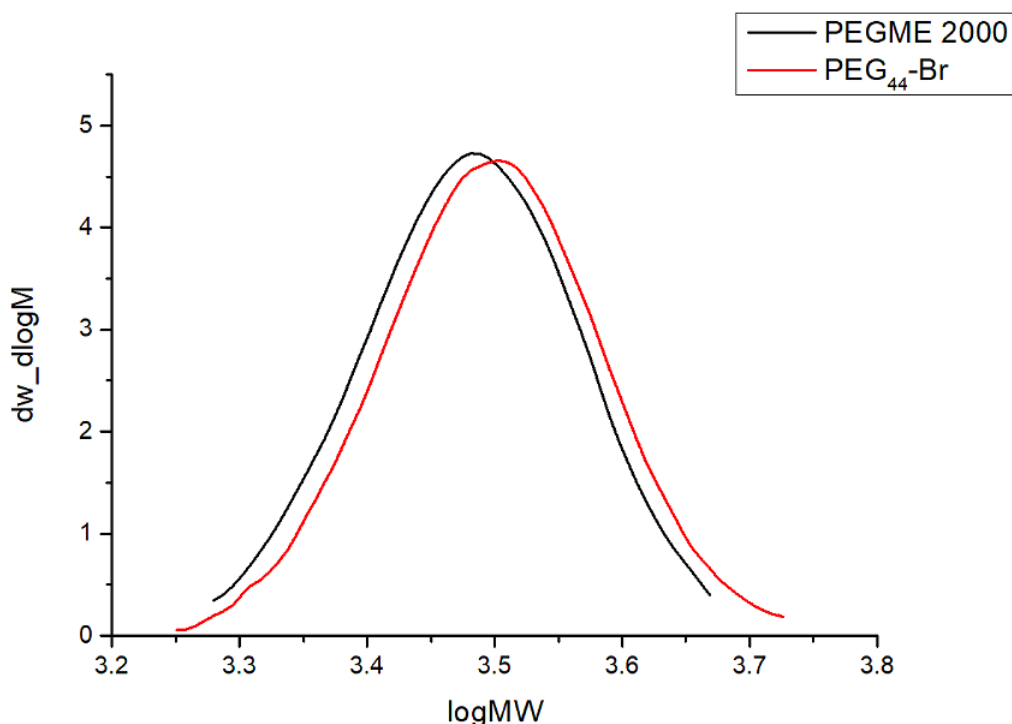


Figure 50. SEC trace of PEGME 2000 overlaid with PEG₄₄-Br.

The molecular weight of these samples was measured by SEC and these were then compared to the M_n values calculated from the $^1\text{H-NMR}$ (integration of the CH_3 end group versus integration of CH_2). On synthesis of the macroinitiator, the molecular weight increased and the SEC results support this by showing a slight increase in the average molecular weight M_n as shown in Figure 50. Even though an increase of 100 is not that significant, it does support what is expected to be seen which is a small increase in molecular weight as the macroinitiator is made. SEC also revealed that both samples had a dispersity index of 1.04 indicating a narrow molecular weight distribution. As only one trace was observed in SEC, this suggested that any unreacted starting material had been successfully removed from the purification step.

Table 2. Molecular weight parameters of macroinitiator and PEGME determined by $^1\text{H-NMR}$ and SEC.

Structure	DP _{PEO}	M_n NMR	M_n SEC	M_w SEC	\mathcal{D}
PEGME	44	2100	3000	3100	1.04
PEO ₄₄	44	2200	3100	3200	1.04

The $^1\text{H-NMR}$ spectra of the PEO macroinitiator and PEGME can be seen overlaid in Figure 51. The $^1\text{H-NMR}$ of PEGME shows a singlet at 2.19 ppm (Peak 3) which confirms the presence of the $-\text{OH}$. This peak is missing from the PEO macroinitiator $^1\text{H-NMR}$ spectrum as the OH is replaced by the ester group. The peak at 4.31 ppm (Peak D) is due to the CH_2 adjacent to the ester bond. The new singlet peak (Peak E) at 1.89 ppm can be seen as the two methyl groups are now next to an electron withdrawing bromine atom. The degree of polymerisation (DP) of the ethylene oxide repeating units was calculated from $^1\text{H-NMR}$ by comparing the methyl integral (CH_3) 3.38 ppm (Peak A) with the ($\text{CH}_2\text{CH}_2\text{O}$) integral (Peak B). The degree of polymerisation of the PEO block for all macroinitiators used in this chapter was found to be 44.

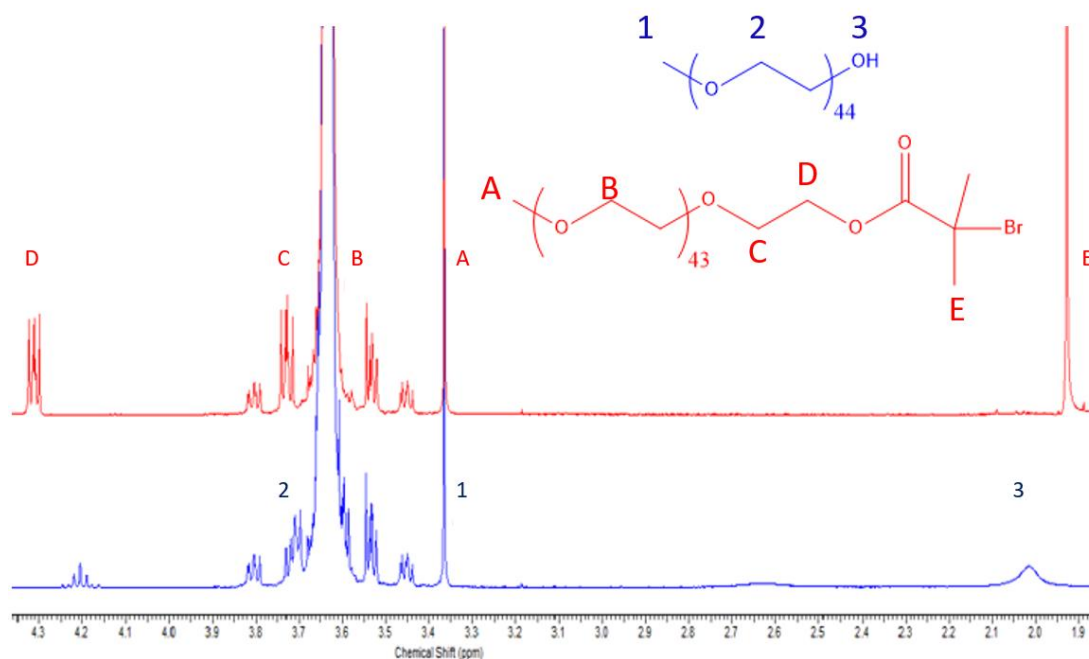


Figure 51. $^1\text{H-NMR}$ spectra overlay of PEGME (Top) and PEO macroinitiator $\text{PEO}_{44}\text{-Br}$ (Bottom). Spectra obtained in CDCl_3

2.3.2 Characterisation of Block copolymers; $\text{PEO-}b\text{-PODMA}$ and $\text{PEO-}b\text{-PDSMA}$ & Homopolymers; PODMA and PDSMA

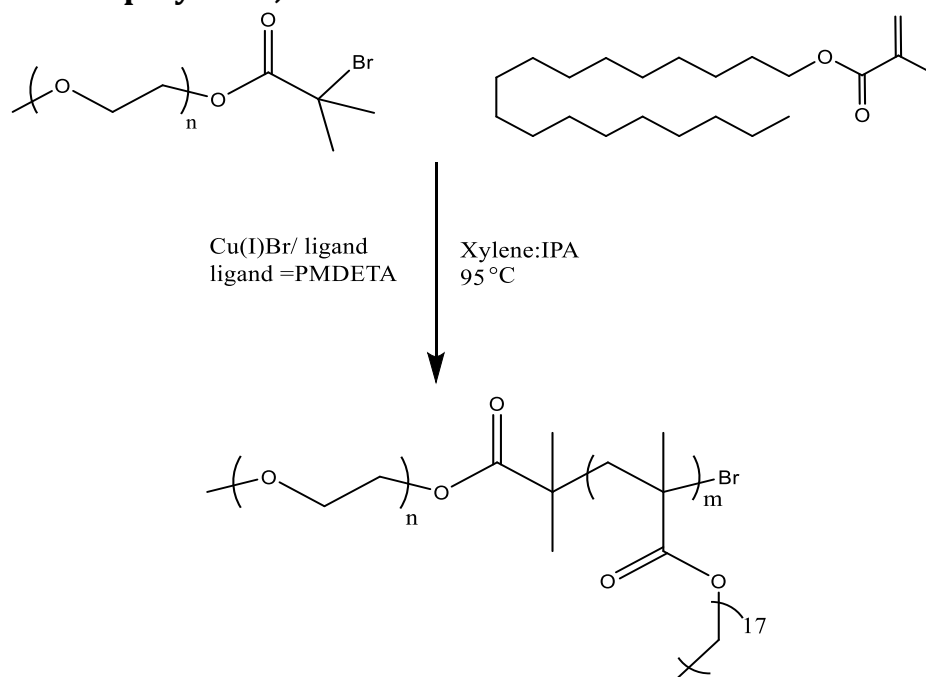


Figure 52. Reaction schemes for the synthesis of $\text{PEO-}b\text{-PODMA}$.

Both block copolymers $\text{PEO-}b\text{-PODMA}$ & $\text{PEO-}b\text{-PDSMA}$ were synthesised by atom transfer radical polymerisation (ATRP) using the PEG_{44}Br macroinitiator as shown in Figure 52. Prior to precipitation, monomer conversion was determined from an NMR analysis of the reaction mixture (Figure 53) by comparing the integral of the polymer peak (Peak F) with the two monomer peaks (Peaks E & D) on the block copolymer NMR spectrum.

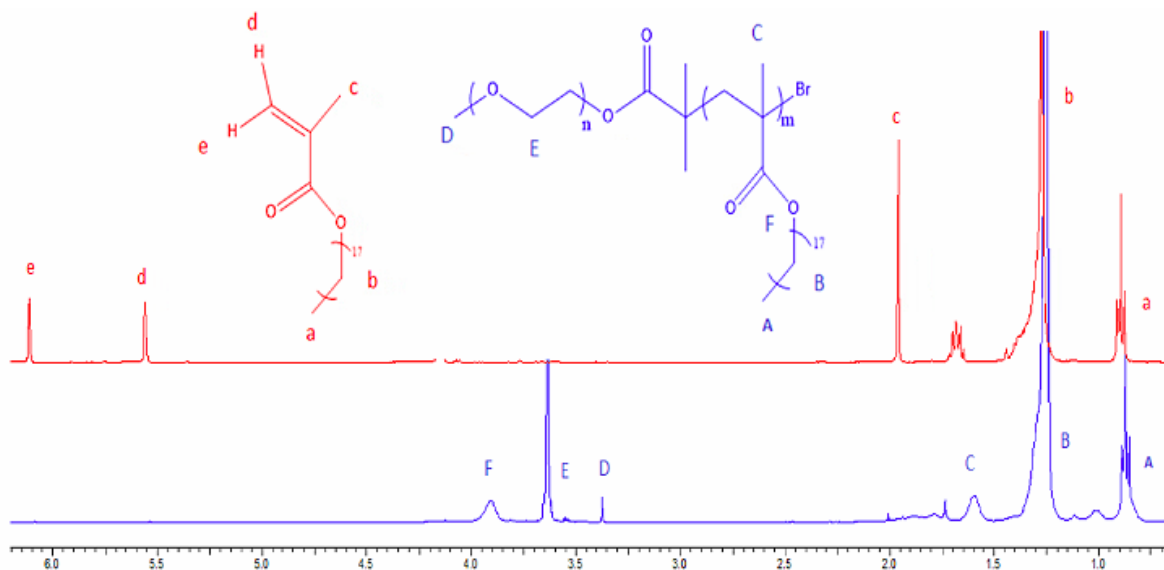


Figure 53. $^1\text{H-NMR}$ spectra overlay of octadecyl methacrylate monomer ODMA (Top) and block copolymer $\text{PEO}_{44}\text{-}b\text{-PODMA}_{26}$ (Bottom) overlaid. Spectra obtained in CDCl_3 .

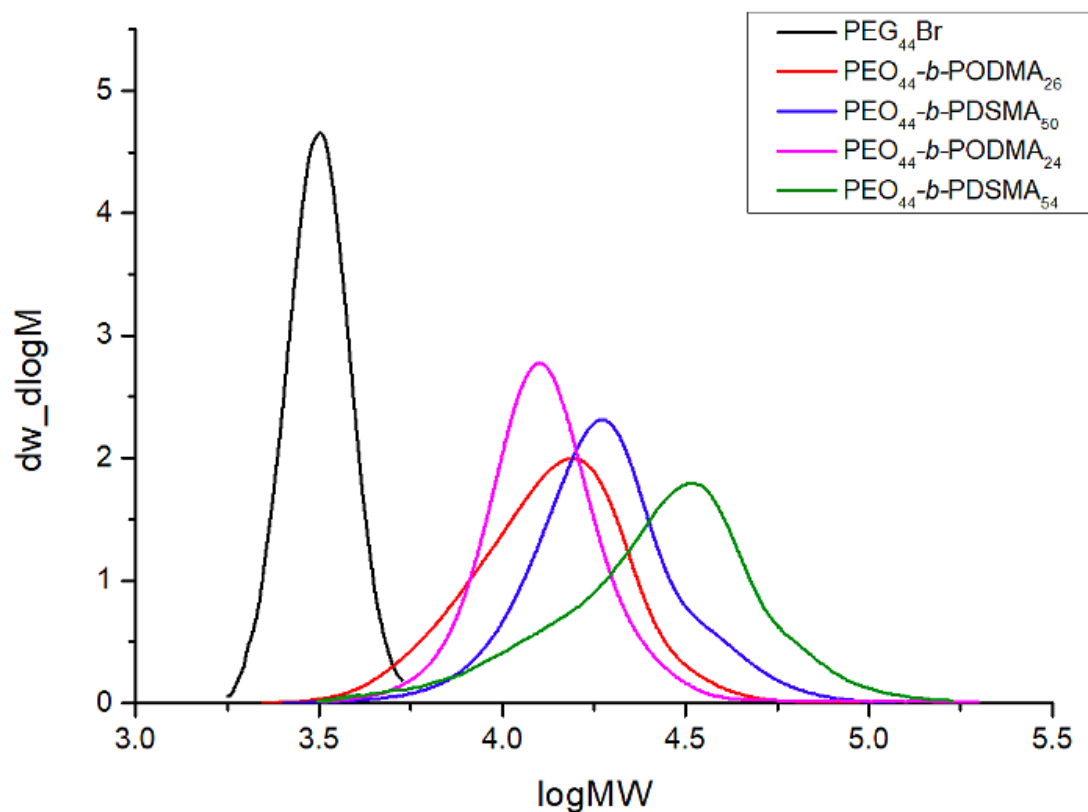


Figure 54. SEC traces of macroinitiator and block copolymers overlaid.

Table 3. Molecular weight parameters of block copolymers determined by $^1\text{H-NMR}$ and SEC.

Structure	PEO (wt %)	M_n NMR	NMR	M_n SEC	M_w SEC	\bar{D}
			Conversion %			
$\text{PEO}_{44}\text{-}b\text{-PODMA}_{26}$	18	10900	99.1	12000	15000	1.26
$\text{PEO}_{44}\text{-}b\text{-PODMA}_{50}$	10	19000	98.6	16900	21300	1.26
$\text{PEO}_{44}\text{-}b\text{-PDSMA}_{24}$	18	11600	98.1	12100	14500	1.20
$\text{PEO}_{44}\text{-}b\text{-PDSMA}_{54}$	10	23400	99.1	2140	31900	1.40

The molecular weight distribution of the PEO macroinitiator overlaid with block copolymer traces clearly shows that there has been a significant increase in molecular weight (Figure 54). This is a strong indication that the ATRP reaction has gone to completion and the block copolymer has been made. The SEC trace shows the block copolymers with PEO weight fraction of 0.18 & 0.10. The reason for PEO₄₄-*b*-PDSMA₅₄ to have a slightly higher polydispersity than the other block copolymers is most likely due to failure to remove all starting material from the purification step. This SEC trace shows a shoulder where something of lower molecular weight has come off second. As the desired block copolymer will be high molecular weight this will come off first and SEC supports this for PEO₄₄-*b*-PDSMA₅₄. This means that the lower molecular weight will be unreacted PEG₄₄-Br.

The molecular weight parameters for all block copolymer synthesised is displayed in Table 3. The molecular weight obtained for all 4 block copolymers is consistent with the phase diagram (Figure 46) and when these block copolymers are self-assembled, bicontinuous nanospheres should be seen under TEM.

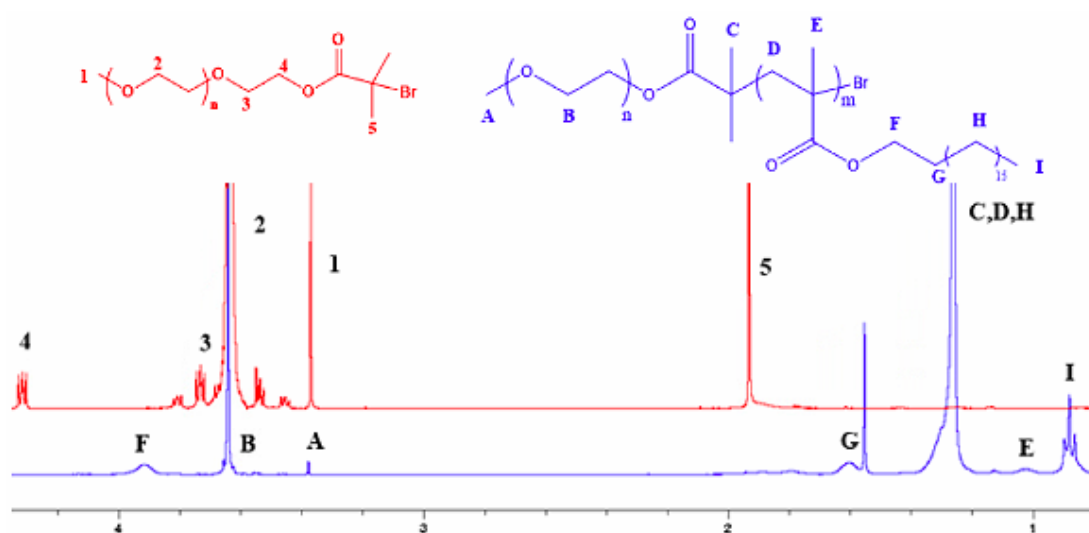


Figure 55. ¹H-NMR overlay of macroinitiator (Top) and block copolymer PEO₄₄-*b*-PODMA₂₆ (Bottom) overlaid. Spectra obtained in CDCl₃

The ¹HNMR spectrum of the macroinitiator was compared to the PEO₄₄-*b*-PODMA₂₆ NMR spectra (Figure 55) to further determine that the polymerisation had gone to completion. All other block copolymers made in this chapter gave similar ¹HNMR with differences just seen with the DP of each BCPs. This matched with literature²⁵ assignments, which further proved that the correct block copolymers were synthesised. The degree of polymerisation for the macroinitiator was calculated by comparing peak 2 to peak 1, which was the known methyl group. The block copolymer DP was calculated by using the same methyl group integral (Peak A) and this was compared to Peak F at 4.3 ppm due to the CH₂ adjacent to the ester group.

Synthesis of homopolymers

The ¹HNMR spectra of the ethyl α-bromoisobutyrate and PODMA can be seen overlaid in Figure 56. The ¹HNMR of ethyl α-bromoisobutyrate gives three signals. The triplet at 1.28 ppm (Peak A) confirms CH₂ group next to the ester, the signal at 4.16 ppm is the CH₃ (Peak B) and the singlet at 2.02 ppm are the two methyl groups (Peak C). There are more peaks

seen with the ^1H NMR of PODMA, the main one being at 3.80 ppm which is the CH_2 next to the oxygen atom (Peak F). To calculate the degree of polymerisation (DP) for the homopolymer from ^1H NMR, Peaks B and F would normally be used. The DP could not be worked out from H-NMR due to signals merging and overlapping with each other. Molecular weight parameters from the SEC measurements were used instead.

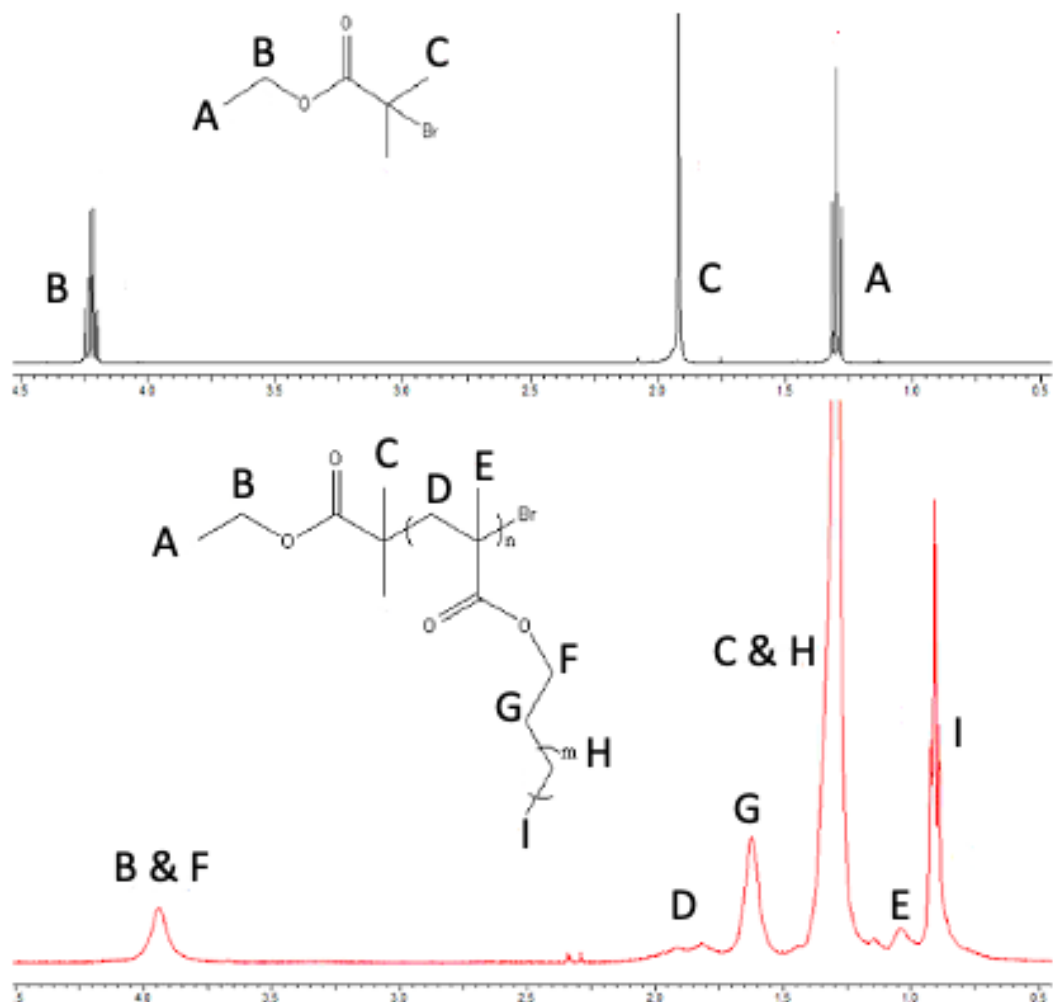


Figure 56. ^1H NMR overlay of ethyl α -bromoisobutyrate (Top) and homopolymer PODMA₈₀ (Bottom) overlaid. Spectra obtained in CDCl_3 .

The two homopolymers displayed similar molecular weights but both had relatively large dispersity indices ($\mathcal{D} > 1.5$).

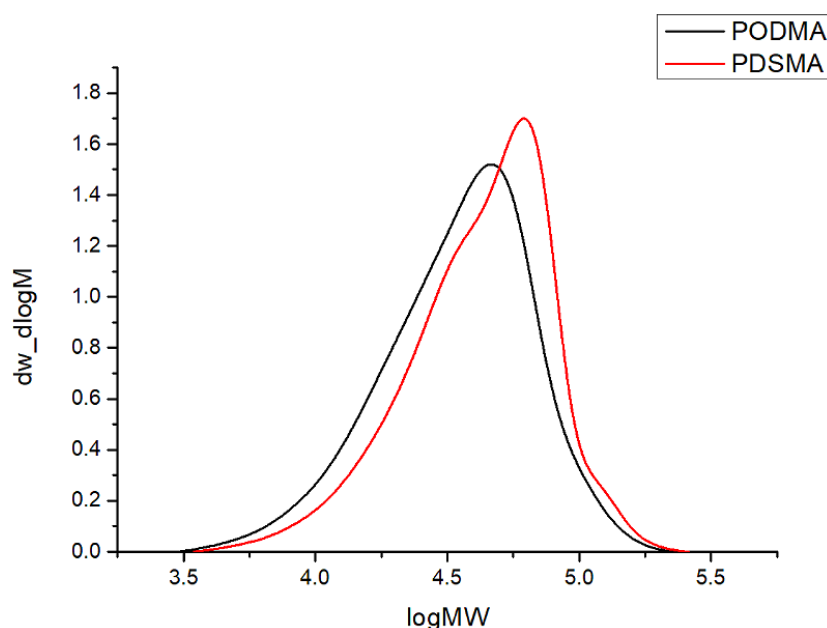


Figure 57. SEC traces of the two homopolymers made by ATRP.

Table 4. Molecular weight parameters of homo polymers determined by SEC.

Structure	DP Targeted	DP Achieved	$M_{n\text{ SEC}}$	$M_{w\text{ SEC}}$	\bar{D}
PODMA	50	80	27200	42000	1.54
PDSMA	50	83	32700	49800	1.52

A degree of polymerisation of 50 was targeted for the homopolymers but molecular weight parameters from SEC suggested the degree of polymerisation was closer to 80. A potentially reason for this is that less ethyl α -bromoisobutyrate initiated at the start of the ATRP reaction. Another possible reason is that there is a higher degree of error associated with the SEC. The calibration samples used to calibrate the SEC instrument rely on a linear relationship of polystyrene standards. Polystyrene is another polymer but is very different to PODMA and PDSMA. This means that the results recorded from SEC are relative rather than absolute which could explain differences seen in molecular weights. As the main objective is to get the homopolymers to mix completely, if the degree of polymerisation is similar the two homopolymers will still be able to be used.

Percentage Yield

A literature method²⁵ was followed for the synthesis of block copolymers where ethanol was used to precipitate the product after the reaction mixture was passed through an alumina column.¹¹ However, percentage yields using ethanol as the non-solvent were found to be very low despite the high monomer conversions observed by ¹HNMR (Table 5). This led to the literature method being adapted and acetonitrile was used as the non-solvent in the precipitation instead. An increase in yield was observed.

Table 5. Percentage yields obtained for block copolymers.

Structure	PEO (wt %)	NMR Conversion %	Ethanol Percentage Yield%	Acetonitrile Percentage Yield%
PEO ₄₄ - <i>b</i> -PODMA ₂₆	18	99.1	11	62
PEO ₄₄ - <i>b</i> -PODMA ₅₀	18	98.6	14	61
PEO ₄₄ - <i>b</i> -PDSMA ₂₄	10	99.1	-	28
PEO ₄₄ - <i>b</i> -PDSMA ₅₄	10	98.6	-	34
PODMA ₈₀	-	99.3	-	57
PDSMA ₈₃	-	98.9	-	59

2.3.3 Self-Assembly of PEO-*b*-PODMA & PEO-*b*-PDSMA and blends

The established preparation procedure followed in this chapter used the solubility parameters for PODMA, DSMA, THF and water, which are shown in Table 6.²⁶ PODMA, PDSMA and PEO have solubility parameters that are extremely close to that of THF (9.1 cal/cm³). These values suggest that these polymers should be soluble in THF as opposed to water. When the self-assembly is carried out, this might lead to the formation of THF-polymer rich droplets in water when the water is added slowly. As the water content increases, a phase separation occurs of the PODMA and water or PDSMA and water and aggregation results.

Table 6. Solubility parameters for block copolymers obtained from literature.²⁶

Compound	Solubility parameter (cal/cm ³)
Water	23.4
THF	9.1
Polyethylene glycol	10.5
Poly(octadecyl methacrylate)	7.8
Poly(docosyl methacrylate)	8.2

Block copolymers that have low PEO weight fractions and high degrees of polymerisation of the ODMA or DSMA block (PEO₄₄-*b*-PODMA₅₀ and PEO₄₄-*b*-PDSMA₅₄), require a greater volume of cosolvent otherwise the solid polymer reforms in the solvent mix and precipitates.²⁴ When water is added slowly, the PEO blocks in the block copolymer are well hydrated. This means that the PODMA blocks as well as a small amount of THF, aggregate to minimize interaction with water. It is the degree of polymerisation which seems to be the most important parameter and influences how successful this micellisation is. When only THF is present, the polymer chains are well solvated and can extend. It is the addition of water that causes these chains to collapse, to minimise the exposure of the PODMA block to the surrounding water molecules. Thus, increasing the DP which means an increase in molecular weight, makes this transformation far more difficult. This is because the ability to segregate from the increasingly hydrophilic water environment is inhibited which causes the polymer to precipitate out into solution.

PEO-*b*-PODMA, PEO-*b*-DSMA & blends of the two polymers were dissolved in THF followed by the slow addition of deionised water at a rate of 5.15 mL/hr. Dialysis was carried out to displace the THF. This was performed in 4 litres of distilled water for 24

hours. Over this time the water was changed twice. After 24 hours it was assumed that all THF had been removed which was confirmed by ^1H NMR analysis of the mixture in the dialysis membrane. This is shown in Figure 15.

The mass of each polymer used in each preparation was varied to make self-assembled solutions of 0.1, 1.0 and 5.0 wt% self-assembled solutions. Quantities of THF and water used are given in Table 7. Solutions at 0.1 & 1.0 wt% produced self-assembled samples that did not precipitate. Solutions at 5 wt% showed slight precipitation of the block copolymers and a lot of precipitation for the block copolymer blends.

Following the previous method²⁴ used before, the volume of THF used in preparation was increased from 4 mL to 9 mL (THF) for the copolymers with PEO 18 wt % and from 6 mL to 9 mL (THF) for the copolymers with PEO 10 wt % in order to make a 5 wt% solution. When the volume of THF was increased to 9 mL, no precipitation was observed for the block copolymers.

However, attempts were made to make 5 wt% solutions with blends of the two block copolymers but precipitation resulted when 6, 9 and 10 ml of THF were used for the initial stage of self-assemble. To eventually make 5 wt% solutions of the blends, a 1.0 wt% sample was made and water was evaporated off to make the sample more concentrated. All final volumes used in the self-assembly preparations are given in Table 7.

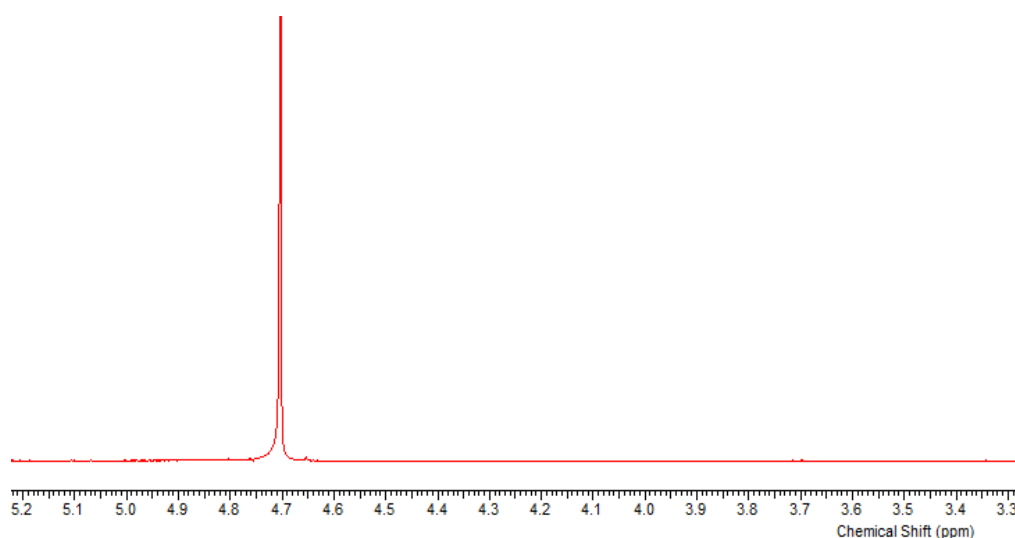


Figure 58. ^1H -NMR of dialysis sample after 24 hours.

The block copolymer dispersions were then analysed using dynamic light scattering (DLS) and transmission electron microscopy (TEM) to determine the size and dispersity of the aggregates.

Table 7. Quantities used for the self-assembly of block copolymers and blends. Self-assembled concentration is defined as the amount of polymer to water in the sample. A 5 wt% solution would mean 5% polymer to 95% water.

Polymers	Self-assembled concentration wt %	Mass of polymer used (g)	THF Volume (mL)	Water Volume (mL)	Total Volume (mL)
18 PEO wt %	0.1	0.01	4	6	10
	1	0.1	4	6	10
	5	0.5	9	1	10
10 PEO wt %	0.1	0.01	6	4	10
	1	0.1	6	4	10
	5	0.5	9	1	10
Blends	0.1	0.01	6	4	10
	1	0.1	6	4	10

Self-assembly of PEO₄₄-*b*-PODMA₂₆ & PEO₄₄-*b*-PDSMA₂₄ and blends.

The relative PEO to PODMA content is an important parameter when determining aggregate morphology.²⁴ When the hydrophilic content (PEO wt fraction) is greater than 0.45, the formation of micelles is likely to result. The structure for the conventional micelle would involve the PEO chains forming the corona and the PODMA chains forming the micelle core. The longer the coronal chains are, the greater the inter-coronal repulsion is when compared to shorter chains. This means that the surface area of coronal chains is therefore larger and aggregation results in smaller particles less than 100nm.

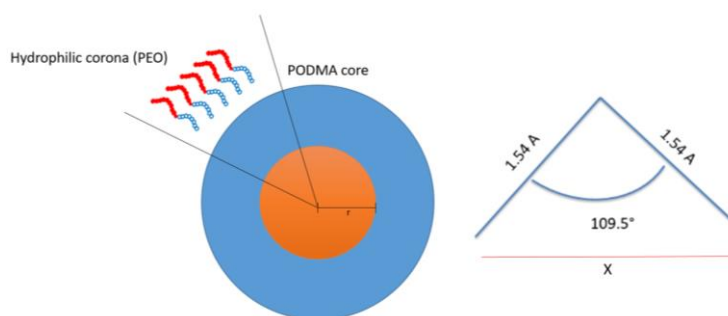


Figure 59. Block copolymer structure of the conventional micelle and tetrahedral bond angle between three carbon atoms.

The average length of a block copolymer micelle (Figure 59) can be calculated for PEO₄₄-*b*-PODMA₂₆ & PEO₄₄-*b*-PDSMA₂₄. Assuming a fully extended all anti conformation chain, the maximum length of a micelle can be calculated. X can be calculated to be 2.515 Å. X is the distance between 1st and 3rd carbon in an anti-conformation.

The following formula was then used to calculate the length of a block copolymer micelle fully stretched out.

Equation 2.7 Calculate the maximum length of a micelle.

$$((n-1) \times 2.515) + 1.225$$

Where n is the degree of polymerisation and 1.225 is half the length of a C-C bond.

For PEO₄₄-*b*-PODMA₂₆ the fully extended chain length was calculated to be 175 nm and for PEO₄₄-*b*-PDSMA₂₄ it was 170 nm. This means that any structures observed by DLS and/or TEM below these lengths are most likely to be micelles.

Table 8. TEM and DLS results for block copolymers and blends (PEO 18 wt %).

Sample(s)	wt %	N _{Aver} Diameter/ (nm) TEM	N _{Aver} Diameter / (nm) DLS	CONTIN (nm) DLS	Đ DLS
PEO ₄₄ - <i>b</i> -PODMA ₂₆	0.1	304±67	144±37	373	0.18
	1.0	184±99	42±5	193/396	0.37
	5.0	300±93	120±5	350	0.22
PEO ₄₄ - <i>b</i> -PODMA ₂₆ 75:25	0.1	218±100	120±6	255	0.25
	1.0	306±87	43±3	50/251	0.76
PEO ₄₄ - <i>b</i> -PDSMA ₂₄	0.1	170±87	102±7	385	0.27
	1.0	296±94	50±4	57/344	0.47
PEO ₄₄ - <i>b</i> -PODMA ₂₆ 25:75	0.1	212±94	122±44	87/381	0.21
	1.0	350±82	241±73	620	0.24
PEO ₄₄ - <i>b</i> -PDSMA ₂₄	0.1	249±94	122±44	37/429	0.31
	1.0	234±61	82±4	138	0.24
	5.0	265±93	122±8	394	0.24

Previous work¹¹ showed that bicontinuous nanospheres formed when the PEO weight fraction was between 0.1- 0.3 and the molecular weight was less than 20,000 KDa. The phase diagram (Figure 46) constructed from this previous testing, predicted that bicontinuous nanospheres would form for a PEO 18 wt % when the molecular weight was around 12.5 KDa.¹⁵ From the DLS measurements (Figure 60 & Figure 61) taken from each block copolymer at PEO 18 wt % and blends, most results were around the 100nm. The exact sizes of the aggregate structures seen using DLS is displayed in Table 8. Most of the DLS results were bimodal distributions and when CONTIN analysis was carried out a higher average in size can be seen. This suggests that there are block copolymer micelles present at the smaller size and strong evidence to suggest that bicontinuous nanospheres

or a much larger particle has formed at the larger size. Bicontinuous nanospheres range from 100-500 nm and so these results are within the size range for this morphology to form.

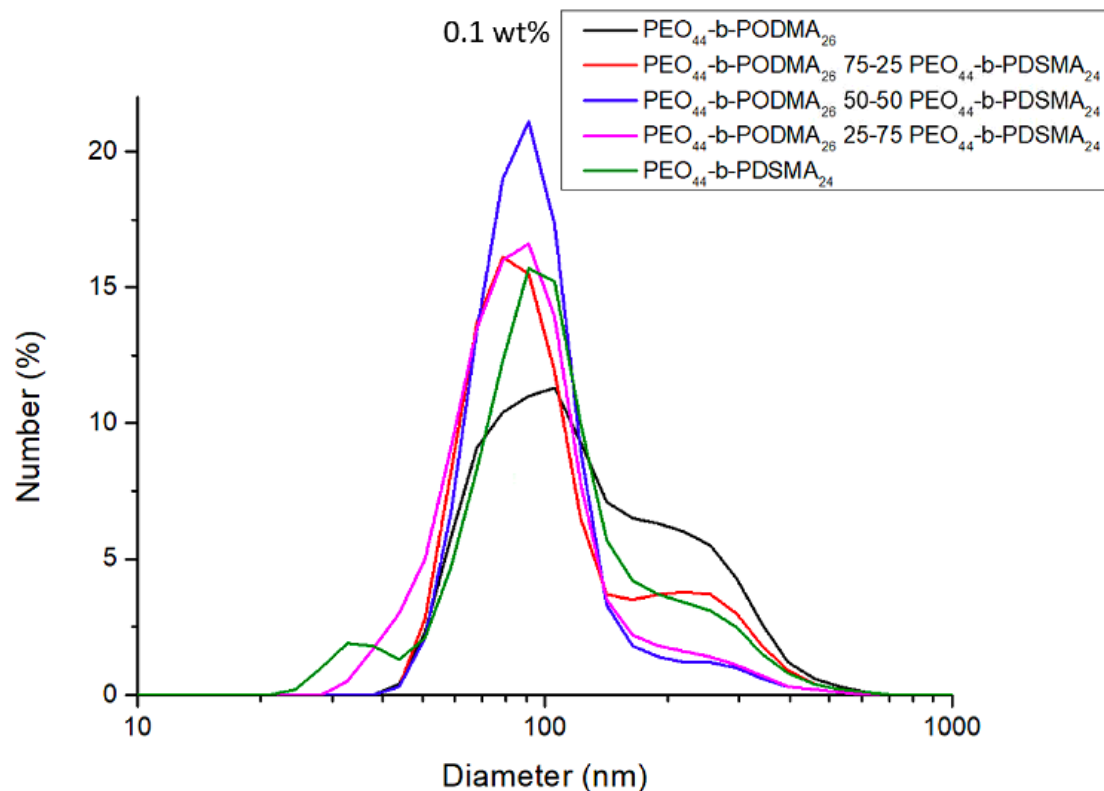


Figure 60. DLS results overlaid for PEO 18 wt % and blends at 0.1 wt% solutions in water. DLS measurements performed at a temperature used 25°C.

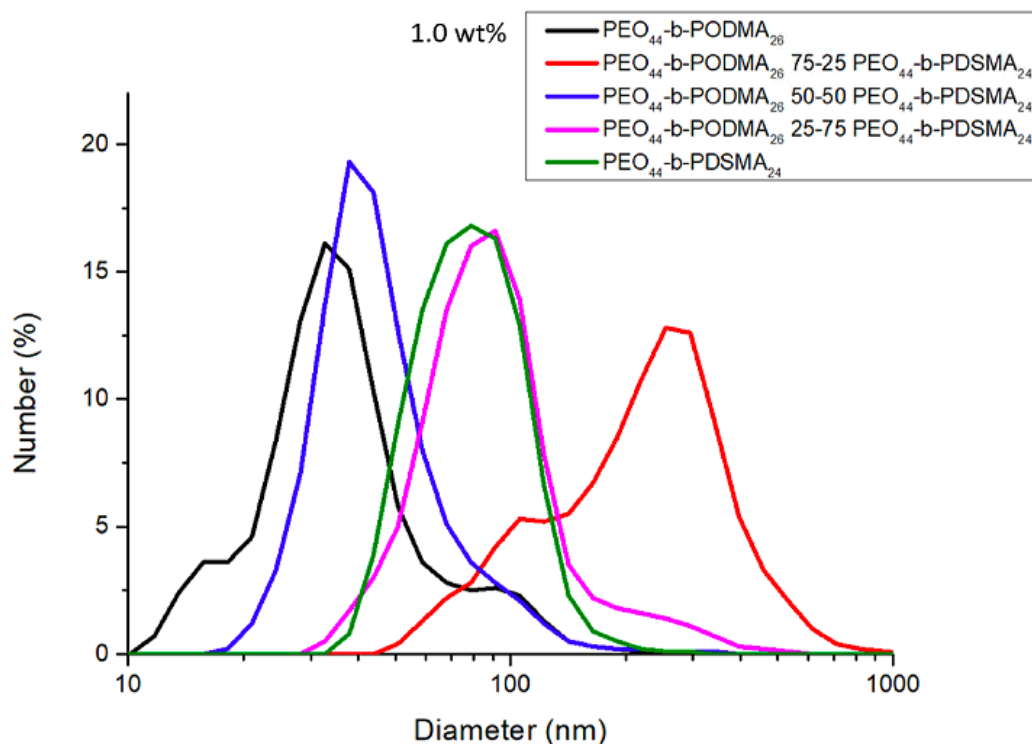


Figure 61. DLS results overlaid for PEO 18 wt % and blends at 1.0 wt% in water. DLS measurements performed at a temperature used 25°C.

The molecular weight of the PEO 18 wt % block copolymers was around 12.0 KDa (PEO₄₄-*b*-PODMA₂₆ M_n 12000 & PEO₄₄-*b*-PDSMA₂₄ M_n 12100) and bicontinuous nanospheres were predicted to form around 12.5 KDa. The TEM analysis supported the supposition that bicontinuous nanospheres were made.

For the block copolymers of PEO 18 wt % with ODMA and DSMA, spheres were observed and in some cases an internal structure inside the spheres could be seen. These markings suggest an internal structure which is further indication of bicontinuous nanospheres. Figure 63 shows a clear example of the markings on some of the spheres seen under TEM. The TEM images also suggest micelles are formed, especially at 1.0 wt solution as there are spheres much smaller than 100 nm.

TEM images for the block copolymers of PEO 18 wt % with ODMA and DSMA showed two different classes of spheres (Figure 20). A larger particle which could be evidence of bicontinuous nanospheres >100nm and a smaller particle sphere which could be the formation of block copolymer micelles which was less <100 nm. This matched with the CONTIN analysis carried out for DLS (Table 8).

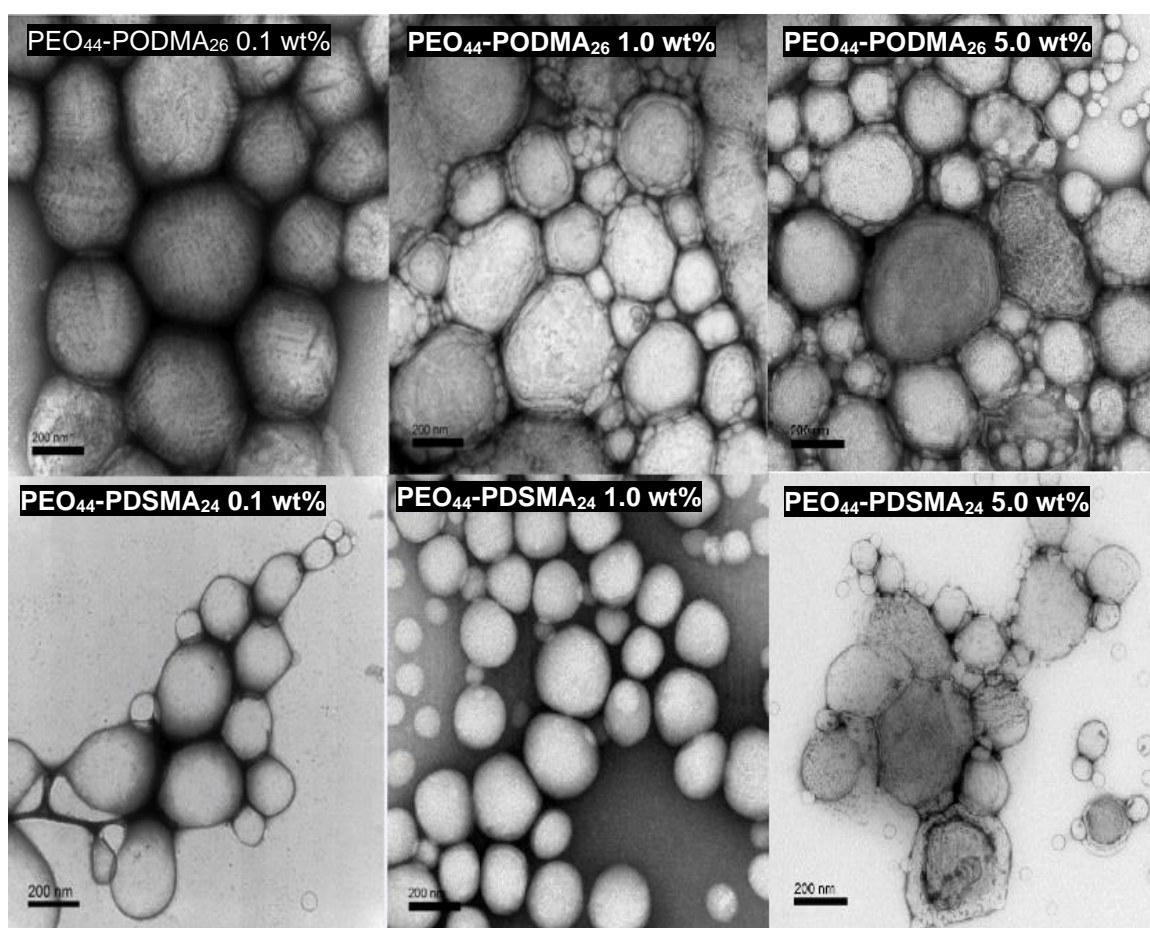


Figure 62. TEM analysis of PEO 18 wt % of block copolymers (scale bars all 200 nm).

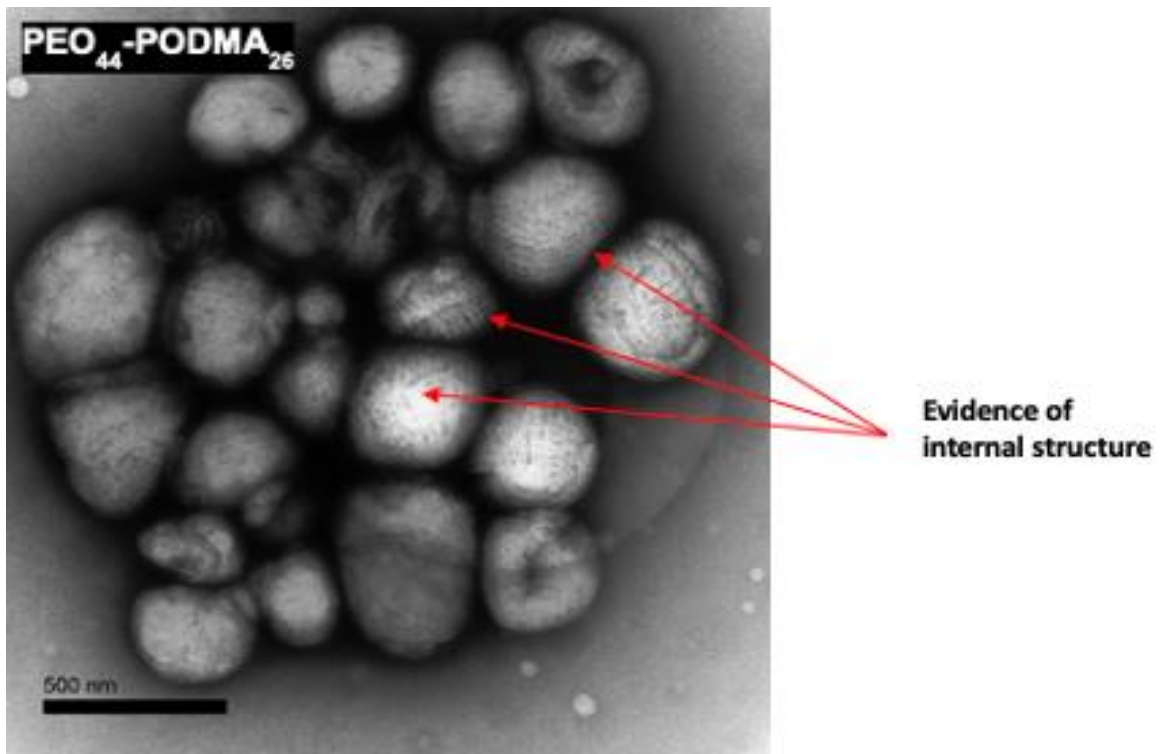


Figure 63. TEM image to show evidence of an internal structure suggesting a bicontinuous aggregate structure.

TEM images for the block copolymers blends at PEO 18 wt % is shown in Figure 64. Like what was seen above for the block copolymers, two classes of spheres were seen. There is strong evidence to suggest that block copolymer micelles are present along with bicontinuous nanospheres.

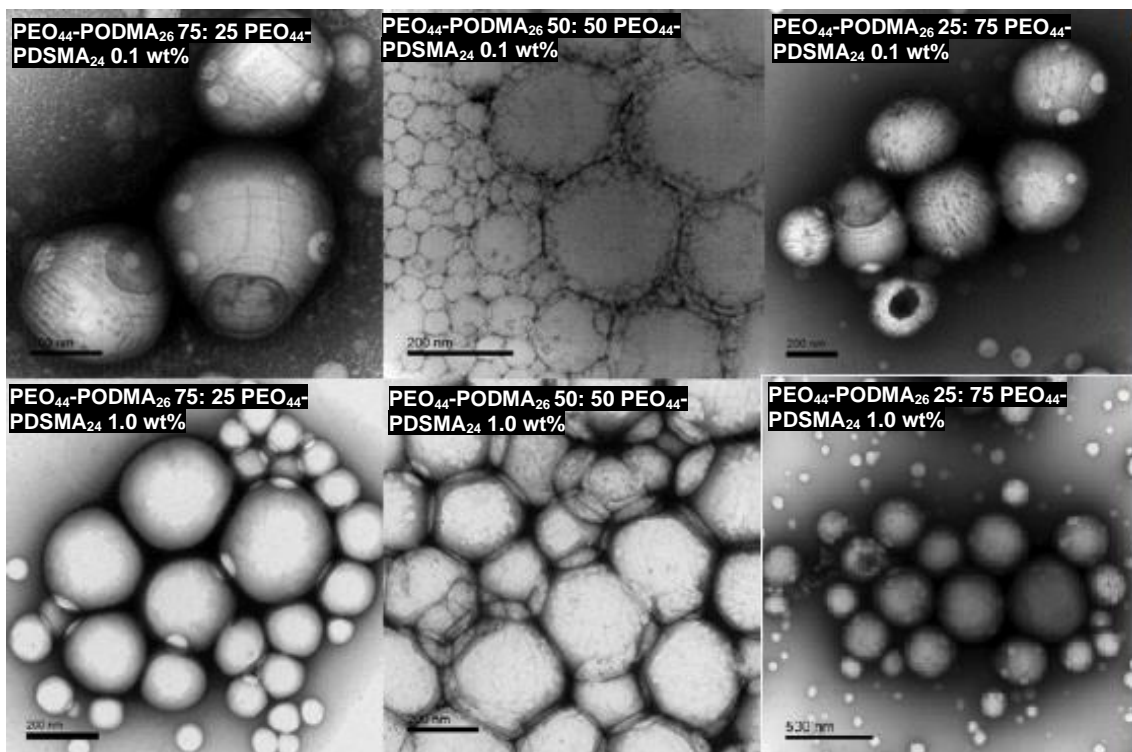


Figure 64 TEM analysis of PEO 18 wt % polymer blends (scale bars clockwise, 200, 200, 200, 500, 200 and 200 nm).

Self-assembly of PEO₄₄-*b*-PODMA₅₀ & PEO₄₄-*b*-PDSMA₅₄ and blends (PEO 10 wt %)

Table 9. TEM and DLS results for block copolymers and blends (PEO 10 wt %). Self-assembled concentration is defined as the amount of polymer to water in the sample.

Sample(s)	wt %	N _{Aver} Diameter/ (nm) TEM	N _{Aver} Diameter / (nm) DLS	CONTIN (nm) DLS	Đ DLS
PEO ₄₄ - <i>b</i> -PODMA ₅₀	0.1	189±44	140±24	328	0.27
	1.0	283±57	88±4	136/565	0.37
	5.0	233±68	106±4	185	0.42
PEO ₄₄ - <i>b</i> -PODMA ₅₀ 75:25	0.1	211±66	261±50	94/392	0.14
	1.0	188±45	87±6	166	0.24
PEO ₄₄ - <i>b</i> -PDSMA ₅₄	0.1	251±97	103±5	244	0.34
	1.0	290±62	107±8	309	0.35
PEO ₄₄ - <i>b</i> -PODMA ₅₀ 25:75	0.1	260±34	111±5	257	0.22
	1.0	277±49	89±4	130/623	0.47
PEO ₄₄ - <i>b</i> -PDSMA ₅₄	0.1	206±56	150±18	402	0.35
	1.0	197±44	92±16	144	0.50
	5.0	256±85	81±7	222	0.29

There has not been much research carried out on block copolymer of PEO 0.1 weight fraction at molecular weight 20 KDa. The phase diagram (Figure 46) suggests that bicontinuous nanospheres should form at these parameters.¹¹ Using the same formula as before, the size of block copolymer micelles for the two 10 PEO wt% can be calculated.

$$((n-1) \times 2.515) + 1.225$$

Where n is the degree of polymerisation

$$\text{PEO}_{44}\text{-}b\text{-PODMA}_{50} ((94-1) \times 2.515) + 1.225 = 235 \text{ nm}$$

$$\text{PEO}_{44}\text{-}b\text{-PDSMA}_{54} ((98-1) \times 2.515) + 1.225 = 245 \text{ nm}$$

This means that anything smaller than 235 nm for PEO₄₄-*b*-PODMA₅₀ and 245 nm PEO₄₄-*b*-PDSMA₅₄ are most likely to be block copolymer micelles.

From the DLS measurements (Figure 65 & Figure 66) taken from each block copolymer and blends, most results were around the 100nm. Bicontinuous nanospheres range from 100-500 nm and so these results are within the size range for this aggregate to form. As

the maximum size of a micelle was calculated to 245 nm then it is hard to tell from the DLS results what aggregate structures have formed. In most cases, the self-assembled solutions at 0.1 & 1.0 wt% are consistent with each other. In most cases the distributions seem to be monomodal indicating that most of the sizes of the aggregates present are around 100nm. There does seem to be some aggregates present at around 50nm.

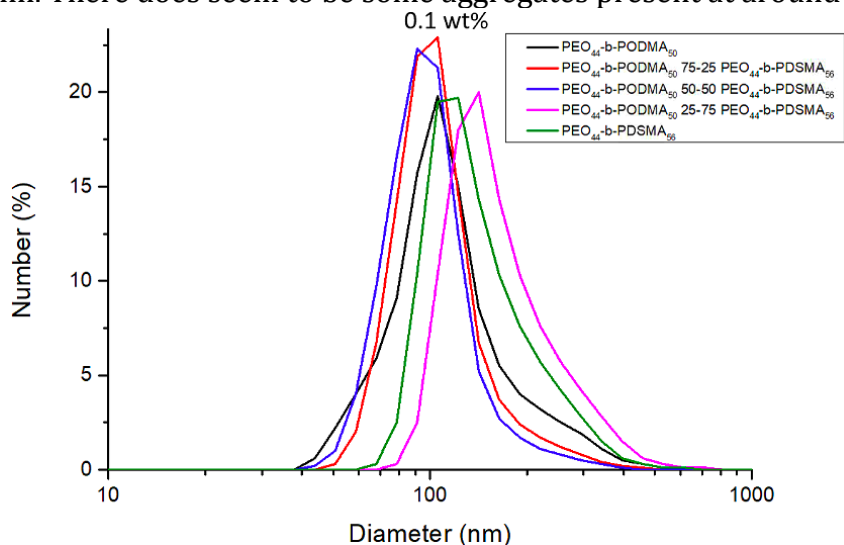


Figure 65. DLS results overlaid for PEO 10 wt % and blends at 0.1 wt% solutions. DLS measurements performed at a temperature used 25°C.

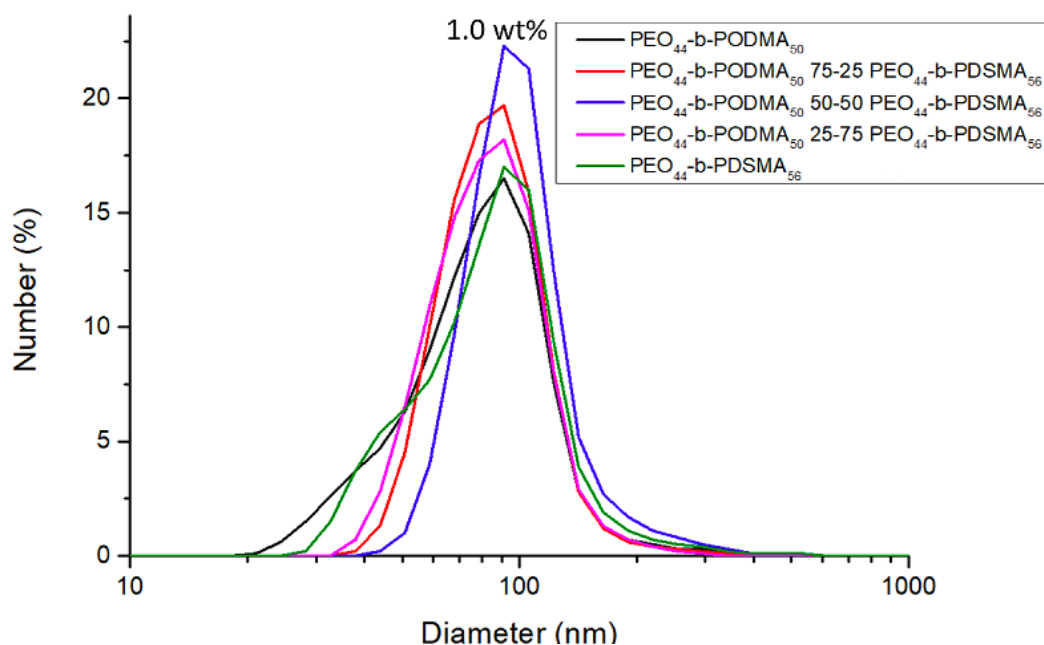


Figure 66. DLS results overlaid for PEO 10 wt % and blends at 1.0 wt% solutions. DLS measurements performed at a temperature used 25°C.

The TEM images (Figure 67 & Figure 68) were recorded for the PEO 10 wt % block copolymers. In all cases, spheres were observed with some of the larger spheres showing markings. This is evidence for bicontinuous nanospheres. The larger spheres are also in the correct size range for bicontinuous nanospheres. In most cases, block copolymer micelles can be seen at a size range of 50 nm.

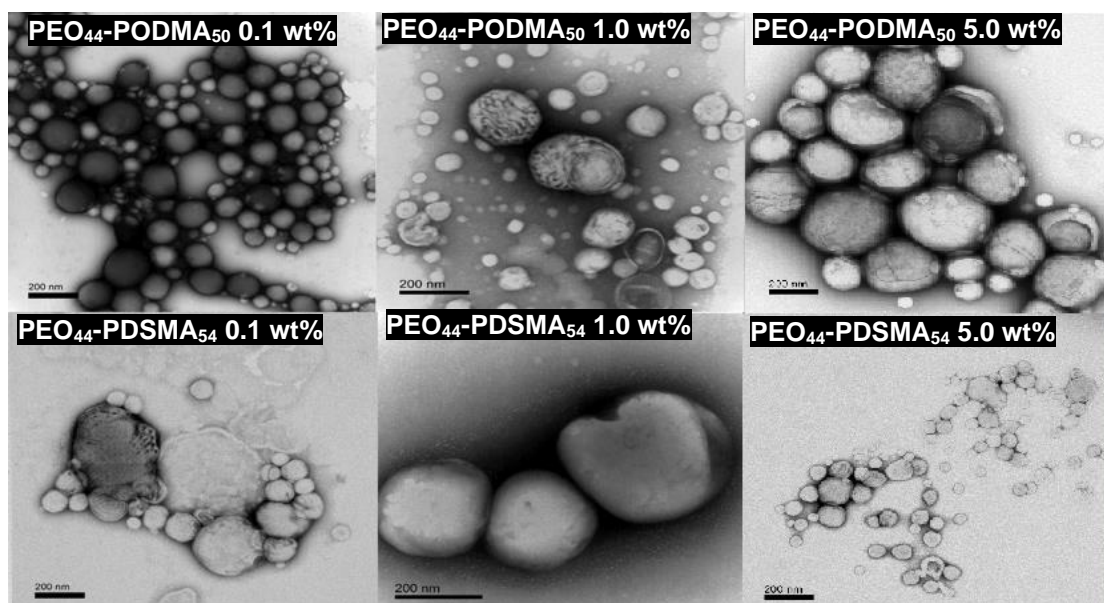


Figure 67. TEM analysis of PEO 10 wt % of block copolymers. (scale bars clockwise, 200, 200, 200, 200, 200 and 200 nm).

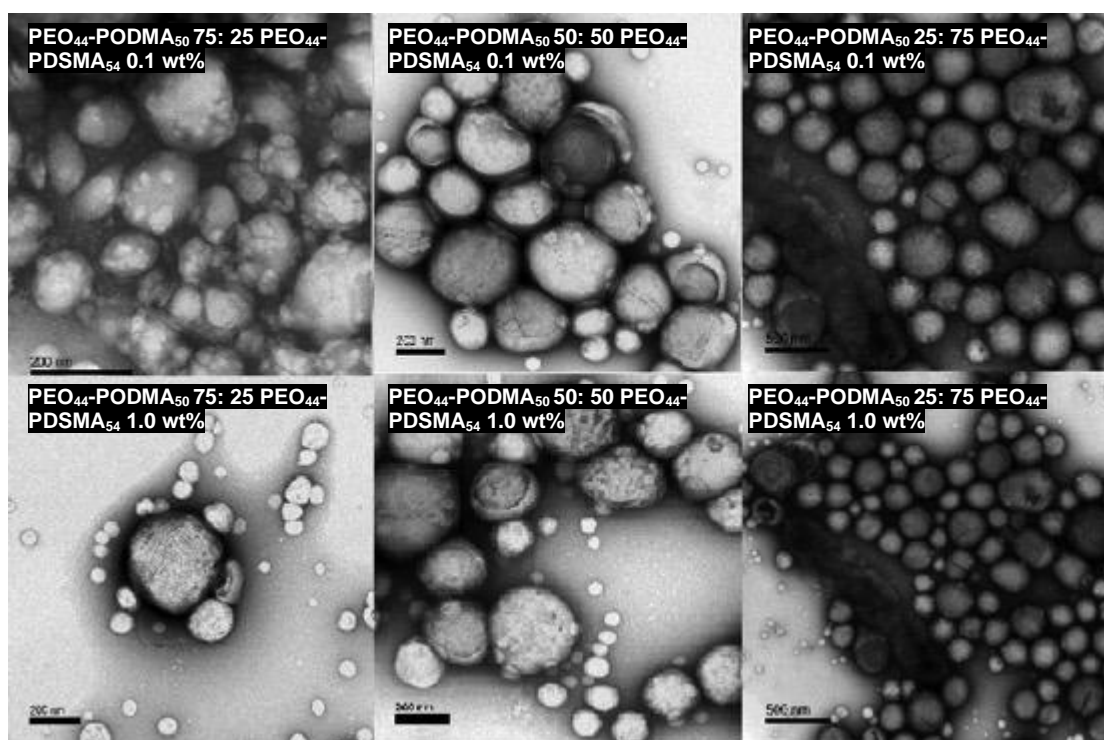


Figure 68. TEM analysis of PEO 10 wt % polymer blends. (scale bars clockwise, 200, 200, 500, 200, 500 and 500 nm).

TEM was conducted on block copolymer and blends at PEO 10 wt%. Spheres were observed along with markings on the surface of the larger ones which is evidence for an internal structure. As the solution is increased from 0.1 to 1.0%, there seems to be an increased in block copolymer micelles being observed. In summary, there seems to be a combination of bicontinuous nanospheres present with block copolymer micelles in the blends of the two block copolymers.

2.3.4 Thermal analysis of bulk block copolymers and polymer blends (DSC)

To achieve bicontinuous nanospheres with thermo-responsive properties it is necessary for the octadecyl and docosyl side chains to crystallise when self-assembled (as opposed to simply forming amorphous structures). Previous studies of the melting transition points of poly(alkyl acrylate)s and poly(alkyl methacrylate)s were carried out by Rehberg and Fisher in 1948.²⁰ It was discovered that when there are only a few carbon atoms found within the alkyl side chain (1-7 carbons for acrylates & 1-11 carbons for methacrylates) only a glass transition point is observed. However, when there were more than 8 carbons for acrylates and 12 carbons for methacrylates melting transition points were observed. As the number of carbon atoms were increased, this melting transition temperature also increased. The reason for this is due to an increase in crystallinity in the side chains which results in an increase in melting point.²⁰ Further research carried out since 1948 showed that it is in fact only the outer methylene units that contribute to the crystal lattice.²⁷ In fact, the methylene units closest to the polymer backbone do not contribute to the side chain crystallinity at all.

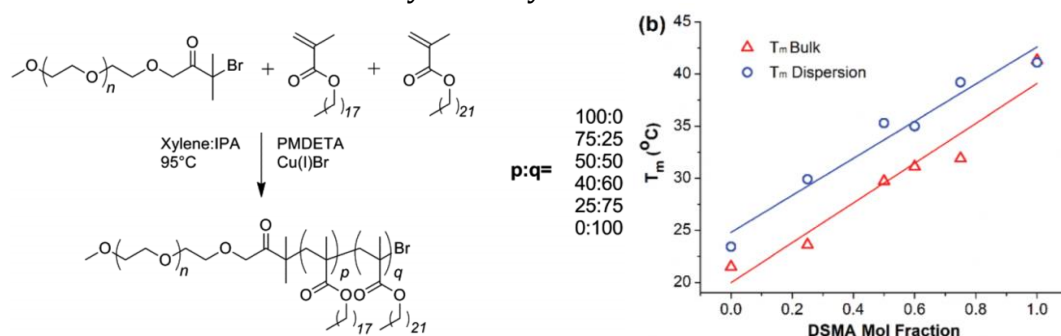


Figure 69-70. Reaction scheme for the synthesis of the carbon 18 & carbon 22 side chains & DSC results of block copolymers taken from previous work.²²

Past work has shown that poly(ethylene oxide)-*block*-poly(docosyl methacrylate) has a T_m higher than poly(ethylene oxide)-*block*-poly(octadecyl methacrylate).²² A series of block copolymers were tested in bulk and in aqueous dispersions as shown in Figure 70. It was also shown that copolymerising the two monomers ODMA and DSMA in the hydrophilic block gave control of the T_m between 21.5°C and 41.3°C. This was expected as the T_m of the carbon 18 side chain was 21.5°C and the T_m of the carbon 22 side chain was 41.3°C so a copolymerisation of these side chains should fall between these values.

For all block copolymers that were synthesised, thermal analysis was carried out on bulk samples and results were compared to literature values.²⁸ ΔH_f (enthalpy change of fusion) and D_c (degree of crystallinity) were calculated for the block copolymers. The area (J/g) was used to calculate the enthalpy of fusion ΔH_f (kJ/mol) in Equation 2.8. Where A is the area (J/g), MW is the average molecular weight of the side-chain repeat unit (253 for PODMA & 309 for PDSMA) and as the hydrophobic block represents 82 or 90 wt% of the block copolymer, this was taken into account by multiplying by 1.22 or 1.1.

The degree of crystallinity (D_c) identifies how much of the polymer is in the crystalline state. The D_c of the hydrophobic block was calculated using Equation 2.9, where ΔH_f is the enthalpy change of fusion for the hydrophobic block and ΔH_f° is the enthalpy of fusion measured for a theoretically 100% crystalline polymer. For PODMA & PDSMA these values are 242.86 J/g and 296.83 J/g respectively.²⁹

Equation 2.8

$$\Delta H_f = A \left(\frac{1}{1000} \right) MW \times 1.22/1.1$$

Equation 2.9

$$D_c = \frac{\Delta H_f}{\Delta H_f^\circ} \times 100$$

Table 10 Thermal properties recorded by DSC for bulk block copolymers.

Structure	Onset °C	Peak °C	ΔH_f J/g	ΔH_f (kJ/mol)	D_c (%)
PEO ₄₄ - <i>b</i> -PODMA ₂₆	22.9	26.3	69.0	21.3	8.8
PEO ₄₄ - <i>b</i> -PODMA ₅₀	23.0	23.3	77.7	21.6	8.9
PEO ₄₄ - <i>b</i> -PDSMA ₂₄	40.9	45.7	113.4	42.8	14.4
PEO ₄₄ - <i>b</i> -PDSMA ₅₄	42.2	45.3	138.7	47.1	15.9

Bulk block copolymers containing the ODMA block had a T_m lower than the bulk block copolymer of DSMA (Table 10). This is because there is an additional four CH₂ groups on the DSMA side chain which can crystallise. Results also showed that as the number of methacrylate side chains in the block copolymer increases so does the D_c as expected from the literature.²⁸ A small increase in the degree of crystallinity (D_c) was seen for the two block copolymer which contained a ODMA and the two block copolymer which contained DSMA blocks, when the side chain increases from approximately 25 to 50. This has not been commented on before in literature for methacrylates but due to the more methacrylate units being present, there is an increase in the degree of crystallinity.

Mixtures of the ODMA and DSMA copolymers of various weight fractions were prepared. These were analysed by DSC to ascertain thermal behaviour and the degree of blending. Ratios used were the following:(ODMA:DSMA) 75:25, 50:50 & 25:75. The DSC thermograms for the copolymers and blends of PEO 18 wt % are shown in Figure and the thermal property data is displayed in Table 11.

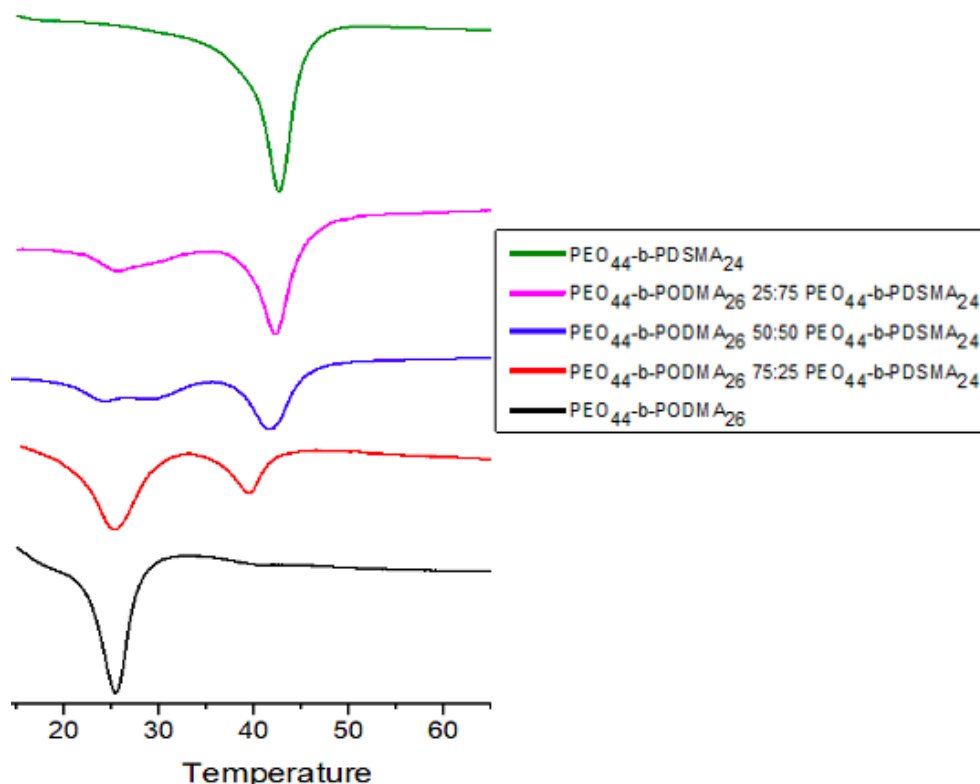


Figure 71. DSC thermograms for PEO 18 wt % block copolymer and blends.

Table 11. Thermal properties recorded by DSC for bulk block copolymers and blends at PEO 18 wt %.

Structure	Onset °C	Peak °C	Area J/g	Total Area J/g	ΔH_f (KJ/Mol)	D_c (%)
PEO₄₄-b-PODMA₂₆	22.9	26.3	69.0	69.0	21.30	8.8
PEO₄₄-b-PODMA₂₆ 75:25	21.4	24.8	53.1	73.1	23.8	9.28
PEO₄₄-b-PDSMA₂₄	36.1	38.9	20.0			
PEO₄₄-b-PODMA₂₆ 50:50	21.9	25.3	33.6	78.4	25.8	9.56
PEO₄₄-b-PDSMA₂₄	39.8	42.6	44.8			
PEO₄₄-b-PODMA₂₆ 25:75	22.5	25.6	24.2	80.9	29.1	10.3
PEO₄₄-b-PDSMA₂₄	39.7	42.3	56.7			
PEO₄₄-b-PDSMA₂₄	40.9	45.7	113.4	113.4	42.8	14.4

The DSC thermograms for the copolymers and blends of PEO wt 0.18 are shown in Figure 72 and the thermal property data is displayed in Table 12.

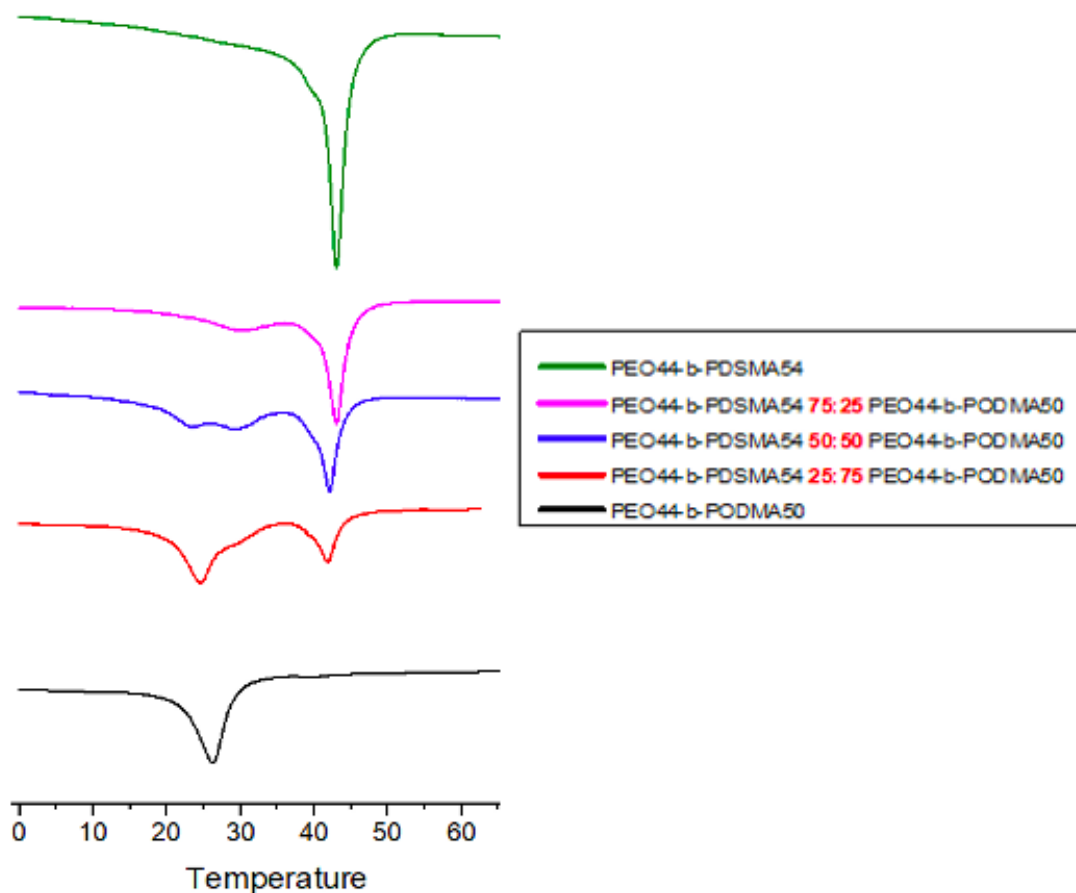


Figure 72. DSC thermograms for 0.10 PEO wt fraction block copolymer and blends

Table 12. Thermal properties recorded by DSC for bulk block copolymers and blends at PEO 0.10 wt.

Structure	Onset °C	Peak °C	Area J/g	Total Area J/g	ΔH_f (KJ/Mol)	D_c (%)
PEO ₄₄ -b-PODMA ₅₀	23.0	23.3	77.7	77.7	21.6	8.9
PEO ₄₄ -b-PODMA ₅₀ 75:25	21	24.3	58.8	82.0	24.1	9.4
PEO ₄₄ -b-PDSMA ₅₄	39.9	41.8	23.2			
PEO ₄₄ -b-PODMA ₅₀ 50:50	20.2	23.6	34.8	86.6	25.7	9.5
PEO ₄₄ -b-PDSMA ₅₄	26.9	29.3	51.8			
PEO ₄₄ -b-PODMA ₅₀ 25:75	24.5	30.2	19.2	88.6	28.8	10.2
PEO ₄₄ -b-PDSMA ₅₄	41.2	43.0	69.4			
PEO ₄₄ -b-PDSMA ₅₄	41.2	43.0	138.7	138.7	47.1	15.9

Analysis of DSC results suggested that in the case for block copolymers of PEO wt fraction of 0.1 & 0.18 that the two block copolymers do not blend completely. In fact, a partial mixing is observed. For a fully miscible blend, one peak is expected and this should be between the melting transition temperatures of the ODMA and DSMA block. For the case of the 50:50 blends, three peaks are seen. The middle peak is around 30°C which would be a reasonable expected temperature for mixing. Figure 73 shows this partial mixing much more clearly by overlaying the 50:50 blends with the straight block copolymers.

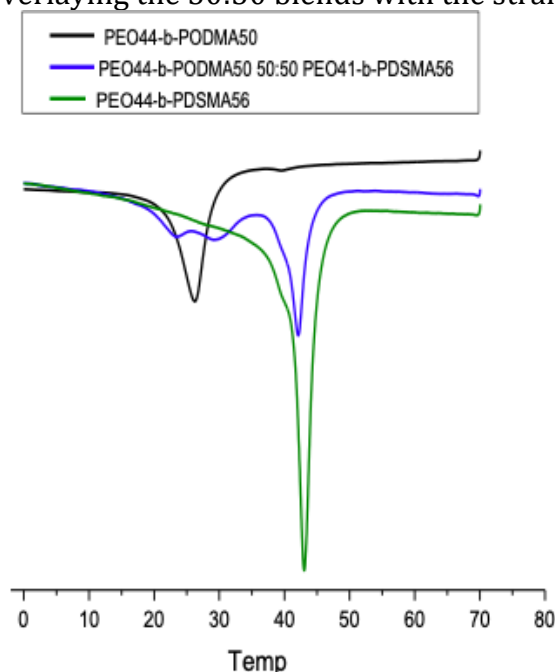


Figure 73. Overlay of DSC thermograms PEO₄₄-b-PODMA₅₀, PEO₄₄-b-PDSMA₅₄ & 50-50 blend

The software on the DSC converts the area of the curves in mw/°C into enthalpy values J/g. The enthalpy values of each DSC thermal analysis trace were taken and plotted against the percentage of methacrylate monomer for each block copolymer and blends. When partial mixing was observed, the ODMA peak and the partial mixing peak overlapped with each other on the DSC trace. As it was hard to separate these peaks it will be called Peak 1 in Figure. Peak 1 is therefore represented by the enthalpy attributable to the PODMA melting transition and the enthalpy attributable to partial mixing. Peak 2 represented in Figure, is the enthalpy attributable to the PDSMA melting transition. Both block copolymer mixtures gave similar results (Figure) for the enthalpy against percentage of methacrylate and the results almost overlay.

ODMA	PEO 0.18 wt		PEO 0.10 wt	
	Peak 1	Peak 2	Peak 1	Peak 2
1.0	69.0	0	77.7	0
0.75	53.1	20.0	58.8	23.2
0.5	33.6	44.8	34.8	51.8
0.25	24.2	56.7	19.2	69.4
0	0	113.4	0	138.7

Table 13. Enthalpy table for block copolymers and blends

The data in Table 13 was used to plot a scatter graph as shown in Figure 74. It shows the enthalpy results for all the block copolymers and blends used at PEO wt fraction of 0.18 & 0.1. This suggests that changing the PEO weight fraction still gives the same enthalpy results from DSC. It also suggests that the degree of partial mixing seen is very similar for the polymer blends at PEO 0.10 wt and 0.18 wt.

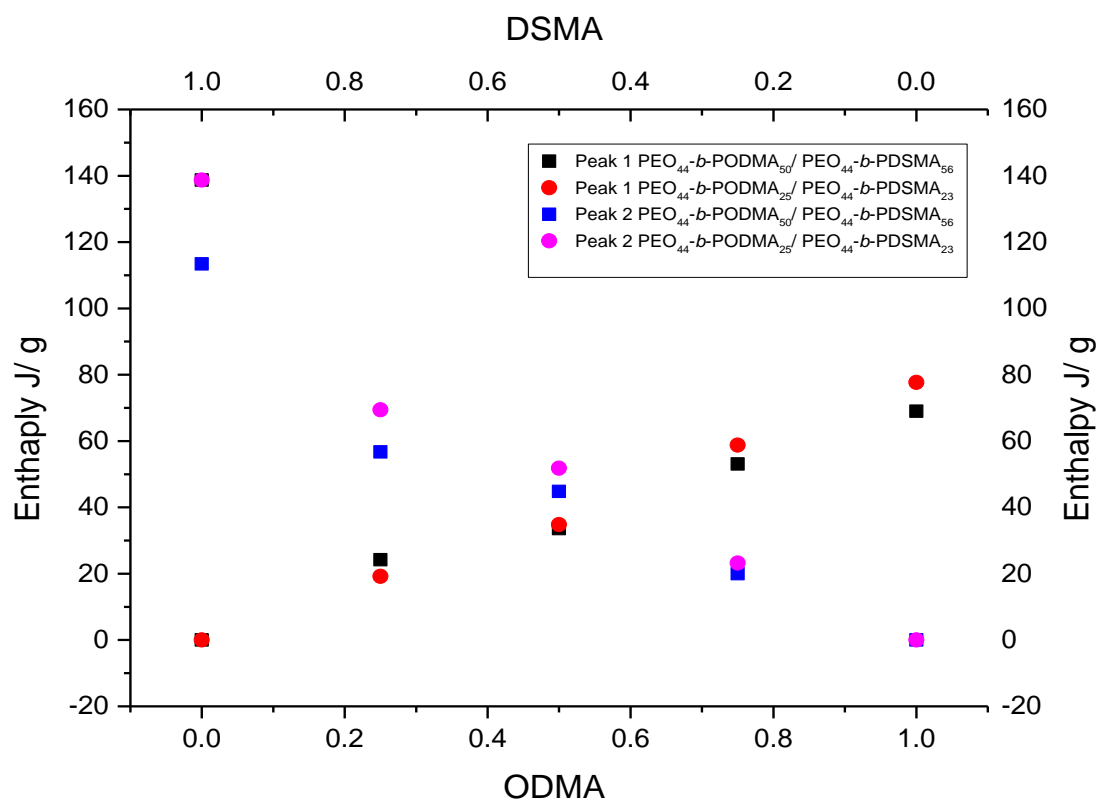


Figure 74. Scatter graph plotted by DSC enthalpy against methacrylate percentage.

Although partial mixing was obtained with the polymeric blends (as three peaks were seen on the DSC thermograms), overall these experiments were deemed unsuccessful. There are signs that if full mixing can be achieved then there could be control on the melting transition temperature of these blends. The main aim was to get a single transition peak in DSC which would move up or down depending on the ratio of ODMA:DSMA.

2.3.5 Thermal analysis of bulk block copolymers blends and copolymerisation species

In attempt to force complete mixing, a copolymerisation species was selected and introduced into the polymer blends. Previous work³⁰ demonstrated that by copolymerising block copolymers with ODMA and DSMA allowed for control and manipulation of melting transition temperature. The rationale here was to assess whether adding a copolymerised species in a small quantity to the block copolymer blends would encourage full mixing. This copolymerisation block copolymer that was synthesised by the same polyethylglycol initiator (PEG₄₄-Br) was prepared previously in our research group.³⁰ The block copolymer used ODMA & DSMA in a 50:50 ratio. Characterisation of the block-co-polymer involving H-NMR & C-NMR was carried out to ensure the sample had not degraded with time.

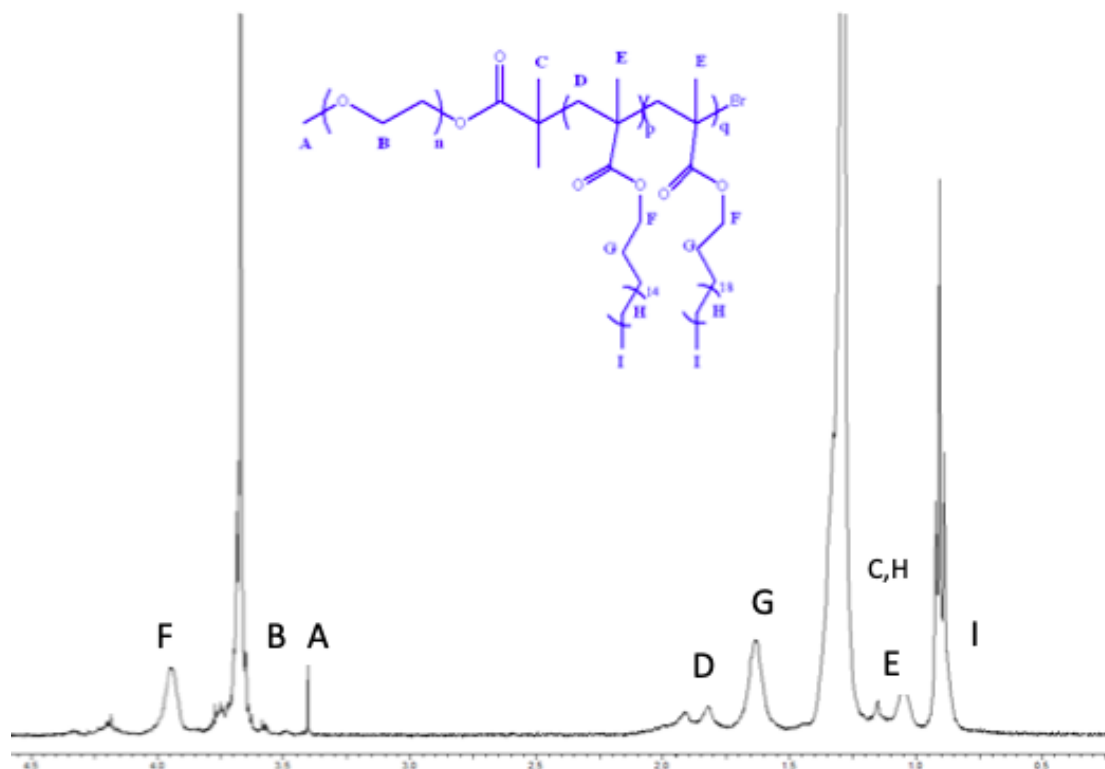


Figure 75. ^1H NMR of PEO-*b*-PODMA₁₂-co-PDSMA₁₂). Spectra obtained in CDCl₃.

PEO-*b*-PODMA₁₂-co-PDSMA₁₂ was mixed with 50:50 blend of PEO₄₄-*b*-PODMA₂₆ & PEO₄₄-*b*-PDSMA₂₄ at 2.5%, 5% and 10%. The exact quantities used are displayed in Table 14. DCM was added to the three polymers, until everything was fully dissolved and then was allowed to evaporate off. The reason why this could work is that the copolymerisation species was made up of PDSMA & PODMA in a 50-50 ratio. The intention of adding PEO-*b*-PODMA₁₂-co-PDSMA₁₂ to the blend is that it could interact with both block copolymers and could act like a 'bridge' to force mixing.³¹ All samples were then analysed by DSC.

Table 14. Quantities used for PEO₄₄-*b*-PODMA₂₆ (50-50) PEO₄₄-*b*-PDSMA₂₄ blend with copolymerised block copolymer.

Percentage %	PEO ₄₄ - <i>b</i> -PODMA ₂₆ (g)	PEO ₄₄ - <i>b</i> -PDSMA ₂₄ (g)	Percentage of PEO- <i>b</i> -PODMA ₁₂ -co-PDSMA ₁₂ (50:50) (g)
2.5	0.5	0.5	0.025
5.0	0.5	0.5	0.05
10.0	0.5	0.5	0.1

Results displayed in Figure 76, showed that adding a copolymerised block copolymer (50:50) to a blend of PEO₄₄-*b*-PODMA₂₆ & PEO₄₄-*b*-PDSMA₂₄ (50-50) up to 10%, does not make the blend mix completely. When these results are compared to what was seen previously with the block copolymer blends, the partial mixing is still observed. This means that if full mixing is to be achieved an alternative method needs to be tried.

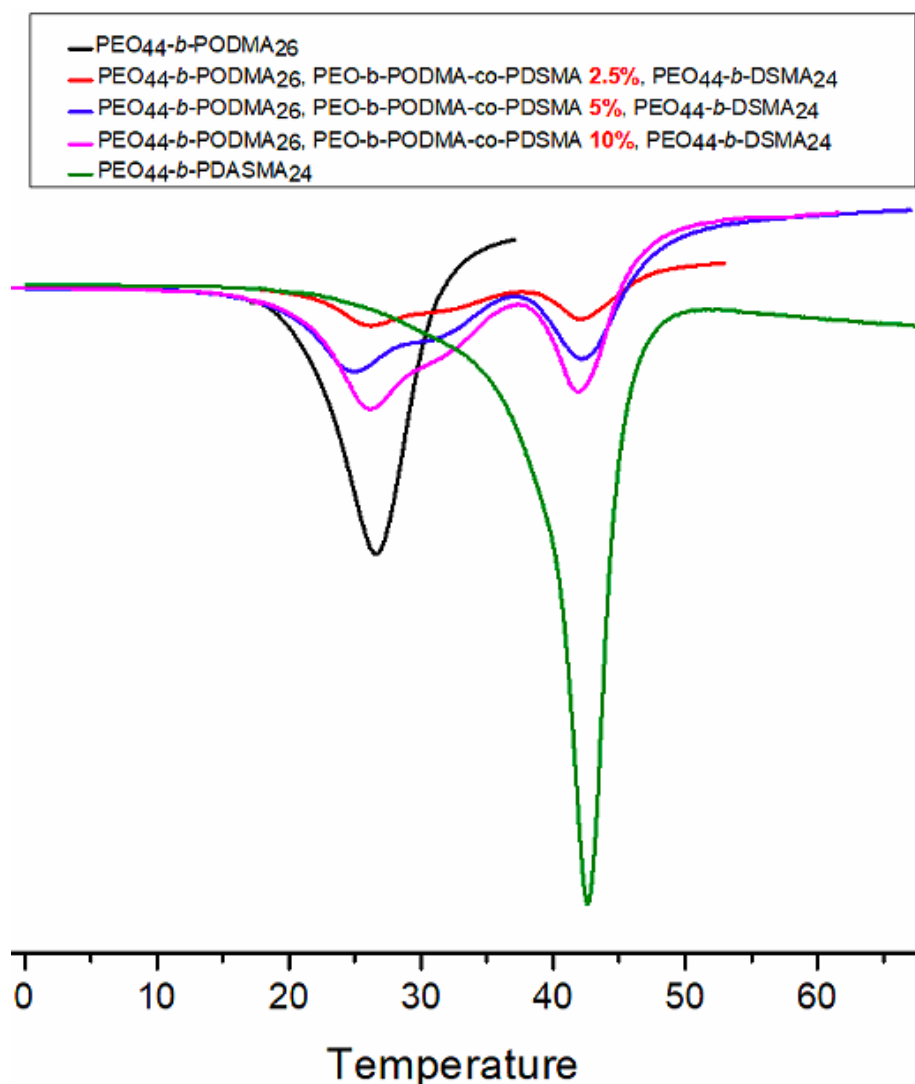


Figure 76. DSC thermograms overlaid for the blends of PEO₄₄-b-PODMA₂₆ & PEO₄₄-b-PDSMA₂₄ with PEO-b-PODMA₁₂-co-PDSMA₁₂.

2.3.6 Thermal analysis of bulk homopolymers and polymer blends (DSC)

In section 2.3.4 studied the thermal analysis of block copolymer and blends. The same work was carried out on the homo polymers of PODMA and PDSMA and blends. If full mixing could be achieved in the homo polymers, it would indicate that the PEO block was affecting the blending process for the block copolymers.

Table 15. DSC parameters for homopolymers.

Structure	Onset °C	Peak °C	Area J/g	Total Area J/g	ΔH_f (KJ/Mol)	D _c (%)
PODMA₈₀	21.1	25.4	55.4	55.4	14.0	5.8
PODMA₈₀ 75:25	20.6	24.7	23.2	59.4	15.9	
PDSMA₈₃	26.5	29.9	3.4			
PDSMA₈₃	39.6	42.9	32.8			
PODMA₈₀ 50:50	21.7	24.4	18.2	76.4	21.5	8.0
PODMA₈₀ 50:50	26.1	31.5	5.4			
PDSMA₈₃	40.7	44.5	52.8			
PODMA₈₀ 25:75	21	24.2	3.2	84.4	24.9	8.8
PODMA₈₀ 25:75	26.1	29.8	5.8			
PDSMA₈₃	40.7	43.2	75.4			
PDSMA₈₃	42.7	44.8	154.3	154.3	47.7	16.1

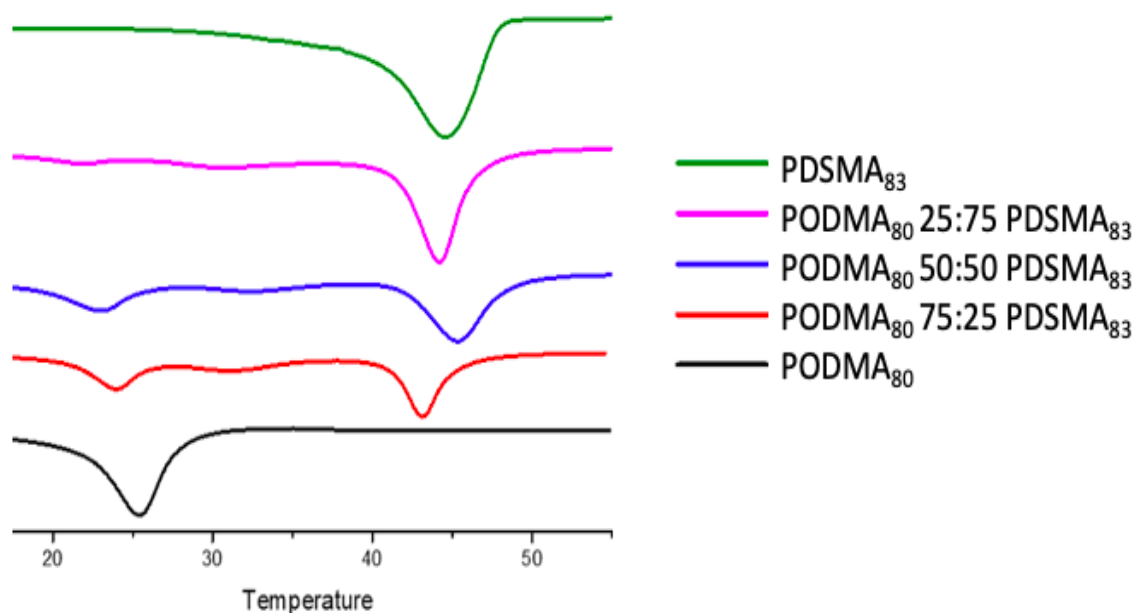


Figure 77. DSC thermograms overlaid for the blends of PODMA₈₀ & PDSMA₈₃ and blends in stack orientation.

The homopolymers of PODMA & PDSMA were synthesised via ATRP. The polymers were then blended in the same ratios as the block copolymers and thermal analysis data as shown in Table 15 and the thermograms of the homopolymers and blends are shown in Figure 77. This was to assess if the partial mixing observed previously was specific to the block copolymers and if the homopolymers involving ODMA and DSMA behaved in the same. The DSC thermograms showed three peaks indicating that partial mixing was being observed again. Figure 78 helps to show the middle transition peak by overlaying the thermograms.

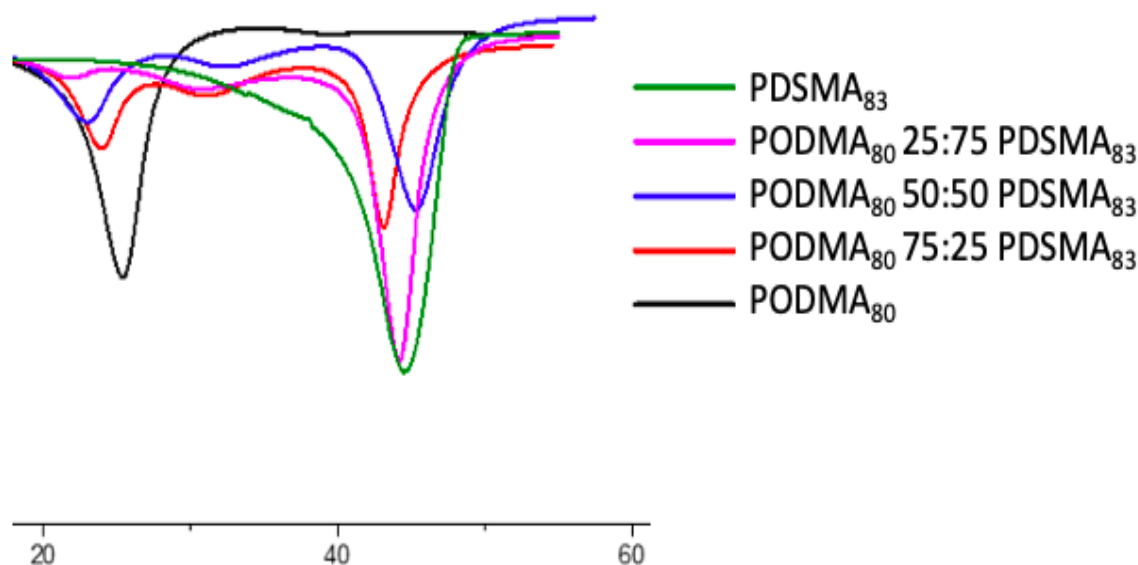


Figure 78. DSC thermograms overlaid for the blends of PODMA₈₀ & PDSMA₈₃ and blends.

Previously in literature,²⁸ PODMA₂₇ has been studied and the degree of crystallinity has been calculated. These results found that PODMA₂₇ has a D_c 35% which is much higher than the D_c calculated for PODMA₈₀.

3.7 Thermal analysis of block copolymers aggregate solutions and polymer blends (DSC)

The research up to this point has concentrated on block copolymer and homopolymer blends on the bulk samples. The self-assembled solutions of the block copolymers and blends were taken and DSC measurements were tested. Thermal analysis was attempted on aqueous solution but a 1 wt% solution was not concentrated enough to show results and anything above this caused precipitation of the block copolymer blends.

Previous work³⁰ demonstrated that DSC could be performed on 5wt% samples. For the straight block copolymer solutions this was not a problem as sample were made up to 5wt%. In order to prepare a more concentrated sample for the block copolymer blends, the self-assembled 1wt% solutions were allowed to evaporate some water off. Each initial self-assembled solution contained 10cm of polymer at 1wt%. By marking 2ml on the glass vial and allowing evaporation to take place to this line it formed a 5wt% solution with no precipitation. DSC measurements were then performed on 5wt% aggregate solutions which displayed a DSC trace.

DSC measurements have been previously tested for block copolymers of ODMA and DSMA as well as copolymerised polymer species. The results of these are shown in Figure 79.

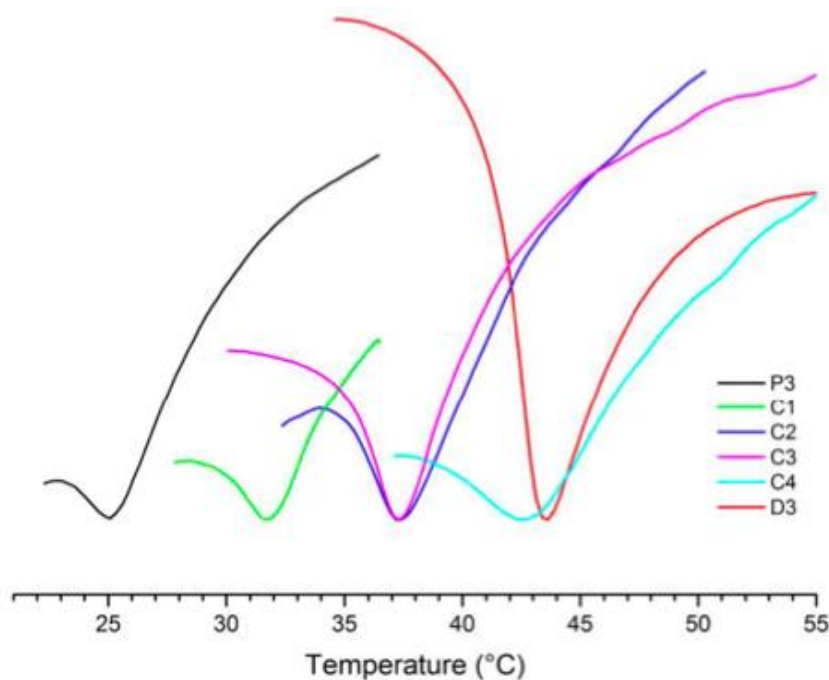


Figure 79. DSC thermogram of P3 (PEO_{49} - b - $PODMA_{21}$) 4wt% aggregate solution, D3 (PEO_{44} - b - $PDSMA_{16}$) 5wt% aggregate solution and C1-C4 (PEO - b -($PODMA$ - co - $PDMSA$)) 5wt% aggregate solution.

DSC measurements of the BCP aggregates were performed using a water filled aluminium pan as a reference sample. The full DSC thermogram is shown for the PEO - b - $PODMA_{50}$ 5wt% aggregate solution as an example to show the start and end point of the curve. It was difficult to get results as the involvement of water seem to make the DSC trace very broad. Figure 80 shows the melting transition of the $ODMA$ block performed in water.

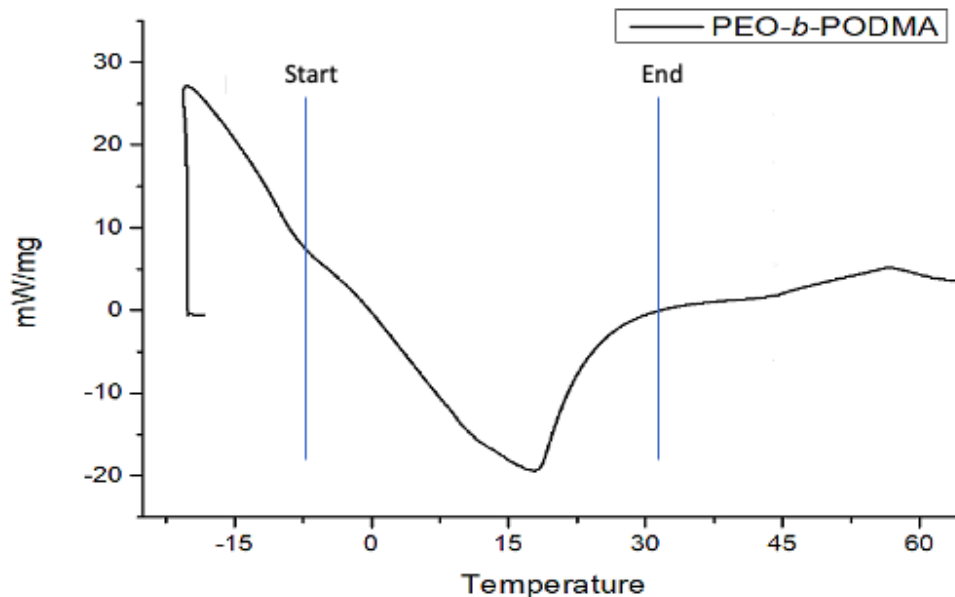


Figure 80. DSC thermogram of PEO - b - $PODMA$ at 5wt% in solutions which demonstrates how difficult it is to place a start and end point of the melting transition.

The peaks of the block copolymers and blends were enlarged to establish the melting transition for each aggregate solution. Figure 81 shows the DSC traces for all block copolymer self-assembled aggregates samples overlaid. The block copolymers self-assembled samples showed a slightly different trend to the bulk samples, with the peak melting transition temperature of PEO_{44} - b - $PODMA_{50}$ occurring around $<20^{\circ}C$ and the

PEO₄₄-*b*-PODMA₅₆ occurring around <40°C. The blends behaved slightly differently than expected. The peak of the 50-50 blend occurred next after the PEO-*b*-PODMA followed by 25-75 and then 75-25. It was expected that the 50-50 should occur in the middle but suggests that the water could be affecting the degree of blending.

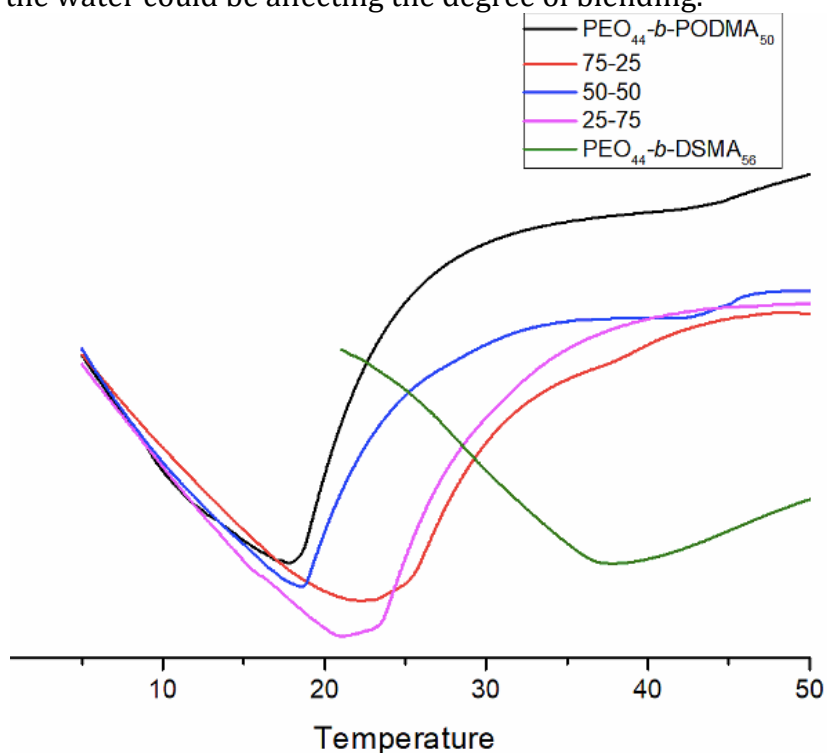


Figure 81. Full DSC heating thermograms of block copolymers and blends aggregate solutions.

The interesting comparison that can be made between the aggregate solutions and bulk samples is that the bulk samples blends produced two or three melting transitions whereas the aggregate solutions only produced one melting transition peak. From previous³⁰ and current testing of aggregate solutions it has been shown that it is difficult to measure these samples with DSC. The reason is that it can be difficult to self-assembled 5wt % solutions without getting precipitation. The involvement of water in DSC also seems to make transitions much broader when compared to the bulk samples. The water could be preventing all the transitions from being observed. This has led to three extreme cases of what might be going on within the micelles.

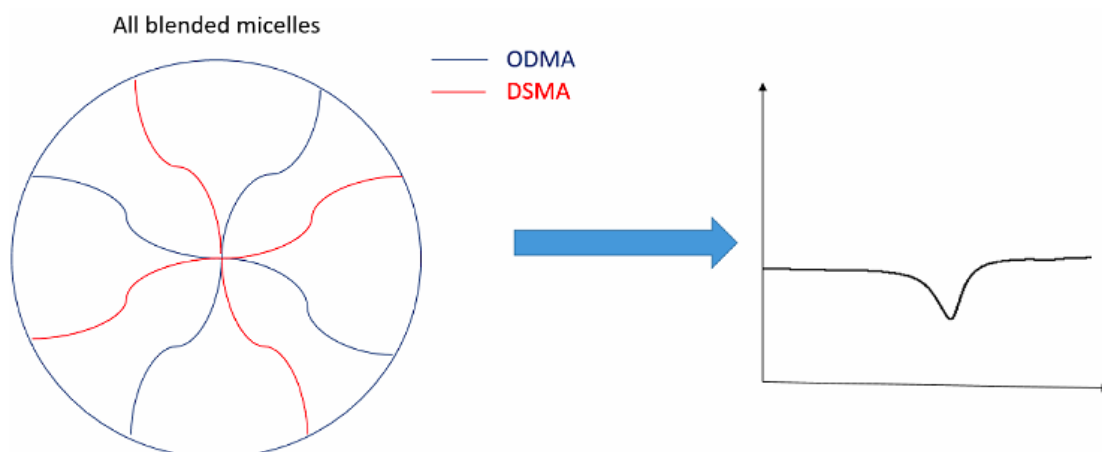


Figure 82. Schematic of blended micelles with an example of what the DSC trace is expected to be if all micelles achieved full mixing.

When the hydrophobic chains are blended in the micelle core, only one transition should be observed by DSC (Figure 82). The aggregate samples tested above, gave one transition at 5wt% indicating that this situation is possible.

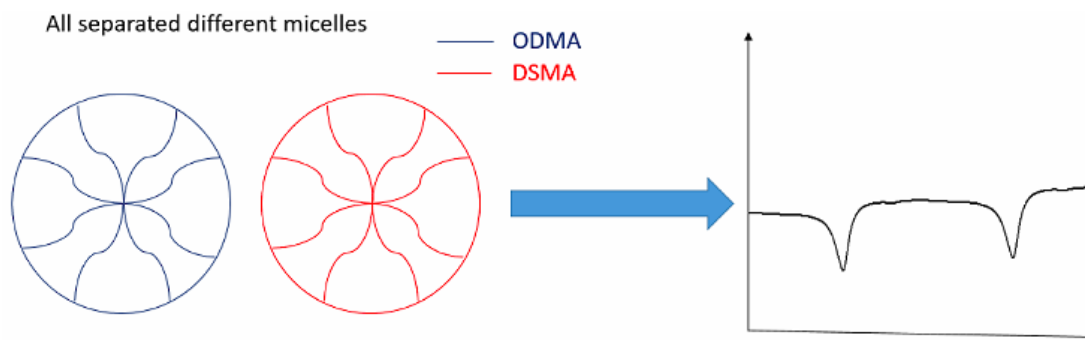


Figure 83. Schematic of separated different micelles with an example of what the DSC trace is expected to be if micelles separate upon mixing.

As the different copolymers self-assemble into discrete micelles then then two melting transition peaks are expected (Figure 83). The peak on the left represents ODMA at the lower melting temperature and the peak on the right is the DSMA at the higher melting temperature. This is not observed for the aggregate samples suggesting that we are not seeing discrete micelles with ODMA and DSMA cores unless the DSC results is being affected by the water in the self-assembly solution.

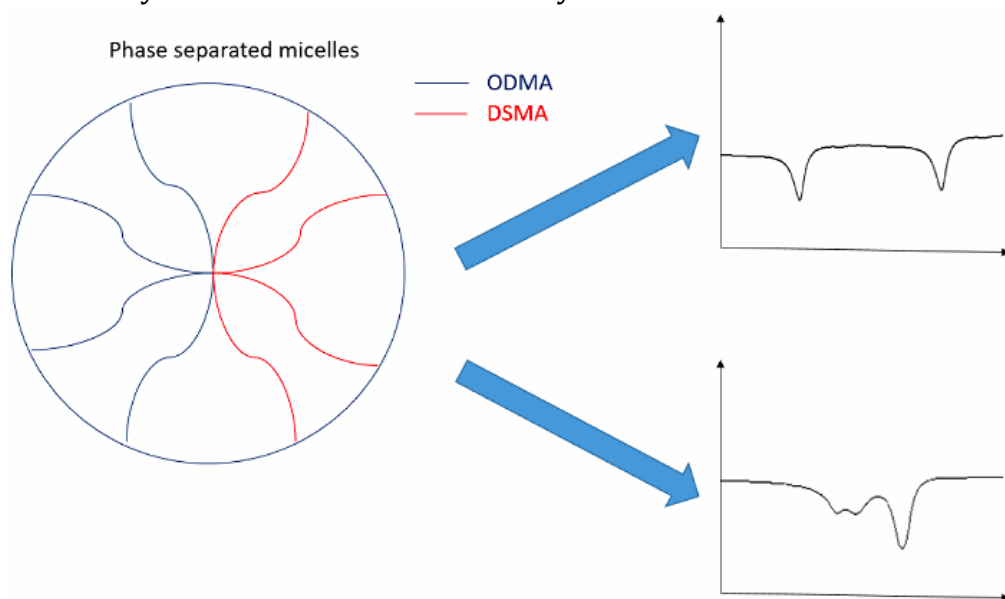


Figure 84. Schematic of phase separated micelles giving rise to two potential DSC traces.

If phase separated micelles are being made then there are two possible scenarios where the DSC trace might show two separate peaks or even three. It appears this is not being seen with the aggregate samples.

Conclusion

Block copolymers of PEO-*b*-PODMA & PEO-*b*-PDSMA were successfully synthesised by ATRP at PEO wt of 0.1 & 0.18%. Using an acetonitrile instead of ethanol like literature stated, allowed for a higher yield to be achieved.

The self-assembly involved using dialysis to form aggregates dispersed in aqueous solutions. These aggregate structures under TEM looked to be a mixture of spherical micelles and bicontinuous nanospheres. This work from this chapter has allowed better understanding how blends of block copolymer behave and when these blends are self-assembled at high concentrations (5wt%) precipitation can occur. What was a new result was that bicontinuous nanospheres seemed to be present when the 0.1wt% block copolymers were self-assembled. This has not been carried out before.

The desired results from this work were to achieve full blending with polymers containing ODMA and DSMA. If this was achieved and a single transition was observed on the DSC trace, this would allow self-assembled aggregate solutions of PEO-*b*-PODMA & PEO-*b*-PDSMA to be manipulated by mixing the solutions in the ratios wanted. DSC results showed that blending of block copolymers (PEO-*b*-PODMA & PEO-*b*-PDSMA) or homopolymers (PODMA & PDSMA) does not allow for manipulation of the melting transition temperature. This was seen through three peaks on the DSC trace with the middle peak coming from partial blending of the two block copolymers or homopolymers. This means that some blending was achieved through discrete regions of ODMA and DSMA. In some situations, there was just two peaks seen indicating that no blending was achieved through discrete regions of ODMA and DSMA.

A novel approach taken in this chapter was to blend with ODMA and DSMA which are very long methacrylate monomers (18 carbon for ODMA & 22 carbon for DSMA). From literature the longest methacrylate monomer to be used in polymeric blends was dodecyl methacrylate²² (DMA) (12 carbon atoms long). Despite full blending not being achieved, the testing carried out in this chapter was very different to what had previously been done. The application of having control on the aggregate solutions through blending and manipulating the melting transition temperature is still desirable. Despite the results from this chapter not allowing for this control on the aggregates species it has paved the way for alternative methods to try to achieve full blending in the self-assembled solutions.

References

- 1 C. Allen, D. Maysinger and A. Eisenberg, *Colloids Surfaces B Biointerfaces*, 1999, **16**, 3–27.
- 2 Y. Mai and A. Eisenberg, *Chem. Soc. Rev.*, 2012, **41**, 5969–5985.
- 3 S. Strandman and X. X. Zhu, *Prog. Polym. Sci.*, 2015, **42**, 154–176.
- 4 M. I. Gibson and R. K. O'reilly, *Chem. Soc. Rev.*, 2013, **42**, 7204–7213.
- 5 J. . Chung, M. Yokoyama, M. Yamato, T. Aoyagi, Y. Sakurai and T. Okano, *J. Control. Release*, 1999, **62**, 115–127.
- 6 P. De, S. R. Gondi and B. S. Sumerlin, , DOI:10.1021/bm701255v.
- 7 C. Porsch, S. Hansson, N. Nordgren and E. Malmström, *Polym. Chem.*, 2011, **2**, 1114–1123.
- 8 D. Giaouzi and S. Pispas, *J. Polym. Sci. Part A Polym. Chem.*, 2019, **57**, 1467–1477.
- 9 C. Wu, R. Ma, H. He, L. Zhao, H. Gao, Y. An and L. Shi, *Macromol. Biosci.*, 2009, **9**, 1185–1193.
- 10 X. Mu, S. Gan, Y. Wang, H. Li and G. Zhou, *Int. J. Nanomedicine*, 2019, **14**, 5415–5434.
- 11 B. E. Mckenzie, F. Nudelman, P. H. H. Bomans, S. J. Holder and N. A. J. M. Sommerdijk, *J. AM. CHEM. SOC*, 2010, **132**, 10256–10259.
- 12 H. Kobayashi, R. Watanabe and P. L. Choyke, *Theranostics*, 2014, **4**, 81–89.
- 13 A. K. Iyer, G. Khaled, J. Fang and H. Maeda, *Drug Discov. Today*, 2006, **11**, 812–818.
- 14 B. E. McKenzie, H. Friedrich, M. J. M. Wirix, J. F. de Visser, O. R. Monaghan, P. H. H. Bomans, F. Nudelman, S. J. Holder and N. A. J. M. Sommerdijk, *Angew. Chemie Int. Ed.*, 2015, **54**, 2457–2461.
- 15 B. E. McKenzie, J. F. de Visser, G. Portale, D. Hermida-Merino, H. Friedrich, P. H. H. Bomans, W. Bras, O. R. Monaghan, S. J. Holder and N. A. J. M. Sommerdijk, *Soft Matter*, 2016, **12**, 4113–4122.
- 16 S. J. Holder, G. Woodward, B. M. Ab and N. A. J. M. Sommerdijk, 2014, **4**, 29.
- 17 Z. Mogri and D. R. Paul, *Polymer (Guildf).*, 2001, **42**, 7765–7780.
- 18 T. Hirabayashi, T. Kikuta, K. Kasabou and K. Yokota, *Polym. J.*, 1988, **20**, 693–698.
- 19 E. F. Jordan, D. W. Feldeisen and A. N. Wrigley, *J. Polym. Sci. Part A-1 Polym. Chem.*, 1971, **9**, 1835–1851.
- 20 C. E. Rehberg and C. H. Fisher, *Ind. Eng. Chem.*, 2005, **40**, 1429–1433.
- 21 K. A. O'Leary and D. R. Paul, *Polymer (Guildf).*, 2006, **47**, 1226–1244.
- 22 O. R. Monaghan, P. H. H. Bomans, N. A. J. M. Sommerdijk and S. J. Holder, *Polym. Chem.*, 2017, **8**, 5303–5316.
- 23 W. I. Goldburg, *Dynamic light scattering*, 1999.
- 24 B. E. McKenzie, H. Friedrich, M. J. M. Wirix, J. F. de Visser, O. R. Monaghan, P. H. H. Bomans, F. Nudelman, S. J. Holder and N. A. J. M. Sommerdijk, *Angew. Chemie*, 2015, **127**, 2487–2491.
- 25 O. R. Monaghan, P. H. H. Bomans, N. A. J. M. Sommerdijk and S. J. Holder, *Polym. Chem.*, 2017, **8**, 5303–5316.
- 26 J. Brandrup, E. H. Immergut, E. A. Grulke, A. Abe, D. R. Bloch, J. Wiley, N. Y. Chichester, W. Brisbane and S. Toronto, *POLYMER HANDBOOK FOURTH EDITION A WILEY-INTERSCIENCE PUBLICATION*, 1999.
- 27 S. A. Greenberg and T. Alfrey, *J. Am. Chem. Soc.*, 1954, **76**, 6280–6285.
- 28 E. Hempel, H. Budde, S. Höring and M. Beiner, *J. Non. Cryst. Solids*, 2006, **352**, 5013–5020.
- 29 E. Hempel, H. Budde, S. Höring and M. Beiner, *Thermochim. Acta*, 2005, **432**, 254–261.

- 30 O. R. Monaghan, *Controlling the Functionality of Block Copolymer Bicontinuous Nanospheres*, 2015.
- 31 W. Arayaprane, P. Prasassarakich and G. L. Rempel, *J. Appl. Polym. Sci.*, 2004, **93**, 1666–1672.

Chapter 3. Structure-property relationships of adenine containing Poly(octadecyl methacrylate) & thymine containing Poly(docosyl methacrylate).

Contents

<i>3.1 Introduction</i>	98
<i>3.2 Experimental</i>	101
3.2.1 Materials.....	101
3.2.2 Apparatus.....	101
<i>3.4 Results and Discussion</i>	110
3.4.1 Synthesis of homopolymers.....	110
3.4.2 Synthesis of styrene based nucleobase monomers.....	110
3.4.3 Development of reactions conditions for ATRP reaction with nucleobase monomers	114
3.4.5 Self-assembly of nucleobase containing block copolymers	126
3.4.6 Proton shifts in H-NMR ¹	131
3.4.6 Thermal analysis of bulk homopolymers containing nucleobases and polymer blends (DSC)	138
3.4.7 Long chain nucleobases monomers	142
3.4.8 Ester functionality nucleobase monomers (TMA & AMA).....	146
<i>Conclusion</i>	152
<i>References</i>	154

3.1 Introduction

The ground work for nucleobases was laid out by Albrecht Kossel who studied the identifying, isolating and naming of nucleobases in 1880 and Hermann Emil Fischer with his work on purine in 1898.¹ This work allowed these biological molecules to be better understood. The structure of deoxyribonucleic acid (DNA) came next in 1950s where it was understood that DNA was a polymeric double helix structure which was bound together through specific hydrogen bonding of complementary nucleobases.² The first pair of complementary nucleobases involves adenine which will selectively bond to thymine. The second pair involves guanine which will selectively bond to cytosine. The structures of these nucleobases are shown in Figure 85.

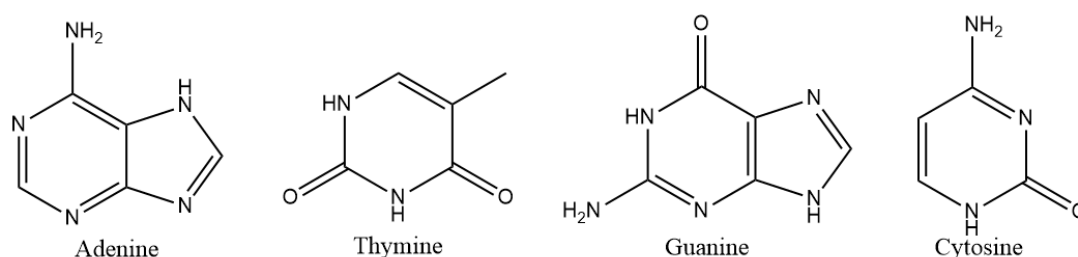


Figure 85 DNA sets of base pairs.

This inspired many to build upon this work with biomimetic syntheses. The first of this early work involved trying to attach nucleobases to naturally occurring polymers such as cellulose.¹ This paved the way for advances using synthetic monomers bearing nucleobase functionality which can be seen in the work of Pitha³ and Takemoto.⁴ It was when advances in controlled living polymerisations⁵ occurred that a larger range of nucleobase functionalised polymers could be made with good control on molecular weight, polydispersity and functionalities. A range of polymerisations such as nitroxide polymerisation (NMP), reversible addition-fragmentation chain transfer (RAFT), atom transfer radical polymerisation and ring opening metathesis polymerisation (ROMP) have all been successfully used to make nucleobase functionalised polymers. A summary of the major advances in controlled living polymerisation with nucleobases is shown in Figure 86.

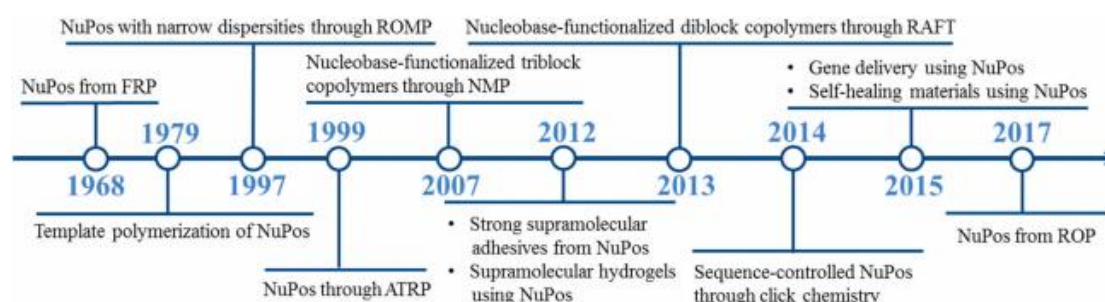


Figure 86 Advances in controlled living polymerisation with nucleobases (NuPos).⁶

This chapter will focus on nucleobases synthesised from ATRP as it is a direct follow on from Chapter 2. Most of the work published has used adenine and thymine as the complementary nucleobases. This can be seen from work published by Marsh,⁷ Van Hest,⁸ Shen⁹ and Lutz¹⁰ who have all used ATRP with nucleobases. This means that there was a

considerable body of literature methods to guide the syntheses described in the experimental of this chapter.

Figure 87 shows to date all the nucleobase monomers that have been successfully polymerised with other monomers to form a functionalised polymer.

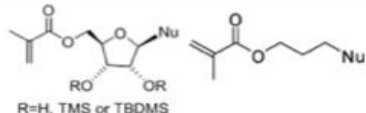
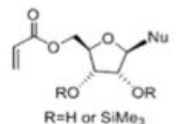
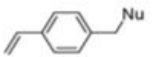
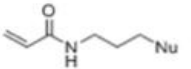
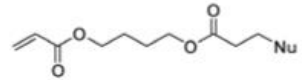
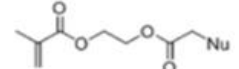
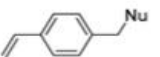
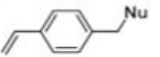
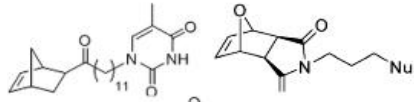
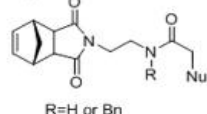
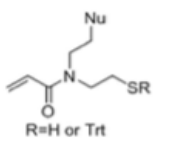
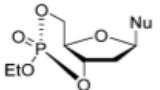

Polymerization method	Monomer structure	Nucleobase (Nu)	DP (no. of nucleobases)
ATRP		A, T, C, G, U	10-60
		A, U	10-100
RAFT		A, T, U	10-100
		A, T, C, G	10-300
		A, T	10-40
		A, T, C	10-100
NMP		A, T, G	20-30
		A, T	10-40
ROMP		A, T, C, G, U	5-40
		A, T, C, G, U	5-40
Click chemistry		A, T	10-30
Ring opening polymerization		T	10-40
Conventional free radical polymerization and other polymerization methods		A, T, C, G, U	80-200
Post-polymerization modifications	—	A, T, C, G, U	1-50

Figure 87 Nucleobase monomers that have been successfully polymerised with other monomers to form a functionalised polymer.

This chapter aimed to use ATRP to synthesize well defined polymers that contained thymine or adenine as the nucleobases with ODMA & DSMA. This was carried out using 1-(4-vinylbenzyl) thymine (VBT) & 9-(4-vinylbenzyl) adenine (VBA) (Figure 88) and having these polymerise into the polymer backbone in a random configuration.

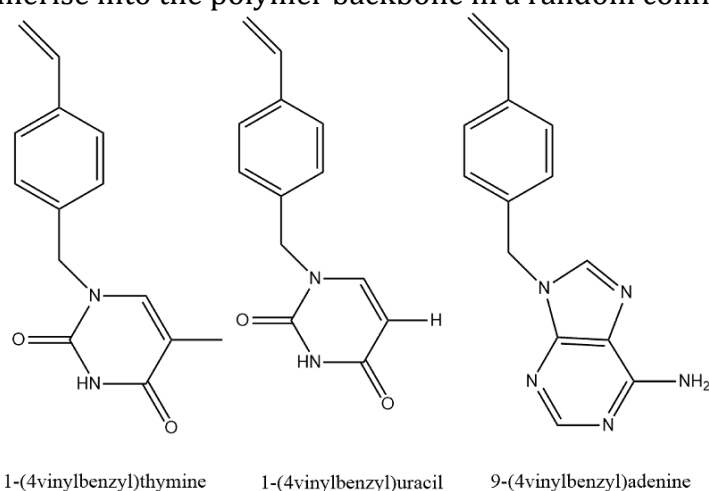


Figure 88 Nucleobase derivatives of thymine, uracil & adenine.

The previous chapter showed how the blends of the homopolymers (PODMA & PDSMA) and block copolymers (PEO-*b*-PODMA & PEO-*b*-PDSMA) showed partial mixing. After studying literature^{11,12,13} and discovering that some blends of polymers can be miscible when nucleobases are incorporated into the polymer backbone, it was thought that complete mixing could be achieved through the hydrogen bond interactions of adenine and thymine as shown in Figure 89. In most cases VBT and VBA seemed to be used to encourage blends to be miscible by the hydrogen bond interaction that takes place with adenine and thymine. DSC analysis will be carried out to access if full mixing can be achieved. The self-assembly of the block copolymers containing VBA and VBT will be carried out to see if BPNs still result.

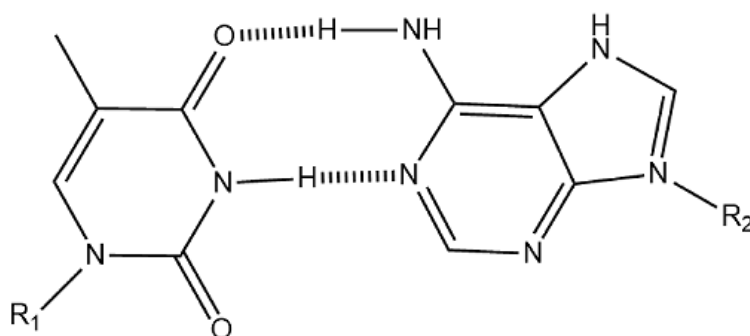


Figure 89 Hydrogen bond interaction between adenine & thymine.

3.2 Experimental

3.2.1 Materials

Copper(I) bromide (98%), copper(I) chloride (99%), hexamethyldisilane, hydroquinone, trimethylsilylchloride, magnesium sulphate (MgSO_4), 4-Vinylbenzyl chloride (90%), Ethyl α -bromoisobutyrate (EBIB), methacryloyl chloride, Sodium hydrogen carbonate, N,N,N',N'-pentamethyldiethylenetriamine (PMDETA) (99%), ethylenediamine, zinc powder, octadecyl methacrylate (ODMA), sodium hydride (NaH), bromoacetyl chloride, docosyl methacrylate (DSMA), hydroethylmethacrylate (HEMA), tris[2-(dimethylamino)ethyl]amine (Me_6TREN) were all purchased from Sigma-Aldrich and used as received. Aluminium oxide for column chromatography was purchased from Acros Organics. Xylene, isopropyl alcohol, tetrahydrofuran (THF), pet ether, chloroform, ethyl acetate, dimethyl sulfoxide (DMSO), dimethylformamide (DMF), dichloromethane (DCM), acetonitrile (analytical reagent grade), potassium carbonate, adenine (99.5%), thymine (99%) and uracil (99%) were purchased from Fisher Scientific and used as received. The deuterated chloroform used in ^1H -NMR and ^{13}C -NMR was purchased from Cambridge Isotope Laboratories. Xylene was purchased from BDH Lab Supplies. 12-bromododecan-1-ol was purchased from Manchester Organics. PODMA and DSMA were synthesised as described in Section 2.2.3, Chapter 2.

3.2.2 Apparatus

All reactions were performed under inert atmosphere (nitrogen) using Schlenk techniques.

Differential scanning calorimetry (DSC)

Differential scanning calorimetry was carried out on bulk samples using a Netzsch DSC 200 Phox. This instrument has a heating range of -150 - 600°C . Thermal analyses were conducted over a range of -20 to 70°C . Each sample was heated at a rate of $10^\circ\text{C min}^{-1}$. Each sample was heated and cooled twice with the transition values taken from the second heating run. Each sample was measured against an empty aluminium pan as a reference.

3.2.3 Synthesis of PODMA and PDSMA via ATRP

The reaction of PODMA and DSMA was discussed in Chapter 2, Section 2.2.3. The synthesis of the two homopolymers remained the same.

3.2.4 Synthesis of 9-(4-vinylbenzyl) adenine (VBA)

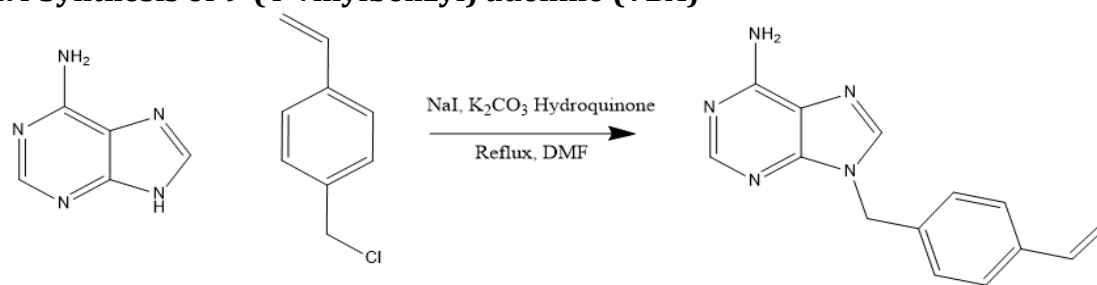


Figure 90 Reaction of 9-(4-vinylbenzyl) adenine VBA.

Method 1 (Antonietti):

Method 1 followed a literature method.¹⁴ A suspension of adenine (6.75 g, 50 mmol), anhydrous potassium carbonate (7.60 g, 55 mmol), NaI (90 mg, 0.6 mmol) and hydroquinone (10 mg 0.09 mmol) were added to a round bottom flask. DMF (100 mL) was added and this was left stirring in nitrogen. 4-Vinylbenzyl chloride (7.1 mL, 50 mmol) was added and reaction mixture was refluxed for 16 hours. The reaction mixture was hot filtered and the solid was washed with hot DMF. Distilled water was added to reaction mixture to precipitate the product. The product was then filtered and dried overnight in a vacuum oven to give a dark brown solid. The final yield was 34%.

Method 2 (Verma):

Method 2 followed a literature method.¹⁵ A round bottom flask was taken and K₂CO₃ (0.61 g, 4.4 mmol) and adenine (0.51g, 3.8 mmol) were added. DMSO (15 mL) was added and reaction mixture was degassed for 1 hour in nitrogen. 4-Vinylbenzyl chloride (0.5 mL, 3.5 mmol) was added slowly and reaction was left for 8 h under nitrogen atmosphere at 30°C. The solvent was evaporated under reduced pressure, and silica gel column chromatography afforded the pure compound as a pale yellow solid. The final yield was 67%.

¹H-NMR (400 Hz, CDCl₃, ppm) δ: 1.79 (broad peak 1H NH₂), 5.21 (d, 1H), 5.29 (s, CH₂), 5.6 (broad peak 1H NH₂), 5.70 (d, 1H), 6.74 (1H HC=CH₂), 7.25 (2H), 7.46 (2H), 7.81 (HC=N), 8.31 (N=CH-N). **¹³C NMR (CDCl₃, ppm) δ:** 47.2, 111.6, 116.2, 127.5, 128.8, 134.2, 136.8, 137.9, 140.2, 148.3, 152.8, 156.2

3.3.5 Synthesis of 1-(4-vinylbenzyl) uracil (VBU)

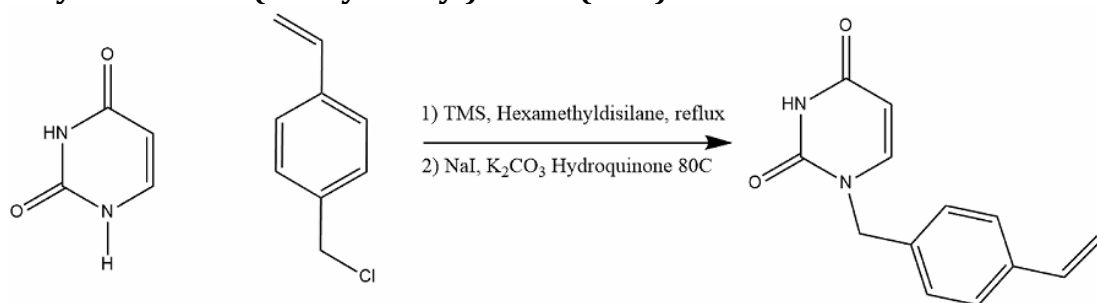


Figure 91 Reaction of 1-(4-vinylbenzyl) uracil VBU.

A literature method was followed for the synthesis of VBU.¹⁴ Uracil (2.25g, 20 mmol) was dissolved in hexamethyldisilane (13mL) in a round bottom flask. Trimethylsilylchloride (1 mL) was added the solution and this was heated under reflux conditions under nitrogen for 24 hours. The excess hexamethyldisilane was distilled off under vacuum and

DMF (10 mL), 4-vinylbenzyl chloride (3 mL, 20 mmol), NaI (30 mg, 0.2 mmol) and hydroquinone (10 ml, 0.09 mmol) were added. The reaction then proceeded at 80°C. After 8 hours the reaction was stopped and allowed to cool to room temperature. Water (150 mL) was then poured into the reaction mixture and after 10 minutes extracted twice with dichloromethane (80 mL). The combined extracts were dried in MgSO₄, filtered and dried in a vacuum oven. The evaporation residue was recrystallised from methanol to give a pale yellow solid. The final yield was 21%.

¹H-NMR (400 Hz, CDCl₃, ppm)δ: 5.30 (d, 1H), 5.76 (s, CH₂), 5.8(1H HC=C), 6.74 (1H HC=CH₂), 7.25 (2H), 7.32 (1H HC=CH-N), 7.46 (2H), 8.51 (1H NH). **¹³C NMR (CDCl₃, ppm) δ:** 52.1, 103.0, 115.1, 126.0, 128.2, 134.8, 135.8, 144.5 150.1 163.4

3.3.6 Synthesis of 1-(4-vinylbenzyl) thymine (VBT)

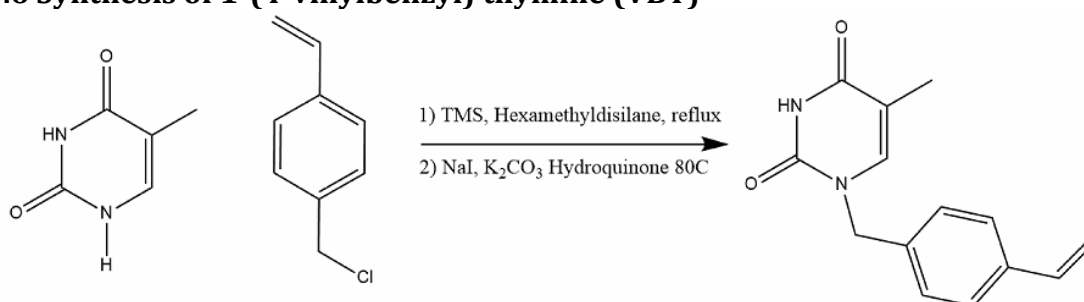


Figure 92 Reaction of 1-(4-vinylbenzyl) thymine VBT.

A literature method¹⁴ was followed for the synthesis of VBT. Thymine (2.50g, 20 mmol) was dissolved in hexamethyldisilane (13mL) in a round bottom flask. Trimethylsilylchloride (1 mL) was added and reaction was reflux under nitrogen for 24 hours. The excess hexamethyldisilane was distilled off under vacuum. The raw silylated thymine was mixed with DMF (10 mL). 4-vinylbenzyl chloride (3 mL, 20 mmol), NaI (30 mg, 0.2 mmol) and hydroquinone (10 ml, 0.09 mmol) was added and reaction proceeded at 80°C for 8 hours. Reaction was stopped, allowed to cool to room temperature and then poured into water (150 mL). After 10 minutes, it extracted twice with dichloromethane (80 mL). The combined extracts were dried in MgSO₄, filtered and dried in a vacuum oven. The evaporation residue was recrystallised from methanol to give a white solid. The final yield was 33%.

¹H-NMR (400 Hz, CDCl₃, ppm)δ: 1.98 (s,3H CH₃), 5.30 (d, 1H), 5.76 (s, CH₂), 5.8(1H HC=C), 6.74 (1H HC=CH₂), 7.25 (2H), 7.32 (1H HC=CH-N), 7.46 (2H), 8.51 (1H NH). **¹³C NMR (CDCl₃, ppm) δ:** 14.0, 52.1, 103.0, 115.1, 126.0, 128.2, 134.8, 135.8, 140.5 150.1 164.4

3.3.7 Synthesis of PODMA-co-PVBA (10 %) via ATRP

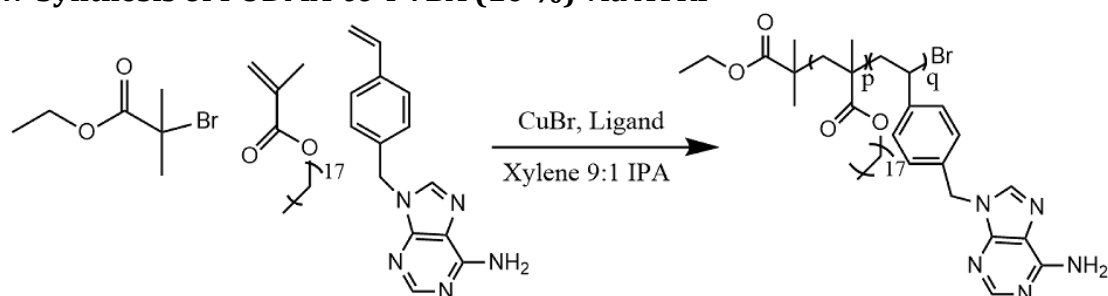


Figure 93 Reaction of PODMAPVBA (10%) via ATRP.

A literature method¹⁶ was adapted for the synthesis of PODMA random copolymer. A typical procedure was as follows. Cu(I)Br (0.017 g, 0.12 mmol) was put into a Schlenk tube with a magnetic stirrer. Ethyl α -bromoisobutyrate (0.023 g, 0.12 mmol) was dissolved in a xylene:IPA mixture (9:1) (4 mL) and added to the Schlenk tube. PMDETA (0.02 g, 0.12 mmol), VBA (0.15g, 10% molar ODMA) and ODMA (2.0 g, 0.006 mol) was added to Schlenk tube which was then sealed and degassed (N_2) for 1 hour. The mixture was then stirred at 95°C for 24 hours under nitrogen. After 24 hours, the reaction was run through alumina column to remove the catalyst and ligand, then half of solvent was evaporated off. The polymer was precipitated out into acetonitrile dropwise at 0°C to give a pale yellow solid. The final yield was 48.5%.

Variations on the above procedure were carried out using CuCl and Me6TREN using the same molar proportions. The random copolymer was characterised by ¹HNMR, ¹³CNMR & GPC.

¹H-NMR (400 Hz, CDCl₃, ppm) δ : 0.80 (triplet, 3H, -(CH₂)₁₇-CH₃), 0.95 (broad peak, 3H, -CH₂-C-CH₃), 1.23 (broad peak, 30H, -(CH₂)₁₄-), 1.72 (broad peak, CH₂(CH₂)₁₄-), 3.85(broad peak, 2H, -COO-CH₂-), 5.26(broad peak Styrene-CH₂-Adenine), 6.98(broad peak (CH)₂(CH)₂), 7.10(broad peak (CH)₂(CH)₂)**¹³C NMR (CDCl₃, ppm) δ :** 14.05, 22.80, 26.08, 28.09, 29.44, 29.86, 31.96, 44.82, 65.0, 168.73, 176.2 GPC M_w 39900, M_n 20600, \bar{D} 1.94

3.3.8 Synthesis of PDSMA-co-PVBT (10 %) via ATRP

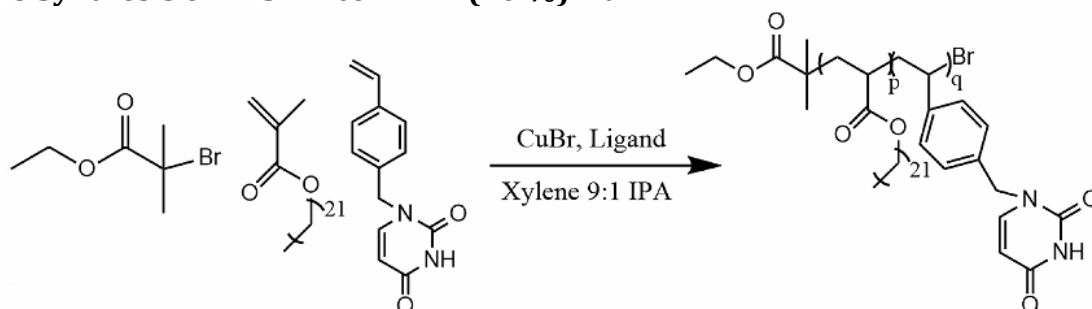


Figure 94 Reaction of PDSMAPVBT (10%) via ATRP.

A literature method was followed for the synthesis of PDSMA random copolymer. Cu(I)Br (0.014 g, 0.10 mmol) was put into a Schlenk tube with a magnetic stirrer. Ethyl α -bromoisobutyrate (0.020 g, 0.10 mmol) was dissolved in xylene:IPA mixture (9:1) (4 mL) and added to the Schlenk tube. PMDETA (0.017 g, 0.10 mmol), VBT (0.125 g, 10% molar DSMA) and DSMA (2.0 g, 0.005 mol) was added to the Schlenk tube which was then

sealed and degassed (N_2) for 1 hour. The mixture was then stirred at $95^\circ C$ for 24 hours under nitrogen. After 24 hours, the reaction was run through alumina column to remove the catalyst and ligand, then half of solvent was evaporated off. The polymer was precipitated out into acetonitrile dropwise at $0^\circ C$ to give a white solid. The final yield was 51%.

Variations on the above procedure were carried out using $CuCl$ and Me_6TREN using the same molar proportions. The random copolymer was characterised by 1H NMR, ^{13}C NMR & GPC.

1H -NMR (400 Hz, $CDCl_3$, ppm) δ : 0.88 (triplet, 3H, $-(CH_2)_{17}-CH_3$), 1.01 (broad peak, 3H, $-CH_2-C-CH_3$), 1.28 (broad peak, 30H, $-(CH_2)_{14}-$), 1.61 (broad peak, $CH_2(CH_2)_{14}-$), 3.92 (broad peak, 2H, $-COO-CH_2-$), 4.73 (broad peak Styrene- CH_2 -Thymine), 6.92 (broad peak $(CH)_2(CH)_2$), 7.04 (broad peak $(CH)_2(CH)_2$) **^{13}C NMR ($CDCl_3$, ppm) δ :** 14.05, 22.80, 26.08, 28.09, 29.44, 29.86, 31.96, 44.82, 65.0, 168.73, 176.2 **GPC** M_w 31900, M_n 22700, \bar{D} 1.41

3.3.9 Attempted synthesis of N,N-bis(pyridine-2-ylmethyl 3-hexoxo-3-oxopropyl) ethane-1,2-diamine (BPED) Ligand

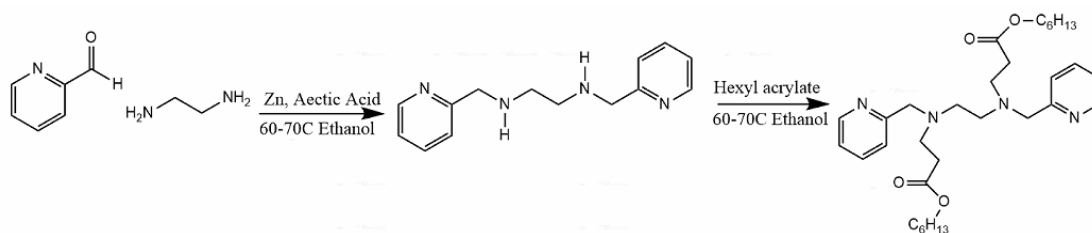


Figure 95 Synthesis of BPED Ligand.

A literature method¹⁷ was followed for the attempted synthesis of BPED ligand. Zinc powder (20.0 g) was left stirring for 2 hours in a mixture of ethylenediamine (3.0 g, 0.050 mol) in ethanol (100 mL) and glacial acetic acid (20 mL) at $70^\circ C$. 2-Pyridinecarboxaldehyde (10.7 g, 0.10 mol) dissolved in ethanol (50 mL) was added to the reaction mixture. More zinc powder and glacial acetic acid was added until a further 70.0g of each had been added at intervals. The reaction was left for 24 hours. The mixture was then allowed to stand at room temperature overnight and then was filtered. The filtrate was evaporated under vacuum to yield a syrupy residue. Sodium hydroxide was then added. It was at this point that the expected brown oil failed to separate and the reaction was deemed unsuccessful.

3.3.10 Synthesis of PEO-*b*-poly(DSMA-co-VBT) (10 %) via ATRP

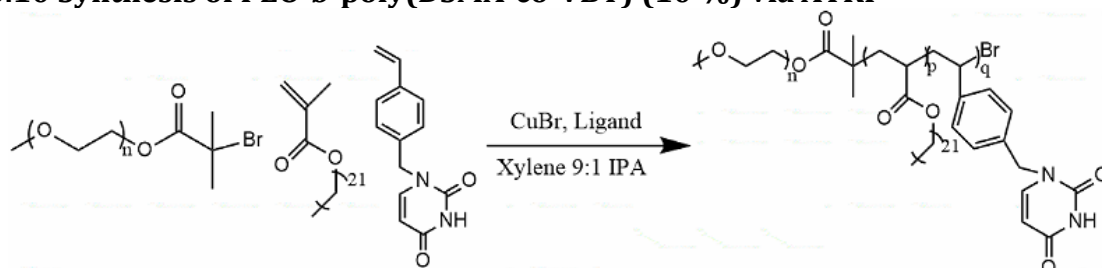


Figure 96 Reaction of PEO-*b*-poly(DSMA-co-PVBT) (10%) via ATRP.

A literature method was adapted for the synthesis of PEO-*b*-poly(DSMA-*co*-PVBT). A typical procedure was as follows. Cu(I)Cl (0.0138g, 0.14 mmol) was put into a Schlenk tube with a magnetic stirrer. Macroinitiator (0.4 g, 0.14 mmol) was dissolved in a xylene:IPA mixture (9:1) (4 mL) and added to the Schlenk tube. Me₆TREN (0.0323g, 0.14 mmol), VBT (0.111 g, 10% molar DSMA) and DSMA (1.82 g, 0.0046 mol) was added to Schlenk tube which was then sealed and degassed (N₂) for 1 hour. The mixture was then stirred at 95°C for 24 hours under nitrogen. After 24 hours, the reaction was run through alumina column to remove the catalyst and ligand, then half of solvent was evaporated off. The polymer was precipitated out into acetonitrile dropwise at 0°C to give a pale white solid. The final yield was 57%.

¹H-NMR (400 Hz, CDCl₃, ppm)δ: 0.88 (triplet, 3H, -(CH₂)₁₇-CH₃), 1.00 (broad peak, 3H, -CH₂-C-CH₃), 1.29 (broad peak, 30H, -(CH₂)₁₄-), 1.54 (broad peak, CH₂(CH₂)₁₄-), 3.30 (Singlet, 3H, CH₃O-), 3.58 (triplet, 4H, -O-CH₂CH₂-O), 3.85(broad peak, 2H, -COO-CH₂-), -) 4.73(broad peak Styrene-CH₂-Thymine), 6.92(broad peak (CH)₂(CH)₂), 7.03(broad peak (CH)₂(CH)₂). **¹³C NMR (CDCl₃, ppm) δ:** 14.05, 22.80, 26.08, 28.09, 29.44, 29.86, 31.96, 44.82, 45.14, 65.0, 70.56, 168.73, 176.2 **GPC** M_w 49000, M_n 25500, Đ 1.92

3.3.11 Synthesis of PEO-*b*-poly(ODMA-*co*-PVBA) (10 %) via ATRP

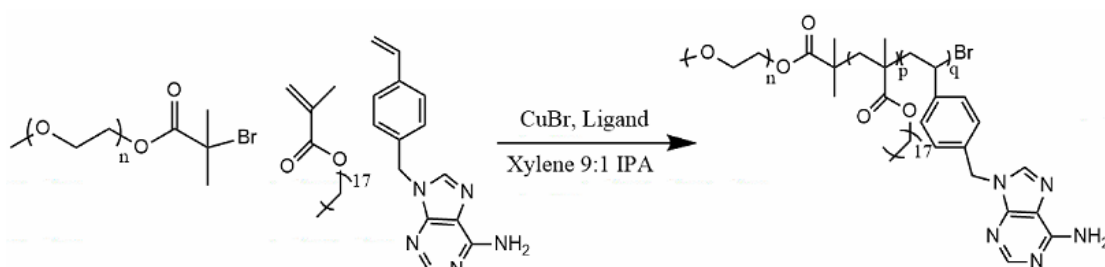


Figure 97 Reaction of PEO-*b*-poly(ODMA-*co*-PVBA) (10%) via ATRP.

A literature method was adapted for the synthesis of PEO-*b*-poly(ODMA-*co*-PVBA). A typical procedure was as follows. Cu(I)Cl (0.0138g, 0.14 mmol) was put into a Schlenk tube with a magnetic stirrer. Macroinitiator (0.4 g, 0.14 mmol) was dissolved in a xylene:IPA mixture (9:1) (4 mL) and added to the Schlenk tube. Me₆TREN (0.0323g, 0.14 mmol), VBA (0.083 g, 10% molar ODMA) and ODMA (1.112 g, 0.0033 mol) was added to Schlenk tube which was then sealed and degassed (N₂) for 1 hour. The mixture was then stirred at 95°C for 24 hours under nitrogen. After 24 hours, the reaction was run through alumina column to remove the catalyst and ligand, then half of solvent was evaporated off. The polymer was precipitated out into acetonitrile dropwise at 0°C to give a pale white solid. The final yield was 52%.

¹H-NMR (400 Hz, CDCl₃, ppm)δ: 0.88 (triplet, 3H, -(CH₂)₁₇-CH₃), 1.00 (broad peak, 3H, -CH₂-C-CH₃), 1.29 (broad peak, 30H, -(CH₂)₁₄-), 1.54 (broad peak, CH₂(CH₂)₁₄-), 3.30 (Singlet, 3H, CH₃O-), 3.58 (triplet, 4H, -O-CH₂CH₂-O), 3.85(broad peak, 2H, -COO-CH₂-), -) 5.35(broad peak Styrene-CH₂-Adenine), 7.13(broad peak (CH)₂(CH)₂), 7.16(broad peak (CH)₂(CH)₂). **¹³C NMR (CDCl₃, ppm) δ:** 14.05, 22.80, 26.08, 28.09, 29.44, 29.86, 31.96, 44.82, 45.14, 65.0, 70.56, 168.73, 176.2 **GPC** M_w 32100, M_n 18000, Đ 1.78

3.3.12 Synthesis of 12-bromododecyl methacrylate

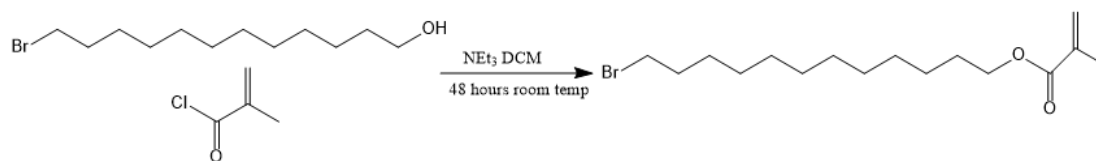


Figure 98 Reaction of 12-bromododecyl methacrylate.

A literature method was adapted for the synthesis of 12-bromododecyl methacrylate.¹⁸ 12-Bromododecan-1-ol (3.5g, 0.0135 mol) and triethylamine (2.0g, 0.0198 mol) were dissolved in DCM (80 mL) and added to a round bottom flask. Methacryloyl chloride (1.52g, 0.0145 mol) was added dropwise at 0°C. The reaction mixture was allowed to warm to room temperature and left for 24 hours. After 24 hours, methanol (10 mL) was added and reaction stirred for 30 mins. Sodium hydrogen carbonate (25 mL) was added and solution was washed twice with water (2 x 20 mL). The organic layer was taken and dried over anhydrous magnesium sulphate for 1 hour and then filtered and vacuumed down to give an orange oil. This was further purified by column chromatography (10% EtOAc/pet ether) to give a colourless oil. The final yield was 55%.

¹H-NMR (400 Hz, CDCl₃, ppm)δ: δ 6.04 (s, 1H, O₂C-(CH₂)₁₁(CH₃)=CHB), 5.47 (s, 1H, O₂C-(CH₂)₁₁(CH₃)=CHA), 4.07 (t, 2H, -O-CH₂-), 3.34 (t, 2H, Br-CH₂-), 1.86 (s, 3H, O₂C-C(CH₃)=CH₂), 1.76(t, 2H, Br-CH₂-CH₂), 1.61 (t, 2H, -O-CH₂-CH₂), 1.48 (t, 2H, -O-CH₂-CH₂-CH₂), 1.22 (quintet, 2H, -CH₂-CH₂-CH₂-), **¹³C NMR (CDCl₃, ppm) δ:** 18.3, 22.2, 24.8, 26.1, 28.2, 28.3, 28.9, 29.5, 32.9, 34.1, 65.0, 125.2, 136.6, 167.6

3.3.13 Synthesis of 12-(thymin-1-yl)dodecyl methacrylate (TDM)

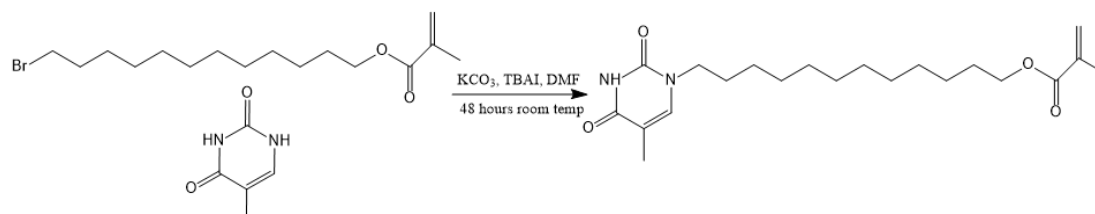


Figure 99 Reaction of 12-(thymin-1-yl)dodecyl methacrylate.

A literature method¹⁸ was adapted for the synthesis of 12-(thymin-1-yl)dodecyl methacrylate. Thymine (0.895g, 0.0071 mol) was dissolved in DMF (50 mL) and potassium carbonate (0.99g, 0.0071 mol) was added followed by TBAI (0.165g, 0.45mmol). 12-Bromododecyl methacrylate (1.01g, 0.0027 mol) was added dropwise to this mixture with stirring at 0°C. The reaction was stirred at room temperature for 2 days. Reaction mixture was filtered and concentrated in vacuo. The resulting solid was extracted by DCM. This was purified by column chromatography (10% MeOH in DCM) to give a yellow solid. The final yield was 28%.

3.3.14 Synthesis of 12-(adenin-9-yl)dodecyl methacrylate (ADM)

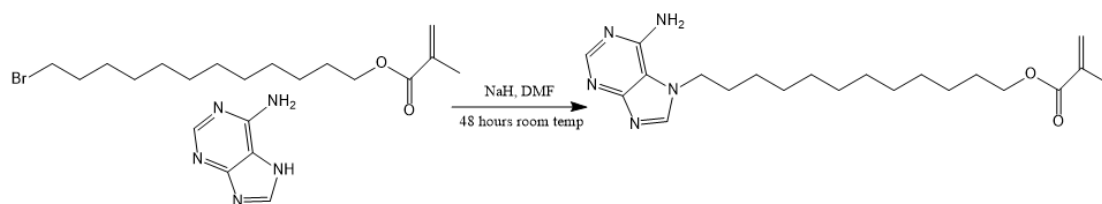


Figure 100 Reaction of 12-(adenin-9-yl)dodecyl methacrylate.

A literature method was adapted for the synthesis of 12-(adenin-9-yl)dodecyl methacrylate. Solution of adenine (0.5 g, 0.0037 mol) was dissolved in DMF (50 mL). Sodium hydride (0.262g, 0.012 mol) was added slowly and left for 1 hour until no more gas was produced. 12-bromododecyl methacrylate (0.992g, 0.0027 mol) was added dropwise at 0°C. The reaction was allowed to proceed at room temperature for 2 days. Reaction was stopped by adding saturated NH₄Cl and left for 30 minutes. The solution was filtered and concentrated in vacuo. The resulting solid was extracted by DCM. Column chromatography (10% MeOH in DCM) was attempted but could not isolate final product. ¹HNMR of the reaction mixture suggested that 12-(adenin-9-yl)dodecyl methacrylate was present in a small quantity.

3.3.15 Synthesis of 2-(2-bromoacetyl) ethyl methacrylate

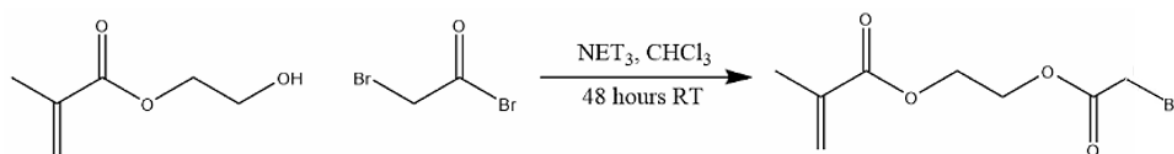


Figure 101 Reaction of 2-(2-bromoacetyl) ethyl methacrylate.

A literature method¹⁹ was followed for the attempted synthesis of 2-(2-bromoacetyl) ethyl methacrylate. Hydroxyethylmethacrylate (HEMA) (13 g, 0.1 mol) and trimethylamine (TEA) (15 mL, 0.107 mol) were dissolved in chloroform (300 mL) and added to round bottom flask. Bromoacetyl chloride (8.3 mL, 0.1 mol) was added dropwise at 0°C. The reaction mixture was then left for 48 hours at room temperature. After 48 hours, the unreacted bromoacetyl chloride was quenched by the addition of methanol (5 mL). The solution was left to stir for 30 minutes where it was poured into saturated NaHCO₃ (100 mL). The reaction mixture was washed twice with water (2 x 100 mL). The organic layer was collected and dried with anhydrous MgSO₄, filtered and concentrated to give a brown oil. The product was further purified by column chromatography with 20:80 ethyl acetate:pet ether mixture to give a colourless oil. The final yield was 40%.

¹H-NMR (400 Hz, CDCl₃, ppm)δ: δ 6.12 (q, 1H, OOC-(CH₃)C=CHA), 5.60 (s, 1H OOC-(CH₃)C=CHB), 4.47 (2H, C=CCOO-CH₂-CH₂), 3.87 (2H, C=CCOO-CH₂-CH₂), 4.10 (s, 2H, Br-CH₂-), 1.95 (3H, OOC-C(CH₃)=CH₂), ¹³C NMR (CDCl₃, ppm) δ 19.1, 44.2, 62.7, 63.5, 119.7, 126.5, 137.0, 141.7, 150.3, 153.2, 166.9, 167.6

3.3.16 Synthesis of 2-(2-(thymine-1-yl)acetoxy) ethyl methacrylate (TMA)

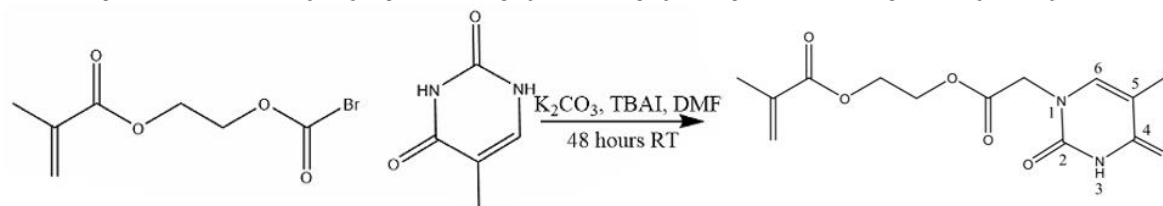


Figure 102 Reaction of 2-(2-(thymine-1-yl)acetoxy) ethyl methacrylate (TMA).

A literature method¹⁹ was followed for the attempted synthesis of 2-(2-(thymine-1-yl)acetoxy) ethyl methacrylate (TMA). Thymine (2 g, 14.2 mmol), anhydrous potassium carbonate (2.21 g, 14.2 mmol) was dissolved in dry DMF (100 mL). This was followed by the addition of TBAI (0.33 g, 0.9 mmol). The reaction mixture was then cooled to 0°C and 2-(2-bromoacetoxy) ethyl methacrylate (2g, 8 mmol) was added dropwise. The reaction was then allowed to proceed at room temperature for 2 days. After 2 days the reaction mixture was filtered and concentrated in vacuo. The resulting solid was extracted by DCM. The product was further purified by column chromatography with 10:90 $CH_3OH:DCM$ mixture to give a colourless oil. The final yield was 34%.

¹H-NMR (400 Hz, $CDCl_3$, ppm)δ: 8.56 (s, 1H pyrimidine NH), 6.95 (d, 1H, pyrimidine NH_2), 6.18 (q, 1H $CH_A=C(CH_3)-COO$), 5.68 (q, 1H $CH_B=C(CH_3)-COO$), 4.58 (s, 2H $OOCH_2$ -purine), 4.48 (s, 2H, $COO-CH_2-CH_2$), 4.41 (q, 2H, $COO-CH_2-CH_2$), 1.86 (t, 3H $OOCH_2-C(CH_3)=CH_2$, **¹³C NMR ($CDCl_3$, ppm) δ** 12.0, 18.3, 48.5, 62.0, 63.9, 111.4, 126.4, 135.8, 140.0, 150.5, 167.1, 167.4

3.3.17 Synthesis of 2-(2-(adenine-9-yl)acetoxy) ethyl methacrylate (AMA)

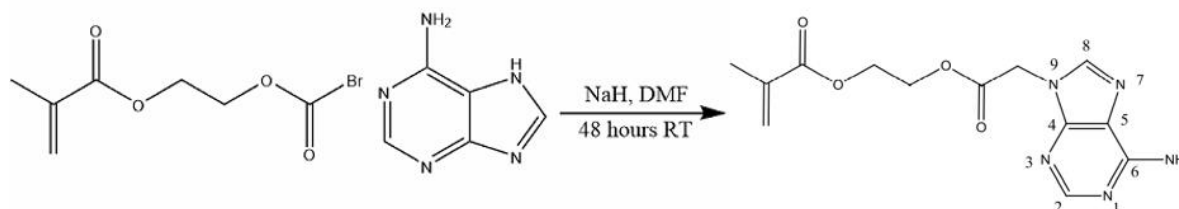


Figure 103 Reaction of 2-(2-(adenine-9-yl)acetoxy) ethyl methacrylate (AMA).

A literature method was followed for the attempted synthesis of 2-(2-(adenine-9-yl)acetoxy) ethyl methacrylate (AMA). Adenine (2.6 g, 19.2 mmol) and NaH (0.764 g, 19.2 mmol) was added to dry DMF (125 mL). The mixture was stirred for 1 hour until no more gas was produced. The reaction mixture was placed in an ice bath and 2-(2-bromoacetoxy) ethyl methacrylate (4 g, 15.9 mmol) was added dropwise at 0°C. The reaction was allowed to proceed room temperature for 2 days. The reaction was then quenched using saturated aqueous NH_4Cl (5 mL). The reaction mixture was filtered and concentrated in vacuo. The solid was extracted by dichloromethane (DCM) and concentrated. The product was further purified by column chromatography with 10:90 $CH_3OH:DCM$ mixture to give a colourless oil. The final yield was 35%.

¹H-NMR (400 Hz, $CDCl_3$, ppm)δ: 8.10 (s, 1H), 8.31 (s, 1H), 6.95 (s, 2H, NH_2), 6.18 (q, 1H $CH_A=C(CH_3)-COO$), 5.68 (q, 1H $CH_B=C(CH_3)-COO$), 5.10 (s, 2H $OOCH_2$ -purine), 4.54 (q, 2H, $COO-CH_2-CH_2$), 4.41 (q, 2H, $COO-CH_2-CH_2$), 1.86 (t, 3H $OOCH_2-C(CH_3)=CH_2$, **¹³C NMR**

(CDCl₃, ppm) δ 168.4, 166.8, 156.4, 153.1, 150.2, 141.6, 135.9, 126.7, 118.7, 63.5, 62.7, 44.3, 18.3

3.4 Results and Discussion

3.4.1 Synthesis of homopolymers

The same homopolymers (PODMA & PDMSA) as made in Chapter 2 were used for Chapter 3. SEC was used to calculate the degree of polymerisation of the homopolymers due to signals overlapping in the ¹HNMR spectra. The SEC data is provided in Table 16.

Table 16 Molecular weight parameters of homo polymers determined by SEC.

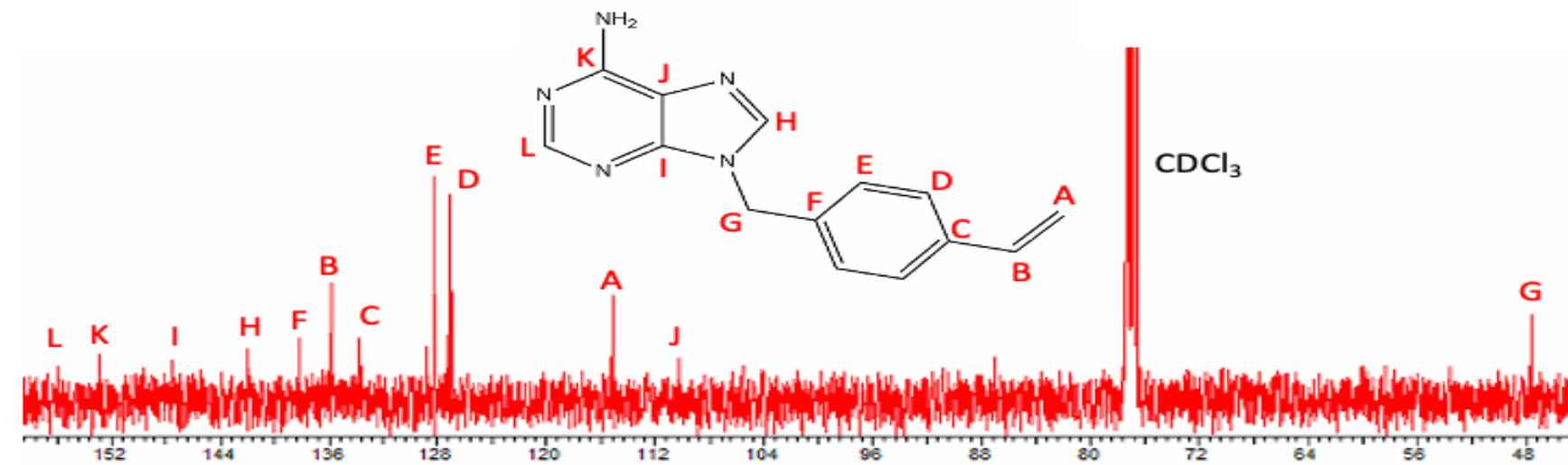
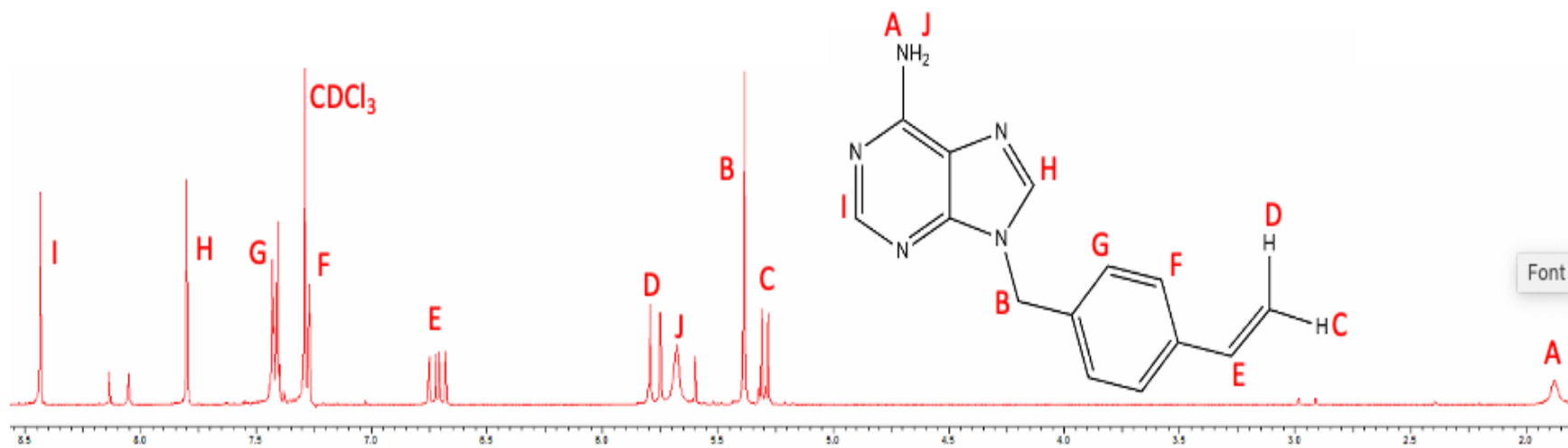
Structure	Dp Targeted	Dp Achieved	M _n GPC	M _w GPC	Đ
PODMA	50	80	27200	42000	1.54
PDSMA	50	83	32700	49800	1.52

3.4.2 Synthesis of styrene-based nucleobase monomers

The desired hydrogen bond interaction which could influence polymer mixing, will only occur between adenine-thymine or adenine-uracil. It was decided that VBA, VBT and VBU would all be made to determine which nucleobase monomers gave the best yields. The synthetic method first followed for the nucleobase monomers was taken from the Antonietti paper and involved a reflux step. A brown solid was obtained which was a different colour to the white solid obtained in the paper. The yields of all the nucleobase monomers were very low; VBA 34%, VBT 33% & VBU 21%. This is a likely cause of the undesired side reactions which caused the percentage yield to be lower than expected.

It was decided at this point that work would proceed using just VBA and VBT as these achieved the highest yields. However, these yields were still very low and a second literature method¹⁵ was found where higher yields were quoted for VBA. The main difference with this method is that there is no reflux step involved and the reaction is kept below 35°C to ensure that the VBA does not polymerise before using it in the future ATRP reaction with the methacrylate monomers. As the temperature is kept below 35°C there is no longer need for the hydroquinone which acts as an inhibitor in the previous method. This improved the percentage yield from 34% to 67%. There was a noticeable difference in colour with the products with the alternative method giving a much whiter product compared to a slight brown seen previously.

NMR confirmed that the synthesis of the nucleobase monomers (VBA, VBT and VBU) had been successfully made are shown in Figures 104-109.



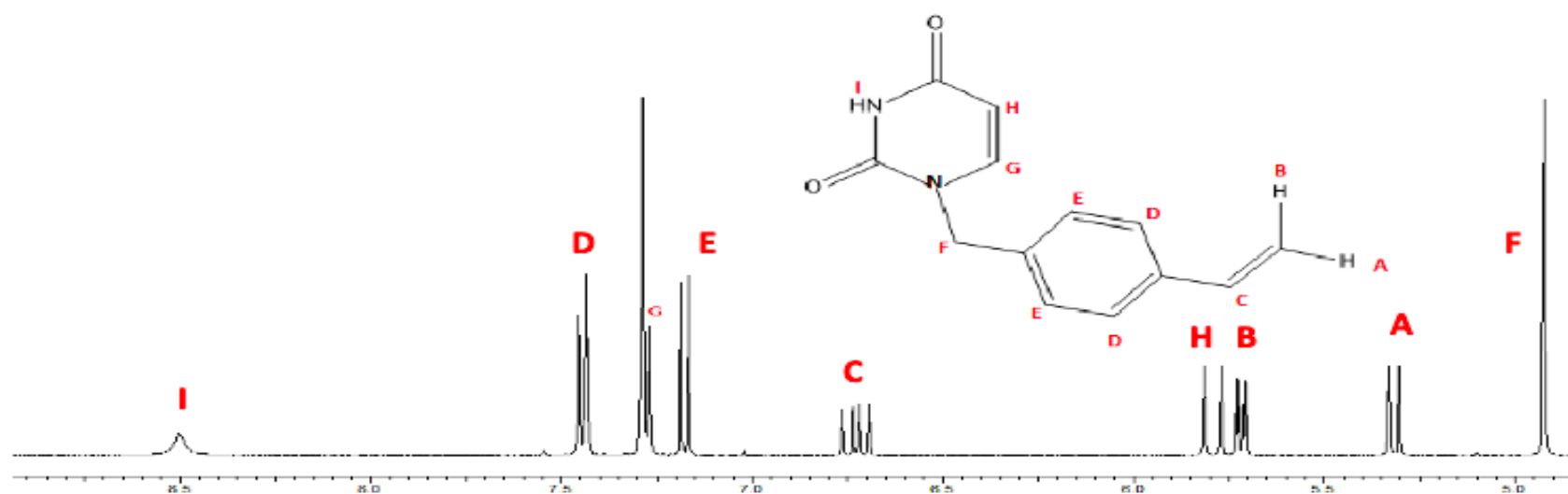


Figure 106 $^1\text{H NMR}$ of 1-(4-vinylbenzyl) uracil VBU in CDCl_3 .

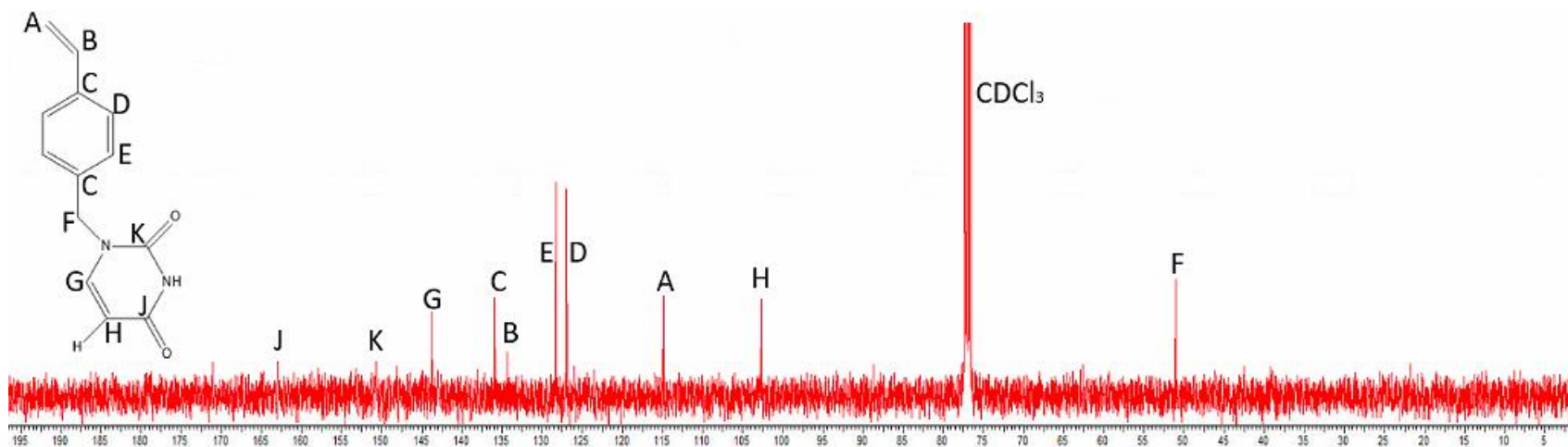
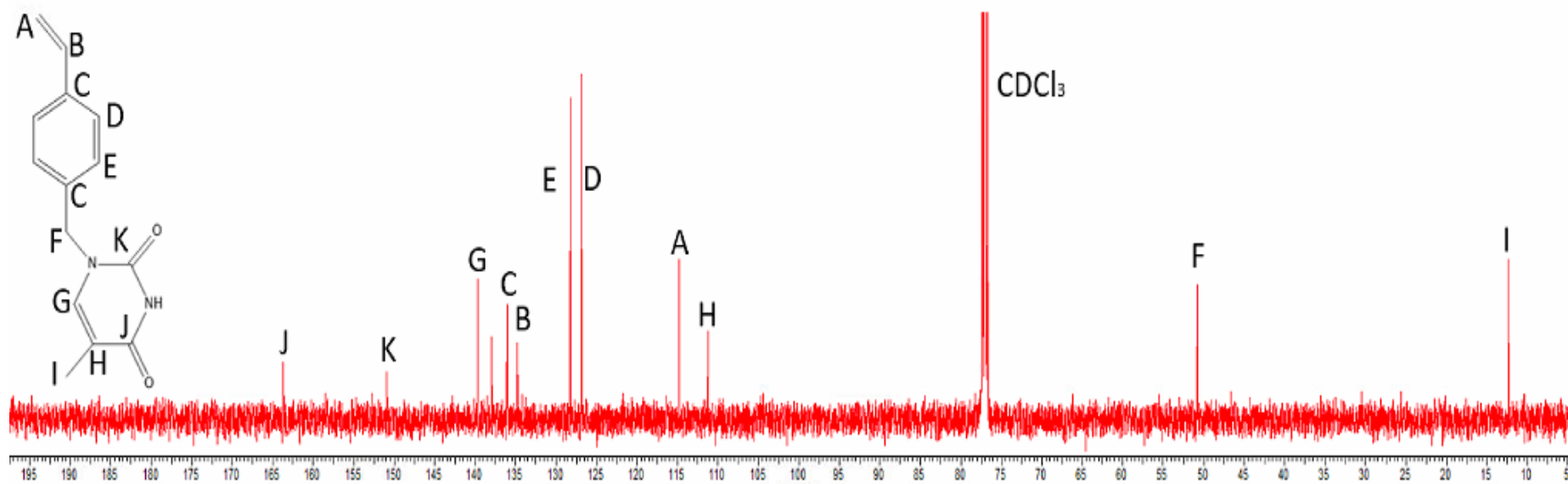
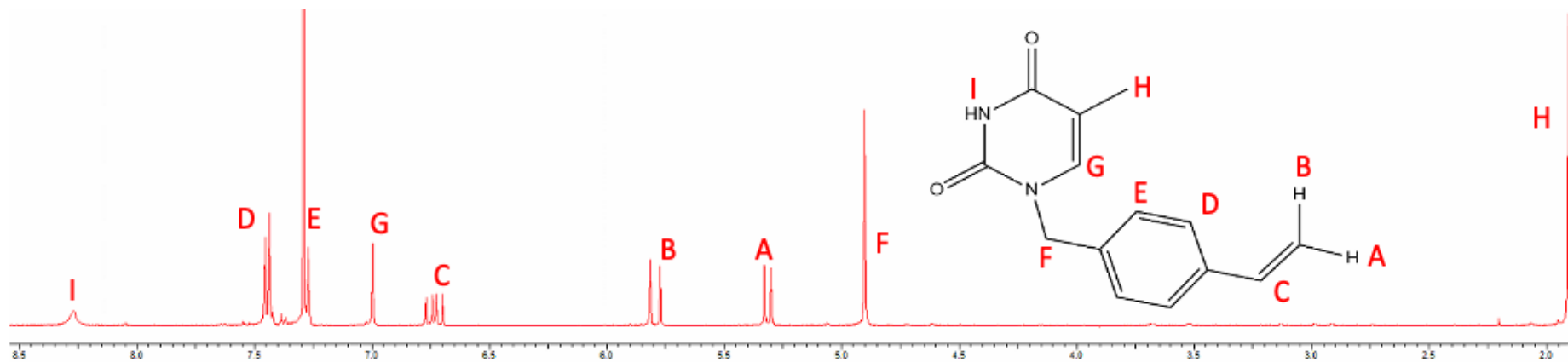


Figure 107 $^{13}\text{C NMR}$ of 1-(4-vinylbenzyl) uracil VBU in CDCl_3 .



3.4.3 Development of reactions conditions for ATRP reaction with nucleobase monomers

Effect of Solvent

Chapter 2 previously used a xylene and IPA 9:1 mixture to carry out ATRP reactions. Using this solvent system for the homopolymers and block copolymers in Chapter 2 showed a high NMR conversion indicating that monomer had converted into polymer efficiently. For this reason, a xylene and IPA 9:1 mixture was used when a ATRP reaction was carried out with the nucleobase monomers (VBT & VBA) with the methacrylate monomers (ODMA & DSMA). ODMA was consistently copolymerised with VBA and DSMA was consistently copolymerised with VBT.

Random copolymers of PODMA-*co*-PVBA and PDSMA-*co*-PVBT were synthesised in a solvent mix of xylene and IPA (9:1 by volume). A 10% molar ratio of nucleobase to methacrylate monomer was used in both cases. When the ATRP reaction was carried out similar results were seen for both nucleobase monomers. The NMR conversion of the methacrylate monomer was <96% and this was expected from the results seen in Chapter 2. However, the NMR conversion of VBA was 23.6% and VBT was 22.6% indicating that very little nucleobase became incorporated within the polymer backbone. A 10 mol% inclusion of both was targeted and only 2 mol% inclusion was obtained.

The polymerisations were repeated several times and the same results obtained (around 2% incorporation of nucleobase monomer), it was hypothesised that the VBA or VBT did not dissolve sufficiently in the xylene due to the hydrophilicity of VBA and VBT is very hydrophilic and dissolves best in polar solvents such as IPA or DMSO. A series of experiments were carried out to assess what solvent system would be best for the ATRP reaction. This was done by taking different solvents at room temperature and seeing if ODMA and VBA dissolved in them.

Table 17 Different solvent system selected to dissolve ODMA & VBA.

Solvent System	Miscibility	
	ODMA	VBA
Xylene 50:50 IPA	Immiscible	Partially
Xylene 50:50 Butanone	Miscible	Immiscible
Xylene 50:50 Ethanol	Miscible	Immiscible
Xylene 50:50 Toluene	Miscible	Immiscible
Xylene 50:50 DMSO	Partially	Miscible
Toluene 50:50 DMSO	Immiscible	Partially
Toluene 50:50 DMF	Immiscible	Partially

From the series of experiment to find a suitable solvent system that works; Xylene 50:50 DMSO & DMF were used as the solvent systems in ATRP reactions using VBA and VBT. Xylene 50:50 DMSO was used as this solvent system seemed to dissolve both VBA & monomer sufficiently and DMF as a literature paper was found to

successfully polymerise a shorter chain methacrylate monomer with VBA & VBT in DMF.

Table 18 Conversion of polymer used for different solvents used in ATRP. All reactions used CuBr as the catalyst, PMDETA as the ligand and performed at 95°C & Targeted 10% molar of VBA or VBT.

Structure	Reaction Solvent	Temperature °C	Time (hrs)	XMA Conversion ^a (%)	VBA/ VBT Conversion ^a (%)
PODMA	Xylene 9:1 IPA	95	24	96.2	-
PDSMA	Xylene 9:1 IPA	95	24	98.0	-
PODMA PVBA	Xylene 9:1 IPA	95	36	98.0	23.8
PDSMA PVBT	Xylene 9:1 IPA	95	36	98.0	22.6
PODMA	Xylene 1:1 DMSO	95	36	97.1	-
PODMA PVBA	Xylene 1:1 DMSO	95	36	14.0	80.0
PDSMA PVBT	Xylene 1:1 DMSO	95	36	16.0	80.0
PODMA	DMF	95	36	96.2	-
PODMA PVBA	DMF	95	36	16.0	0.00

a. Calculated from ¹H NMR

All ATRP reactions were successful on the homopolymers in the three solvent systems selected. A high conversion of methacrylate monomer to polymer was achieved. When the VBA and VBT was introduced, there were surprising results. In xylene 9:1 IPA, 23.8 and 22.6 conversion of VBA & VBT bonded to the backbone respectively. In the xylene 1:1 DMSO 80% of VBA or VBT bonded to the backbone but only a 15% methacrylate conversion was achieved. This was due to the solvent system only partially dissolving the methacrylate monomer. The reaction with DMF was unsuccessful as neither the methacrylate nor VBA polymerised when targeting the random copolymer. The ATRP with just the homopolymer in DMF was successful but it suggested that when the VBA was added it inhibited the polymerisation from happening. As the best results were still the xylene:IPA mixture, this led to the effect of ligand from being tested.

Effect of Ligand

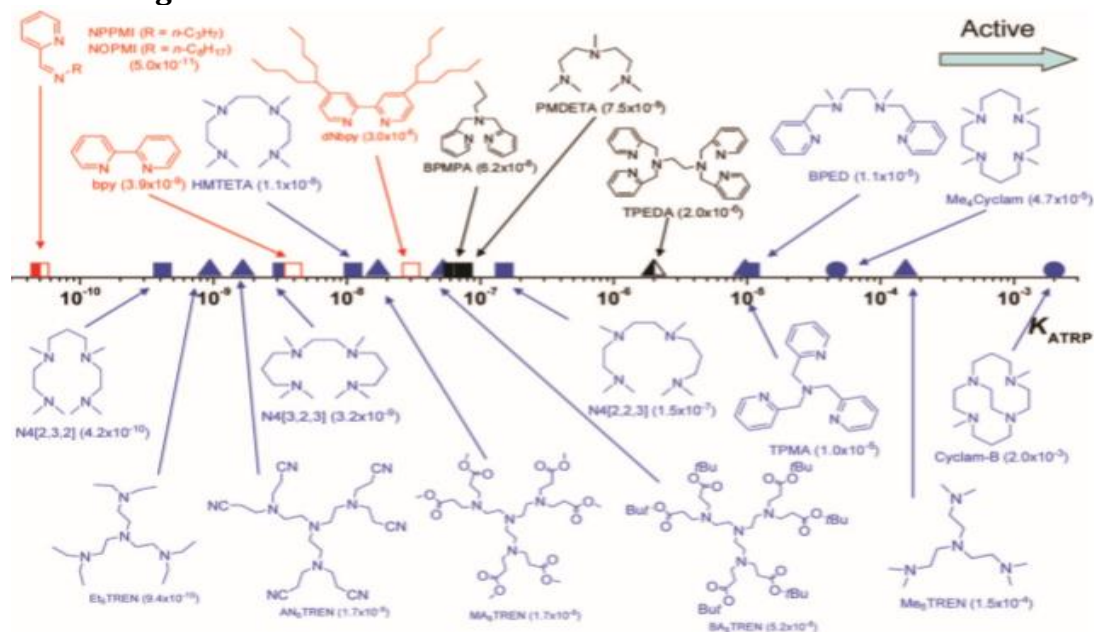


Figure 110 Different ligands available for ATRP.²⁰

For all of the ATRP reactions described above, PMDETA was used as the ligand with CuBr. To improve the reactivity of VBA and VBT it was decided to investigate different ligand systems in the polymerisation. A literature method²¹ was found where *N,N'*-bis(pyridin-2-ylmethyl-3-hexoxo-3-oxopropyl)ethane-1,2-diamine (BPED) was a new tetradentate ligand which could be used in ATRP. A second literature paper²² showed how BPED could be used with VBT, VBU & VBA to achieve high conversions with dodecyl methacrylate (DMA). As BPED is not commercially available, the synthesis of BPED was attempted and was the reason for the literature method described above. Unfortunately, all attempts of the synthesis of BPED were unsuccessful. This meant tris[2-(dimethylamino)ethyl]amine (Me₆TREN) and 2,2'-bipyridine (bpy) were selected instead. The reason for this was to select a ligand that had a higher K_{ATRP} value than PMDETA and one that had a lower value. The conversions from these reactions are shown in Table 19.

Table 19 Selection of different ligands used in ATRP reactions with VBA & VBT. All reactions used CuBr as the catalyst, Xylene 9:1 IPA as solvent system and performed at 95°C for 36 hours & Targeted 10% molar of VBA.

Structure	Ligand	Reaction Solvent	Time (hrs)	XMA Conversion ^a (%)	VBA/ VBT Conversion ^a (%)
PODMA	PMDETA	Xylene 9:1 IPA	36	96.2	-
PODMA PVBA	PMDETA	Xylene 9:1 IPA	36	98.0	23.8
PODMA	Bpy	Xylene 9:1 IPA	36	97.3	-
PODMA PVBA	Bpy	Xylene 9:1 IPA	36	89.3	22.6
PODMA	Me ₆ TREN	Xylene 9:1 IPA	36	99.2	-
PODMA PVBA	Me ₆ TREN	Xylene 9:1 IPA	36	98.0	80.3

a. Calculated from ¹H-NMR

All three ligands have previously been used in ATRP reactions. All three ligands with the homopolymer gave high conversions which meant the reaction was successful. When the bpy ligand was introduced with the VBA a similar conversion of >20% was achieved suggesting that the bpy was equal to PMDETA in relation to polymerising the VBA onto the backbone. When the Me₆TREN was introduced, the highest conversion of 80% was achieved for the VBA. These results suggest that the ligand plays a vital role in the polymerisation of the methacrylate monomer and VBA.

Effect of Catalysts

CuBr has been the catalyst selected previously for the ATRP reactions in this and previous chapters. It was demonstrated that when CuBr was used it allowed block copolymers to be synthesised with accurate molecular weights with low PDI within 24 hours. This part of the chapter investigates the impact that CuCl has as a catalyst when used instead of CuBr. The reaction is expected to proceed slower as the chlorine group is a poorer leaving group compared to the bromine atom.

Two ligands (PMDETA & Me₆TREN) were used in the ATRP reactions which aimed to add 10 mol% of the nucleobase monomer relative to the methacrylate monomer into the copolymer. Results already tested in this chapter shows that changing the ligand has an effect on the VBA/ VBT conversion. Thus both PMDETA and Me₆TREN were studied with CuCl.

Table 20 Conversion of methacrylate & VBT/VBA from different ATRP reactions. All reactions used Xylene 9:1 IPA as the solvent system. Targeted 10% molar of nucleobase to methacrylate.

Structure	Ligand	Catalyst	XMA Conversion (%)	VBA/ VBT Conversion (%)	Mol% inclusion of nucleobase
PODMA	PMDETA	CuBr	96.2	-	-
PDSMA	PMDETA	CuBr	98.0	-	-
PODMA	PMDETA	CuCl	96.2	-	-
PDSMA	PMDETA	CuCl	89.3	-	-
PODMA-co-PVBA	PMDETA	CuBr	98.0	23.8	2.4
PDSMA-co- PVBT	PMDETA	CuBr	98.0	22.6	2.3
PODMA-co- PVBA	PMDETA	CuCl	99.4	23.7	2.4
PDSMA-co- PVBT	PMDETA	CuCl	98.1	24.1	2.4
PODMA-co- PVBA	Me ₆ TREN	CuBr	98.0	80.3	8.0
PDSMA-co- PVBT	Me ₆ TREN	CuBr	94.8	80.8	8.1
PODMA-co- PVBA	Me ₆ TREN	CuCl	94.7	80.1	8.0
PDSMA-co- PVBT	Me ₆ TREN	CuCl	89.7	81.1	8.1

SEC results (Figure 111) were carried out on all homopolymers and random copolymers with the VBT & VBA derivatives first using CuBr as the catalyst.

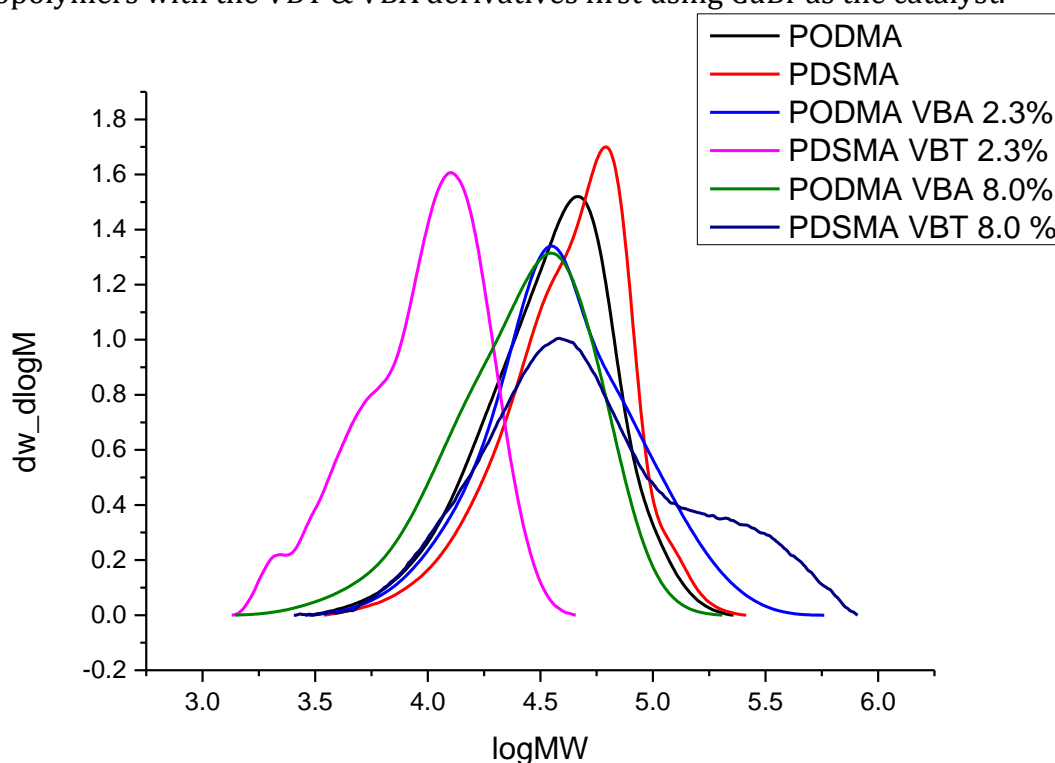


Figure 111 SEC data obtained from polymers made by ATRP which used CuBr as catalyst.

In all cases a DP of 50 was targeted. Although high conversions of methacrylate monomer were obtained along with some conversion of VBA/VBT from the ATRP reactions, the molecular weight varied greatly from each reaction. Results suggest that there was little control on the molecular weight and that VBT was much more challenging in getting the polymer to polymerise at the desired molecular weight. This led to the same reactions being repeated using CuCl.

Table 21 showed the molecular weight and dispersity indices of the polymers made by ATRP using CuBr catalyst. Adding VBT or VBA to the ATRP reaction seemed to increase the polydispersity index. All GPC traces showed a broad peak but in the cases of the VBA/ VBT derivatives this number seemed to increase from 1.5 to 1.7. When the PDI increases, it suggests that there is a range of different molecular weights which is not desirable for polymer chemistry. The causes of this is when polymers terminate too quickly before they have chance to grow or if excess starting material is still present.

Table 21 SEC data for homopolymers and random copolymers synthesised with VBA or VBT using CuBr.

Structure	Dp	Mn	Mw	PDI
PODMA	80	27200	42000	1.54
PDSMA	83	32700	49800	1.52
PODMA-co-PVBA 2.3%	88	29900	53000	1.77
PDSMA-co-PVBT 2.3%	19	7500	11200	1.49
PODMA-co-PVBA 8.0%	76	29900	53000	1.77
PDSMA-co-PVBT 8.0%	58	19500	33400	1.71

The ATRP reactions were repeated with CuCl to slow down the polymerisation rate determining step. This meant that the reaction proceeded much more slowly allowing for better control of the molecular weight. Figure 112 shows the SEC traces overlaid.

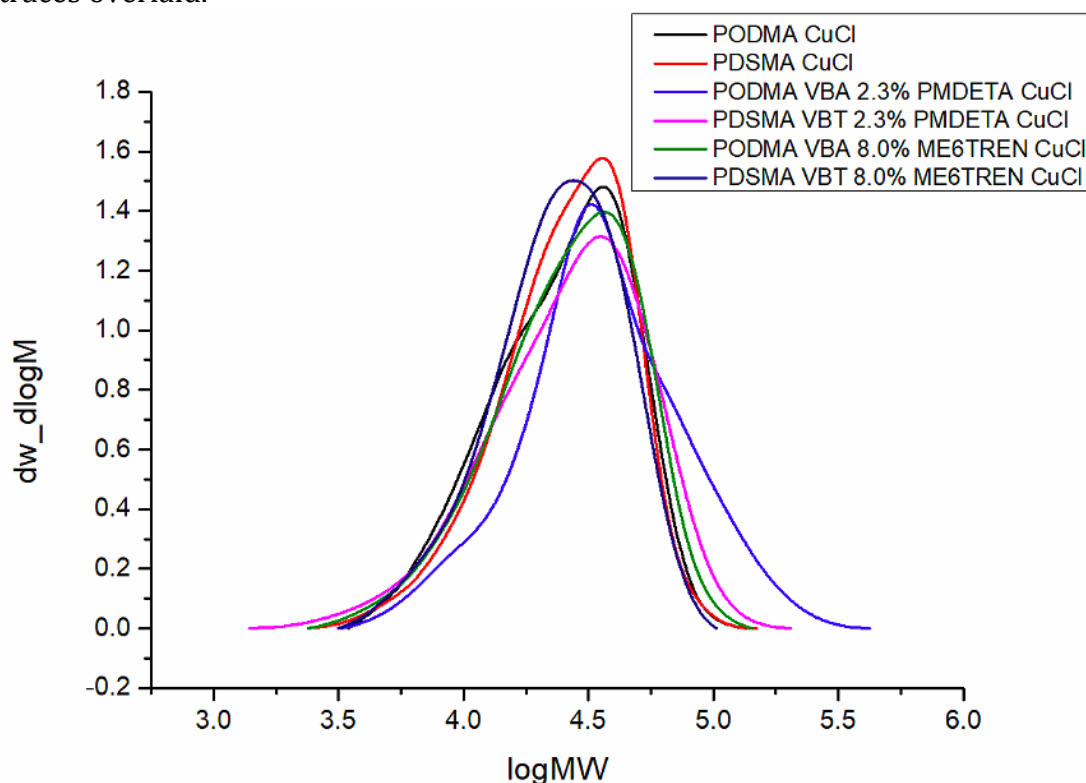


Figure 69 SEC data obtained from polymers made by ATRP which used CuCl as catalyst.

For all the reactions that studied the effect of using different ATRP catalysts, ME₆TREN and xylene:IPA (9:1) was used as the ligand and reaction solvent. Table 22 showed the molecular weight and polydispersity of the polymers made by ATRP using a CuCl catalyst. Comparing the polydispersities with the polymers made by CuBr, shows a significant decrease in PDI when CuCl is used with the exception of PODMA-*co*-PVBA (2.3%).

Table 22 GPC table for homopolymers synthesized with VBA or VBT using CuCl.

Structure	Dp	Mn	Mw	PDI
PODMA	60	20000	28300	1.49
PDSMA	60	23200	30500	1.31
PODMA- <i>co</i> -PVBA 2.3%	61	20600	39900	1.94
PDSMA- <i>co</i> -PVBT 2.3%	58	22700	31900	1.41
PODMA- <i>co</i> -PVBA 8.0%	65	25800	32200	1.24
PDSMA- <i>co</i> -PVBT 8.0%	65	22200	32400	1.45

3.4.4 Increase loading of nucleobase into polymer backbone

The initial work with the nucleobases always targeted a molar ratio of 10% nucleobase to methacrylate monomer. Once the best reaction conditions were worked out (95°C, CuCl, Me₆TREN & xylene 9:1 IPA), a molar ratio of 20% was targeted to assess how much nucleobase monomer could be added. The ¹HNMR of both PDSMA-*co*-PVBT (Figure 113) and PODMA-*co*-PVBA (Figure 114) show how much nucleobase was incorporated into the polymer backbone when 20% was targeted.

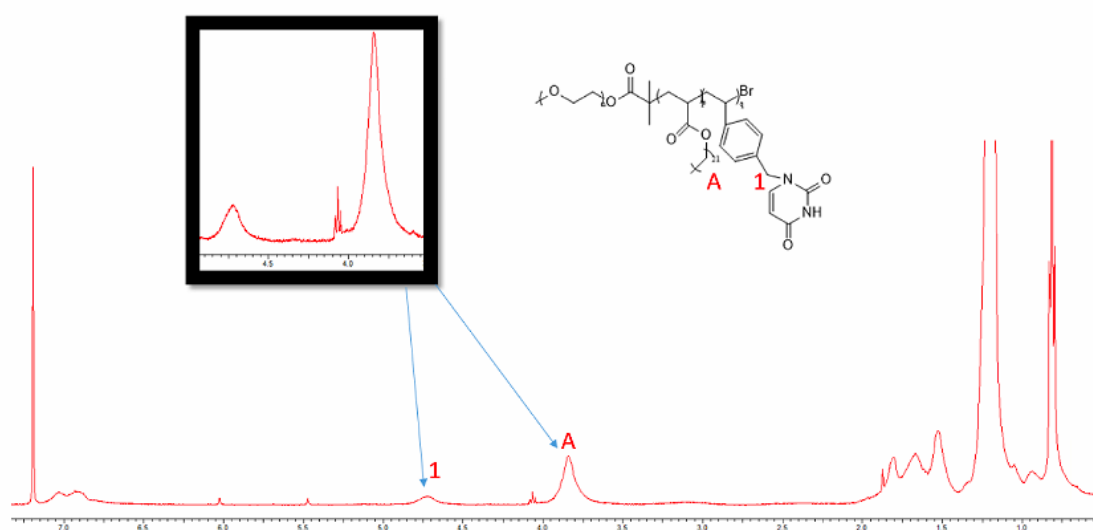


Figure 113 HNMR¹ of PDSMA-*b*-PVBT (18%) in CDCl₃.

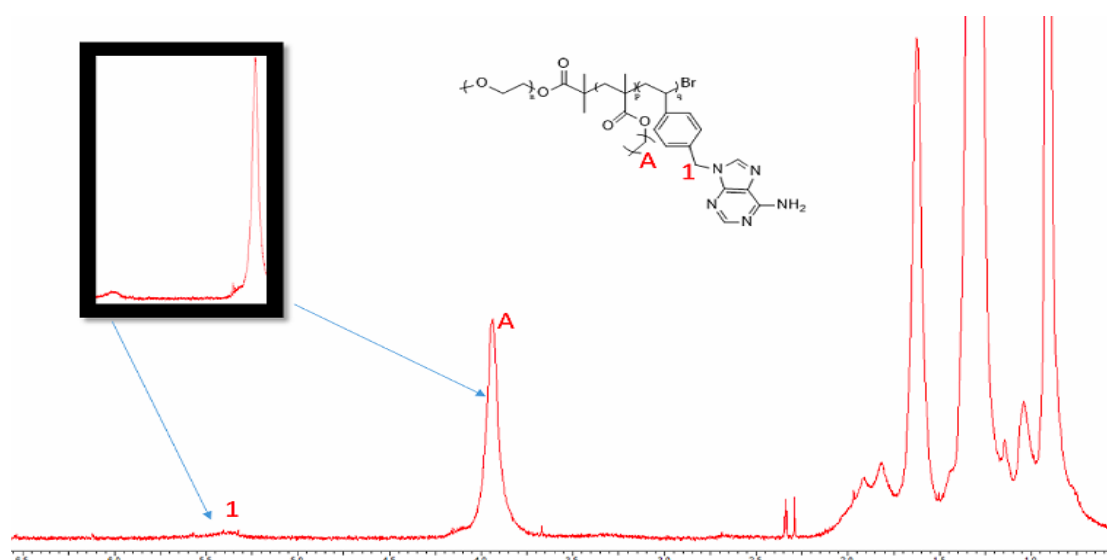


Figure 114 $^1\text{H-NMR}$ of PODMA-b-PVBA (8%) in CDCl_3 .

The two proton NMR show how the amount of VBA or VBT can be calculated. It is simply the integral of Peak 1 compared to the integral of Peak A. Peak 1 in both cases is the CH_2 which is found between the styrene group and the nucleobase group. It is also important to realise that for the VBA, Peak 1 is shown on the $^1\text{H-NMR}$ at 5.29ppm and Peak 1 for VBT comes out at 4.76ppm.

When PDSMA-co-PVBT was targeted at 20% VBT to methacrylate monomer, it was found that 18% of the VBT was incorporated into the polymer backbone. When PODMA-co-PVBA was targeted at 20% VBA to methacrylate monomer, it was found that 8% of the VBA was incorporated into the polymer backbone. There was not an improvement on the amount of VBA being added to the polymer backbone when compared to the PODMA-co-PVBA at 10%. This suggested that the amount of VBA being added to the polymer backbone could be capped at 8%.

SEC analysis was performed on the random copolymers and is shown in Figure 115. The molecular weights of each polymer were similar.

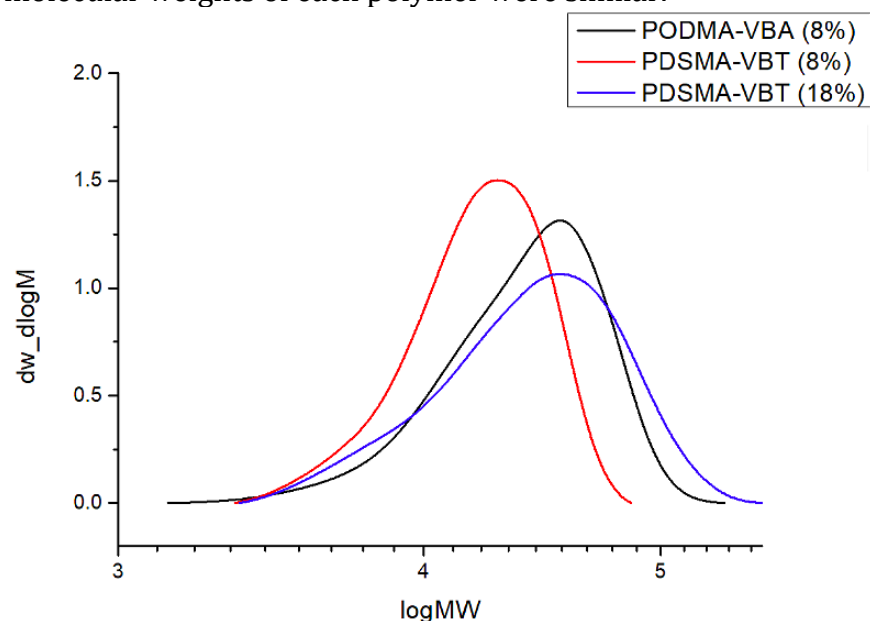


Figure 115 SEC traces of the homopolymers overlaid.

Table 23 SEC data for the three homopolymers overlaid in Figure 31.

Structure	Sample	Dp	Mn	Mw	PDI
PODMA-co-PVBA 8.0%	1	65	25800	32200	1.24
PDSMA-co-PVBT 8.0%	2	65	22200	32400	1.45
PDSMA-co-PVBT 18.0%	3	59	19700	40100	2.04

Table 24 Shows the percentage of VBX species that went onto the polymer backbone.

Table 24 Percentage of VBX species polymerised onto homopolymer backbone.

Structure	Target VBX %	Actual VBX %
PODMA-co-PVBA	10.0	8.0
PDSMA-co-PVBT	10.0	8.0
PODMA-co-PVBA	20.0	8.0
PDSMA-co-PVBT	20.0	18.0

The result seen with VBA matches literature.¹¹ A paper that studied the reactions of VBA and VBT with styrene, where only achieve 8.0% attachment onto the polymer backbone. This same literature paper used VBT with styrene and could only achieve 11.0%. The results above with VBT and DSMA is promising as more VBT was able to be attached onto the polymer backbone than previously seen.

Despite there being a limit on the amount of VBA that can be added to the polymer backbone, these VBA and VBT monomers were taken and reacted with the PEO-Br macroinitiator made in Chapter 2 to make the block copolymer counterparts.

Figure 116 and 117 show the proton NMR of block copolymers containing VBA and VBT. The amount of nucleobase monomer added into the polymer backbone was calculated the same as previously used for the homopolymers. The ¹H-NMR for both block copolymers are shown below. It is important to realise that the even in the block copolymer the thymine peak occurs around 4.76 ppm and the adenine peak occurs around 5.29 ppm like previously seen for the homopolymers.

The degree of polymerisation could be calculated much easier using H-NMR¹ as Peak A can be set to 3. Full calculation of degree of polymerisation was discussed in Chapter 2.

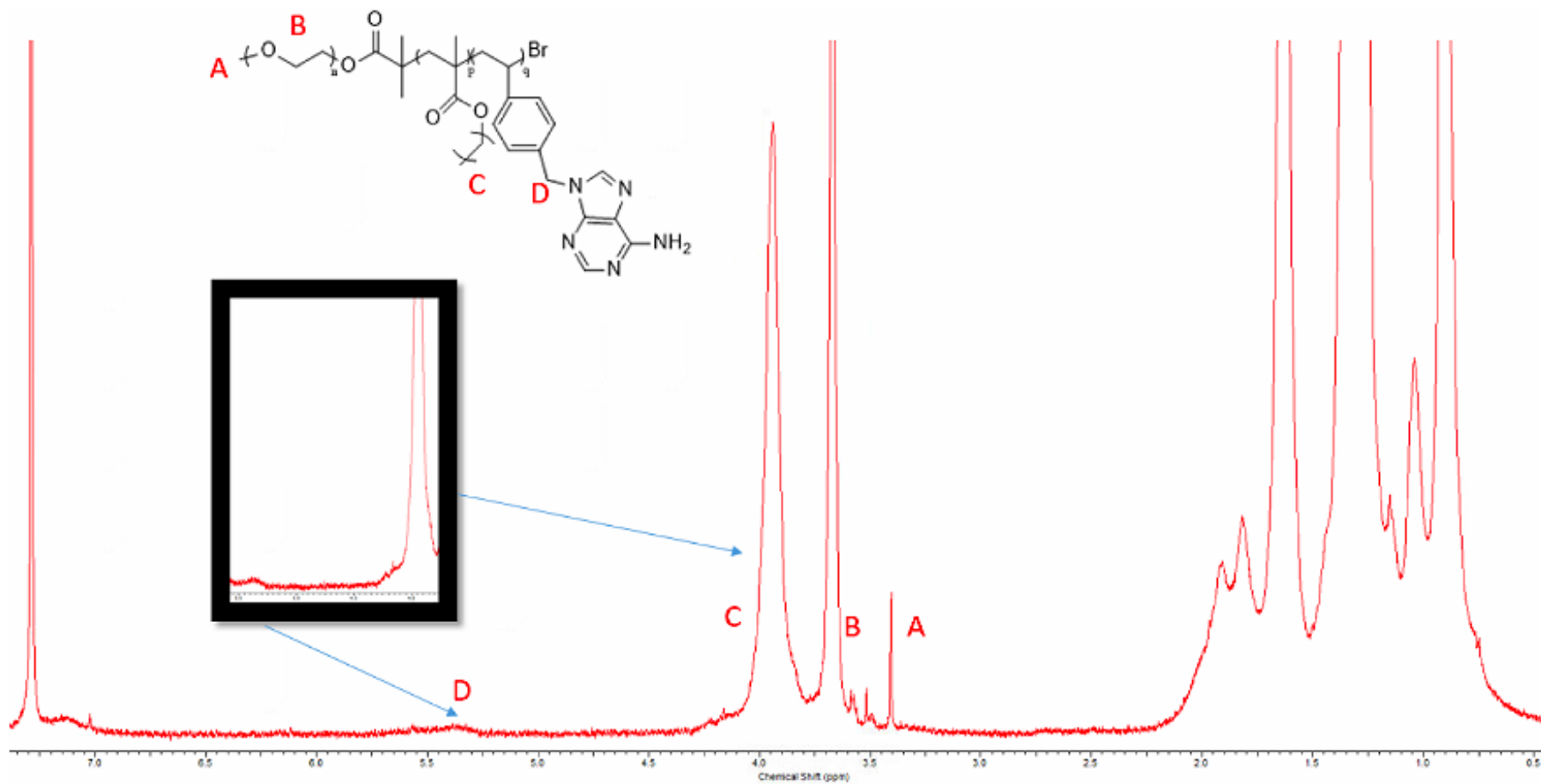


Figure 116 ¹H NMR of PEO-*b*-PODMA-*b*-PVBA in CDCl₃.

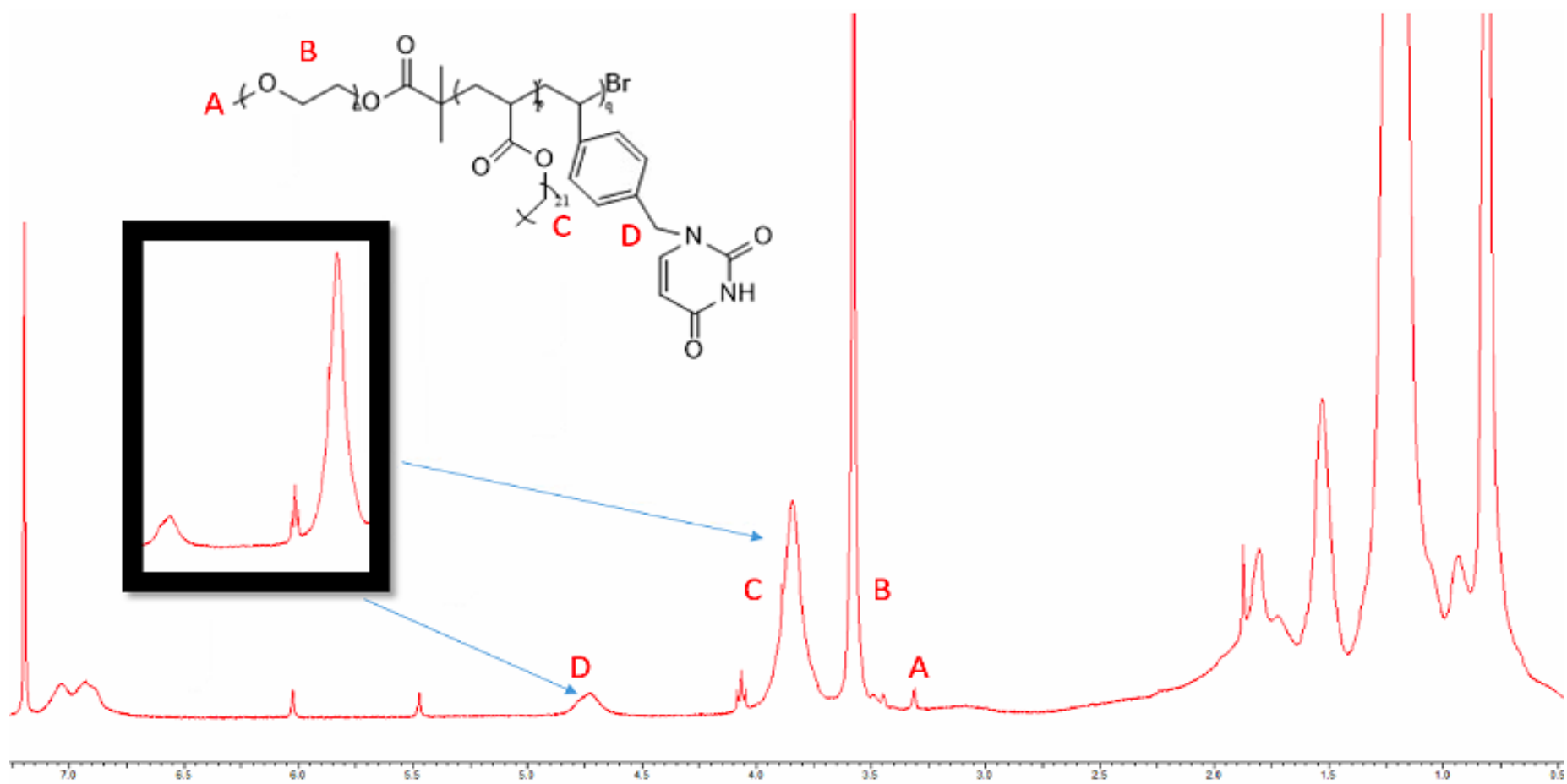


Figure 117 ¹H NMR of PEO-b-PDSMA-b-VBT in CDCl₃.

SEC analysis was performed on the block copolymers containing the nucleobase monomers and is shown in Figure 118. The molecular weights of each block copolymer were similar.

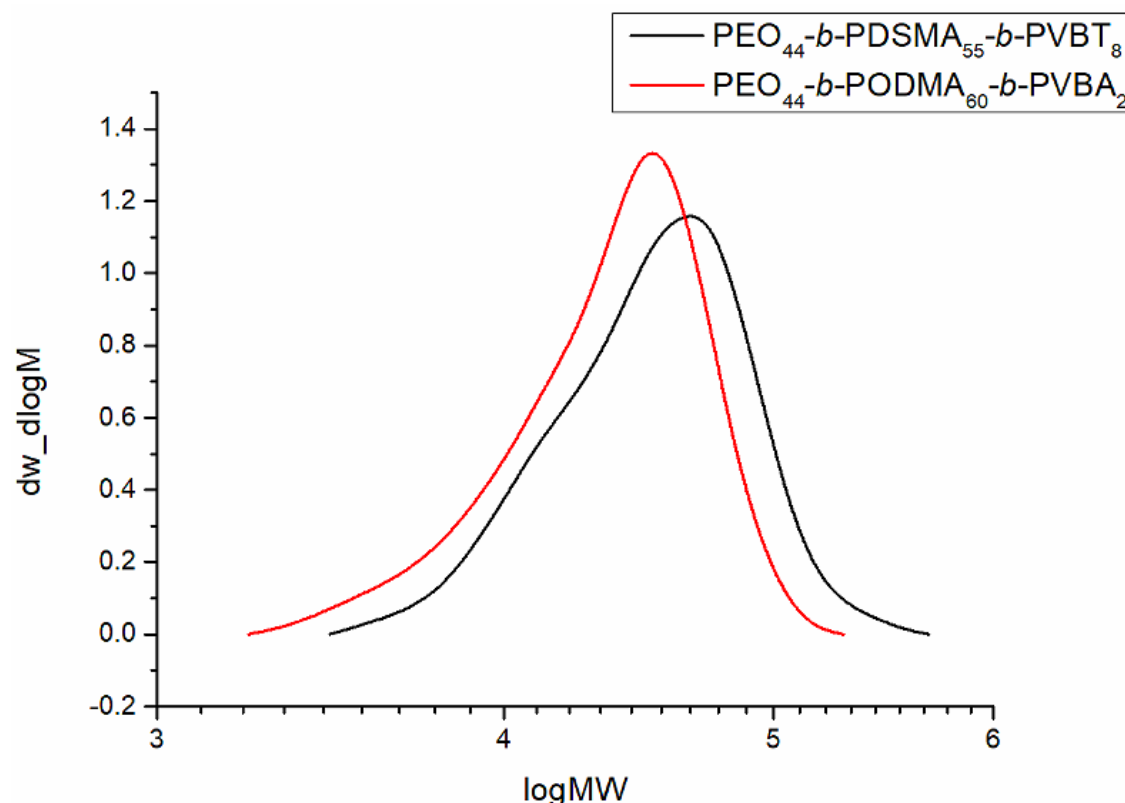


Figure 118 SEC trace of block copolymers overlaid.

Table 25 H-NMR and SEC data for block copolymers with nucleobases attached within polymer backbone.

Structure	M_n NMR	NMR Conversion %	M_n GPC	M_w GPC	\bar{D}
PEO₄₄-b-PODMA₆₀-PVBA₂	22800	86.1	18000	32100	1.78
PEO₄₄-b-PDSMA₅₅-PVBT₈	25700	88.2	25500	49000	1.92

The level of VBA polymerising onto the polymer backbone was less for the block copolymers when compared to the 8% achieved on the random copolymers of PODMA-co-PVBA. This led to a 20% sample being made where the level of VBA was only increased by 0.6% and these results are shown in Table 26.

Table 26 Percentage of VBX species polymerised onto block copolymer backbone.

Structure	Target VBX %	Actual VBX %
PEO-b-PODMA-b-PVBA	10.0	4.0
PEO-b-PDSMA-b-PVBT	10.0	10.0
PEO-b-PODMA-b-PVBA	20.0	4.6

3.4.5 Self-assembly of nucleobase containing block copolymers

The block copolymers containing the nucleobases were self-assembled to see if bicontinuous nanospheres would form. Table 27 showed the quantities used for the self-assembly of the block copolymers containing VBT and VBA.

Table 27 Quantities used for the self-assembly of block copolymers containing nucleobases.

Polymers	Self-assembled concentration wt %	Mass of polymer used (g)	THF Volume (mL)	Water Volume (mL)	Total Volume (mL)
PEO ₄₄ - <i>b</i> -PODMA ₆₀ -PVBA ₂	0.1	0.01	9	1	10
	1	0.1	6	4	10
	1	0.1	9	1	10
PEO ₄₄ - <i>b</i> -PDSMA ₅₅ -PVBT ₈	0.1	0.01	9	1	10
	1	0.1	6	4	10
	1	0.1	9	1	10

First attempts used THF (6mL) with the addition of water (4mL) slowly over time to make a 1.0 wt % concentration but this caused precipitation (Figure).

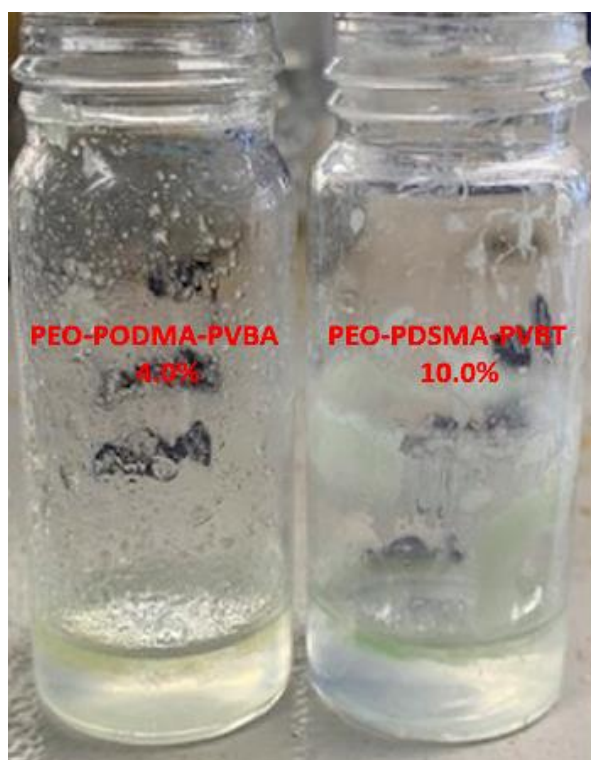


Figure 119 Samples of block copolymers at 1.0 wt% after 4mL of distilled water was added to THF mixture. Demonstrates the amount of precipitation.

The samples at this stage were taken and filtered and the remaining solution was put into the dialysis cassette and self-assembly was attempted. Figure 119 shows slight precipitation after the self-assembly process.

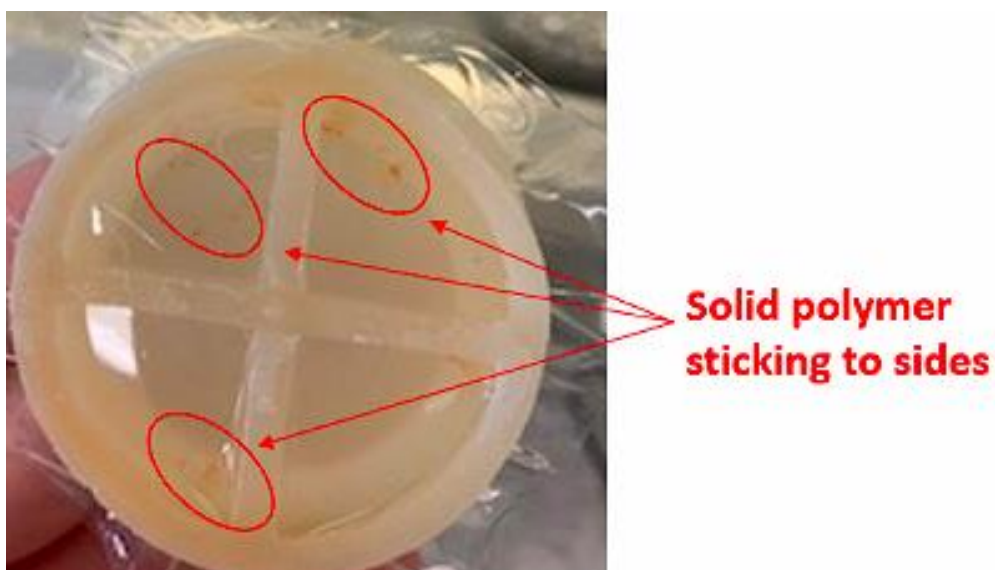


Figure 120 Slight precipitation after the self-assembly process using 6mL THF.

This led to the work being repeated and using THF (9mL) with the addition of water (1mL). Samples did not show any evidence of precipitation and this was then transferred to the dialysis cassette as shown in Figure 121.

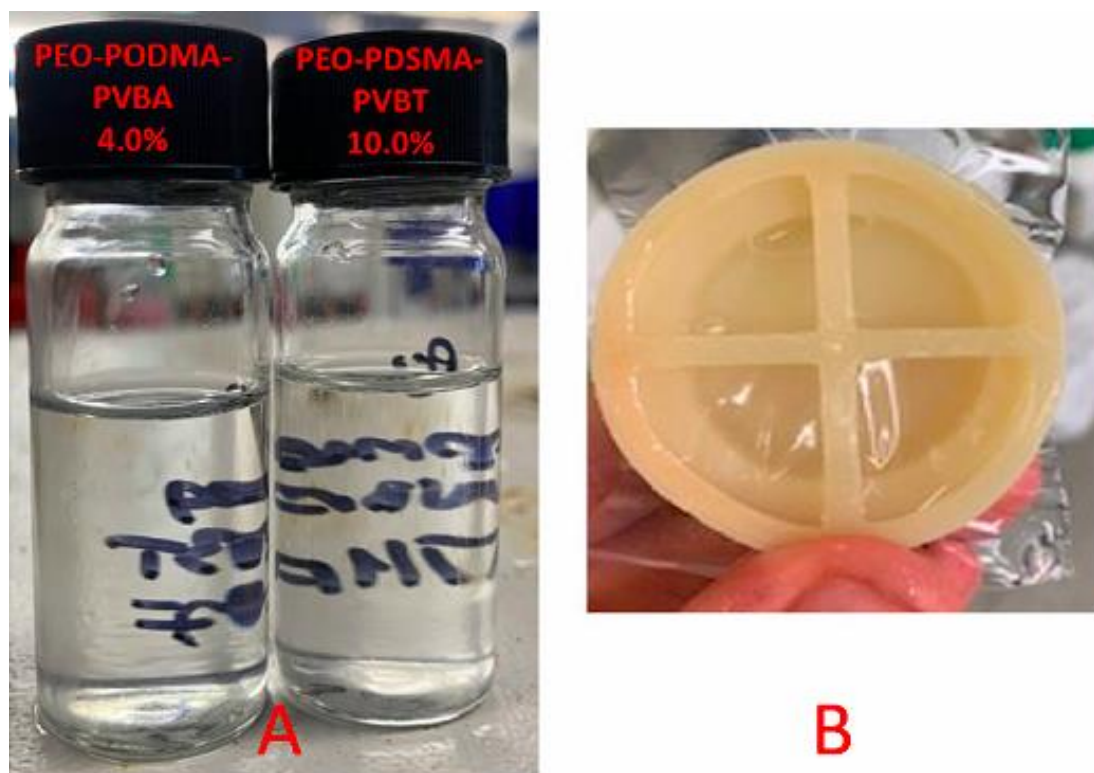


Figure 121 A) No precipitation seen after 1mL of water was added to 9mL THF. B) No precipitation seen after dialysis for 24 hours.

The block copolymer dispersions were then analysed using dynamic light scattering (DLS) and transmission electron microscopy (TEM) to determine the size and dispersity of the aggregates.

PEO₄₄-*b*-PODMA₆₀-PVBA₂ & PEO₄₄-*b*-PDSMA₅₅-PVBT₈

DLS and TEM were carried out on the aggregate samples. The results are shown in Figure 122.

Table 28 TEM and DLS results for block copolymers and blends (PEO 0.10 wt). *N* is the number average of particles present.

Sample(s)	THF mL	wt %	N _{Aver} Diameter / (nm) TEM	N _{Aver} Diameter / (nm) DLS	CONTIN (nm) DLS	Đ DLS
PEO ₄₄ - <i>b</i> -PODMA ₆₀ -PVBA ₂	9	0.1	231.4 ± 17.5	187.3 ± 24	185	0.088
	6	1.0	140.7 ± 39.7	173.0 ± 20	216	0.066
	9	1.0	174.2 ± 35.3	115.5 ± 7	190	0.144
PEO ₄₄ - <i>b</i> -PDSMA ₅₅ -PVBT ₈	9	0.1	113.4 ± 55.2	187.3 ± 22	185	0.085
	6	1.0	109.5 ± 17.5	173.3 ± 13	185	0.078
	9	1.0	150.7 ± 89	118.1 ± 9	190	0.127

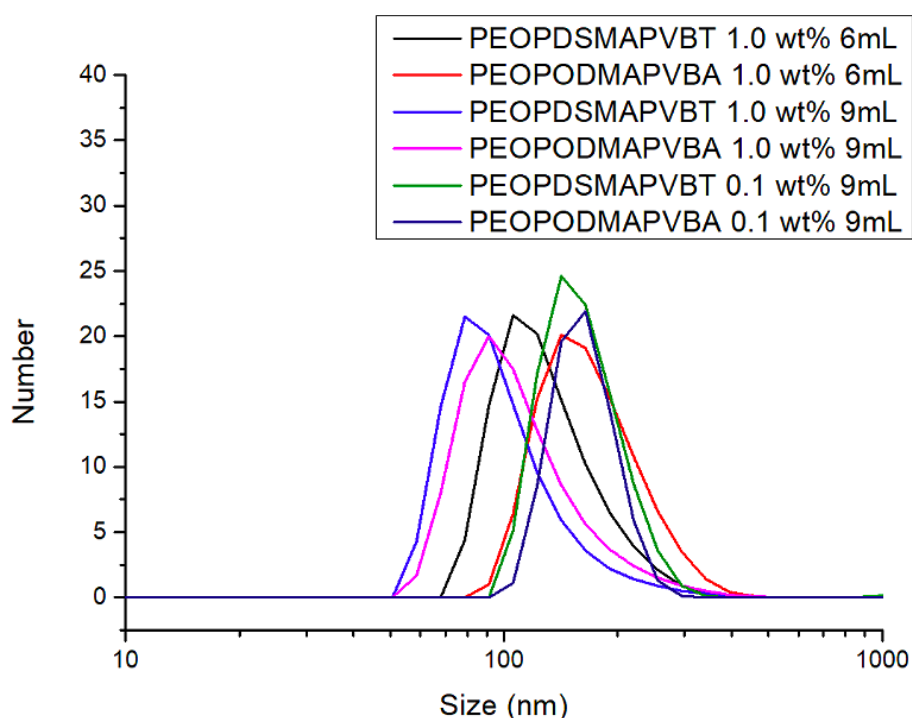


Figure 122 DLS for the self-assembly of BCP containing nucleobases monomers.

Previous work showed that bicontinuous nanospheres formed when the PEO weight percent was between 10-30 wt% and the molecular weight was less than 20,000 KDa. The weight percentage of PEO for both the block copolymers containing the nucleobases were calculated to be 10 wt%. This was planned as one set of block copolymers used in Chapter 2 also had a PEO weight percent of 10 wt% and bicontinuous nanospheres seemed to be present.

The SEC results are shown in Table 29 and show that the molecular weights are around the correct area for bicontinuous nanospheres to form. This information

is used with the phase diagram which can be seen in previous chapters and is displayed once again in Figure 46.

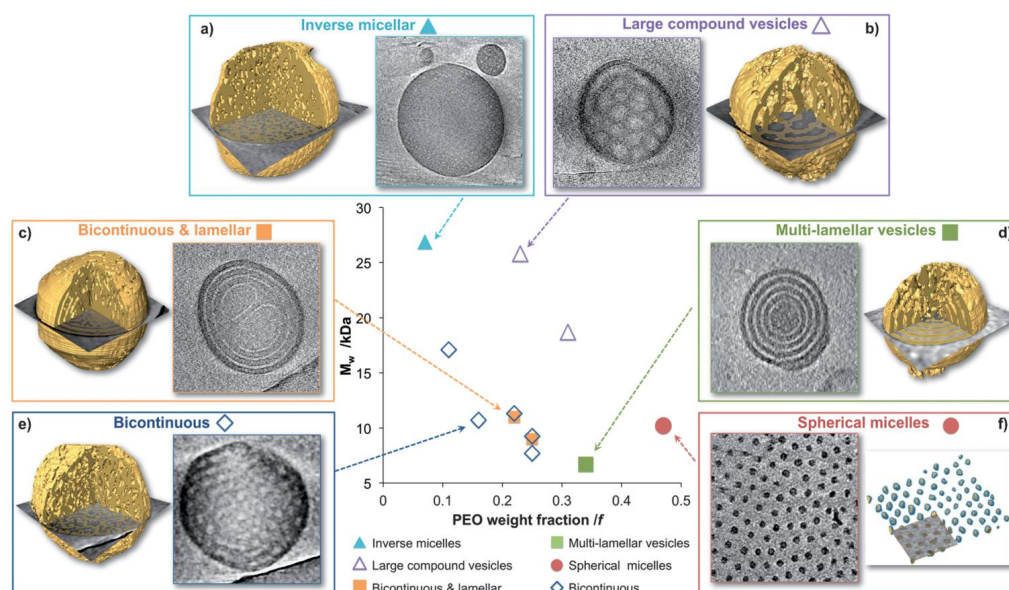


Figure 70 Phase diagram of the self-assembly of PEO-*b*-PODMA block copolymers with corresponding slices through 3D reconstructions¹¹

Table 29 SEC data for block copolymers with nucleobases attached within polymer backbone.

Structure	PEO wt%	M_n NMR	M_n GPC
PEO ₄₄ - <i>b</i> -PODMA ₆₀ -PVBA ₂	10	22800	18000
PEO ₄₄ - <i>b</i> -PDSMA ₅₅ -PVBT ₈	10	25700	25500

DLS measurements for the block copolymers at 10 PEO wt % most hydrodynamic diameters were in the range from 80-200nm with monomodal distributions and this was backed up by CONTIN analysis. The samples at 0.1 wt% and made with 9 mL THF disagree with TEM as the TEM images taken suggest that something smaller can also be seen which is likely to be block copolymer micelles. The three samples of (PEO-PDSMA-PVBT 1.0wt% 9mL and 6mL and 9 mL PEO-PODMA-PVBA 1.0wt%) all give tails on DLS down to 50nm. This is also supported by TEM as small structures can be seen indicating that micelles are present. TEM in some cases suggest that bicontinuous structures are present as some images show spheres with an internal structure. However, in some cases it appears that vesicular structure are present instead.

In all cases there appears to be block copolymer micelles present when TEM was carried out. The samples of PEO-PODMA-PVBA 6 mL 1.0 wt%, PEO-PDSMA-PVBT 9mL 1.0 wt% and PEO-PODMA-PVBA 9mL 0.1% all give vesicles when self-assembled. These vesicles were the largest sized aggregate seen and this is backed but by DLS as the three traces on the right are these three samples. The other three samples (PEO-PDSMA-PVT 6mL 1.0wt%, PEO-PODMA-PVBA 9mL 1.0 & PEO-PODMA-PVBT 9mL 0.1%) produced aggregates of spherical micelles and bicontinuous nature. Some of the larger spheres of around 100 nm have darker regions which could be evidence of an internal structure suggesting bicontinuous nanospheres have formed.

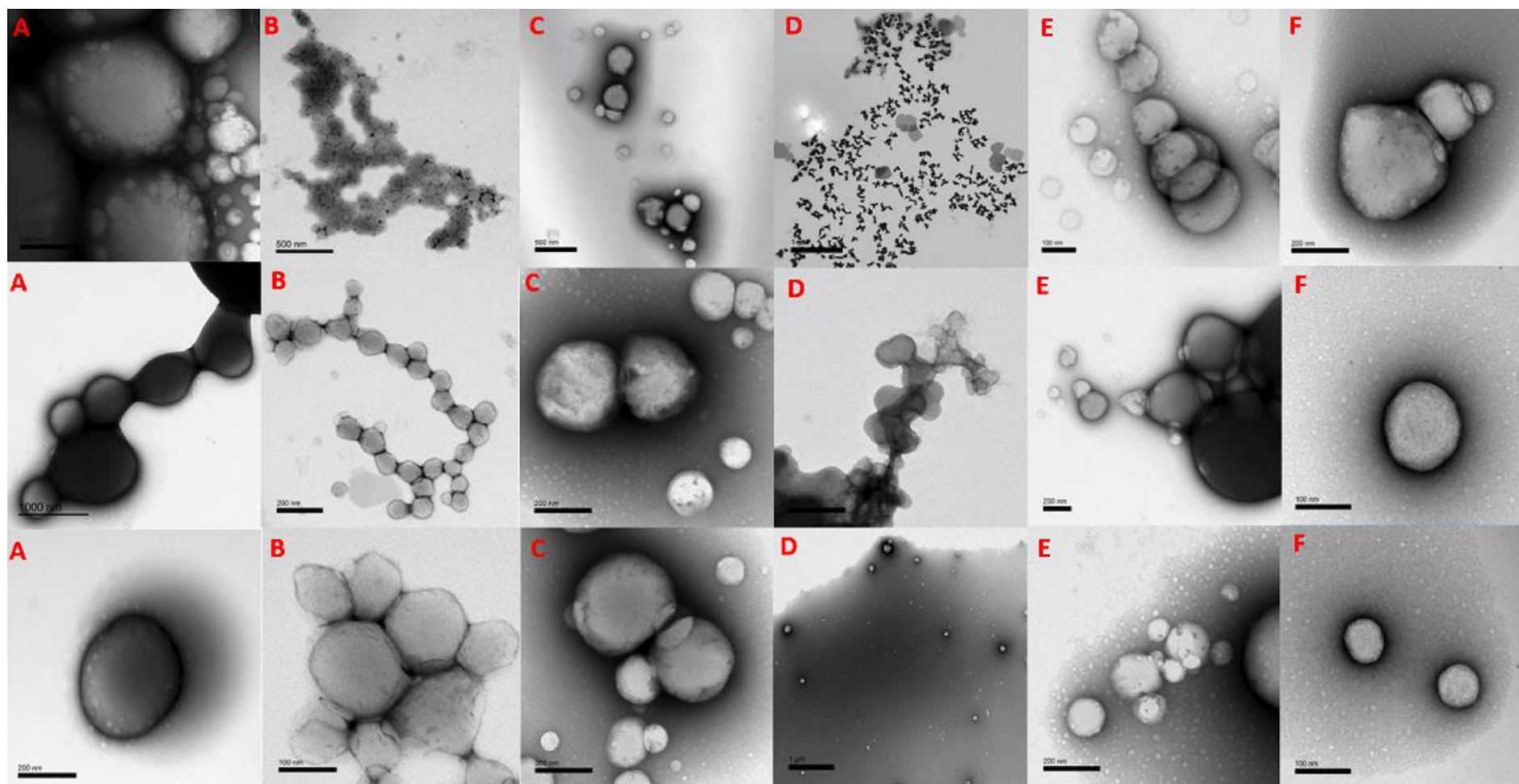


Figure 123 TEM images of BCP with nucleobases monomers incorporated into the polymer backbone; A) 6mL THF PEO-*b*-PODMA-*b*-PVBA 1.0wt%, B) 6mL THF PEO-*b*-PDSMA-*b*-PVBT 1.0wt%, C) 9mL THF PEO-*b*-PODMA-*b*-PVBA 1.0wt%, D) 9mL THF PEO-*b*-PDSMA-*b*-PVBT 1.0wt%, E) 9mL THF PEO-*b*-PODMA-*b*-PVBA 0.1 wt% & F) 9mL THF PEO-*b*-PDSMA-*b*-PVBT 0.1wt%.

3.4.6 H-NMR¹ Titrations

Titration using the H-NMR¹ was carried out to see if the compounds made containing the VBA and VBT were hydrogen bonding to each other. The hydrogen bonding expected is shown Figure 124.

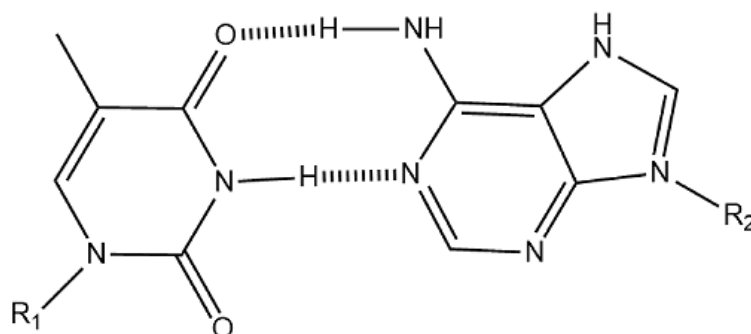


Figure 124 The expected hydrogen bonding that occurs between thymine and adenine.

In order to full fully miscible blends, the polymers of PDSMA and PODMA containing the nucleobases need to hydrogen bond. It was hypothesised that if this hydrogen bonding did take place, it would help the blend to stay miscible.

H-NMR¹ titration with VBA and VBT

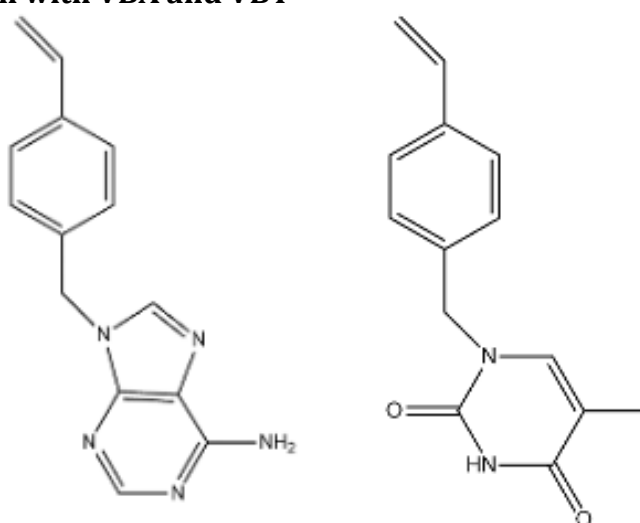


Figure 125 Host species VBA (left) & Guest Species VBT (Right) for H-NMR¹ Titration

Due to the large volumes of publications²³ that have demonstrated that adenine and thymine do interact through hydrogen bonding, it was expected that VBA and VBT should do the same. This led to a solution of the intended guest species VBT (10^{-5} mol in 0.10 mL) which was added in a stepwise fashion to a solution of host VBA (10^{-6} mol in 0.50 mL solvent) at 298 K.

The integrals of the hydrogen bonding signal taken from H-NMR¹ was then recorded and put into a binding programme called 'Bindfit'.²⁴ Bindfit uses the assumption that the free guest is 'silent' and that the first data point used is pure host. It then fits the changes to the signal. For Bindfit to do this a series of data points are need and for this study 22 have been selected.

Spectra were measured and chemical shifts recorded at 22 titration points (0, 0.1, 0.2, 0.3, 0.4, 0.5, 0.6, 0.7, 0.8, 0.9, 1.0, 1.2, 1.4, 1.6, 1.8, 2.0, 2.5, 3.0, 4.0, 5.0, 7.0, 10 equivalents of guest to host).

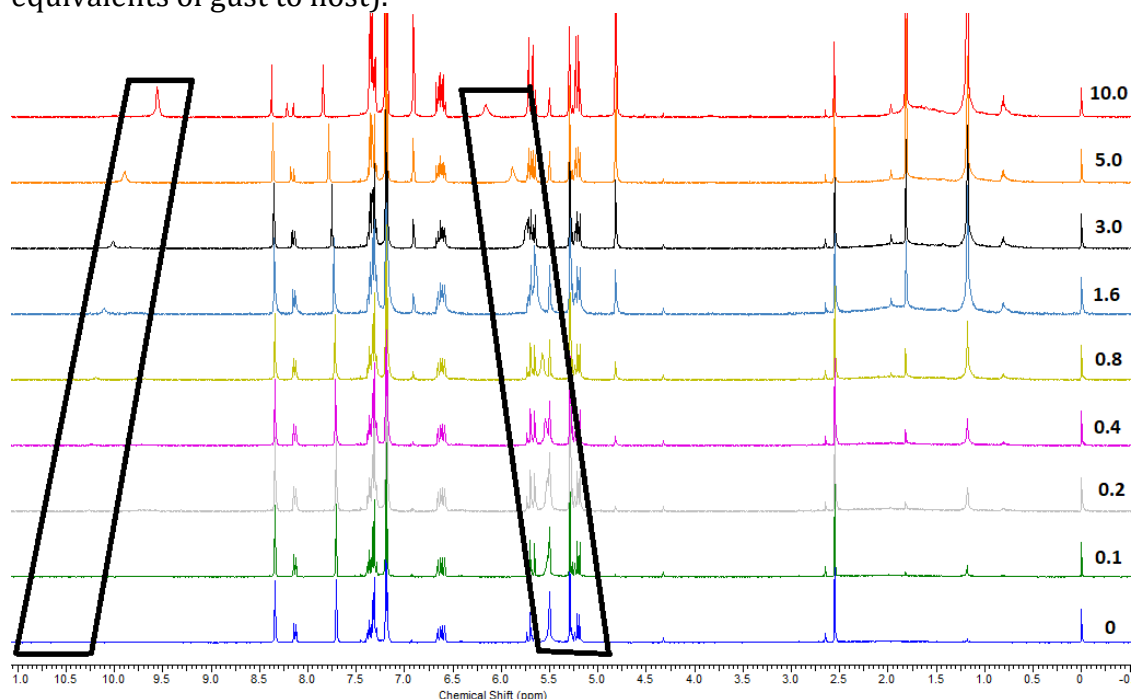


Figure 126 $^1\text{H-NMR}$ Spectra showing the thymine (left) and adenine (right) proton shift when VBA (Host) is titrated with VBT (Guest).

The shift on the left at around 10ppm is the proton signal coming from the thymine. As this undergoes hydrogen bonding to the adenine host this peak shifts up to 11ppm and is highlighted in Figure 126. The shift around 5.25 ppm comes from the proton on the adenine group which shifts to 6 ppm when it undergoes hydrogen bonding with thymine. These shifts are proof that the nucleobase monomers have been successfully made and can interact through hydrogen bonding as intended.

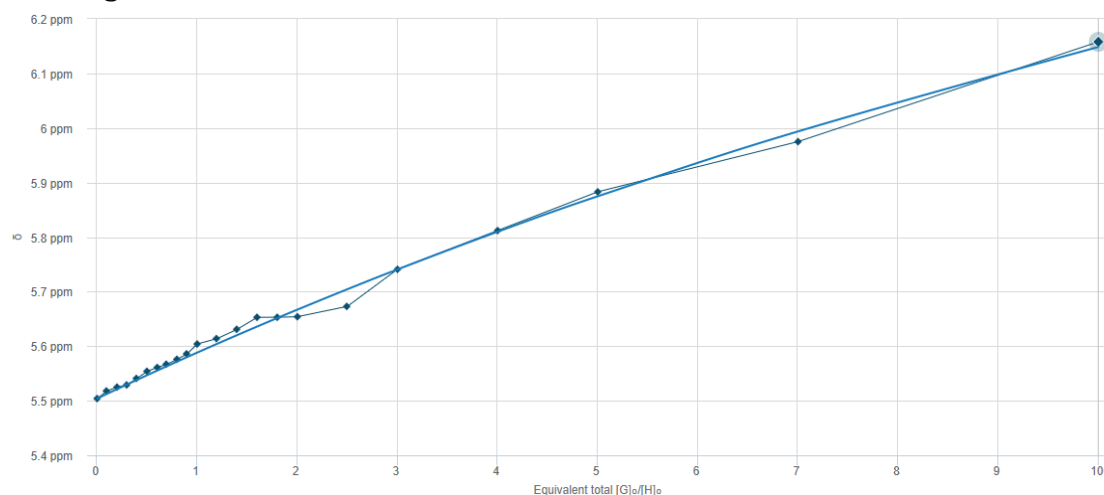


Figure 127 Shows the 22 titration points for the adenine proton shift against the equivalent total $[G]_0/[H]_0$

Figure 127 shows that as the amount of guest (VBT) is added to the host (VBA) over time, that a shift for the proton environment on the adenine is seen. This is due to an increase in hydrogen bonding as more guest is added to the reaction mixture. Bindfit has then performed a non-linear regression on the data so the mole fraction of the species can be shown.

Parameter (bounds)	Optimised	Error	Initial
$K (0 \rightarrow \infty)$	37624.41	± 2.9339	100.00
	M^{-1}	%	M^{-1}

Figure 127 Parameters for the data set for VBA (host) with VBT (guest). K is the binding coefficient.

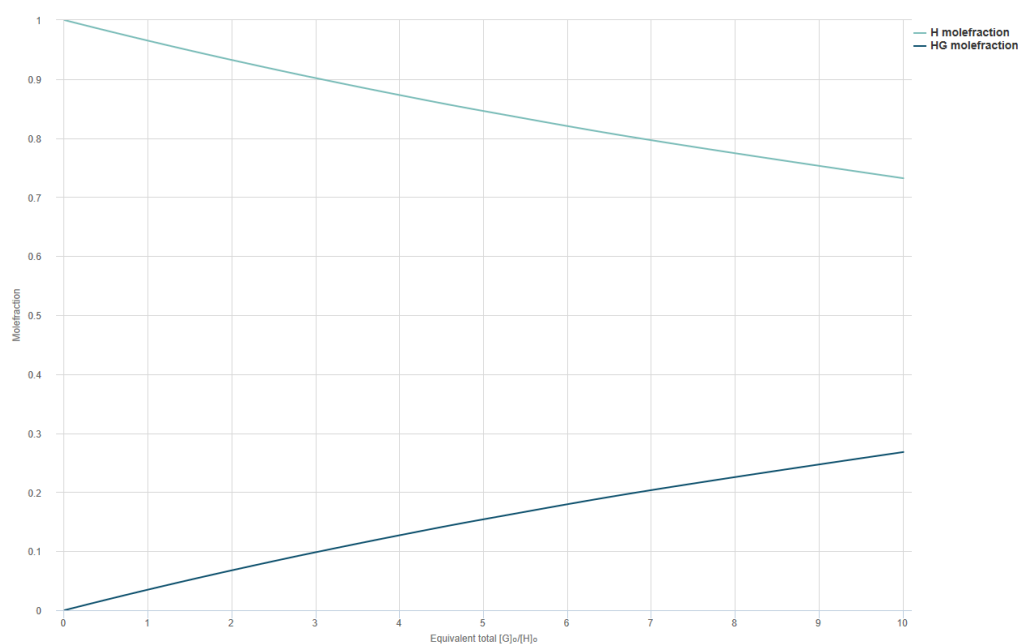


Figure 128 Shows the molefraction of the host and the molefraction of the host and guest change through the titration.

Figure 128 shows how the different species change through the titration. H is the mole fraction of the host and HG is the mole fraction of the host and guest.

H-NMR¹ with VBT and VBA

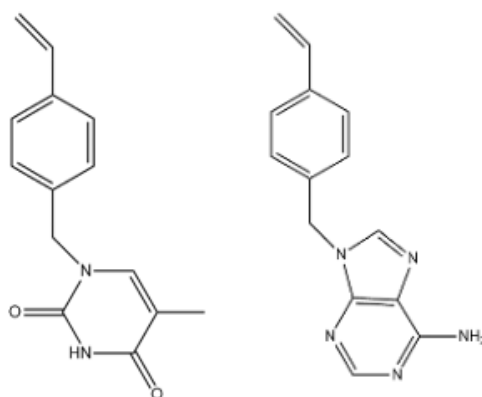


Figure 129 Host species VBT (left) & Guest Species VBA (Right) for H-NMR¹ Titration

A solution of the intended guest species VBA (10^{-5} mol in 0.10 mL) was added in a stepwise fashion to a solution of host VBT (10^{-6} mol in 0.50 mL solvent) at 298 K. This was to assess if there was interaction between the adenine and thymine.

Spectra were measured and chemical shifts recorded at 22 titration points (0, 0.1, 0.2, 0.3, 0.4, 0.5, 0.6, 0.7, 0.8, 0.9, 1.0, 1.2, 1.4, 1.6, 1.8, 2.0, 2.5, 3.0, 4.0, 5.0, 7.0, 10 equivalents of guest to host).

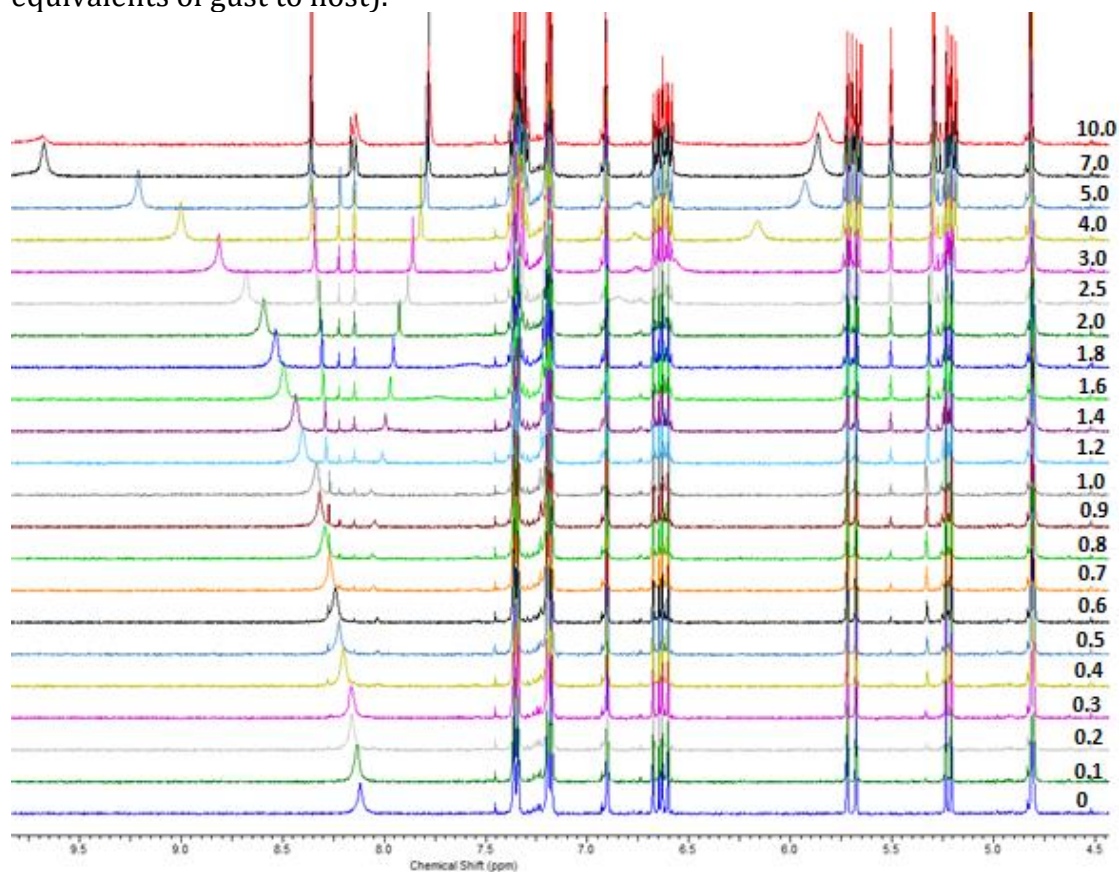


Figure 130 $^1\text{H-NMR}$ Spectra showing the thymine proton shift when VBT (Host) is titrated with VBA (Guest).

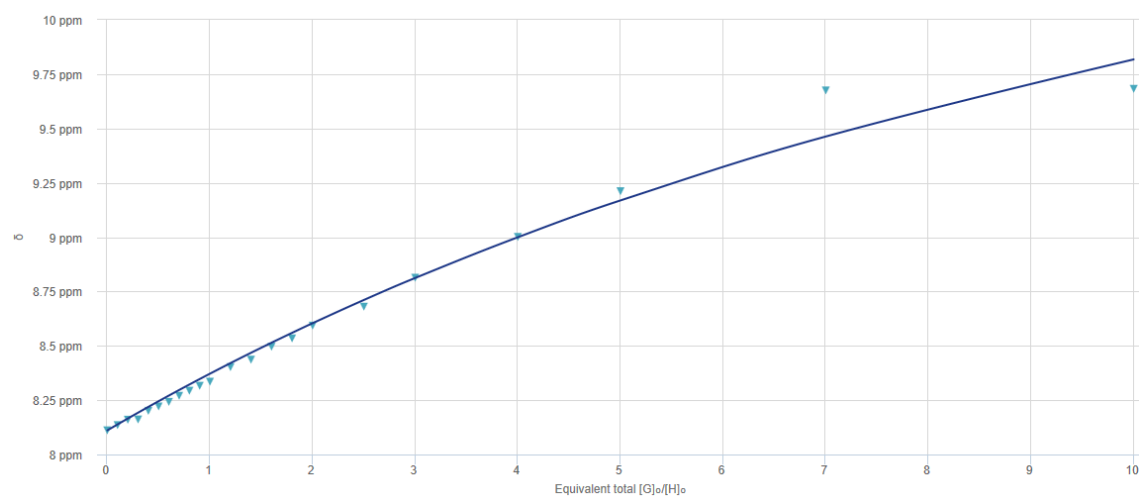


Figure 131 Shows the 22 titration points for the adenine proton shift against the equivalent total $[G]_0/[H]_0$

From Figure 130 and 131 that the shift seen overtime is from the proton on the thymine group and shifts from 8.2 ppm to 9.75 ppm in the titration. As this proton shift occurs due to the hydrogen bonding that is taking place between the VBT and VBA. The bindfit model seems to be a much closer fit than the one seen in Figure 7.

Parameter (bounds)	Optimised	Error	Initial
$K (0 \rightarrow \infty)$	69119.93 M ⁻¹	± 6.3888 %	100.00 M ⁻¹

Figure 132 Parameters for the data set for VBT (host) with VBA (guest). K is the binding coefficient.

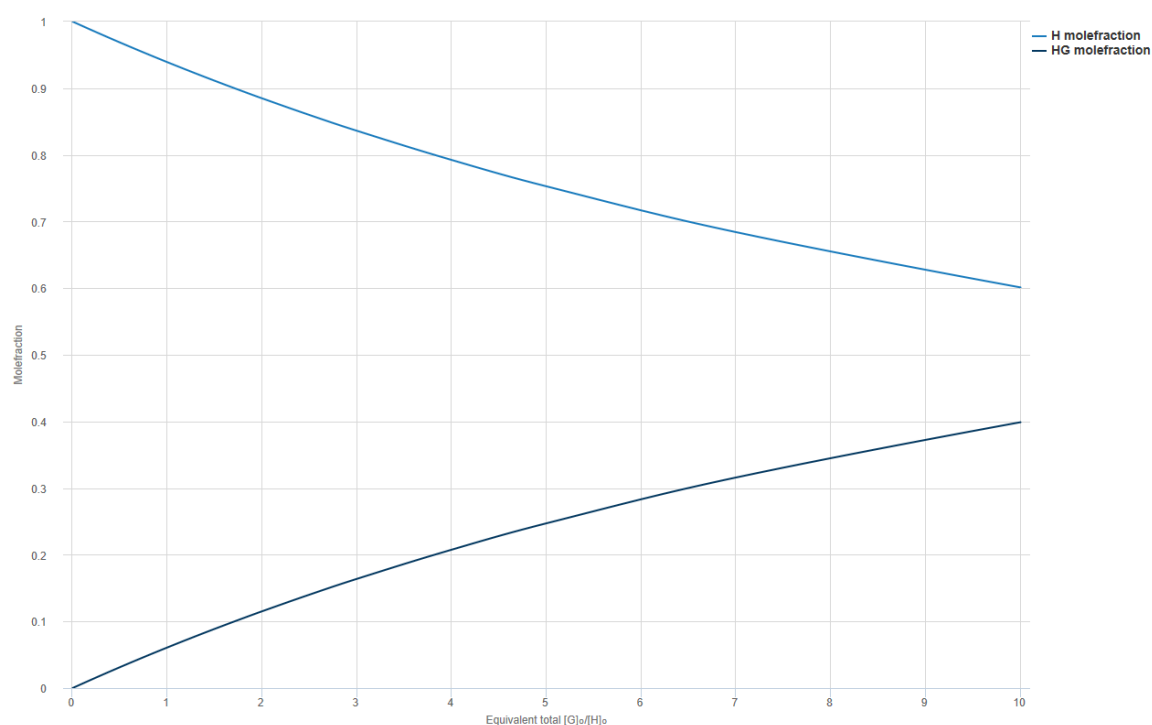


Figure 133 Shows the molefraction of the host and the molefraction of the host and guest change through the titration.

H is the mole fraction of the host and HG is the mole fraction of the host and guest. At the end of the titration the mole fraction of the two species is much closer together than what was seen in Figure 128.

H-NMR¹ with VBA and PDSMAPVBT (18%)

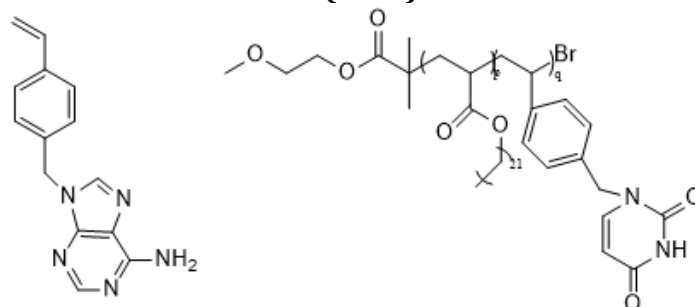


Figure 134 Host species VBA (left) & Guest Species PDSMA-PVBT (18%) (Right) for H-NMR¹ Titration

A solution of the intended guest species PDSMAPVBA (18%) (10^{-5} mol in 0.10 mL) was added in a stepwise fashion to a solution of host VBA (10^{-6} mol in 0.50 mL solvent) at 298 K. This was to assess if there was interaction between the adenine and thymine.

Spectra were measured and chemical shifts recorded at 22 titration points (0, 0.1, 0.2, 0.3, 0.4, 0.5, 0.6, 0.7, 0.8, 0.9, 1.0, 1.2, 1.4, 1.6, 1.8, 2.0, 2.5, 3.0, 4.0, 5.0, 7.0, 10 equivalents of guest to host).

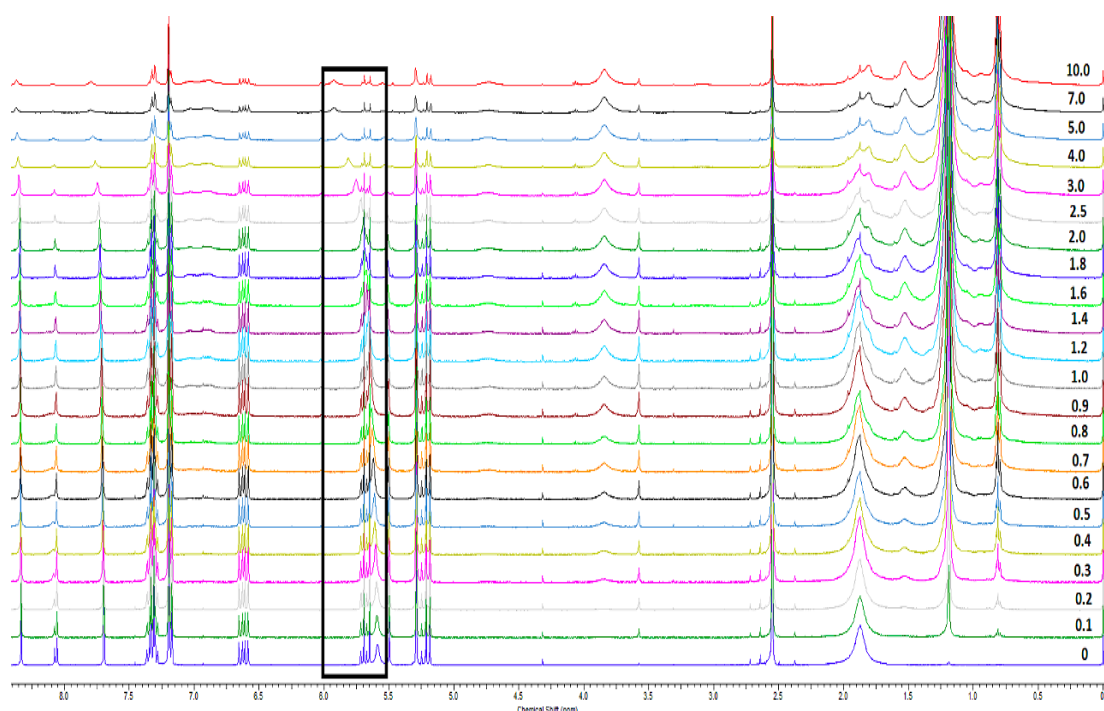


Figure 135 $^1\text{H-NMR}$ Spectra showing the adenine proton shift when VBA (Host) is titrated with PDSMA-PVBT (18%) (Guest).

Figure 135 shows the adenine proton shift when VBA is the host species and PDSMA-PVBT is added over time. It shows that there is hydrogen bonding interaction occurring between VBA and the random copolymer. This is encouraging when targeting fully miscible blends as the next step is to try titrating two random copolymers which contain VBA and VBT to assess if there is interaction between them.

$^1\text{H-NMR}$ with PDSMAPVBT (18%) and PODMAPVBA (8%)

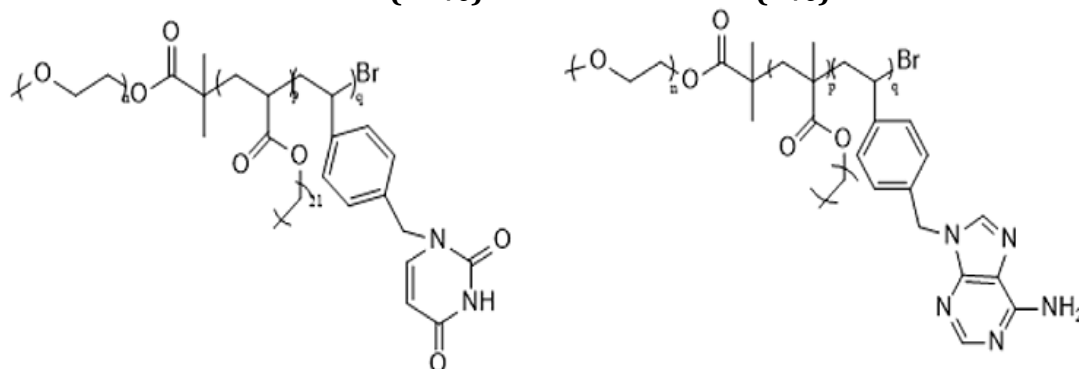


Figure 136 Host species PDSMA-b-PVBT (18%) (left) & Guest Species PODMA-b-VBA (8%) (Right) for $^1\text{H-NMR}$ Titration

A solution of the intended guest species PODMA-*b*-VBA (8%) (10^{-5} mol in 0.10 mL) was added in a stepwise fashion to a solution of host PDSMA-*b*-VBT (18%) (10^{-6} mol in 0.50 mL solvent) at 298 K. This was to assess if there was interaction between the adenine and thymine.

Spectra were measured and chemical shifts recorded at 22 titration points (0, 0.1, 0.2, 0.3, 0.4, 0.5, 0.6, 0.7, 0.8, 0.9, 1.0, 1.2, 1.4, 1.6, 1.8, 2.0, 2.5, 3.0, 4.0, 5.0, 7.0, 10 equivalents of guest to host).

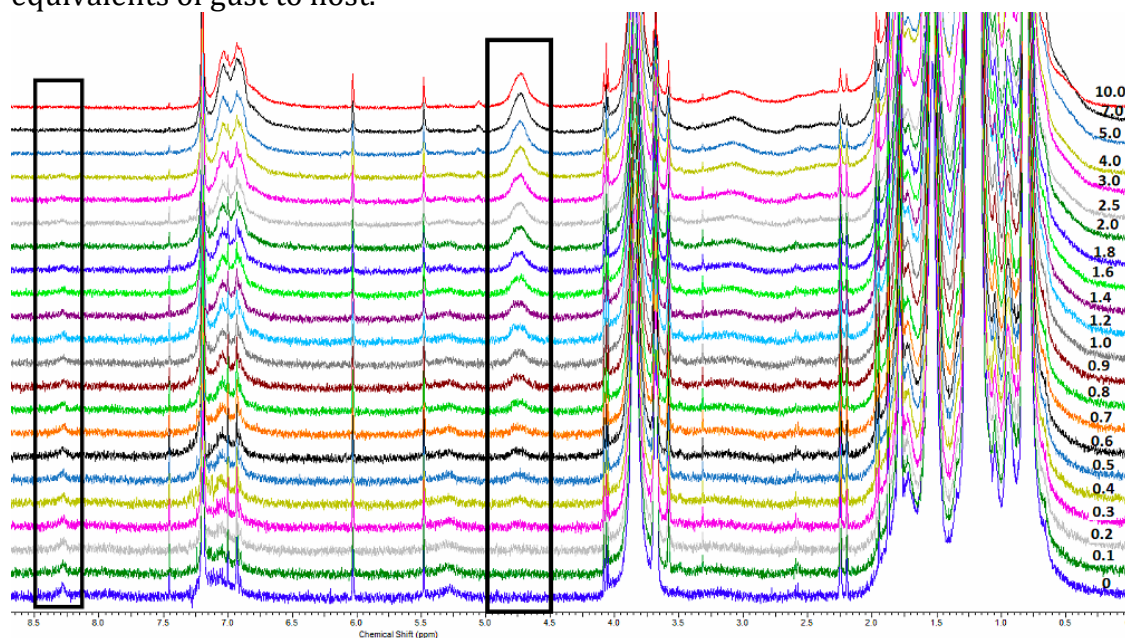


Figure 717 $^1\text{H-NMR}$ Spectra showing the thymine proton shift (left) and adenine proton shift (right) when PDSMA-*b*-VBT (18%) (Host) is titrated with PODMA-*b*-PVBA (8%) (Guest).

The $^1\text{H-NMR}$ titration suggest that hydrogen bonding is not taking place in the two homopolymers as the thymine peak and adenine peak do not shift at all like previously seen with the adenine and thymine monomers. The integrals of these peaks remain constant which is proof that no or very little hydrogen bonding is occurring between adenine and thymine. This is most likely a cause of steric hindrance between the two random copolymers. The hydrogen bonding which would normally take place between adenine and thymine is not taking place and the nucleobase monomers are getting lost along the polymer backbone. The VBA is only 12 carbons and the VBT is only 10 carbon atoms long and when attached to the polymer backbone is not long enough to interact with each other.

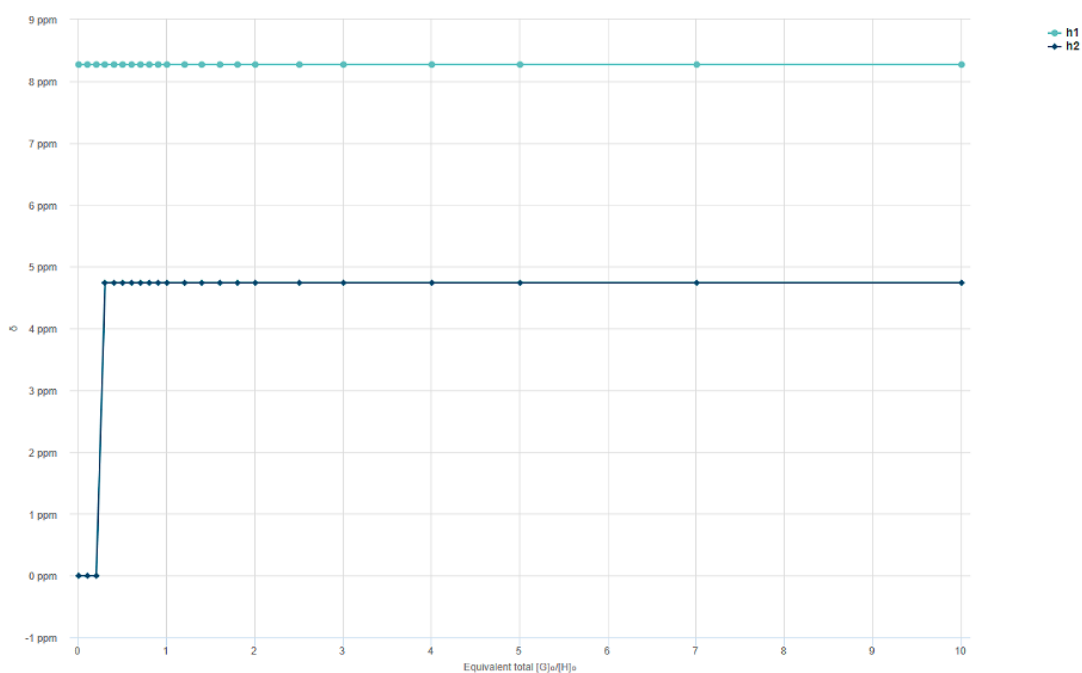


Figure 138 Shows the molefraction of the host (h1) and the molefraction of the host and guest (h2) change through the titration.

Figure 138 shows that there is no interaction taking place between the adenine and thymine during the titration. This is due to a flat line being seen in both cases suggesting that after being fitted, that the integrals of the proton peaks on the thymine and adenine are not changing at all.

3.4.6 Thermal analysis of bulk homopolymers containing nucleobases and polymer blends (DSC)

For both homopolymers that contained VBT or VBA that were synthesised, thermal analysis was carried out on bulk. This was to see whether blends involving the homopolymers were fully miscible or if partial mixing was present again. ΔH_f (enthalpy change of fusion) and D_c (degree of crystallinity) were calculated for the homopolymers. These calculations were previously discussed in Chapter 2 and were calculated in the same way as before.

Table 30 DSC parameters for homopolymers and random copolymers.

Structure	Onset °C	Peak °C	Area J g ⁻¹	ΔH_f (kJ mol ⁻¹)	D_c (%)
PODMA ₈₀	21.1	25.4	55.4	14.0	5.8
PODMA ₆₅ PVBA (8%)	20.7	24.7	28.55	7.2	3.0
PDSMA ₆₅ PVBT (8%)	42.2	44.2	121.0	37.4	12.6
PDSMA ₅₉ PVBT (18%)	41.5	45.8	42.1	13.0	4.4
PDSMA ₈₃	42.7	44.8	154.3	47.7	16.1

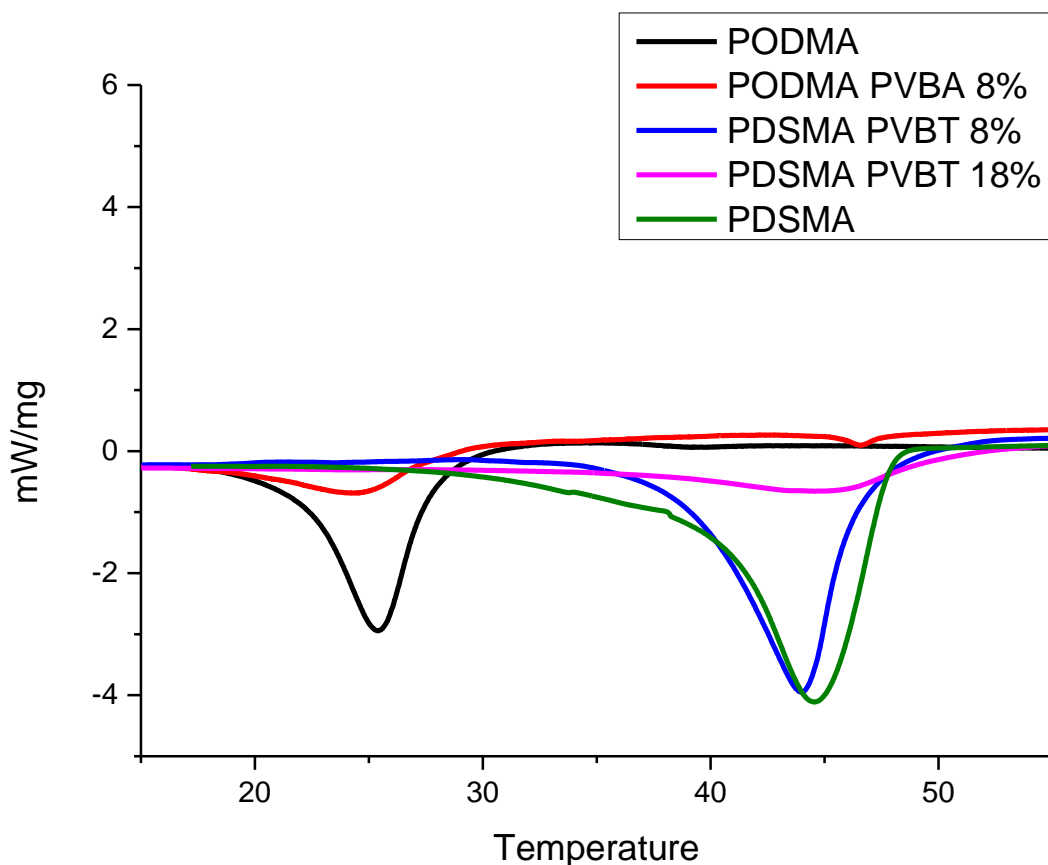


Figure 139 DSC traces of straight homopolymers and homopolymers with VBT and VBA.

DSC result (Figure 139 & Table 30) suggest that the amount of VBA or VBT bonded to the polymer backbone is having an effect on the degree of crystallinity. As the amount of VBT is increased, there is a significant drop in the docosyl methacrylate side chains being able to crystallise.

After the random copolymers containing VBT or VBA were tested using DSC, blends of each were tested to see if the problem of having partially miscible polymer blends was overcome. What was wanted was a single peak that would be in the middle of the two polymer blends as discussed in Chapter 2. To see if this has been achieved a 50:50 blend of the two polymers was made and then tested. The sample preparation was the same as described in Chapter 2, where 5g of each polymer was added to a vial and dissolved in DCM. The DCM was then allowed to evaporate off.

Table 31 DSC data for random copolymers containing VBA and VBT at 8%.

Structure	Onset °C	Peak °C	Area J/g	ΔH_f (KJ/Mol)	D_c (%)
PODMA PVBA 8%	20.7	24.7	28.55	7.2	3.0
50:50 Blend	21.0	24.4	29.82	18.0	6.7
	39.7	42.7	34.1		
PDSMA PVBT 8%	42.2	44.2	121.0	37.4	12.6

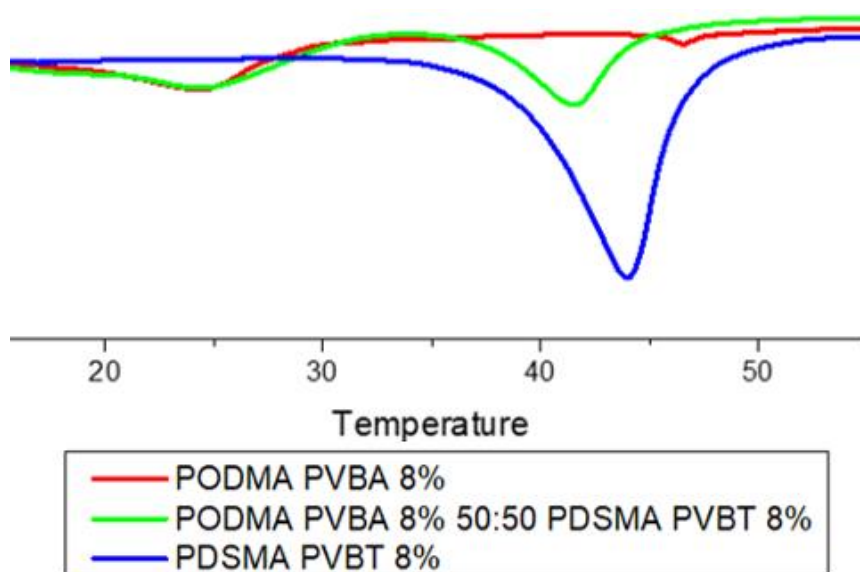


Figure 140 DSC traces of homopolymer at 8% with VBA and VBT.

The DSC results from the random copolymers and blend suggest that even though the nucleobase is present on the polymer backbone it is still not forming a miscible blend. This is because two distinct peaks are seen for the blend at 8%.

The next experiment to try to encourage a miscible mixture was to use the random copolymer containing VBA at 8% with the random copolymer containing VBT at 18%. A 50:50 sample was made and then tested. The DSC data is displayed in Table 17.

Table 32 DSC data for random copolymers containing VBA 8% and VBT at 18%.

Structure	Onset °C	Peak °C	Area J/g	ΔH_f (KJ/Mol)	D_c (%)
PODMA PVBA 8%	20.7	24.7	28.55	7.2	3.0
50:50 Blend	20.5	24.9			
PDSMA PVBT 18%	41.5	45.8	42.1	13.0	4.4

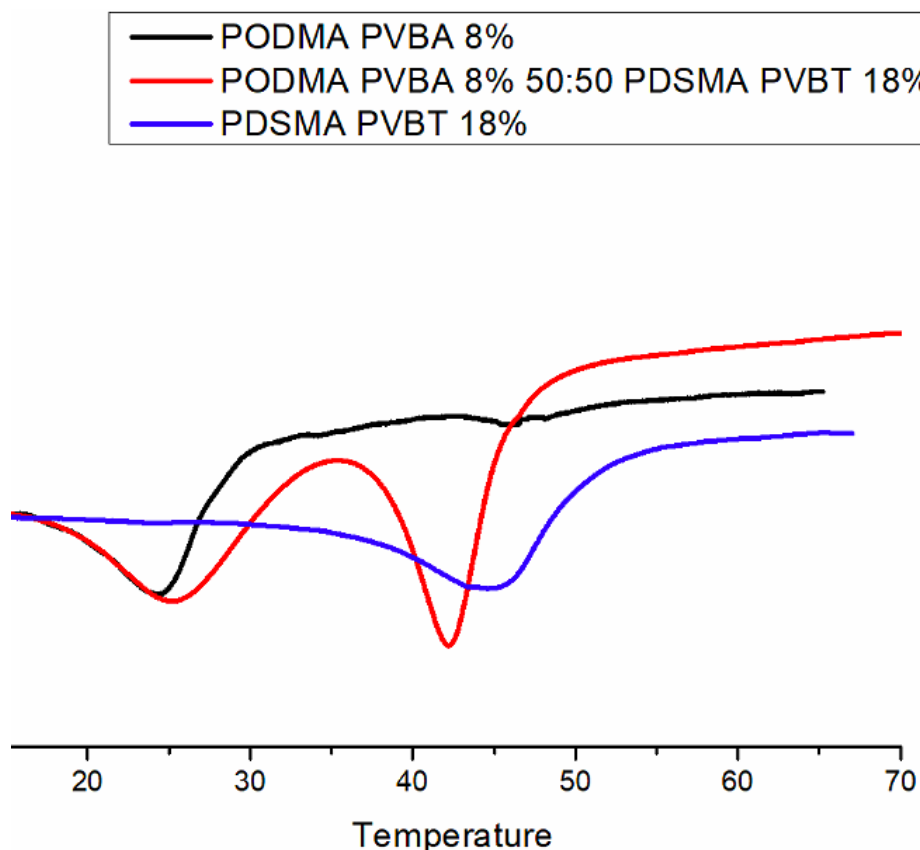


Figure 141 DSC traces of random copolymer at 8% and 18% with VBA and VBT.

The DSC results (Figure 141) for a blend of random copolymers at 8 and 18% showed similar results to the blend at 8%. It suggests no partial mixing and a fully miscible blend still has not been achieved. The final experiment to try was using a blend of the block copolymers containing the nucleobase monomers. Having a PEO block could encourage mixing and the results are shown in Figure 142.

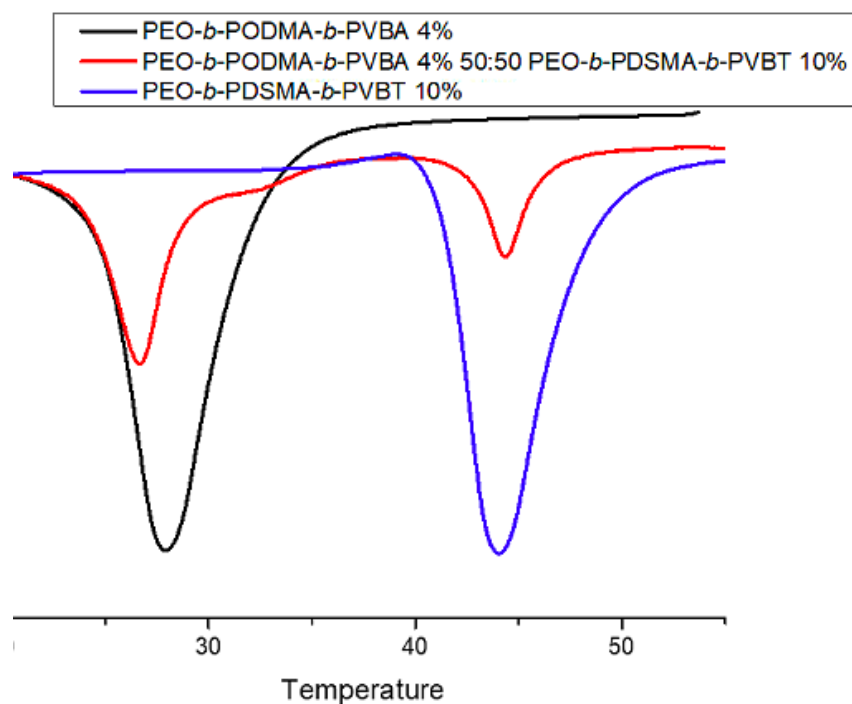


Figure 142 DSC traces of block copolymer at 4% and 10% with VBA and VBT.

The DSC results (Figure 142) for the block copolymers containing VBT and VBA suggest a partial miscible mixture with 3 peaks being observed for the 50:50 blend. Incorporating nucleobase monomers onto the polymer backbone has not led to a fully miscible mixture. It is thought that there is steric hindrance with VBT and VBA monomers and that these nucleobase monomers are too short in carbon atoms to have an effect on the mixing properties. This is backed up by the NMR titrations, where there was no hydrogen bond interaction between two random copolymers containing VBT and VBA. The T_m that takes place occurs in the outer most methyl groups which are the furthest from the polymer backbone. The interaction of VBT and VBA might not be long enough to have an effect and the desired hydrogen bond interaction that these base pair share could be being lost.

3.4.7 Long chain nucleobases monomers

VBA and VBT showed that these monomers were not long enough to force mixing through hydrogen bonding. It was concluded that the interaction between VBT and VBA was getting lost along the polymer backbone. This led to increasing the chain length of the nucleobase monomer. This led to the testing of 12-(thymine-1-yl)dodecyl methacrylate and 12-(adenine-9-yl)dodecyl methacrylate.

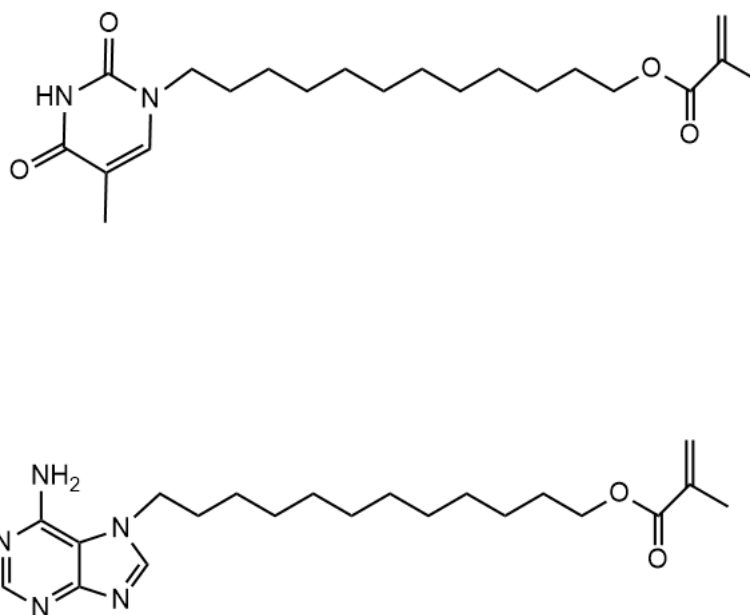


Figure 143 Chemical structures 12-(thymine-1-yl)dodecyl methacrylate and 12-(adenine-9-yl)dodecyl methacrylate.

The longest monomer that could be found in literature which could help to increase the carbon chain length was 3-bromopropyl methacrylate. This meant that this method was used but adapted which allowed for 12-bromododecan-1-ol to be used instead of 3-bromopropanol. The H-NMR (Figure 144) confirmed that 12-bromododecyl methacrylate was made with 45% percentage yield. It also meant that 12-bromododecyl methacrylate is the longest methacrylate monomer synthesised to date.

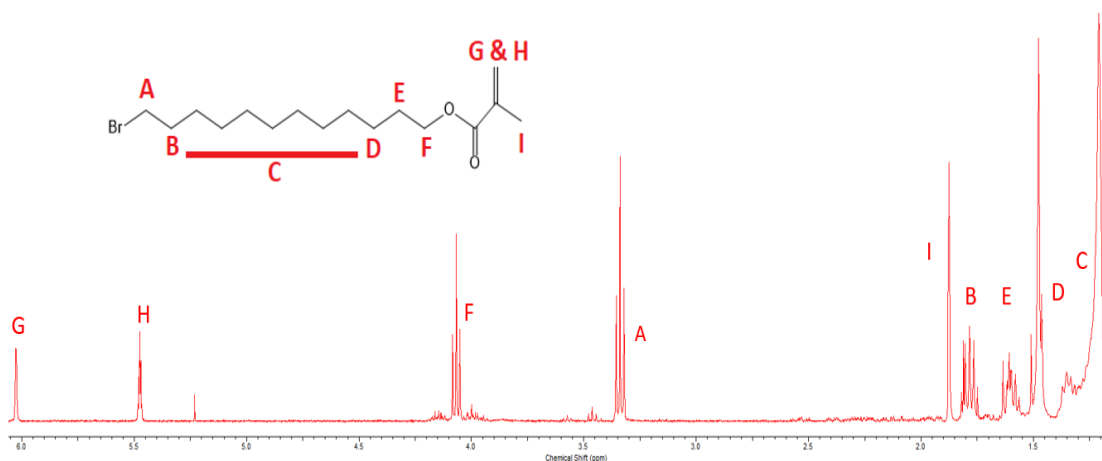


Figure 144 ^1H NMR of 12-bromododecyl methacrylate

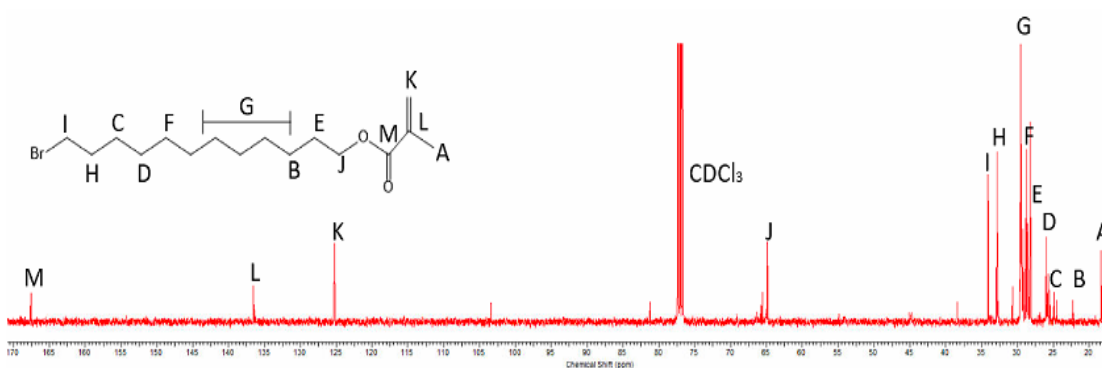


Figure 145 ^{13}C NMR of 12-bromododecyl methacrylate

The main proton signals in Figure 144 were peaks G & H which confirmed the double bond. Peak F was a triplet which was found at 4.06ppm which confirmed the ester group and peak A which was a triplet that confirmed the two protons next to the bromine atom. Peak I was important for confirming the methyl group at the end of the molecule. Despite only a 45% percentage yield being obtained, this led to the methacrylate monomer being taken and reacted with adenine and thymine to make 12-(adenin-9-yl)dodecyl methacrylate (ADM) and 12-(thymin-1-yl)dodecyl methacrylate (TDM).

The reaction of 12-(thymin-1-yl)dodecyl methacrylate (TDM) was attempted first as the reaction with thymine seemed to be much more straight forward when VBT was made compared to VBA.

Figure 146 shows the proton NMR of 12-bromododecyl methacrylate and TDM. The NMR conversion was calculated from peak 1 which is the CH_2 next to the bromine atom on the starting material and peak D which is the proton environment next to the thymine group. This was calculated to be 45%. Column chromatography was used to try and purify the reaction mixture but it was proven very difficult to isolate pure product of TDM.

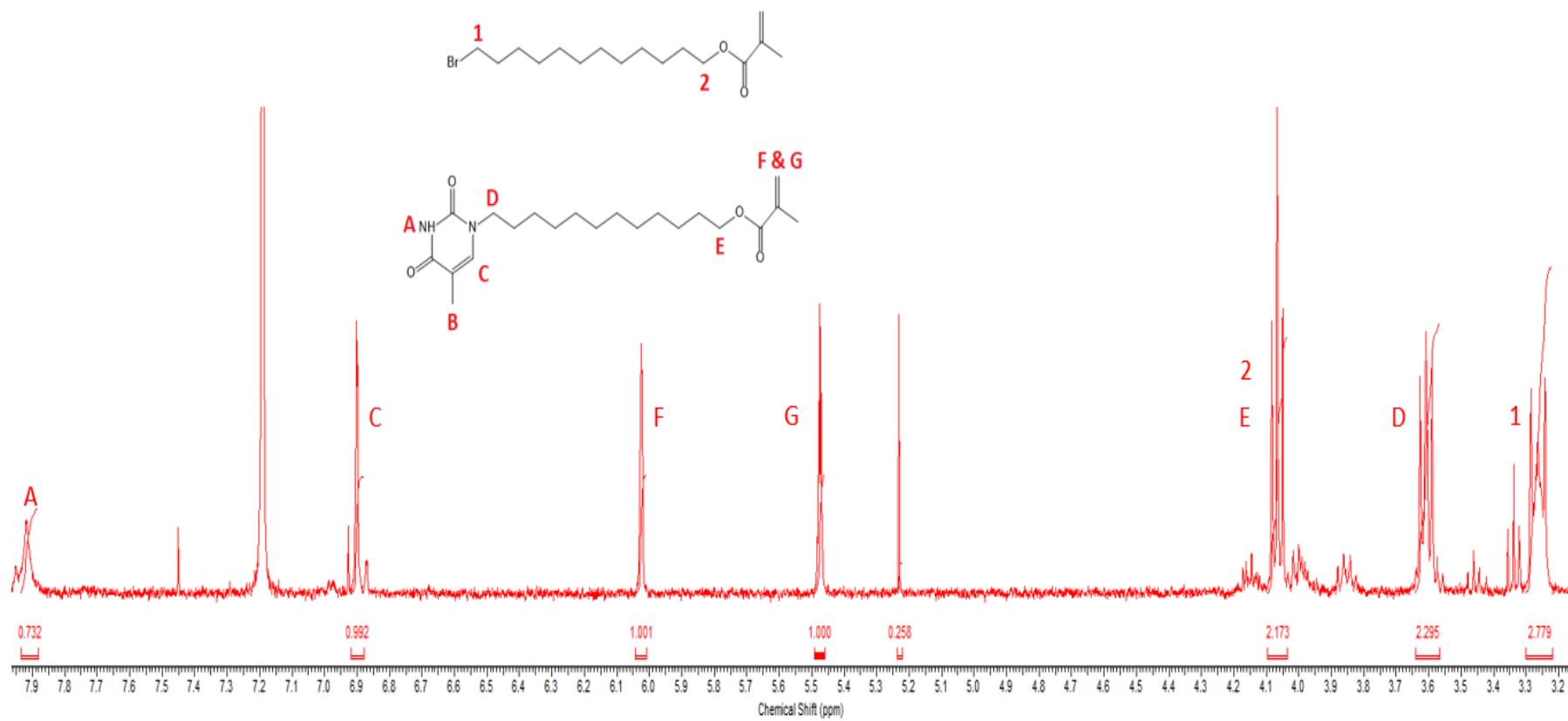


Figure 146 ^1H NMR of 12-(thymine-1-yl)dodecyl methacrylate (TDM).

Many reactions were carried out to synthesise ADM and the same outcome was achieved every time. This was that the H-NMR (Figure 147) of the reaction mixture confirmed that ADM has been made but only at 20% (NMR conversion). This was calculated from the integral of peak 1 which is the CH₂ next to the bromine atom on the starting material and peak D which is the proton environment next to the adenine group. The low yields were not ideal, as a large amount of this monomer was needed to be used in the next step of polymerising with the ODMA monomer.

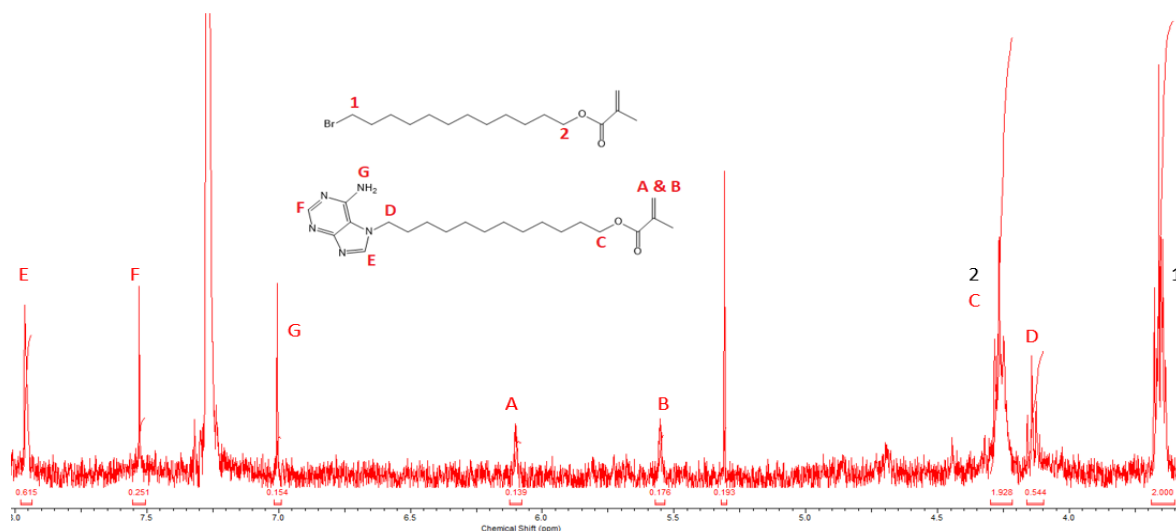


Figure 147 ¹H NMR of 12-(adenin-9-yl)dodecyl methacrylate (ADM).

Purification was attempted on ADM to remove the starting material and a cleaner proton NMR was ran.

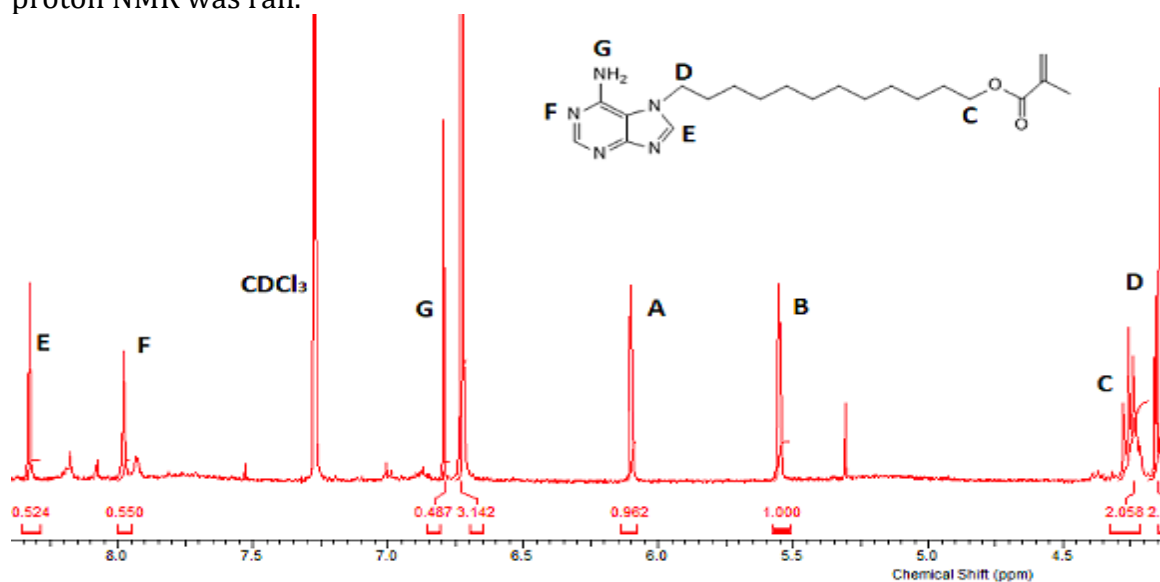


Figure 148 ¹H NMR of 12-(adenin-9-yl)dodecyl methacrylate (ADM).

3.4.8 Ester functionality nucleobase monomers (TMA & AMA)

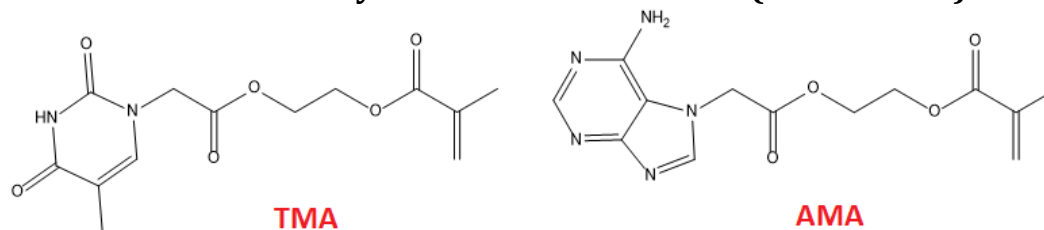


Figure 728 schematic of two monomers of , 2-(2-(adenine-9-yl)acetoxy) ethyl methacrylate (AMA) and 2-(2-(thymine-1-yl)acetoxy) ethyl methacrylate (TMA)

After researching papers published in literature,^{19,26} two monomers of , 2-(2-(adenine-9-yl)acetoxy) ethyl methacrylate (AMA) and 2-(2-(thymine-1-yl)acetoxy) ethyl methacrylate (TMA) were discovered at higher yields. AMA and TMA were quoted at around 69% for both. Previously, literature had quoted 38% yield for a long carbon adenine monomer and ADM synthesised in this chapter could only be purified at 20%. This therefore meant that switching to TMA and AMA should offer better yields of nucleobase monomers to work with. The reason for this is that AMA or TMA has incorporation of the C=O bond which makes the C-Br more reactive. There are two low-energy empty orbitals; π^* of the C=O bond and σ^* of the C-Br bond which are used to make a new molecular LUMO ($\pi^* + \sigma^*$) which has lower energy than the previous empty orbitals. This means that nucleophilic attack occurs much more easily meaning that higher yields are achieved. It was also calculated that AMA and TMA were also still longer than VBT and VBA. This meant that TMA and AMA were to be used to try and achieve full mixing of PODMA and PDSMA.

2-(2-bromoacetoxy)ethyl methacrylate had to be made first which would then react with thymine or adenine to give TMA or AMA. The NMR for 2-(2-bromoacetoxy)ethyl methacrylate is shown in Figure 149.

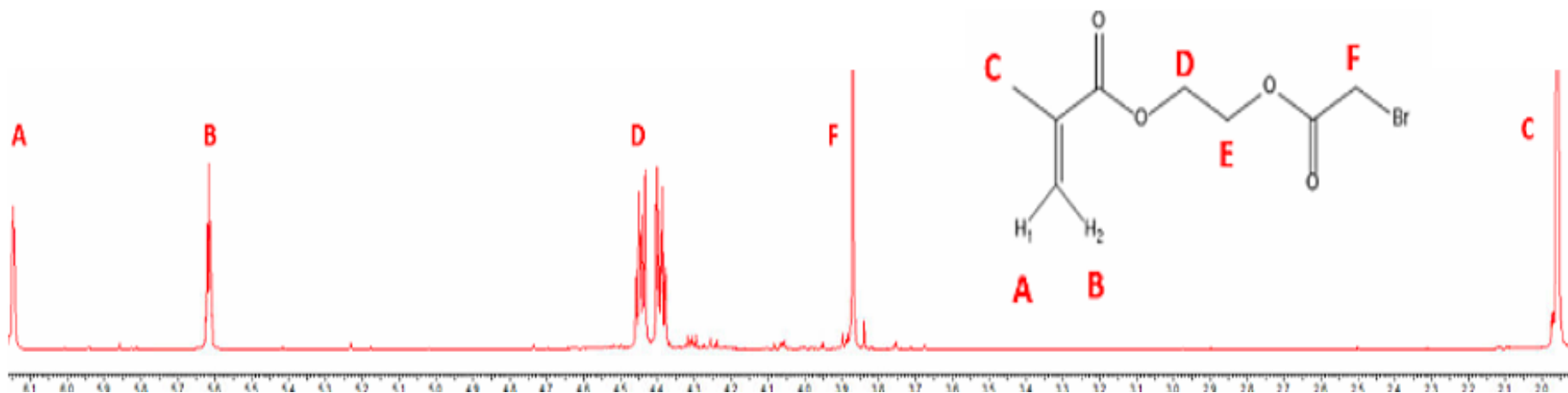


Figure 149 $^1\text{H NMR}$ of 2-(2-bromoacetoxy)ethyl methacrylate

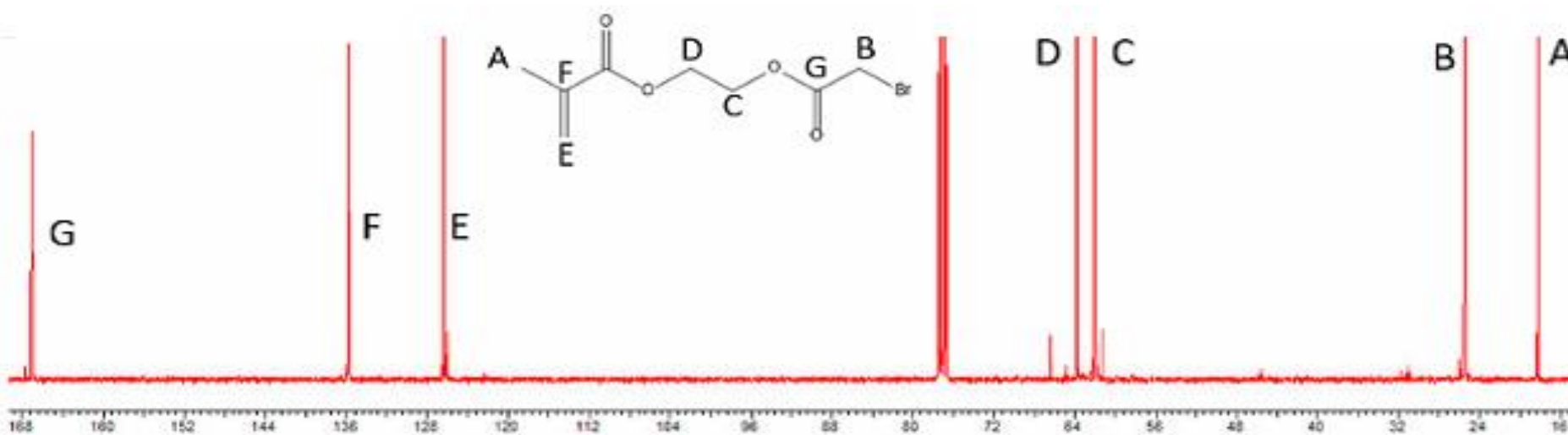


Figure 148 $^{13}\text{C NMR}$ of 2-(2-bromoacetoxy)ethyl methacrylate

2-(2-bromoacetoxy)ethyl methacrylate was taken and used to make AMA and TMA. The reaction of TMA was carried out first.

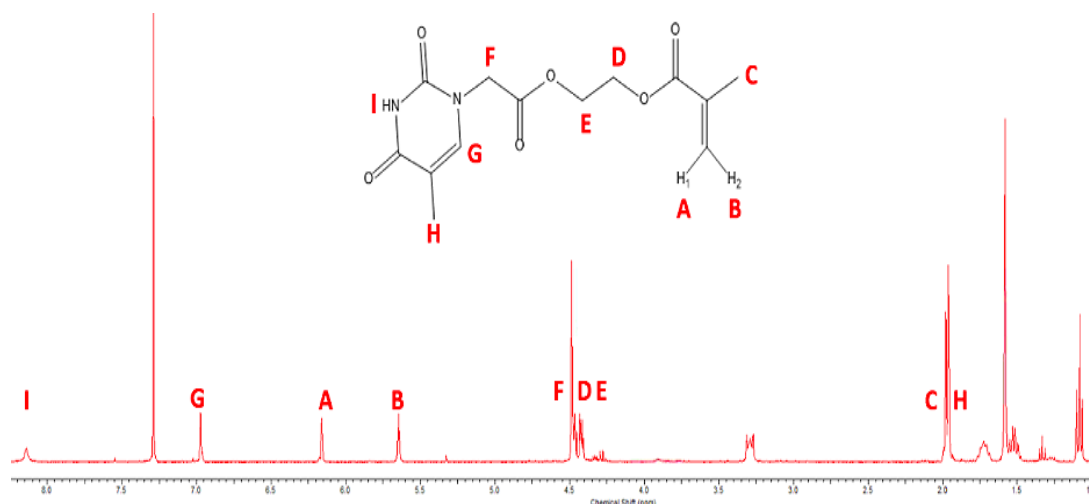


Figure 73 $^1\text{H NMR}^1$ of TMA.

Figure 149 shows the proton NMR of TMA. Between 1.0- 1.5ppm there are some proton signals which belong to TBAI as well as a large water peak at 1.5ppm. The impure TMA monomer was taken dissolved in DCM and washed 6 times in distilled water. The DCM was then separated and dried for 1 hour in MgSO_4 . This was then filtered and the solution was vacuumed down to give a much purer TMA monomer and is shown in Figure 150.

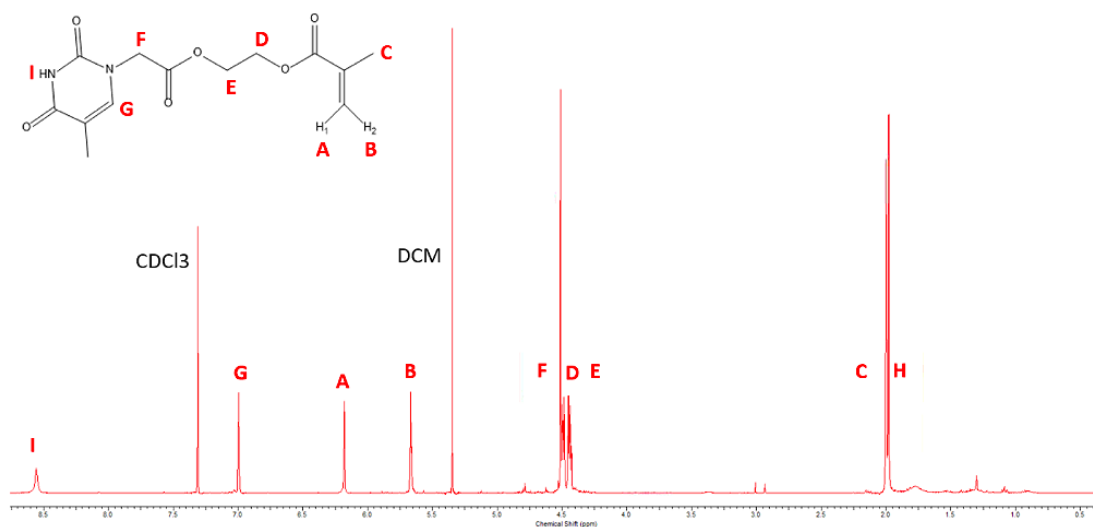


Figure 150 $^1\text{H NMR}^1$ of TMA after washing with distilled water.

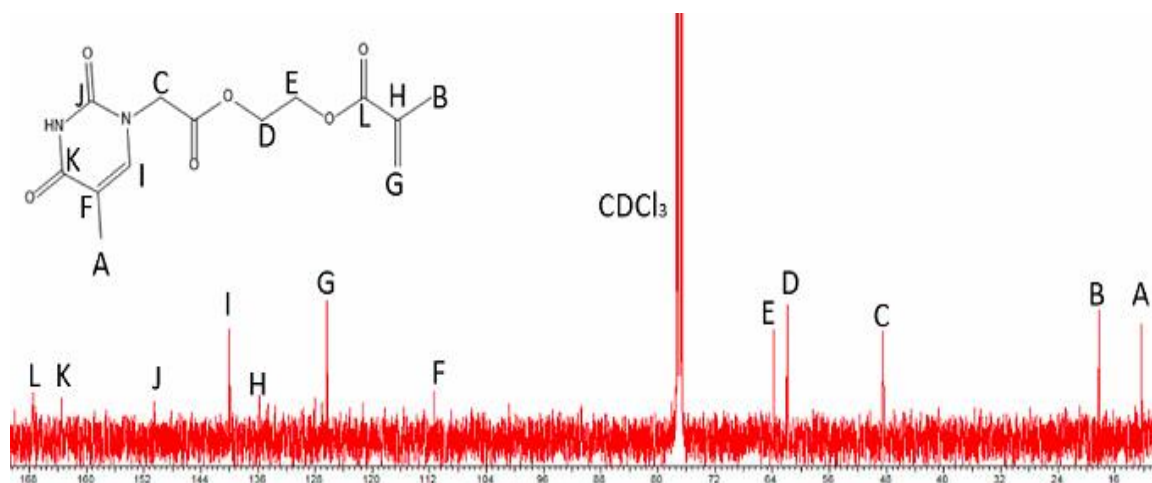


Figure 151 ^{13}C NMR of TMA.

The second reaction involved making AMA which was then characterised by NMR.

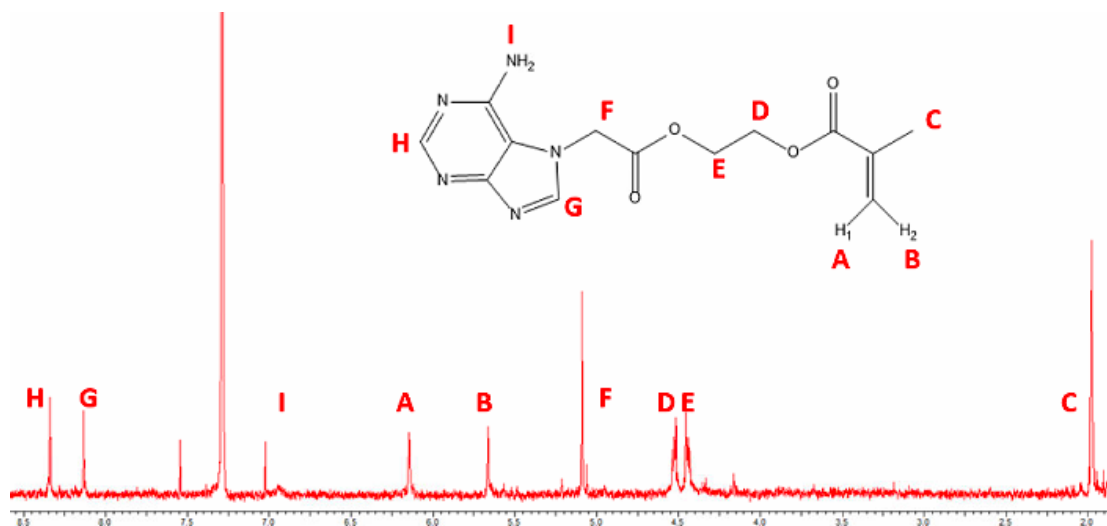


Figure 152 ^1H NMR of AMA.

After pure samples of AMA and TMA were made, they were taken and reacted with the conditions worked out for the VBT and VBA nucleobase monomers.

Table 33 Reaction conditions used for the ATRP reaction of methacrylate monomers with AMA and TMA.

Condition	Chemical
Ligand	Me ₆ TREN
Catalyst	CuCl
Reaction Solvent	Xylene: IPA (9:1)
Temperature	95°C

The ATRP reaction was set up and everything weighed out, looked like it was fully dissolved. The reaction was left over the weekend for 2 days. After 48 hours, the H-NMR for both reactions involving AMA and TMA showed a polymer peak indicating the ODMA and DSMA had polymerised but the nucleobase monomer peaks were absent from the H-NMR.

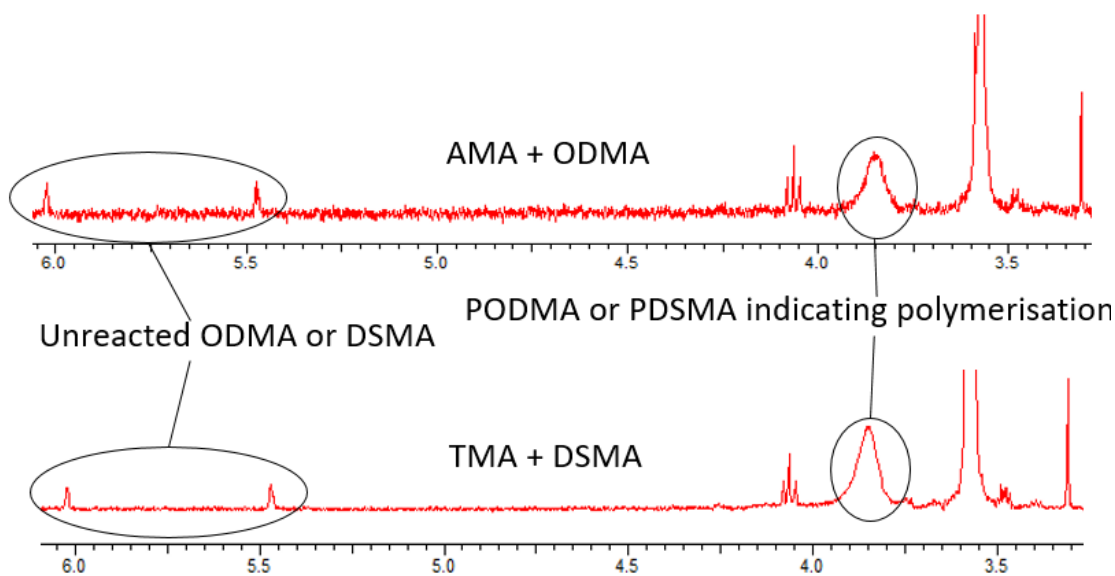


Figure 153 $^1\text{H-NMR}$ of the ATRP reaction involving block copolymers with AMA and TMA. Polymer peak at 3.8ppm indicating block copolymer had been made. Solvent CDCl_3 .

The NMR conversions were monitored and the reaction had stopped polymerising for ATRP with AMA 88.1% and TMA 92.9%. This meant that most of ODMA and DSMA had polymerised. The proton peaks of AMA and TMA were not visible in the NMR but as these peaks can be difficult to see so the block copolymers were purified to see if the resulting polymer had any of the nucleobase attached.

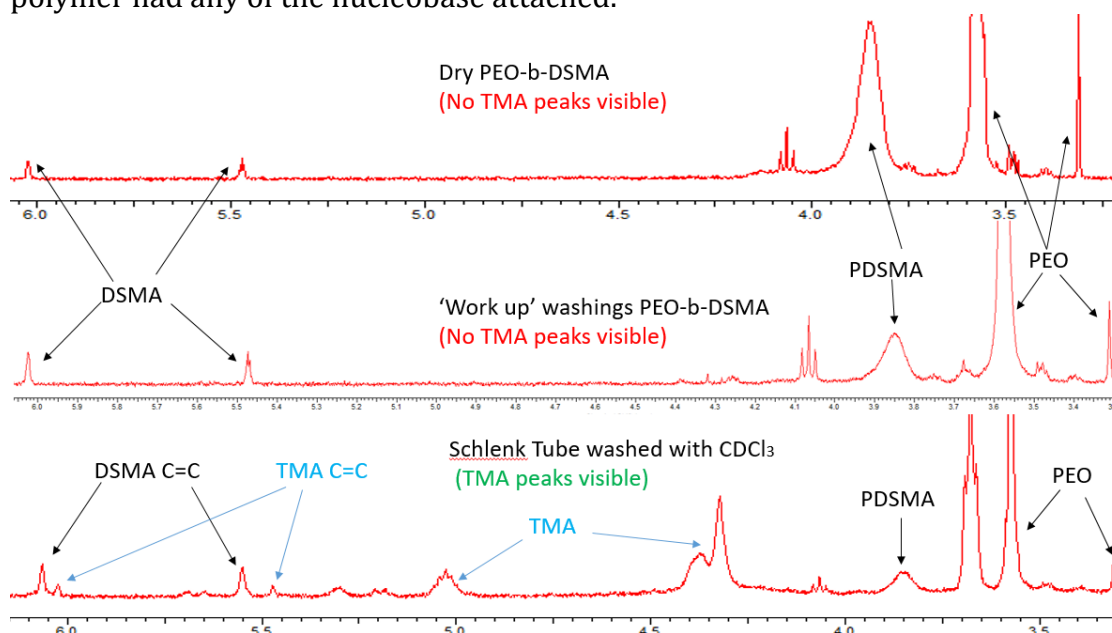


Figure 154 $^1\text{H-NMR}$ of the ATRP reaction involving block copolymers with AMA and TMA. Traces show where the ATA or TMA was after purification of block copolymer. Solvent CDCl_3 .

After the work up the resulting block copolymer showed no indication that neither AMA nor TMA had polymerised into the polymer backbone from the H-NMR. An H-NMR was taken of the purification washings and this also showed no present of AMA and TMA. It was when deuterated chloroform was added to the Schlenk tube and a proton NMR was taken of the inside of the reaction vessel, that AMA or TMA peaks could be seen. When xylene and IPA is used as a reaction solvent, the AMA or TMA will complex to the copper ligand meaning that it does not polymerise into the polymer backbone. This reaction was

repeated using DMF (a much polar solvent) with just the TMA to try and overcome this problem.

The ATRP reaction involving TMA with DSMA and the PEO-macroinitiator was repeated in DMF. From the early testing in this chapter, it was shown that DSMA does polymerise in DMF with a high NMR conversion. It was determined that when VBT was used in DMF it prohibited the polymerisation. As TMA was behaving differently to VBT, DMF was used to try and overcome the issue of TMA interacting with the copper ligand. In fact the solvent used was DMF:IPA (9:1) which allowed the IPA to be a hydrogen donor for the reaction. The reaction was left on for 48 hours initially but H-NMR suggested that a lot of unreacted DSMA was still present and a polymer peak for the PDSMA was not seen. It was after 72 hours that a small polymer peak looked to be forming but the integral didn't increase for 96 hours. It was at this point it was worked up but no block copolymer could be obtained that had TMA bonded into the polymer backbone.

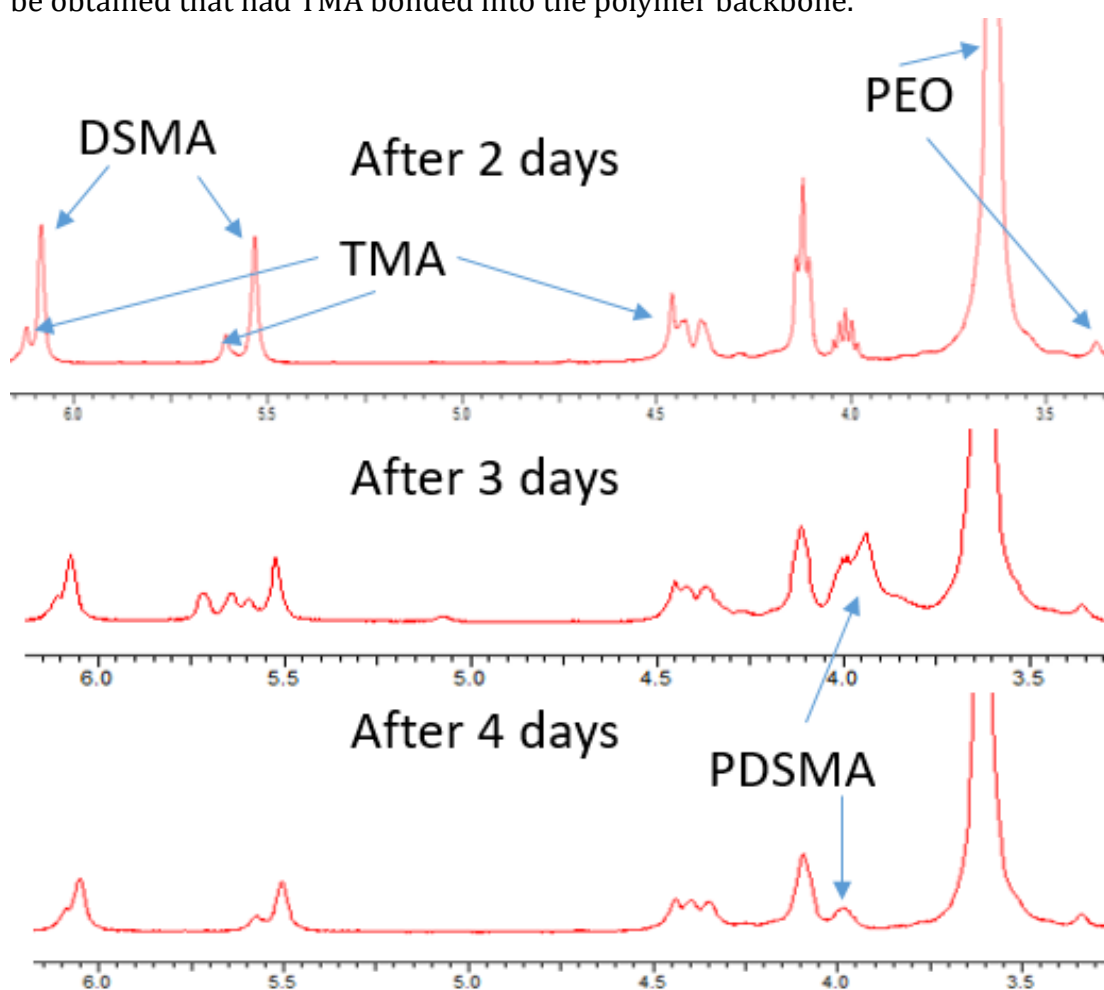


Figure 155 $^1\text{H-NMR}$ of the ATRP reaction involving DSMA with TMA. Solvent CDCl_3 .

After NMR was carried out on the block copolymer, SEC was carried out to check to see if the polymerisation had worked. NMR suggested that a small amount of DSMA had polymerised.

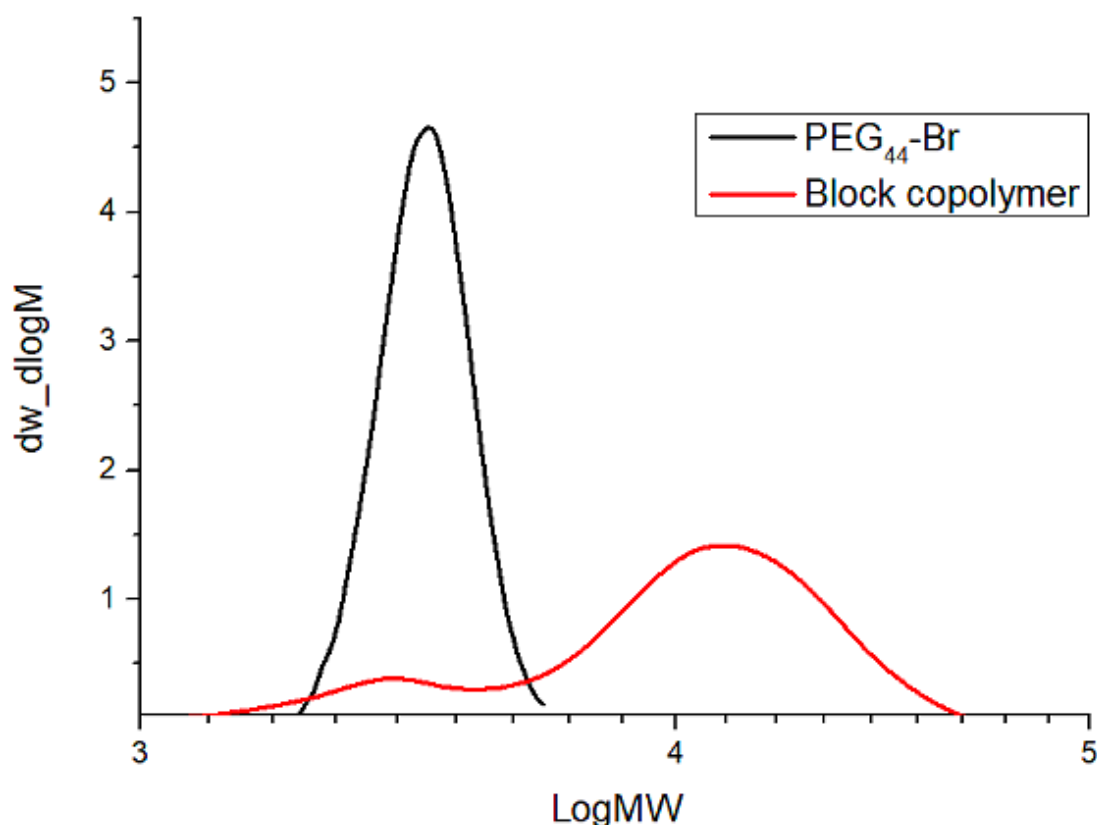


Figure 156 SEC trace of block copolymer made in DMF overlaid with the macroinitiator.

Structure	Mn	Mw	PDI
PEO- <i>b</i> -PDSMA-PTMA	7100	13300	1.86

SEC confirmed that the molecular weight had increased along with the sample containing some unreacted macroinitiator. However, the integral of the polymer peaks indicate that the molecular weight is extremely low when a DP of 50 was targeted.

Conclusion

A series of different nucleobase monomers were successfully made and characterised in this chapter. VBA and VBT were successfully attached onto the polymer backbone of homopolymers of PODMA and PDSMA as well as the block copolymers PEO-*b*-PDSMA and PEO-*b*-PODMA. What was novel about this chapter was that nucleobase monomers were added to long methacrylate monomers to form random and block copolymers. This has not been done before with methacrylate monomers as long as 18 and 22 carbon atoms. However, it was difficult to get these nucleobase monomers onto the polymer backbone and in most cases a lot less than the desired amount was added. The block copolymers containing VBT VBA were self-assembled and in some cases a combination of micelles, vesicles and bicontinuous nanospheres could be seen which has not been done before with nucleobases.

Blending polymers is difficult to do and trying to do this through nucleobase monomers still offer challenges. This chapter tried to blend two very long methacrylate polymers together and showed that if hydrogen bonding from the nucleobase is to be successful then for long polymers, long nucleobase monomers are needed. This chapter also showed

that long straight nucleobase monomers are challenging to make as side reaction take place and only offer low yields. However the synthesis of TDM & ATM were the longest nucleobase monomers now made in literature. Ester functionality within the nucleobase monomer, allowed the bromine group to become more reactive and allows for better percentage yields.

The final conclusion of this chapter showed how nucleobase monomers interact with the copper catalyst and ligand which can lead to the nucleobase not taking part in the polymerisation. This could be improved by using RAFT which does not use copper in the reaction to overcome this problem.

References

- 1 R. Mchale and R. K. O'reilly, , DOI:10.1021/ma300895u.
- 2 J. D. Watson and F. H. C. Crick, *Nature*, 1953, **171**, 737–738.
- 3 J. Pitha and P. O. P. Ts'o, *J. Org. Chem.*, 1968, **33**, 1341–1344.
- 4 K. Kondo, H. Iwasaki, N. Ueda, K. Takemoto and M. Imoto, *Die Makromol. Chemie*, 1968, **120**, 21–26.
- 5 K. Matyjaszewski and J. Spanswick, *Mater. Today*, 2005, **8**, 26–33.
- 6 J. Li, Z. Wang, Z. Hua and C. Tang, *J. Mater. Chem. B*, 2020, **8**, 1576.
- 7 A. Marsh, A. Khan, M. Garcia and D. M. Haddleton, *Chem. Commun.*, 2000, 2083–2084.
- 8 H. J. Spijker, A. J. Dirks and J. C. M. Van Hest, in *Polymer*, Elsevier BV, 2005, vol. 46, pp. 8528–8535.
- 9 H. Tang, M. Radosz and Y. Shen, *J. Polym. Sci. Part A Polym. Chem.*, 2006, **44**, 6607–6615.
- 10 J.-F. Lutz, R. Nehring and A. F. Thünemann, *SOLUTION SELF-ASSEMBLY OF SYNTHETIC COPOLYMERS BEARING COMPLEMENTARY NUCLEIC ACID FUNCTIONALITIES*, .
- 11 S. W. Kuo and R. S. Cheng, *Polymer (Guildf.)*, 2009, **50**, 177–188.
- 12 J.-F. Lutz, A. F. Thünemann and R. Nehring, *J. Polym. Sci. Part A Polym. Chem.*, 2005, **43**, 4805–4818.
- 13 S.-W. Kuo, *Polym. Int.*, 2009, **58**, 455–464.
- 14 M. Sedlák, P. Šimůnek and M. Antonietti, *J. Heterocycl. Chem.*, 2003, **40**, 671–675.
- 15 S. G. Srivatsan, M. Parvez and S. Verma, *Chem. - A Eur. J.*, 2002, **8**, 5184–5191.
- 16 B. E. Mckenzie, F. Nudelman, P. H. H. Bomans, S. J. Holder and N. A. J. M. Sommerdijk, *J. AM. CHEM. SOC*, 2010, **132**, 10256–10259.
- 17 O. R. Monaghan, *Controlling the Functionality of Block Copolymer Bicontinuous Nanospheres*, 2015.
- 18 H. J. Spijker, F. L. Van Delft and J. C. M. Van Best, *Macromolecules*, 2007, **40**, 12–18.
- 19 Y. Kang, *Synthesis and Self-Assembly of Nucleobase-containing Polymers by RAFT Techniques*, 2015.
- 20 W. Tang, Y. Kwak, W. Braunecker, N. V. Tsarevsky, M. L. Coote and K. Matyjaszewski, *J. Am. Chem. Soc.*, 2008, **130**, 10702–10713.
- 21 S. Ding, Y. Shen and M. Radosz, *J. Polym. Sci. Part A Polym. Chem.*, 2004, **42**, 3553–3562.
- 22 J.-F. Lutz, A. F. Thünemann and R. Nehring, *J. Polym. Sci. Part A Polym. Chem.*, 2005, **43**, 4805–4818.
- 23 S. Varlas, Z. Hua, J. R. Jones, M. Thomas, J. C. Foster and R. K. O'Reilly, *Macromolecules*, 2020, **53**, 9747–9757.
- 24 P. Thordarson, *Chem. Soc. Rev.*, 2011, **40**, 1305–1323.
- 25 E. Hempel, H. Budde, S. Höring and M. Beiner, *Thermochim. Acta*, 2005, **432**, 254–261.
- 26 Y. Kang, A. Lu, A. Ellington, M. C. Jewett and R. K. O'Reilly, *ACS Macro Lett.*, 2013, **2**, 581–586.

**Chapter 4. Self-Assembly of poly(methyl methacrylate)-*block*-poly-4-vinyl pyridine
(Collaborative work with Ryan Lauder part of Dr Steven Howdle University of
Nottingham)**

Table of Contents

4.1 Introduction.....	157
4.2 Experimental.....	159
4.2.1 Materials used by University of Kent.....	159
4.2.2 Materials used by University of Nottingham.....	159
4.2.3 Apparatus	159
Self-assembly procedures.....	159
Dynamic Light Scattering (DLS)	160
Transmission Electron Microscopy (TEM)	160
Characterisation performed at University of Nottingham	160
4.2.4 Reactions.....	161
Synthesis PMMA-P4VP (RAFT) in Supercritical CO ₂	161
Synthesis PMMA ₇₆ -Br (ATRP).....	161
Synthesis PMMA-Cl (ATRP)	162
Attempted synthesis PMMA- <i>b</i> -P4VP (ATRP)	162
4.3 Results and Discussion	162
4.3.1 Microstructure of PMMA- <i>b</i> -P4VP at University of Nottingham	162
4.3.2 Synthesis PMMA-Br via ATRP	165
4.3.3 Synthesis PMMA-Cl via ATRP	168
4.3.4 Synthesis PMMA- <i>b</i> -P4VP via ATRP	169
4.3.5 Characterisation and Self-assembly of PMMA- <i>b</i> -P4VP	172
Characterisation of PMMA- <i>b</i> -P4VP	172
Self-Assembly of PMMA- <i>b</i> -P4VP at University of Kent.....	173
4.3.6 Self-assembly of PEO ₄₄ - <i>b</i> -PODMA ₂₆ in Ethanol	191
4.3.7 Attempted synthesis of P4VP- <i>b</i> -PODMA.....	193
Polymerisation in scCO ₂	193
Conclusion	195
References	196

4.1 Introduction

A class of materials commonly referred to as metal oxides have properties which makes them of use to applications¹ involving catalysis,² solar cells,³ energy storage,⁴ photonics⁵ and gas sensing.⁶ All the applications listed benefit from morphologies that provide increased storage, better diffusion and increased reactivity. This means that metal oxides that have well-defined and repeating structures on both the micron and nano scale have attracted much interest.⁷⁻⁸

The most common approaches to their synthesis taken use soft templating, hard templating and hydro/solvo-thermal routes. These approaches use hydrolytic or nonhydrolytic sol gel precursors to achieve the final structure of the material.¹ Syntheses that uses a hydrosolvothermal approach offers morphological control. This is demonstrated by the fabrication of diverse morphologies that have short diffusion distance. Examples being nanoparticles,⁹ microspheres that are porous,¹⁰ hollow particles¹¹ and nanowires.¹² Having said this, synthesis involving hydrothermal routes does have some drawbacks, the main one being that the size of the morphology of the templated material is usually poor when compared to other approaches.¹³

Approaches that use hard templating, show that it is an effective method for producing well-defined ordered mesoporous materials but sees drawbacks in practicality and scalability.¹⁴ This leaves the soft templating approach, which is described as more versatile, flexible and promising for large scale procedures when compared by contrast to the other two methods. This approach allows the mesopore structure to be controlled by controlling the reaction conditions used in the synthesis as well as the properties of the template molecules.¹⁵⁻¹⁶

Recent studies have used soft templating routes using pluronic block copolymers (BCP) due to them being commercial available.¹ Pluronic block copolymers also allow a range of mesoporous materials that have high surface area, diverse compositions, pore structures that can be varied and tuneable pore sizes.¹⁶⁻¹⁷ There is a limitation for using pluronics which comes from their restrictive block chemistry, compositions, molecular weight, high oxygen content and exhibit lower glass transition temperatures compared to their non-Pluronic counterparts. Controlled radical synthesis of BCPs (via reversible addition-fragmentation chain-transfer (RAFT) and atom transfer radical polymerisation (ATRP)) allows BCPs to be made easily through facile and cheap routes.

The Howdle group at the University of Nottingham has worked on a facile, one pot, solvent free method where using RAFT polymerisation allows for nanostructured BCP microparticles to be made in supercritical carbon dioxide.¹⁸ The microparticles made were shown to be structurally diverse and different morphologies could be made by changing the composition and chemical structure. The way they do this is by using poly(methyl methacrylate)-*block*-poly(4-vinylpyridine) (PMMA-*b*-P4VP) BCP microparticle which can be used for a range of metal oxide materials and is shown in Figure 157.

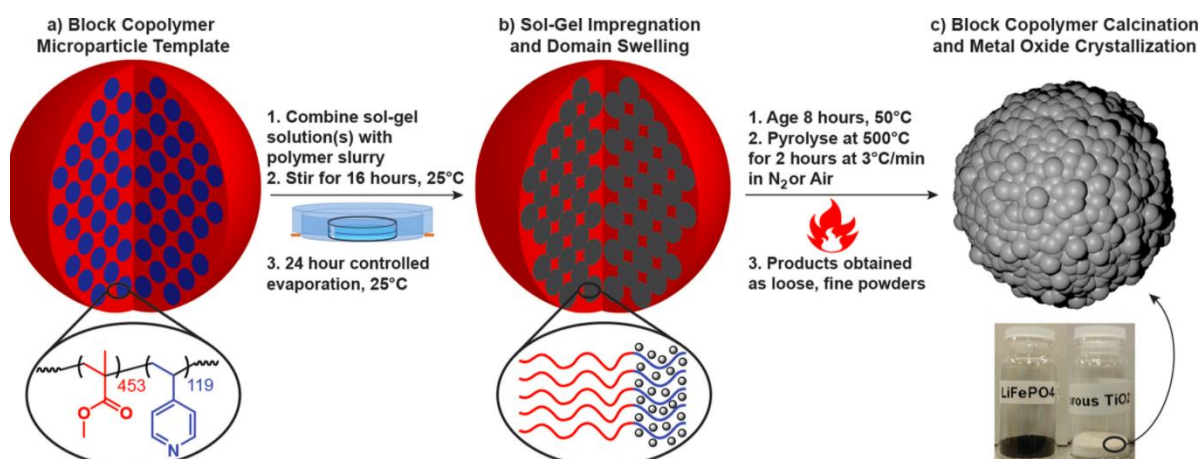


Figure 157 Shows the BCP microparticle sol-gel templating as well as the calcination process. A) Shows the BCP microparticle template where there is an internal morphology of P4VP spheres within a PMMA matrix. B) The P4VP spheres start to swell in ethanol causing sol-gel impregnation. C) BCP template is removed by calcination causing metal oxide crystallisation at 500 °C in air or nitrogen.¹

One reason for using 4-vinylpyridine is that it is a common hydrophilic block which has successfully allowed metal oxides in films to be made. A second advantage is that a range of different morphologies has been made when 4-vinylpyridine is used.¹⁹ The Howdle group have used two metal oxide systems which were titanium dioxide (TiO_2) and LiFePO_4 . Titanium dioxide has many applications, a few being pigments, photocatalysis, photovoltaics and electrical energy storage.²⁰ LiFePO_4 was selected as it is a more specialised class of material which is starting to be used more in industry.

The PMMA-*b*-P4VP template was made by using RAFT dispersion polymerisation in super critical carbon dioxide. The standard method targeted PMMA-*b*-P4VP molecular weight of 57.8 KDa (\bar{M}_n 1.34) with a weight fraction of P4VP to be 0.22. Previously it has been observed that when the weight fraction of P4VP is between 0.1-0.35, the morphology of P4VP spheres surrounded by PMMA matrix occurs (Figure). It is within this range that the microparticle structure is retained upon mixing P4VP with selective solvent such as ethanol.²¹

Previously, PMMA-*b*-P4VP was used successfully to produce P4VP spheres in a PMMA matrix which ranged from 12-200 nm by altering the molecular weight of the two blocks. This has paved the way for future work to look at templated synthesis of other BCP morphologies such as lamellar or bicontinuous aggregate structures. The University of Nottingham could not achieve these structures and since the work of PEO-*b*-PODMA led to bicontinuous nanospheres, a collaborative project was started. This chapter aims to self-assemble PMMA-*b*-P4VP in water and ethanol to access the different morphologies available which could be used in the templating process with the main aim of trying to form lamellar or bicontinuous structures. Samples of PMMA-*b*-P4VP were first prepared by RAFT polymerisation but ATRP will also be used to target polymers with lower molecular weight. The Howdle Group have found it difficult to make block copolymers with low molecular weight and does appear to be a limit on what they can make.

4.2 Experimental

4.2.1 Materials used at University of Kent

2-bromoisobutryl bromide (BIBB) (98%), , N,N,N'N'N"-pentamethyldiethylenetriamine (PMDETA) (99%), octadecyl methacrylate (ODMA) tris[2-dimethylamino]ethyl]amine (Me₆TREN), methyl methacrylate (MMA) and Triethylamine (TEA) (99%) were all purchased from Sigma-Aldrich and used as received. Ethanol, tetrahydrofuran (THF), methanol, dimethylformamide (DMF), copper bromide (CuBr), copper chloride (CuCl), 4-vinyl pyridine (4VP) and hydrochloric acid (HCl)(36%) were purchased from Fisher Scientific and used as received apart from the hydrochloric acid, which was turned into a 0.1M solution. Distilled water used as obtained from University of Kent. The deuterated chloroform used in ¹H-NMR and ¹³C-NMR was purchased from Cambridge Isotope Laboratories.

4.2.2 Materials used at University of Nottingham

Methyl methacrylate (MMA, ProSciTech, 99%) and 4-vinylpyridine (4VP, Acros Organics, 95%) were purified by eluting through a basic alumina column to remove inhibitor. 2,2'-azobis(2-methylpropionitrile) (AIBN, Sigma Aldrich, 98%) was purified by recrystallisation from methanol. Dry CO₂ (BOC, SFC grade, 99.99%), 2-(dodecylthiocarbonothioylthio)-2-methylpropionic acid (DDMAT, Sigma Aldrich, 98%) RAFT agent and poly(dimethylsiloxane) monomethyl methacrylate (PDMS-MA, Fluorochem, Mn ~10 kg mol⁻¹) stabiliser were used as received.

4.2.3 Apparatus

All reactions were performed under inert atmosphere (nitrogen) using Schlenk techniques.

Self-assembly procedures

A typical procedure for the self-assembly of PMMA-*b*-P4VP consisted of using the following: a syringe pump brought from Semat Technical Limited which added solvents at 0.075 mL per minute and dialysis membrane (MW 12-14 kDa) brought from MEDICELL international Ltd. Distilled water was used as obtained.

The block copolymer (0.1 or 0.01 g) was dissolved in THF (X mL) and stirred in an oil bath at 60°C. Deionised water was added dropwise (at 4.5 mL h⁻¹) using a syringe pump (Semat technical Limited, 220 Voltz, 0.1 Amps, 50 Hz) and the volume of THF containing the BCP was made up 10 mL. After addition of distilled water, the solution was transferred to 10 mL dialysis cassette (MEDICELL International Ltd) fitted with a dialysis membrane (MW 12-14 kDa). This was left spinning in 4 L of deionised water at 60°C for 24 hours. In this time the water was changed twice. The aggregates formed were analysed using dynamic light scattering (DLS) and transmission electron microscopy (TEM). Figure shows the self-assembly process using distilled water. The same method was used

for ethanol but the dialysis was carried out in 1L ethanol for 24 hours where the solution was changed four times.

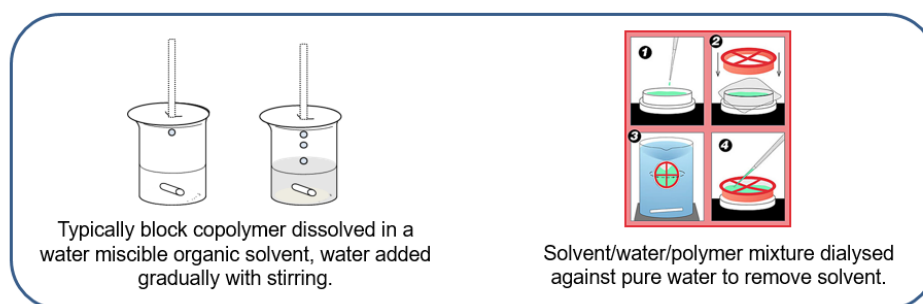


Figure 158 Demonstrating the process of self-assembly. The block copolymer is first dissolved in an organic solvent which is then transferred to a dialysis cassette where dialysis is carried out for 24 hours.

Dynamic Light Scattering (DLS)

All dynamic light scattering measurements were performed on a Malvern High Performance Particle Sizer (Nano Zetasizer HPPS HPP5001). This instrument contains a laser with a wavelength of 633 nm. The measurements were carried out using a clean quartz cuvette, which holds 1 mL of sample. Samples were first filtered using a 1.2 μm filter and then measurements were carried out at a temperature of 25°C for the BCP aggregates. 11 measurements were recorded with the first measurement being discarded and average values taken from the remaining 10.

Transmission Electron Microscopy (TEM)

The self-assembled block copolymer aggregates had transmission electron microscopy carried out on them using a JEOL JEM (200-FX) TEM instrument (120 kV). Samples of 5 μL were pipetted onto a carbon coated copper grid (200 mesh) and allowed to evaporate off for 10 minutes. Any excess sample was removed using suction. 5 μL of uranyl acetate (5%) was put onto the grid to stain the sample and any excess was removed by suction.

Characterisation performed at University of Nottingham

The University of Nottingham performed gel permeation chromatography (GPC) which was used to measure the molecular weight and dispersity of the polymers. An Agilent 1260 infinity SEC system was used with a Wyatt Optilab dRI detector. The mobile phase was a solvent mixture of chloroform and ethanol (9:1) with triethyl amine stabiliser (1% v/v). Samples were injected at a flow rate of 0.5 mL min⁻¹ and passed through a guard column followed by two separation columns (2 x Agilent PLgel 5 μm mixed C). The system was calibrated using PMMA narrow standards (M_n range: 0.5-2,000 kg mol⁻¹).

Scanning electron microscopy (SEM) was used to characterise the morphology of polymer aggregates. Samples were imaged using a JEOL 6490LV SEM at an accelerating voltage of 10 kV after first being coated with a 6 nm layer of platinum.

4.2.4 Reactions

All reactions were performed either by RAFT or ATRP polymerisation.

Synthesis of PMMA-P4VP (RAFT) in Supercritical CO₂

The following procedure was used to synthesise a PMMA₅₀₀-*b*-P4VP₁₆₂ block copolymer. MMA (7.5 g, 74.9 mmol), AIBN (12.3 mg, 0.15 mmol), DDMAT (54.6 mg, 0.07 mmol) and PDMS-MA polymeric stabiliser (0.5 g) were mixed in a sealed vial at 0 °C and degassed by purging with argon for 30 minutes. Meanwhile a 60 mL autoclave was degassed by flushing with CO₂ at 1-2 bar for 30 minutes. The monomer solution was added to the autoclave via syringe against a positive pressure of CO₂ to prevent the ingress of air. The autoclave was then sealed, pressurised to 50 bar and heated to 65 °C before further addition of CO₂ to the reaction pressure of 241 bar.

After stirring at 300 rpm for 24 hours, a small sample of the PMMA first block was collected through the outlet tap for analysis. Then, a degassed solution of 4VP (3 g, 28.5 mmol) and AIBN (7.5 mg, 0.05 mmol) was added to the autoclave via a high-performance liquid chromatography (HPLC) pump (Jasco PU-4180) at a flow rate of 0.5 mL min⁻¹. After a further 24 hours, the reaction was cooled to room temperature, slowly vented and the PMMA-*b*-P4VP product collected as an off-white, dry free-flowing powder (9.48 g, 86% yield).

Synthesis of PMMA₇₆-Br (ATRP)

A literature method²² was followed and adapted for the synthesis of PMMA₇₆-Br. A general procedure used methyl methacrylate (MMA) (1 g, 9.99 mmol) dissolved in toluene (5mL) in a round bottom flask. This was degassed with nitrogen by bubbling for 30 minutes. CuBr (14.3 mg, 0.1 mmol) were added to a dried Schlenk and degassed in nitrogen for 30 minutes. The degassed MMA was transferred to the Schlenk tube. PMDETA (34.6 mg, 0.2 mmol) and initiator ethyl α -bromoisobutyrate (Eib-Br) (19.5 mg, 0.1 mmol) were added and reaction mixture and this was degassed by bubbling with nitrogen gas for a further 30 minutes at room temperature. The reaction mixture was then heated at 90°C with stirring for 24 hours. Subsequently THF was added to reaction mixture and the resultant mixture was run through an alumina column to remove catalyst and ligand. The reaction mixture was then evaporated off using a rotatory evaporator to remove most of the THF. The product was then precipitated in cold methanol and filtered collecting PMMA₇₆-Br as the product. Percentage yield 61%. **¹H-NMR (400 Hz, CDCl₃, ppm) δ : 4.03 (2H, CH₃CH₂O-), 3.53 (3H, CH₃O-), 1.75 (2H, CH₂CCH₃)** **¹³C NMR (CDCl₃, ppm) Fig δ : 16.4, 18.7, 44.5, 44.9, 51.8, 52.4, 177.1, 177.8 M_n = 7,600**

The same method above was used for PMMA₁₇₀-Br where PMMA (2g 0.020 mol) was used and PMMA₂₂₆-Br where PMMA (3g 0.030 mol) was used. The quantities of initiator, catalyst and ligand remained the same. Percentage yields of PMMA₁₇₀-Br & PMMA₂₂₆-Br were 57 % and 50 % respectively.

Synthesis of PMMA-Cl (ATRP)

A literature method²² was followed and adapted for the synthesis of PMMA₁₀₆-Cl. A general procedure used methyl methacrylate (MMA) (5.32 g, 0.053 mol) dissolved in toluene (5mL) in a round bottom flask. This was degassed with nitrogen by bubbling for 30 minutes. CuBr (0.07 g, 0.49 mmol) were added to a dried Schlenk and degassed in nitrogen for 30 minutes. The degassed MMA was transferred to the Schlenk tube. PMDETA (0.17 g, 0.98 mmol) and initiator methyl 2-chloropropionate (0.06 g, 0.49 mmol) were added and reaction mixture and this was degassed by bubbling with nitrogen gas for a further 30 minutes at room temperature. The reaction mixture was then heated at 90°C with stirring for 24 hours. Subsequently THF was added to reaction mixture and the resultant mixture was run through an alumina column to remove catalyst and ligand. The reaction mixture was then evaporated off using a rotatory evaporator to remove most of the THF. The product was then precipitated in cold methanol and filtered collecting PMMA₁₀₆-Cl as the product. Percentage yield 54 %. ¹H-NMR (400 Hz, CDCl₃, ppm) δ: 3.53 (3H, CH₃O-), 1.74 (2H, CH₂CCH₃) ¹³C NMR (CDCl₃, ppm) Fig δ: 16.4, 18.7, 44.5, 44.9, 51.8, 52.4, 177.1, 177.8

The same method above was used for PMMA₁₃₇-Cl where PMMA (7.0 g 0.07 mol) was used. The quantities of initiator, catalyst and ligand remained the same. Percentage yield of PMMA₁₃₇-Br were 52 %.

Attempted synthesis PMMA-*b*-P4VP (ATRP)

A literature method²³ was followed for the attempted synthesis of PMMA-*b*-P4VP. The PMMA-Cl macroinitiator (100 mg) was dissolved in DMF (0.5 mL) in a Schlenk tube. CuCl (2.6 mg 0.026 mmol) was added to the Schlenk tube and degassed by bubbling nitrogen gas through it for 1 hour. Me₆TREN (0.006g, 0.026 mmol) was then added and the mixture degassed a further 30 minutes. 4-vinylpyridine (0.1 g, 0.95 mmol) was added and the reaction mixture was degassed a further 30 minutes. After degassing, the reaction was heated at 50°C with stirring for 24 hours. Further reactions were carried out following the above procedure but at temperature 80°C .

4.3 Results and Discussion

4.3.1 Microstructure of PMMA-*b*-P4VP at University of Nottingham

The main aim of this project was to make different BCP aggregate structures for use as templates at the University of Nottingham. The current application performed by University of Nottingham involved making a slurry of PMMA-*b*-P4VP block copolymer microparticles. This was achieved by taking the BCP (1g) and dispersing it in ethanol (40 mL).¹ The University of Nottingham took SEM images of all the samples before sending them to The University of Kent (Figure 159). They also took TEM images of PMMA₄₅₃-*b*-P4VP₁₁₉ (Figure 160).

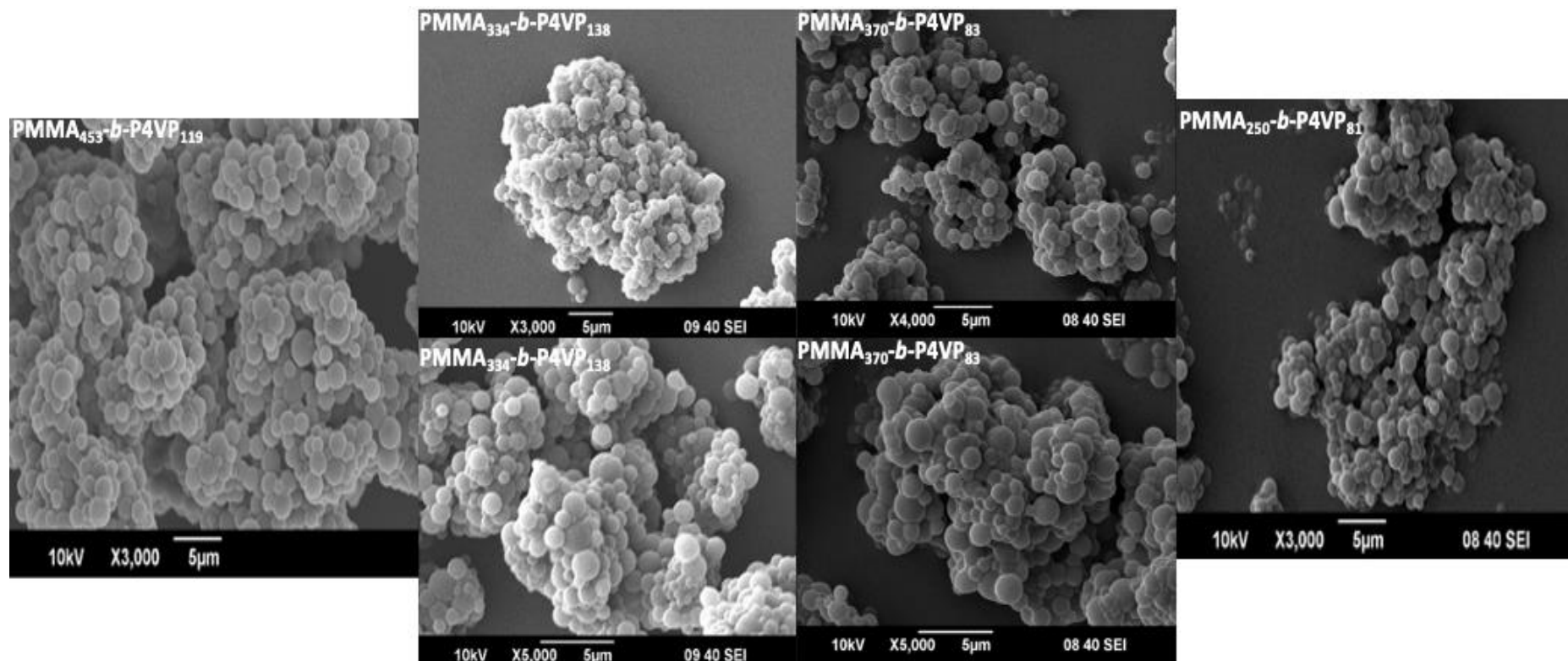


Figure 159 SEC images of the BCP microparticle templates for all the samples sent in for testing. Achieved by mixing in ethanol and using a BCP containing 10-35wt% of P4VP.

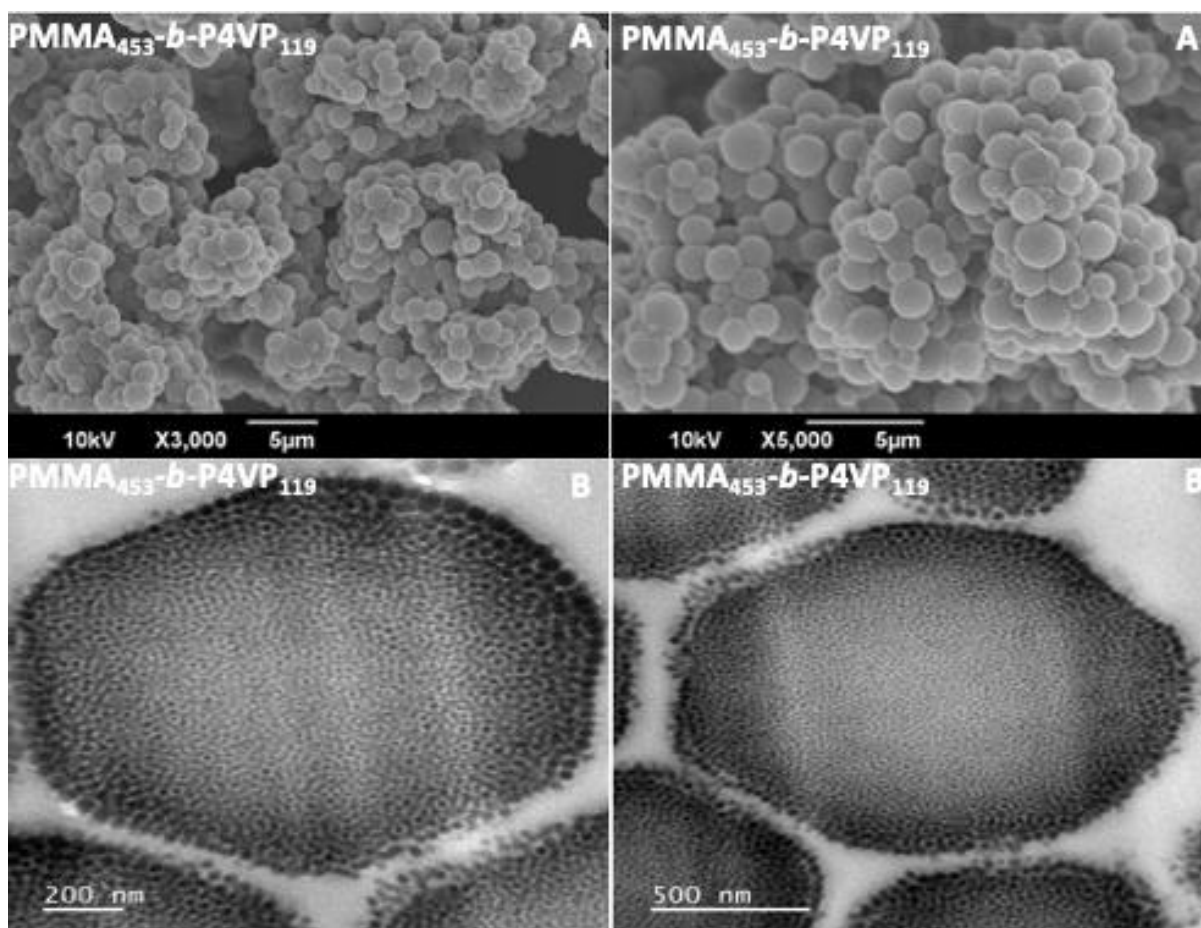


Figure 160 SEM (A) and TEM images (B) of $PMMA_{453}\text{-}b\text{-}P4VP_{119}$ after mixing in ethanol. The University of Nottingham describe it as a morphology of P4VP spheres within a PMMA matrix. Dark regions (B) correspond to I_2 stained P4VP. Sample displays a spherical self-assembled morphology.

The composition of each $PMMA\text{-}b\text{-}P4VP$ was chosen from a recent study²⁴ where it was demonstrated that a 10-35 wt% of P4VP gave rise to a morphology of P4VP spheres in a PMMA matrix when mixing with a selective solvent such as ethanol. The TEM images reveal a homogenous composition of microparticles, each possessing the internal morphology of PMMA matrix embedded with P4VP spheres with a domain size of ~ 29.5 nm. As the basis of this work is to examine what other structures can be achieved with $PMMA\text{-}b\text{-}P4VP$, it is important to compare any new structures with the microparticles shown above. This will ensure that anything new being observed is different from what has previously been witness at Nottingham. As the application described involves ethanol, it was important to make sure that this solvent was used in the self-assembly of $PMMA\text{-}b\text{-}P4VP$. Thus, self-assembly was carried out in both solvents.

4.3.2 Synthesis PMMA-Br via ATRP

The initial objective of the work described in this chapter, was to make a series of PMMA-Br samples with different molecular weights. These would then be taken and reacted with 4VP to produce samples of PMMA-*b*-P4VP with various molecular weights. 3 samples of PMMA-Br of different molecular weights were synthesised. The reaction involving ethyl α -bromoisobutrate and methyl methacrylate went to completion and formed PMMA-Br in all cases.

After it was clear that PMMA-Br had been successfully made it was purified through an alumina column, followed by precipitation from THF into methanol. Despite there being a distinct band of green on the column, some copper had leaked out and still remained in the polymer. This can be seen by the first workup producing a blue sample and when this was placed in an oven it turned to a green colour.



Figure 160 (Right) Sample of PMMA-Br after the first purification stage showing blue polymer indicating copper leakage. (left) Sample of PMMA-Br after first purification stage after it had been in the oven for at 80°C for an hour. Green colour indicating present of copper.

The purification stage was repeated using methanol to precipitate out PMMA-Br and separate it from starting material and the copper. It took a total of 5 washes to eventually produce a white sample. This can also explain why the percentage yields of the three samples were so low (Table 34) when the NMR conversions suggested that most of the MMA had reacted.

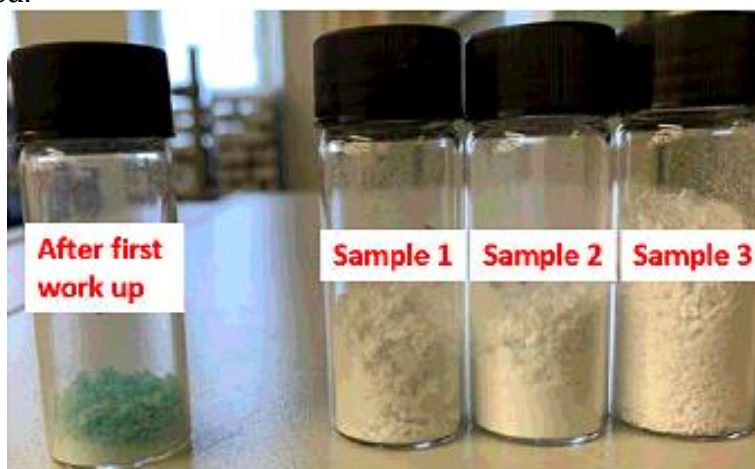


Figure 741 The three samples of PMMA-Br after being purified 5 times in methanol.

Table 34 Percentage Yields of PMMA-Br made by ATRP

Structure	Percentage Yield (%)
PMMA ₇₆ -Br	60.7
PMMA ₁₇₀ -Br	57.3
PMMA ₂₂₆ -Br	50.3

Proton and carbon NMR was used to characterise the purified samples of PMMA-Br. The three samples of PMMA-Br all showed similar proton and carbon NMR traces. A typical ¹H NMR spectrum is shown in Figure 162 and a typical ¹³C NMR spectrum in Figure 163 of the purified samples of PMMA-Br.

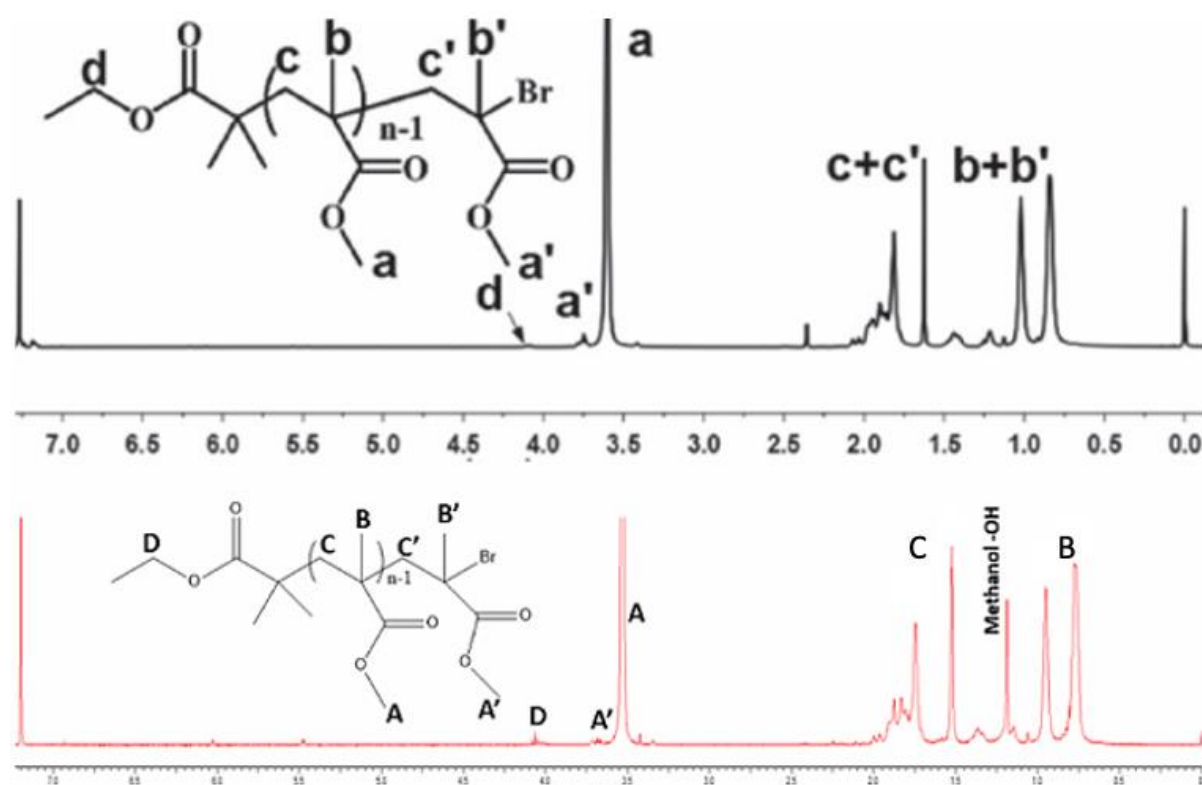


Figure 162 A comparison of the NMR spectra for PMMA-Br from the literature (top) and this project (PMMA₇₆)

The proton NMR closely matches the literature paper²² from which the procedure for making PMMA-Br was taken. NMR conversion was calculated from the integrals of the monomer signals that occur around 5.5 and 6.0 ppm and compared to Peak A (PMMA signal) (Table 35)

Table 35 NMR conversion and percentage yields of the three PMMA-Br made by ATRP.

Sample	Structure	NMR Conversion (%)	Percentage yield (%)
1	PMMA ₇₆ -Br	96.4	60.7
2	PMMA ₁₇₀ -Br	94.6	57.3
3	PMMA ₂₂₆ -Br	98.2	50.3

Carbon NMR was also used to characterise each sample and was carried out also. This can be seen below in Figure .

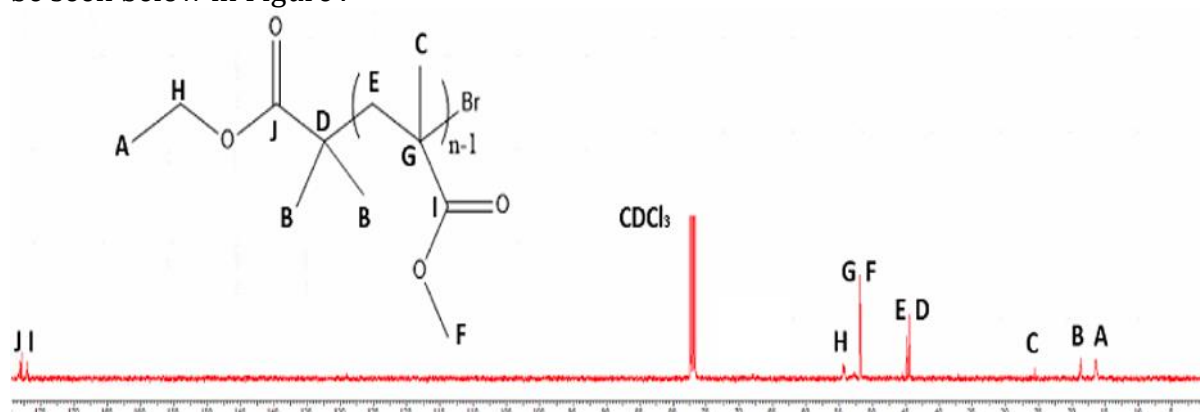


Figure 163 ^{13}C NMR of PMMA₇₆-Br synthesised by ATRP.

Peak C provides further evidence that the bromine atom is at the end of the molecule as the electron withdrawing bromine and ester group would make peak C occur at around 27ppm.

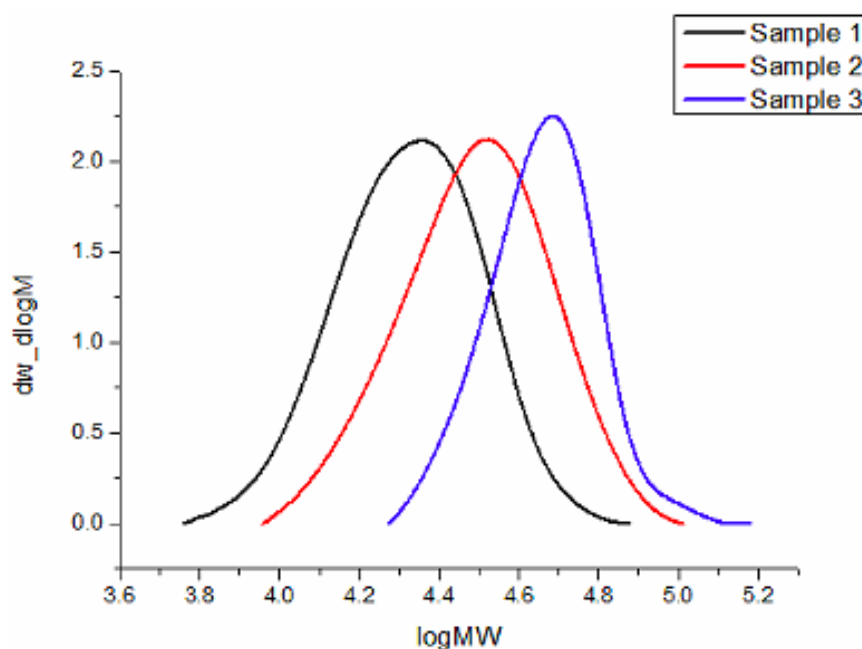


Figure 164 SEC trace of the three samples of PMMA-Br made by ATRP. PMMA₇₆-Br (Sam 1), PMMA₁₇₀-Br (Sam 2) & PMMA₂₂₆-Br (Sam 3).

The only differences between the three samples of PMMA-Br were the difference in initiator to monomer molar ratios. Three DP values were targeted (Table 36) and the theoretical DPs were 100, 200 & 300. PMMA₇₆-Br & PMMA₁₇₀-Br were very close to the theoretical DPs calculated. PMMA₂₂₆-Br was much further away from the theoretical despite the H-NMR suggesting that most of the monomer had been converted to polymer. A possible reason for this is that if the initiator only partial initiates, then DP can change. In all cases, H-NMR was monitored for a few days to ensure that integrals of monomer-polymer peaks stayed the same suggesting that the reaction had finished.

Table 36 NMR and GPC results on DP and molecular weights of the three samples of PMMA-Br made. DP were calculated from H-NMR.

Structure	DP	Theoretical DP	M _n NMR	Theoretical Mn	M _n GPC	M _w GPC	Đ
PMMA ₇₆ -Br	76	100	7,600	10,000	19,400	22,900	1.20
PMMA ₁₇₀ -Br	170	200	17,000	20,000	28,400	40,000	1.18
PMMA ₂₂₆ -Br	226	300	22,600	30,000	32,300	43,300	1.34

4.3.3 Synthesis PMMA-Cl via ATRP

The same method which was used for the synthesis of PMMA-Br was taken and used for PMMA-Cl. Once the polymerisation had gone to completion, it was purified and the product was collected.

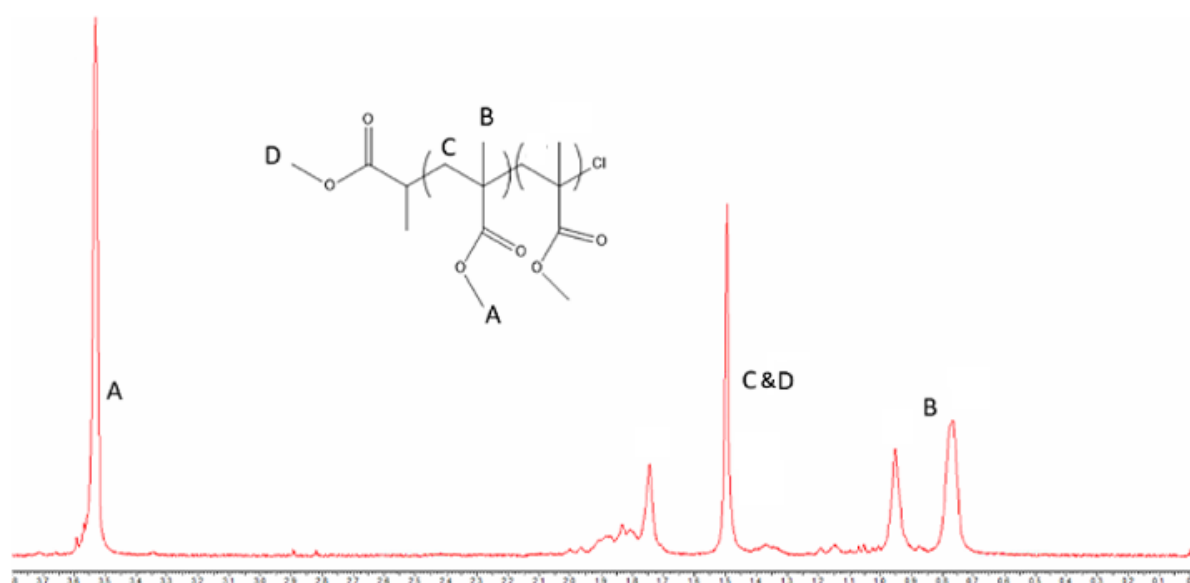


Figure 165 Proton NMR of PMMA-Cl made via ATRP.

The proton NMR closely matched that of PMMA-Br. The main difference between PMMA-Br and PMMA-Cl was that a different initiator was used.

Previously in an earlier chapter, the calculation of DP was discussed. It is the CH₂ integral on the α -bromoisobutyrate which is used to calculate DP from proton NMR. This peak is missing on methyl 2-chloropropionate and makes calculating DP from proton NMR difficult as the methyl groups on the methyl 2-chloropropionate appear to fall within similar regions of the PMMA. This means that GPC was used to calculate the DP for the PMMA-Cl initiators.

Table 37 GPC data on the two samples of PMMA-Cl made by ATRP.

Structure	DP	Theoretical DP	Theoretical Mn	M _n GPC	M _w GPC	Đ
PMMA ₁₀₆ -Cl	106	108	10,800	10,600	12,500	1.18
PMMA ₁₃₇ -Cl	137	143	13,700	13,700	15,700	1.14

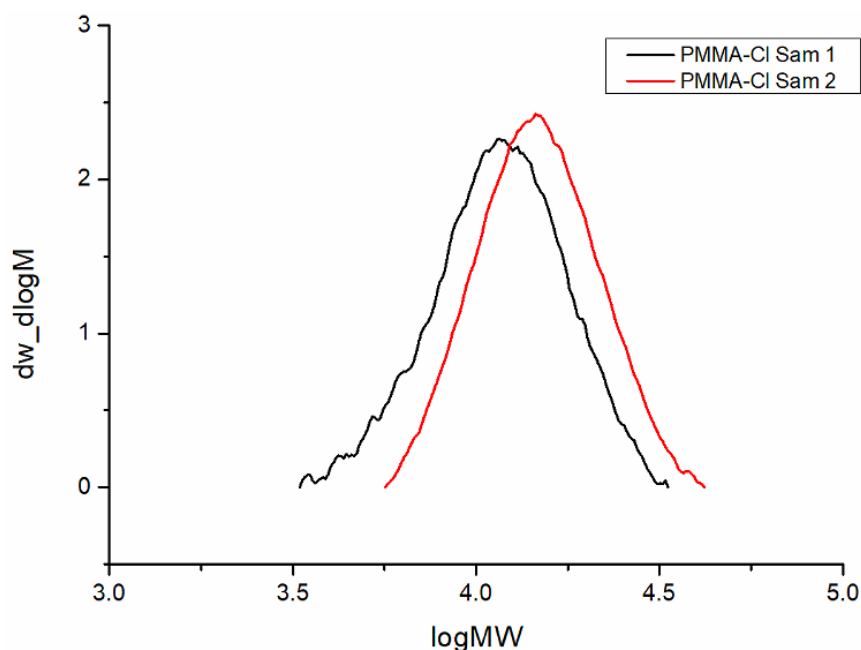


Figure 166 GPC traces of the two PMMA-Cl samples made by ATRP. PMMA₁₀₆-Cl (Sam1) & PMMA₁₀₆-Cl (Sam 2). GPC carried out in THF and PS standards were used to calibrate the instrument.

GPC analysis carried out on the two samples did show a slight difference in molecular weight which is expected.

4.3.4 Synthesis PMMA-*b*-P4VP via ATRP

4-vinylpyridine was purchased to assess whether it was possible to make a block copolymer of PMMA-*b*-P4VP by ATRP. The issue that the University of Nottingham were having was that they could make a block copolymer of PMMA-*b*-P4VP by RAFTs polymerisation but could not achieve any complex morphologies from this block copolymer. When they saw that our work allowed bicontinuous nanospheres to be made from PEO-*b*-PODMA, they were interested. This allowed a collaborative project to take place and gave us an opportunity to work with a new polymer to see if micelles of bicontinuous nature could be achieved.

The current samples sent in from the University of Nottingham were made via RAFTs and the molecular weight was not able to get any lower than 33,500 KDa. The block copolymers involving PEO-*b*-PODMA which gave bicontinuous nanospheres were self-assembled in water at molecular weights >33,500 KDa. It was hypothesised that if more complex structures were to form from self-assembly, then the molecular weight would need to be lowered. As there seemed to be a limit with RAFTs, it offered an opportunity for ATRP to make the desired block copolymer at lower molecular weights.

The samples of PMMA-Br were taken and reacted via ATRP with 4VP to make the desired block copolymers. Table 38 shows the parameters used for the attempted synthesis of PMMA-*b*-P4VP.

Table 38 Shows the quantities used for the attempted synthesis of PMMA-*b*-P4VP.

Structure	Moles of PMMA-Br	PMMA-Br (g)	Moles of 4VP	4VP (g)	Targeted P4VP Fraction
PMMA ₇₆ - <i>b</i> -P4VP ₁₈	6.58 x10 ⁻⁵	0.5	1.18 x10 ⁻³	0.12	0.2
PMMA ₇₆ - <i>b</i> -P4VP ₁₈	6.58 x10 ⁻⁵	0.5	2.04 x10 ⁻³	0.21	0.3
PMMA ₁₇₀ - <i>b</i> -P4VP ₄₀	2.94 x10 ⁻⁵	0.5	1.18 x10 ⁻³	0.12	0.2

The method was fairly similar to the synthesis of PMMA-Br & PMMA-Cl. The main difference was that CuCl was used to slow the reaction down and a strong coordinating ligand (Me₆TREN) was used to try and prevent the 4VP from coordinating to the catalyst.

Several reactions were carried out (Table 38). All reactions were monitored by taking samples every day up to Day 8 where the reaction was deemed unsuccessful if the monomer peaks could still be seen. The way this was monitored was by taking a sample and subjecting them to NMR analysis after it had been run down a microcolumn. In all cases, NMR demonstrated that little to no polymerisation of the 4VP was taking place (Figure 167).

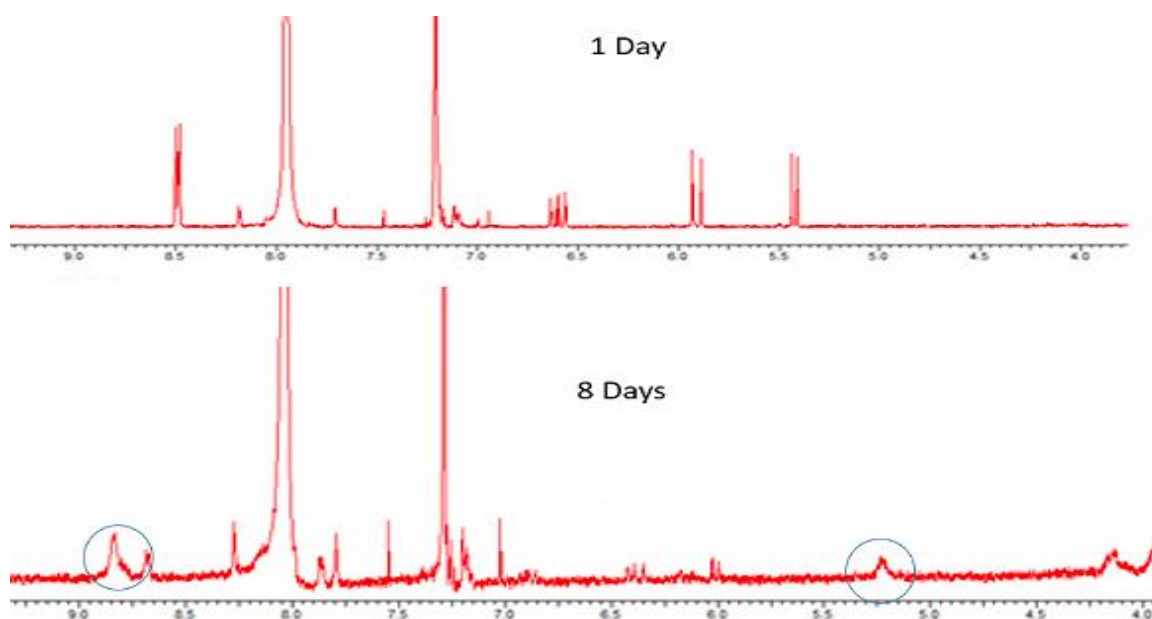


Figure 167 Proton NMR of the attempted ATRP reaction of PMMA-*b*-P4VP. (Top) is 1 day after the ATRP reaction was put on. (bottom) is Day 8 after ATRP reaction was set up showing that proton signals have changed.

If any polymerisation was taking place, then an increase in molecular weight should be seen. Samples were also taken for GPC analysis and are shown in Figure 168. There is no increase in molecular weight which suggest no polymerisation has taken place.

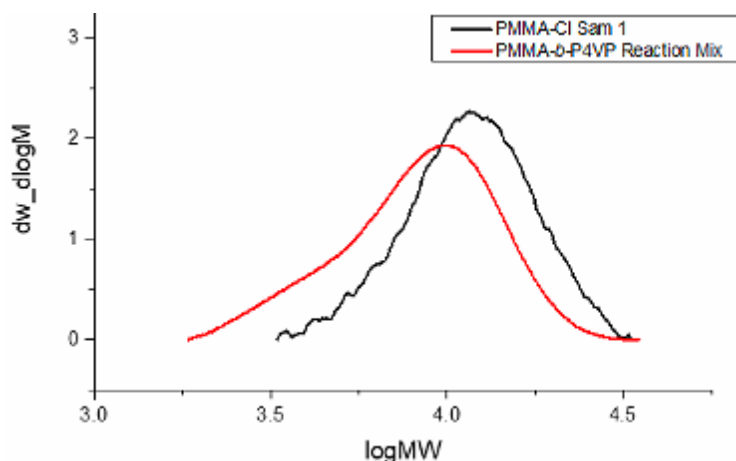


Figure 168 Reaction mixture after 8 days and at start of ATRP reaction suggesting that no polymerisation is happening.

It is well known that 4VP can pose a challenging problem for ATRP reactions. The 4VP and P4VP are strong coordinating ligands that compete for the binding of metal catalyst in these systems. There is a possibility that the pyridine will coordinate to the copper in the polymerisation solution. Pyridine-coordinated copper complexes are not effective catalysts for ATRP thus making it difficult to make PMMA-*b*-P4VP by ATRP.²³

There are many factors to consider in order to try and get the ATRP reaction to work. The first was using chlorine (Cl) as the halogen offers advantages since the strong C-Cl bond balances the activation/deactivation of the CuCl/Me₆TREN complex.²³ This offers a suitable concentration of active radicals helping the ATRP reaction. The chlorine atom is also a worse leaving group than bromine which helps to limit SN₂ nucleophilic attack of pyridine molecules on the terminating and initiating alkyl halide groups which is a likely side reaction.

At this point PMMA-Cl was made and the ATRP reaction was repeated using this initiator. The ATRP reaction was repeated using PMMA-Cl and left for a few days. A proton NMR was taken each day but it showed that the monomer peaks of the 4VP were not changing and that no polymerisation was occurring. This was repeated again and the same happened. It was deemed at the point that it was not going to be feasible to make PMMA-*b*-P4VP via ATRP for this project. The reaction NMR after a few days is shown below (Figure 169) indicating the unchanged monomer peaks.

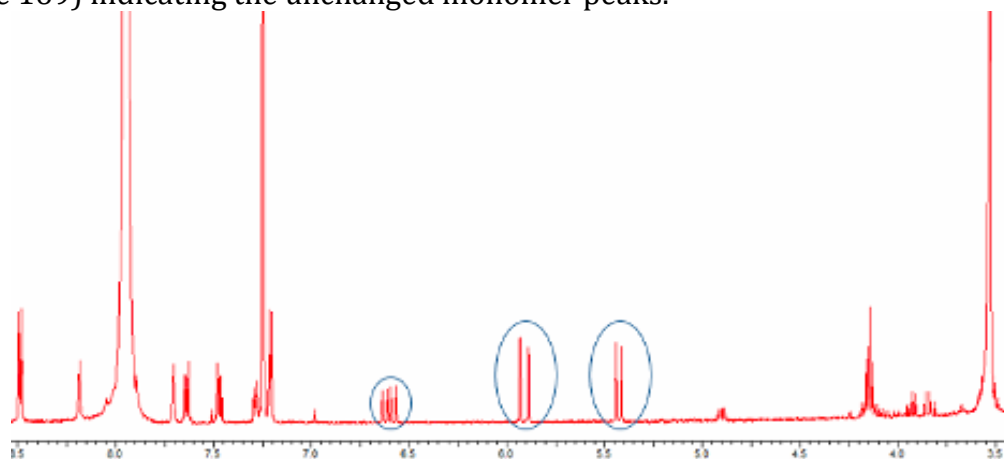


Figure 169 Proton NMR after a few days of attempted synthesis of PMMA-*b*-P4VP made from the PMMA-Cl initiator. The peaks circled are from 4VP suggesting that no or little polymerisation is happening.

At this point, a literature paper²⁵ was found where there was significant improve on the rate of polymerisation when the temperature was increased from 40-60°C when polymerising using 4-vinylpyridine to make a PS-*b*-P4VP block copolymer.

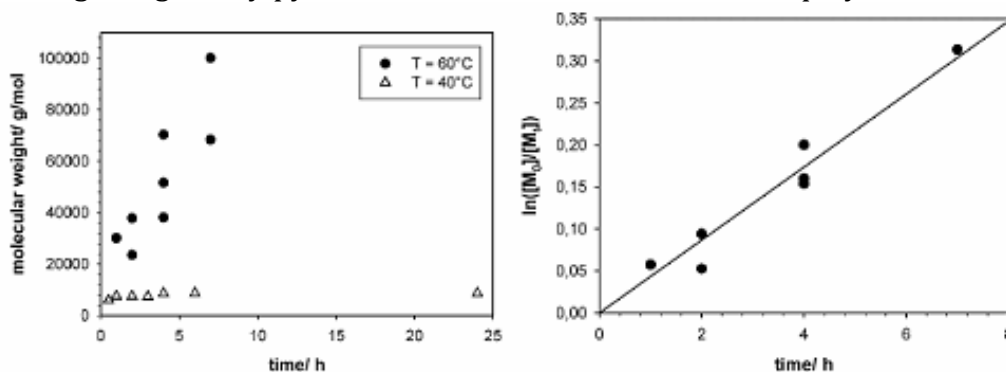


Figure 170 The result of increasing the reaction temperature when making PS-*b*-P4VP²⁵ showed that polymerisation occurred much more quickly. (left) shows molecular weight increasing over time when reaction was performed at 60°C. (right) Shows a linear relationship as the monomer is converted to polymer over time.

The final attempt was to try increasing the reaction temperature. At this point the reaction was repeated at 80°C but when a proton NMR was taken the monomer peaks were clearly visible. This suggested that increasing the temperature was having no or little effect on the ATRP reaction.

4.3.5 Characterisation and Self-assembly of PMMA-*b*-P4VP

Characterisation of PMMA-*b*-P4VP

Samples made at the University of Nottingham were supplied to Kent to be self-assembled. The main aim was to self-assemble different aggregate morphologies than the spherical BCP microparticles previously achieved for PMMA-*b*-P4VP. All samples were characterised by NMR and GPC. A representative NMR spectrum is shown in Figure 171. The compositions of the copolymers with respect to MMA and 4VP are given in Table 39, alongside the molecular weight parameters.

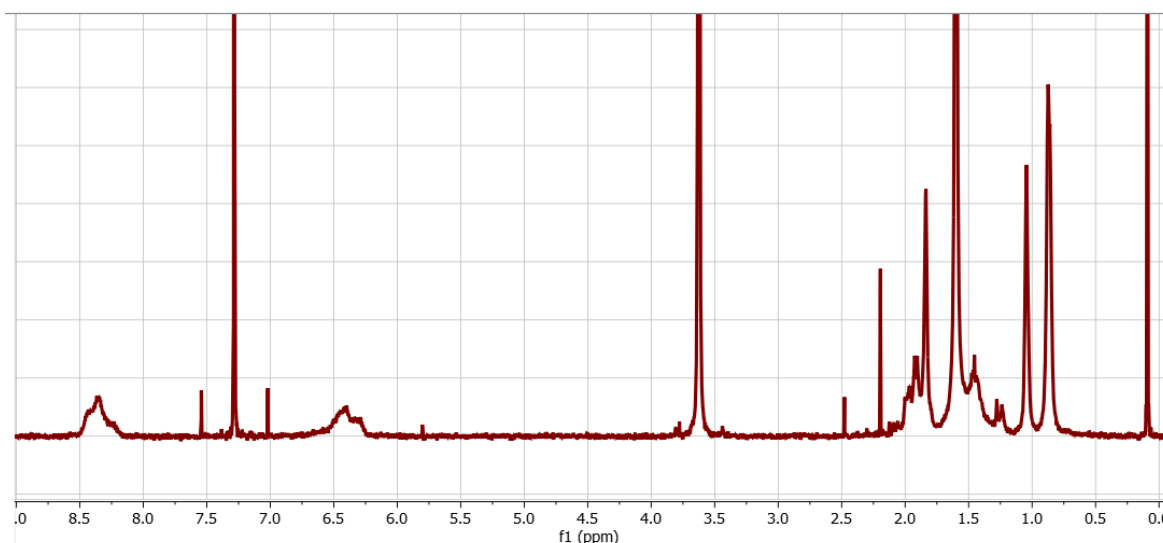


Figure 171 ¹H NMR of PMMA-*b*-P4VP made via RAFTs in CDCl₃.

RAFT polymerisation involves using free radicals to polymerise a substituted monomer in the presence of a chain transfer agent. Typical RAFT agents include thiocarbonylthio compounds. Polydimethylsioxane (PDMS-MA) is used and the University of Nottingham have shown that adding PDMS-MA stabilizer before or during the polymerisation allows manipulation of the size of the microparticle. Peak at 0.1 ppm is the PDMS-MA stabiliser. The Peak at 0.5-2.5 ppm is the polymer backbone as well as the RAFT agent. At 3.6 ppm is the methyl group of the PMMA. And the signals at 6.4 and 8.4 are the pyridine ring on the P4VP. All the samples sent in for self-assembly had identical proton NMRs.

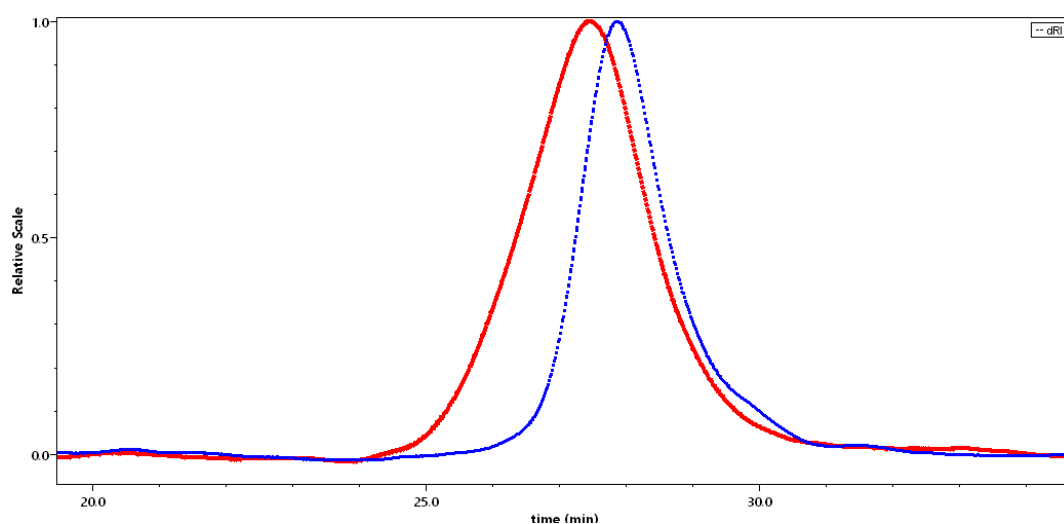


Figure 172 (Blue) PMMA made first by RAFT. (Red) is the block copolymer of PMMA₄₅₃-b-P4VP₁₁₉.

GPC analysis was carried out on the samples which demonstrated that the molecular weight is increasing. This means that the 4VP are successfully being added to the PMMA polymer which is made first.

Table 39 Compositions and molecular weight parameters of Nottingham PMMA-*b*-PVP samples.

Sample	Structure ^a	P4VP wt Fraction ^a	M _n GPC ^b	Đ
1	PMMA ₄₅₃ - <i>b</i> -P4VP ₁₁₉	0.22	64200	1.45
2	PMMA ₃₇₀ - <i>b</i> -P4VP ₈₃	0.30	47900	1.27
3	PMMA ₃₃₄ - <i>b</i> -P4VP ₁₃₈	0.19	45700	1.30
4	PMMA ₂₅₀ - <i>b</i> -P4VP ₈₁	0.25	33500	1.34

a. Determined from NMR. b. Determined from GPC

Self-Assembly of PMMA-*b*-P4VP at University of Kent

Self-Assembly of Poly (methyl methacrylate-*block*-4-vinylpyridine) PMMA-*b*-P4VP in Water

The same self-assembly procedure was used for all of the PMMA-*b*-P4VP samples sent by University of Nottingham. A sample of PMMA-*b*-P4VP self-assembled in aqueous solutions using a non-solvent addition procedure followed by dialysis. The block copolymer was first dissolved in a known volume of THF and distilled water was added slowly at 0.075 mL per minute at 60°C to make the total volume to 10 mL. The block copolymer was self-assembled at 0.1 wt% & 1.0 wt% solutions.

PMMA₄₅₃-*b*-P4VP₁₁₉ (0.22 wt fraction) Mn 64200

The first sample received from the University of Nottingham was PMMA₄₅₃-*b*-P4VP₁₁₉ which meant that the early testing just used this sample. As this was the first time this polymer had been self-assembled using dialysis it was unknown what quantity of THF would provide the best results. This led to using a range of different volumes of THF to see which volume would provide the better results. The different volumes of THF used are shown in Table 40.

Sample Preparation

The exact quantities of polymer and water used in each case are given in Table 1 below.

Table 40 Quantities used in the self-assembly of PMMA-*b*-P4VP samples

Self-assembled Concentration wt %	Mass of polymer used (g)	THF Volume (mL)	Water Volume (mL)	Total Volume (mL)
0.1	0.01	9.0	1.0	10
	0.01	7.5	2.5	10
	0.01	6.0	4.0	10
1.0	0.1	9.0	1.0	10
	0.1	8.0	2.0	10
	0.1	7.0	3.0	10
	0.1	6.0	4.0	10

Micelle maximum size

The calculation used to determine the maximum micelle size has been discussed before. The same calculation was used to determine the maximum size of a simple spherical micelle for PMMA₄₅₃-*b*-P4VP₁₁₉ which was found to be 144 nm. This means that anything seen on the TEM images bigger than 144 nm is unlikely to be a simple micelle and is a different aggregate species.

Summary 0.1 wt% samples PMMA₄₅₃-b-P4VP₁₁₉

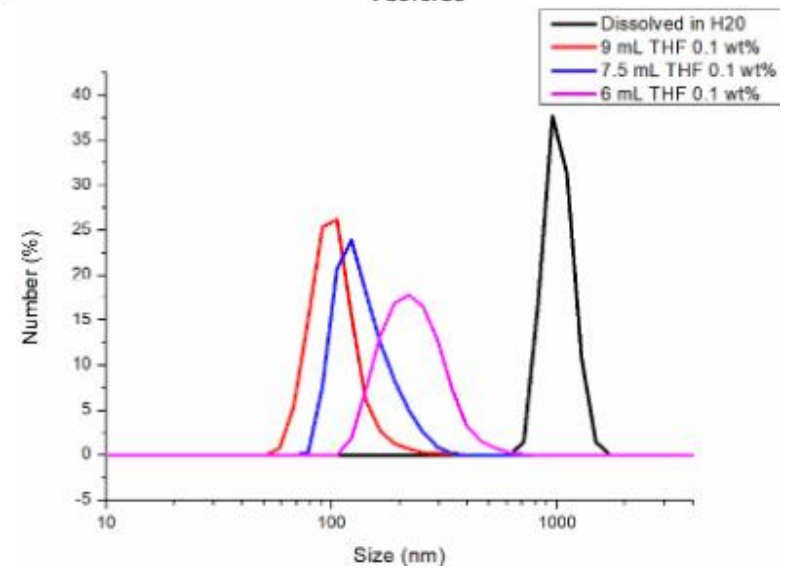
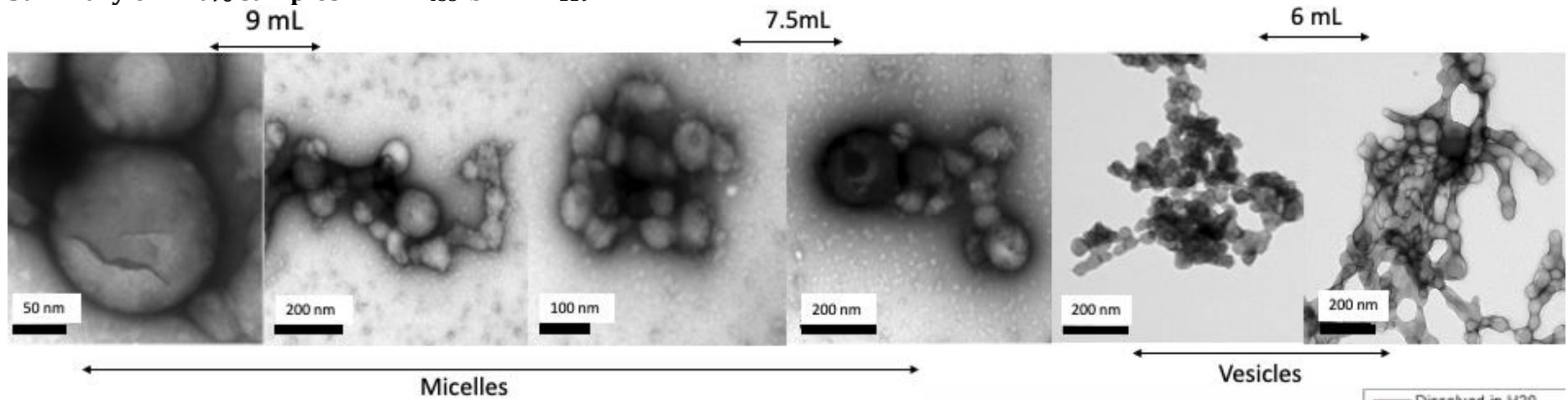


Figure 173 Summary results of PMMA₄₅₃-b-P4VP₁₁₉ self-assembled at 0.1 wt% solutions where spherical micelles and vesicles are present.

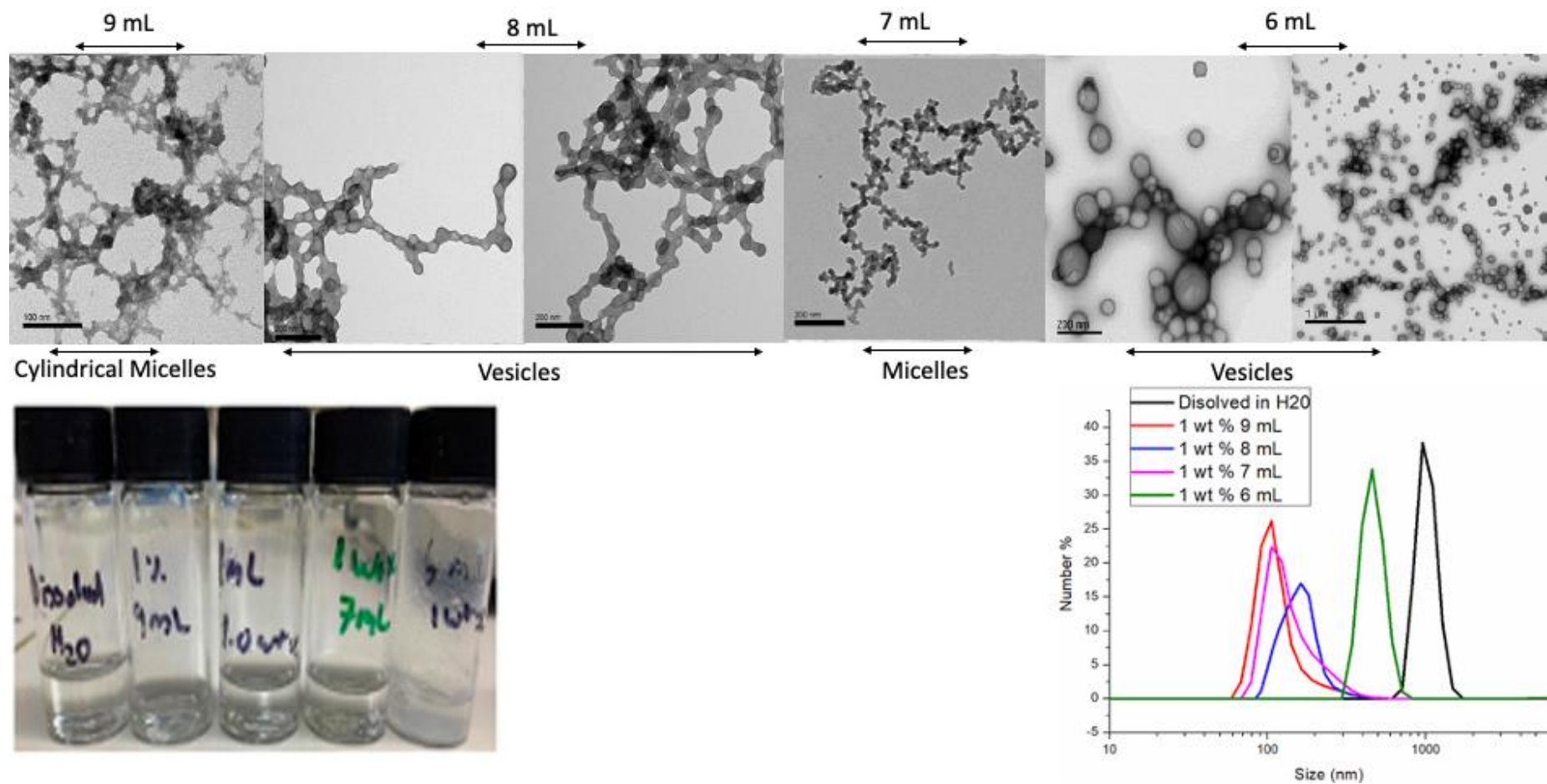


Figure 174 Summary results of $PMMA_{453}\text{-}b\text{-}P4VP_{119}$ self-assembled at 1.0 wt% solutions where micelles and vesicles are present.

0.1 wt% Samples

When PMMA₄₅₃-*b*-P4VP₁₁₉ was self-assembled at 0.1 wt % solutions (Figure 173), spherical micelles and vesicles were seen. The TEM solutions were all clear which suggested that there were submicron particles. Looking at the DLS result there seems to be a trend when increasing the volume of THF. As less THF is used, the aggregates seem to be getting larger.

9ml

The typical diameters for the aggregates seen by TEM was 50 to 100 nm with a few larger particles being observed. It is difficult to comment whether these larger particles are micelles or vesicles. A similar size distribution was observed by DLS analysis. Thus, these are most likely simple micelles.

7.5 ml

The typical diameters for the aggregates seen by TEM was 50 to 120 nm; a similar size distribution was observed by DLS analysis. Thus, these are most likely spherical micelles. Some of the block copolymers micelles formed in the 7.5 mL THF, looked to be a little bigger than the micelles formed in 9 mL. Dynamic light scattering (DLS) also supports this as most particles seen are slightly bigger than 100 nm.

6ml

The TEM micrographs show that vesicles seem to be present. Typical size ranges of these vesicles seem to be around between 20-40 nm. Dynamic light scattering (DLS) does not support the TEM images and suggests that there are bigger individual particles present. There seems to be a trend that as less THF is added, the aggregation of the micelle structures seem to increase. The size of the micelles also seem to get slightly smaller from TEM as less THF is used.

1.0 wt% Samples

9ml

The TEM micrographs show that cylindrical micelles seem to be present but they are connected by 'web-like' structure. The cylindrical micelles are very small (20-30 nm). Dynamic light scattering (DLS) does not support the TEM images and suggests that there are bigger individual particles present. It could be the aggregation of micelles which has allowed the DLS to measure particles that are bigger than what actually is in solution.

8ml

The TEM micrographs show that vesicles seem to be present and are around 20-30 nm. Dynamic light scattering (DLS) does not support the TEM images and suggests that there are bigger individual particles present. It could be the aggregation of vesicles which has allowed the DLS to measure particles that are bigger than what actually is in solution.

7ml

The TEM micrographs show that micelles seem to be present. Large structures can be seen in the TEM images as these micelles aggregate together and range from 20-40 nm. Dynamic light scattering (DLS) does not support the TEM images and suggests that there are bigger individual particles present.

6ml

The aggregate structures observed by TEM are most likely to be vesicles. When the spheres that look 'transparent' it is a strong indication that vesicular type structures. Looking at the size of these structures, there seems to be very small vesicles at around (20-30 nm) as well as bigger vesicles. The TEM images show build-up of particles where they are coming together to form larger structures. Dynamic light scattering (DLS) does not support the TEM images and reports that bigger particles are being observed. This difference is due to the aggregation of vesicular structures which has allowed the DLS to measure particles that are bigger than what actually is in solution.

The structures seen with the self-assembly of PMMA₄₅₃-*b*-P4VP₁₁₉ in water is very different from what was previously seen in the Nottingham results. The first key difference is that vesicular structures are present as the particles look transparent. Nothing like this was observed with the Nottingham results. Before the self-assembly at Kent took place, the PMMA₄₅₃-*b*-P4VP₁₁₉ microparticles had a much more ordered structures but the micelles and vesicles present here are very dispersed and spread out. The initial results do suggest a difference in the particles present after self-assembly. It is important to remember that the results from Nottingham did use ethanol to form their microparticles. This will lead to further self-assembly using ethanol instead of water to see if this makes a difference to the particles formed.

Self-Assembly of Poly (methyl methacrylate-*block*-4-vinylpyridine) PMMA-*b*-P4VP in water varying pH

Previously a block copolymer of polystyrene and 4-vinylpyridine was self-assembled in water and the pH was varied.²⁶ The molar weight of this polymer was about 10,000 KDa and the vinyl pyridine molar content was between 19-53%. It was reported that as the pH is changed from 5.1 to 1.0 the block copolymer aggregates changes. At pH range of 5-3 the nanoparticles are a spherical shape, uniform and around 100nm in diameter. As the pH is lowered to pH 2-1 the nanoparticle develops a multicore structure. An example of a multicore structure is shown in Figure 175.

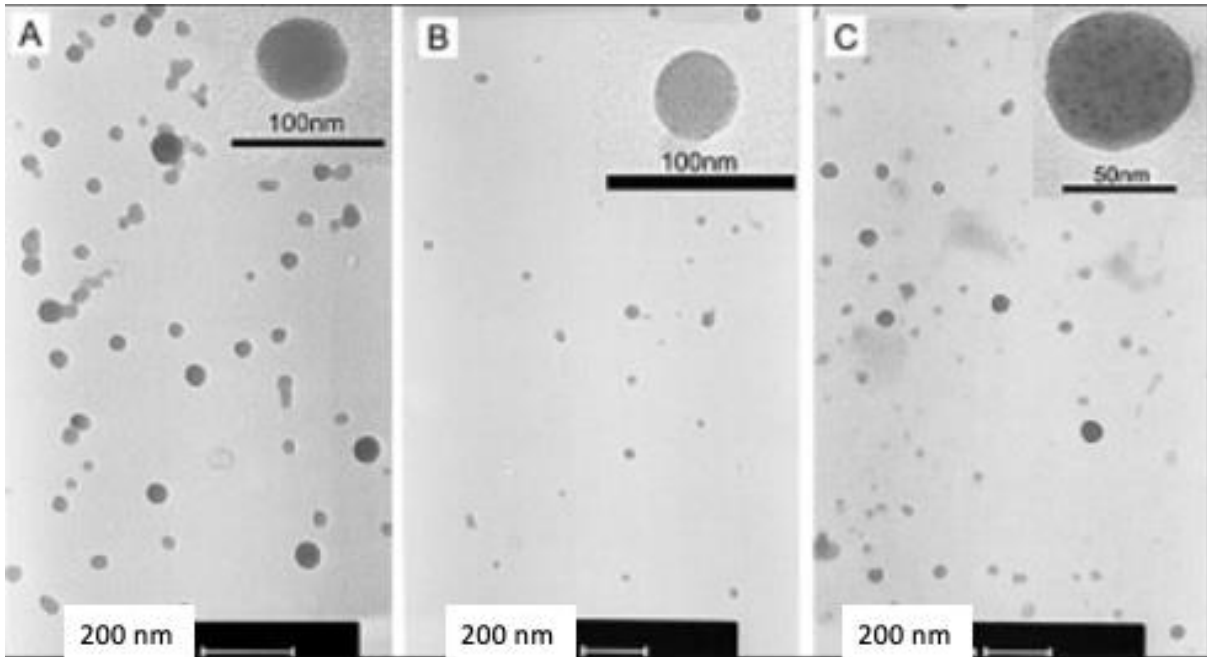


Figure 175 Multicore structure(C) when a block copolymer of polystyrene and 4-vinylpyridine was self-assembled in water and the pH was varied.²⁶ A) pH 5, B) pH 3 & C) pH 1

As the pH is lowered using HCl, the formation of the nanoparticle will be driven by the electrostatic repulsion of the protonated 4VP within the block copolymer. This can actually be seen in **Error! Reference source not found.** 177 where a 1.0wt% of P MMA₄₅₃-*b*-P4VP₁₁₉ was self-assembled and the pH was then varied. The structure becomes much more uniform as the protonated 4VP try to get further away from one another. Figure 176 further demonstrates how multicore structures are formed when acid is added to the self-assembled solution.

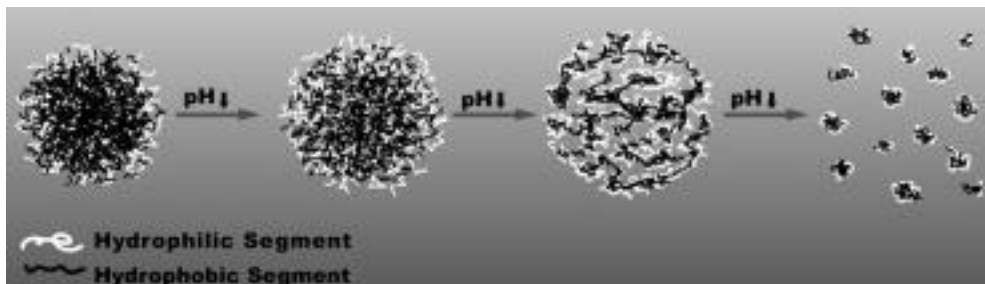


Figure 176 Shows block copolymer aggregates changing as the pH is lowered.

How ionised the P4VP is in water can be calculated from the following equation:

$$K_a = \frac{\alpha^2 C}{1 - \alpha}; pK_a = -\log K_a$$

Where K_a is the acid dissociation constant, C is the concentration of the acidic solution and α is the degree of dissociation of the acid.

Using $pK_a = 5.2$ of pyridine and the assumption that there is 1 mole of P4VP present, then the degree of dissociation is 0.0025 suggesting that none of it is dissociated in water and that the acidity of the pyridine will be mainly ionised.

The pH was varied by adding HCl 0.1M to the self-assembly of PMMA-*b*-P4VP to assess whether nanoparticles could develop a multicore structure when self-assembled at pH 1 and 2.

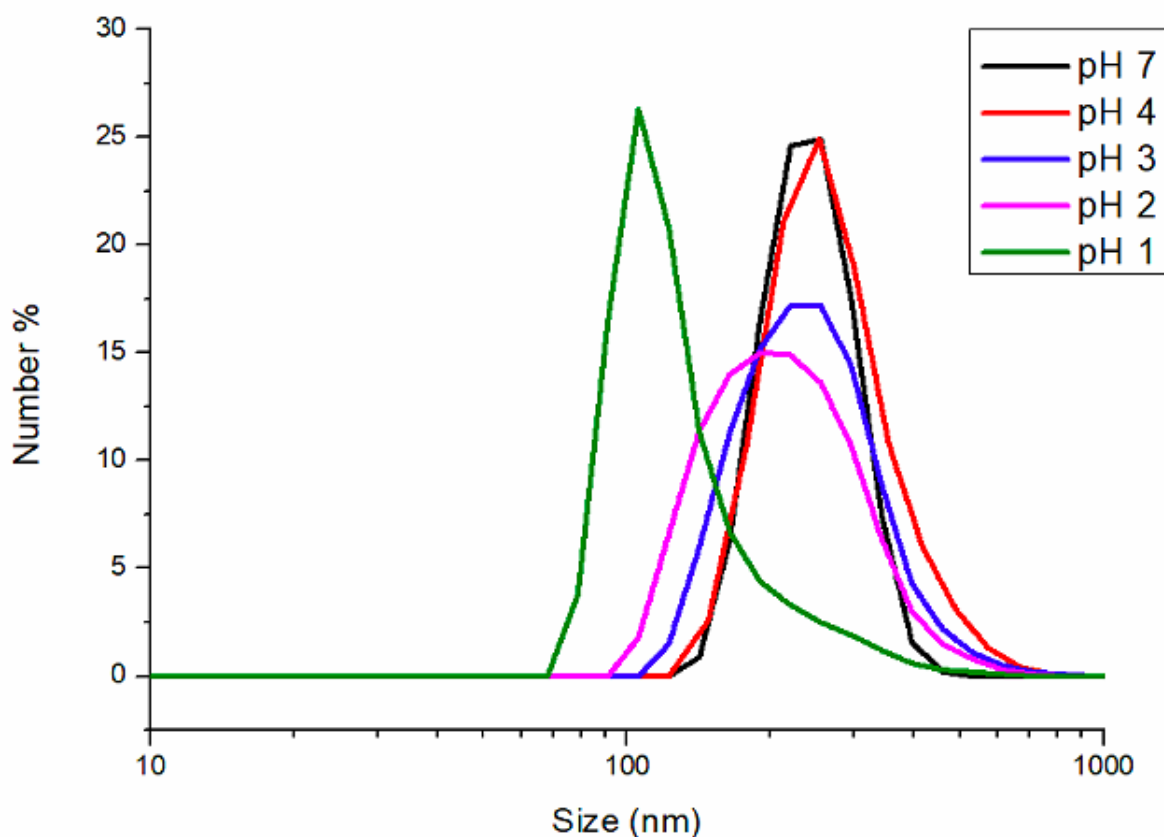


Figure 177 DLS Results for self-assembled 1.0 wt% aggregates using 6 mL THF with varied pH.

The addition of HCl 0.1 M was added to see if any other morphologies would form and if there was any effect to the structure of the micelles previously seen. There seems to be a slight trend that as the pH is lowered and becomes more acidic, the size of the particle gets smaller. Vesicles seem to be present at pH 1. This is seen with DLS but also shown in the TEM images. There seems to be agglomeration forming from the micelles at the higher pH but when HCl is added the particles seem to become more uniform and this agglomeration is witness less. This is very much the repulsion that is occurring between each 4VP group after it has been protonated from the acid. This matches what is seen in literature with smaller particles being seen at the more acidic conditions.

1.0 wt% Sample

A 1.0 wt% sample of PMMA-*b*-P4VP (0.22 wt fraction hydrophilic: hydrophobic) was self-assembled in 6 mL distilled water. Hydrochloric acid 0.1M was added to the sample to bring the pH to 1. DLS and TEM was carried out to see if by varying the pH changed the aggregate species from forming.

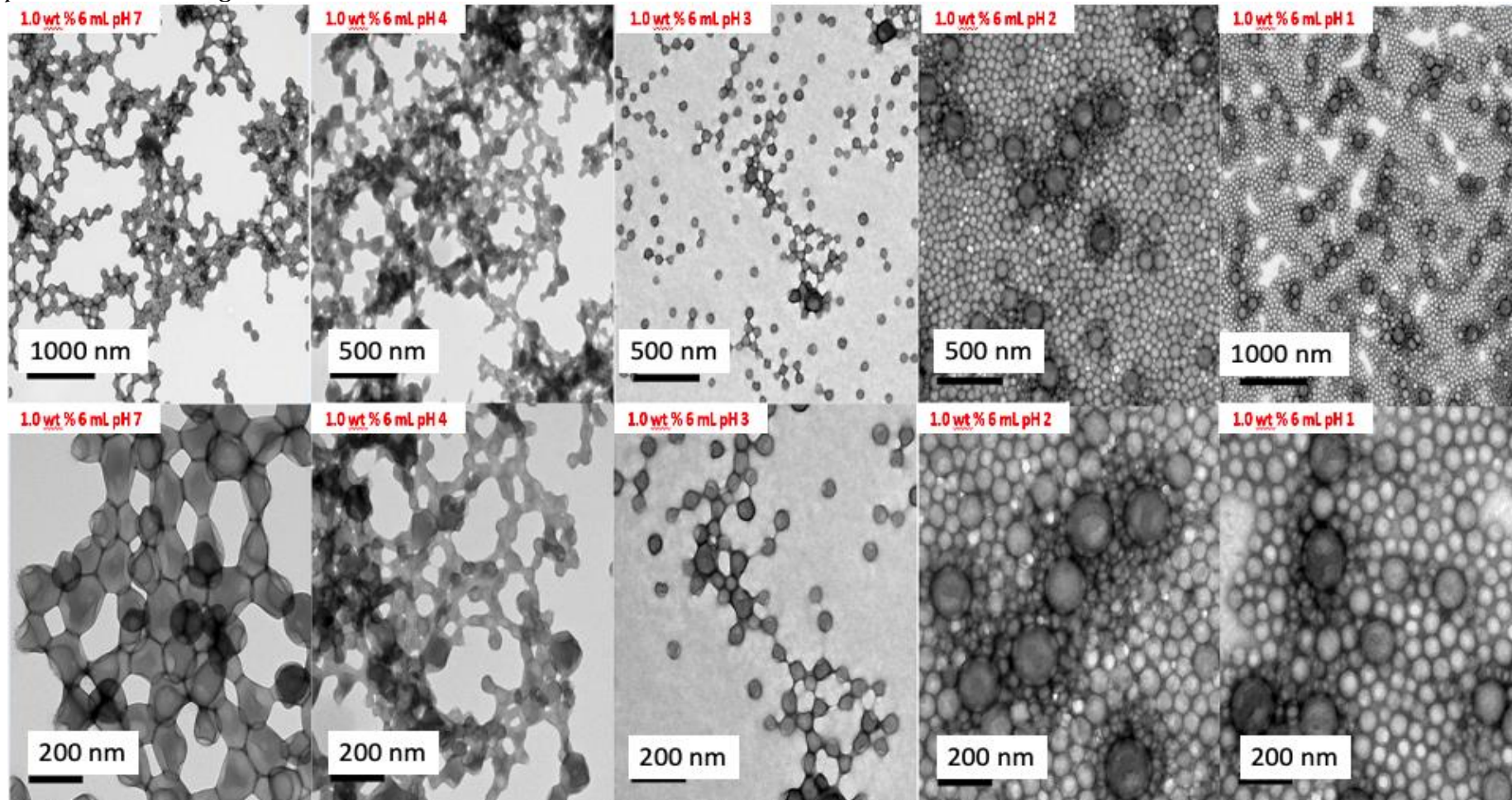


Figure 178 TEM Images of 1.0 wt% aggregates self-assembled at different pH using 6 mL THF.

Self-Assembly of Poly (methyl methacrylate-*block*-4-vinylpyridine) PMMA₄₅₃-*b*-P4VP₁₁₉ in Ethanol

A key step in using PMMA₄₅₃-*b*-P4VP₁₁₉ with metal oxides is using selective solvents such as ethanol to retain the microparticle structure.²¹ Due to this, self-assembly was performed in ethanol to determine which aggregates structures form. The Hilderbrand solubility parameters²⁷ are shown in Table 41 which allows determination of whether water or ethanol is a better solvent for poly vinyl pyridine.

Table 41 Hilderband solubility parameters for PVP in the two solvent systems used for self-assembly.²⁸

Compound	Solubility parameter (mPa ^{1/2})
Water	48.0
Ethanol	26.5
PVP	21.3

This suggest that ethanol is a much better solvent for PVP as the solubility parameters for ethanol and PVP and much closer together than they are for water.

A sample of PMMA₄₅₃-*b*-P4VP₁₁₉ (0.22 wt fraction hydrophilic: hydrophobic) was self-assembled in ethanol. The self-assembly of this block copolymer was carried out using dialysis. The block copolymer was first dissolved in a known volume of THF (6 mL) and ethanol was added slowly at 0.075 mL per minute at 60°C to make the total volume to 10 mL. Polymer was self-assembled at 0.1 wt% & 1.0 wt% solutions.

Sample Preparation

The exact quantities of polymer and ethanol used in each case are given in Table 42 below.

Table 42 Quantities used in the self-assembly of PMMA-*b*-P4VP

Self-assembled Concentration wt %	Mass of polymer used (g)	THF Volume (mL)	Ethanol Volume (mL)	Total Volume (mL)
0.1	0.01	6.0	4.0	10
1.0	0.1	6.0	4.0	10

0.1 & 1.0 wt% 6mL THF (Ethanol)

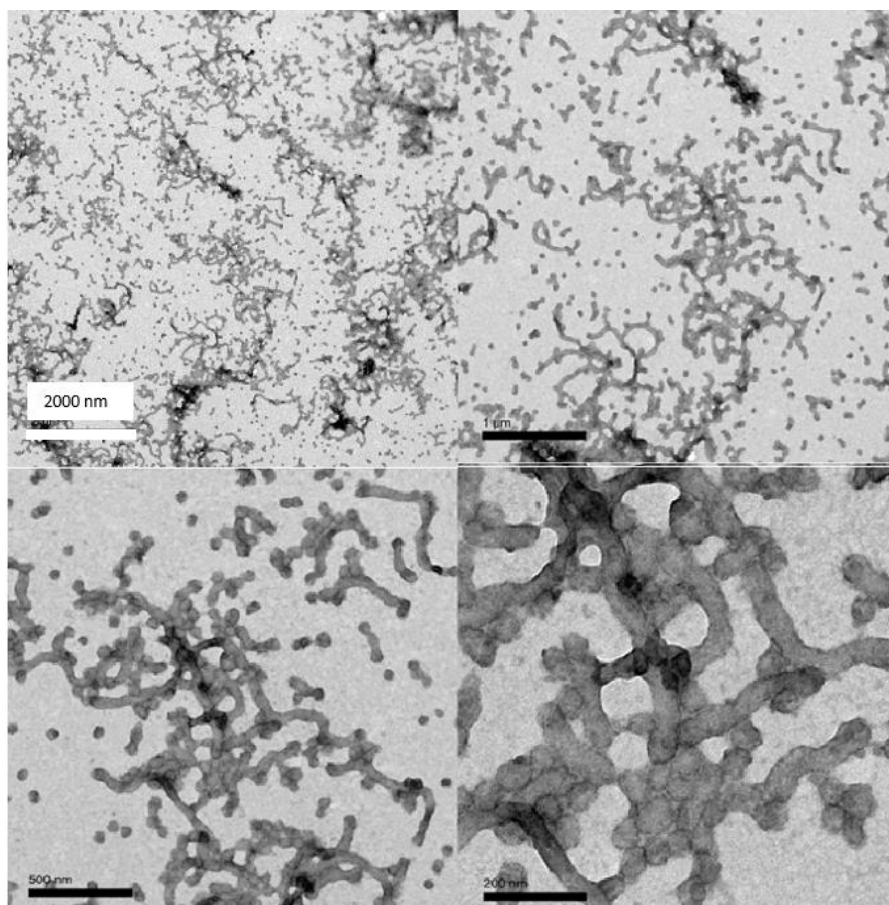


Figure 179 TEM Images of 0.1 wt% self-assembled in ethanol using 6 mL THF.

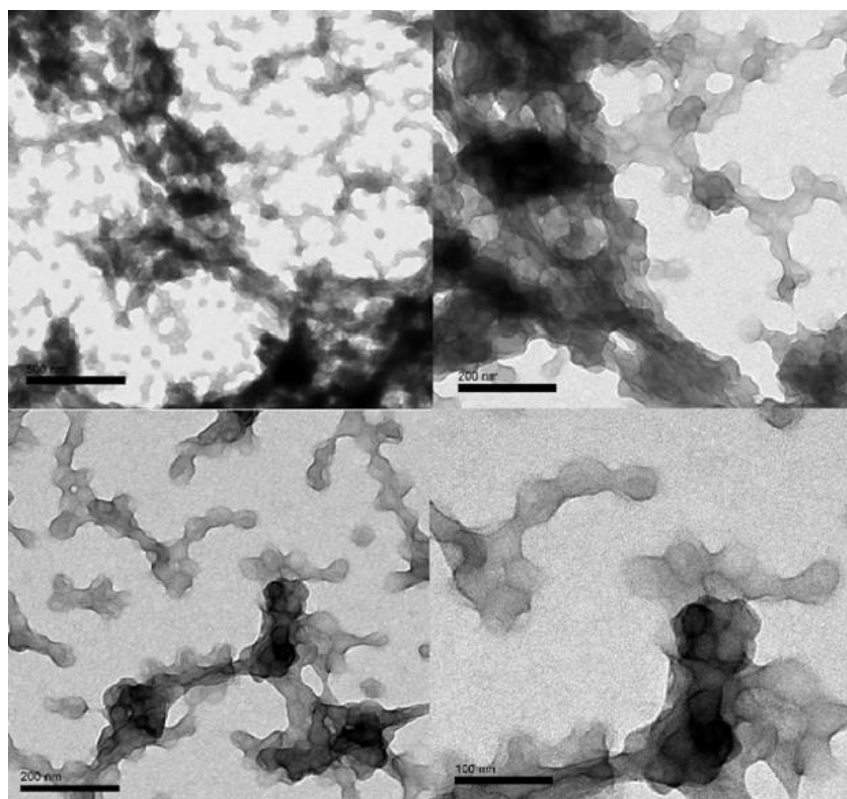


Figure 180 TEM Images of 1.0 wt% self-assembled in ethanol using 6 mL THF.

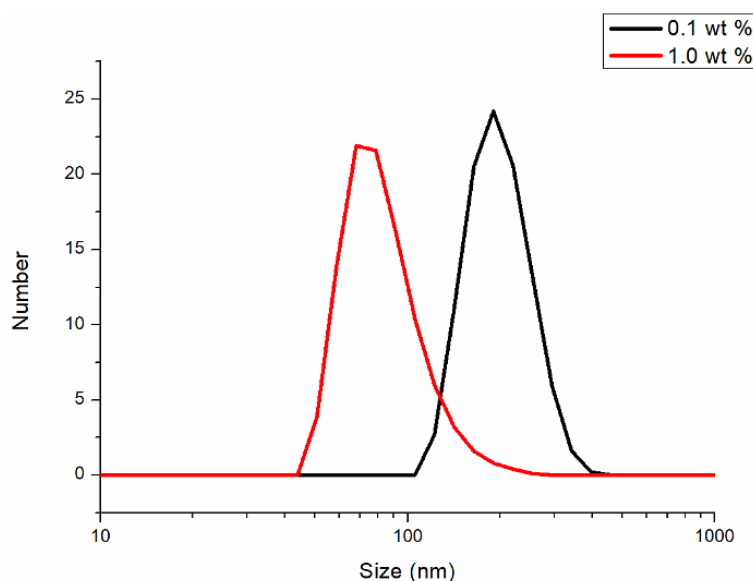


Figure 181 DLS results of 0.1 and 1.0 wt% self-assembled in ethanol using 6 mL THF.

The 0.1 wt% solution (Figure 179) at THF (6mL) is very interesting as the TEM images show spherical micelles along with cylindrical micelles which has not been observed in the other solutions so far. Looking at the size of these micelles, they are very small (20-30 nm) but the cylindrical micelles are much bigger. The TEM images show aggregation where particles are coming together to form larger structures. Dynamic light scattering (DLS) does support the TEM images and reports that bigger particles are being observed. The cylindrical micelles are big and will have a bigger radius of gyration.

The 1.0 wt% solution (Figure 180) TEM images show spherical micelles along with cylindrical micelles. Looking at the size of these micelles, they are very small (20-30 nm) but the cylindrical micelles are much bigger. This is very similar to what was seen with the 0.1 wt% solutions. The TEM images show aggregation where particles are coming together to form larger structures. Dynamic light scattering (DLS) does not support the TEM images and reports that bigger particles are being observed. This difference is due to the aggregation of micelles/ cylindrical structures which has allowed the DLS to measure particles that are bigger than what actually is in solution.

A summary of results of PMMA₄₅₃-*b*-P4VP₁₁₉ can be seen in Figure 182. When PMMA₄₅₃-*b*-P4VP₁₁₉ was self-assembled at 1.0 wt % solutions, spherical micelles and vesicles can be seen. Most of the TEM solutions were all clear which suggested that there were submicron particles. In the case of 6mL, the solution was cloudy suggesting much larger particles. This could be a result of agglomeration of the micellar and vesicular structures.

When PMMA₄₅₃-*b*-P4VP₁₁₉ was self-assembled at 1.0 wt % solutions in ethanol and water, spherical micelles, cylindrical micelles and vesicles can be seen. All of the TEM solutions made in ethanol were all clear which suggested that there were submicron particles which is supported by DLS. TEM images show that there was aggregation of the micellar structures where these particles are coming together to form larger structures. These results suggest that as there is a change in the self-assembly solvent (water to ethanol) different morphologies will form. For the ethanol solutions cylindrical micelles were seen but not vesicles and for the water solutions vesicles were seen but not cylindrical micelles.

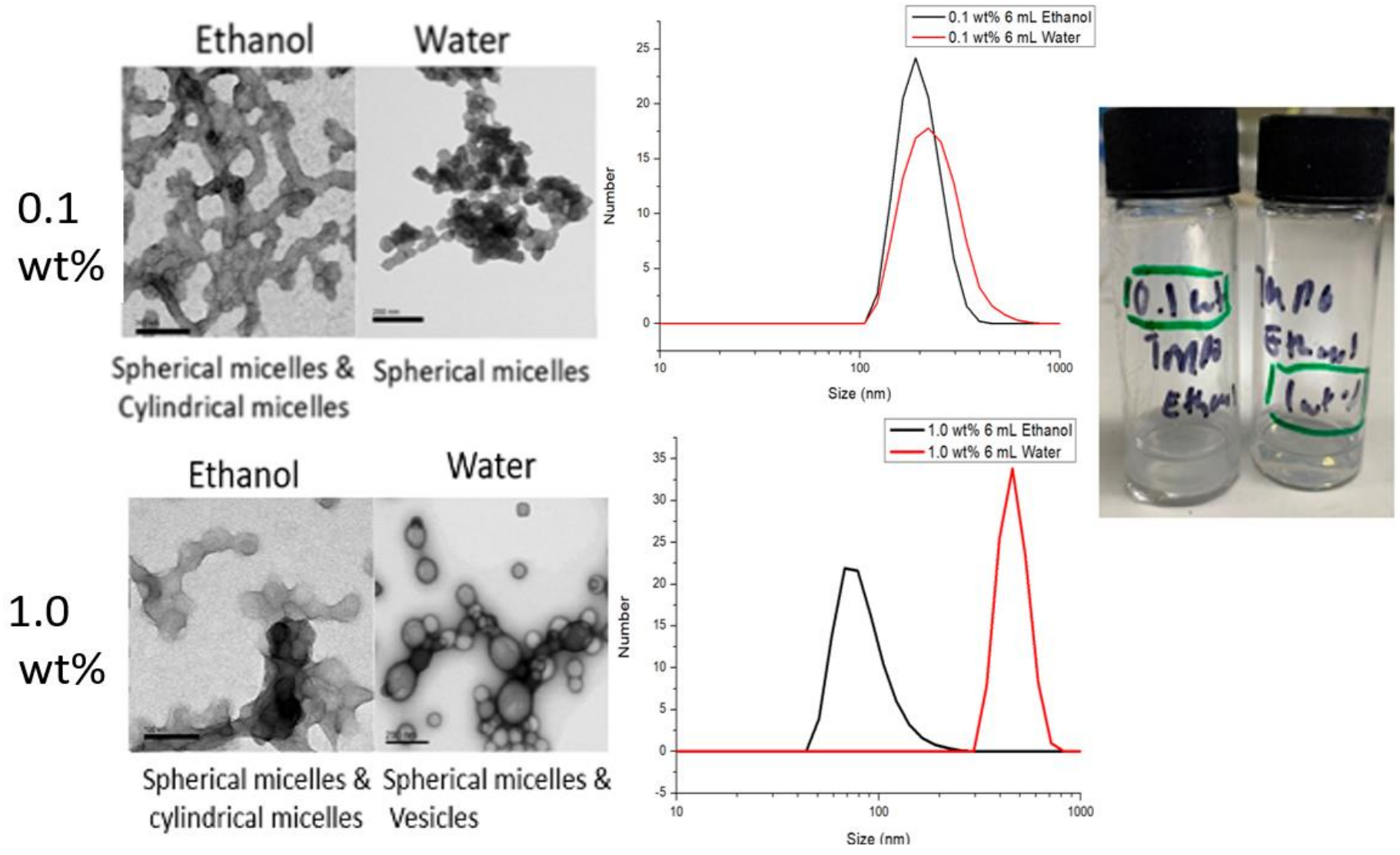


Figure 182 Summary results of $PMMA_{453}\text{-}b\text{-}P4VP_{119}$ self-assembled in ethanol where spherical micelles, cylindrical micelles and vesicles are present.

Self-Assembly of remaining Poly (methyl methacrylate-*block*-4-vinylpyridine) Samples in water and ethanol

Table 43 Shows the remaining PMMA-*b*-P4VP samples to self-assembled in water and ethanol along with the first sample of PMMA₄₅₃-*b*-P4VP₁₁₉.

Sample	P4VP wt fraction	Mn	Max Micelle Size (nm)
PMMA ₄₅₃ - <i>b</i> -P4VP ₁₁₉	0.22	64,200	144
PMMA ₃₃₄ - <i>b</i> -P4VP ₁₃₈	0.30	47,900	144
PMMA ₃₇₀ - <i>b</i> -P4VP ₈₃	0.19	45,700	114
PMMA ₂₅₀ - <i>b</i> -P4VP ₈₁	0.30	33,500	83

The remaining samples were self-assembled in the same way as the first sample of PMMA₄₅₃-*b*-P4VP₁₁₉. Two concentration were made (0.1 wt% and 1.0 wt%) for the water and ethanol self-assemblies. DLS and TEM were performed on all samples made.

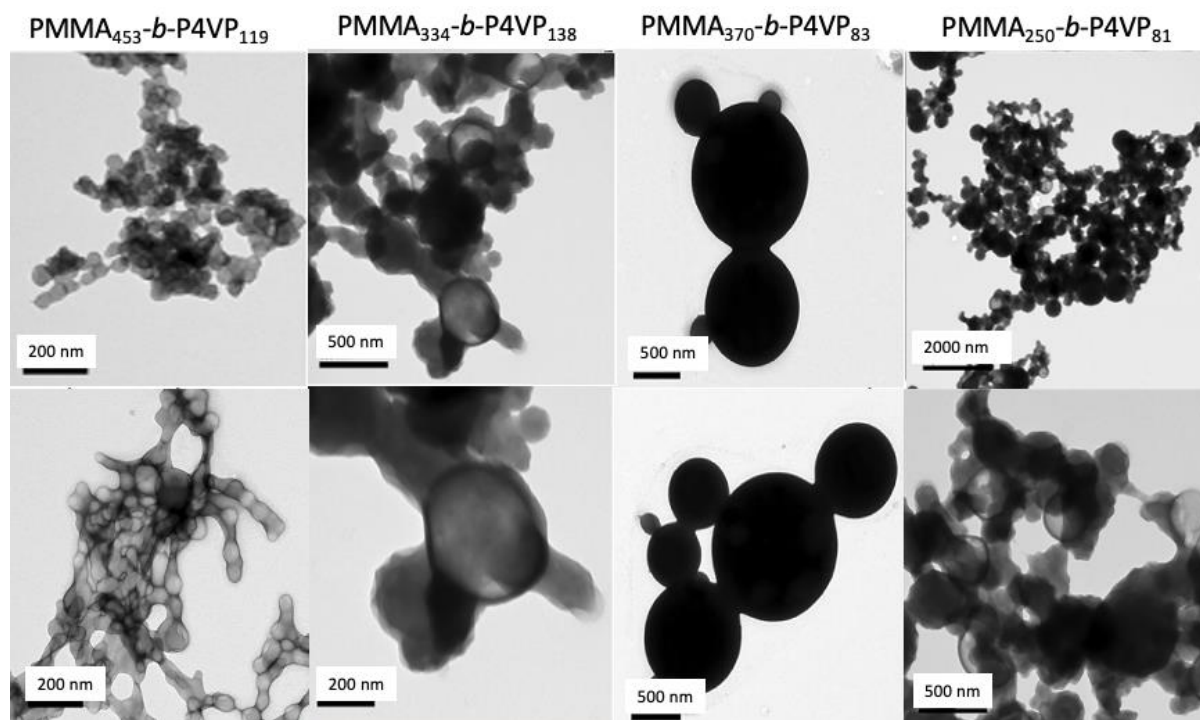


Figure 183 TEM images of self-assembly 0.1wt% in water using 6 mL THF.

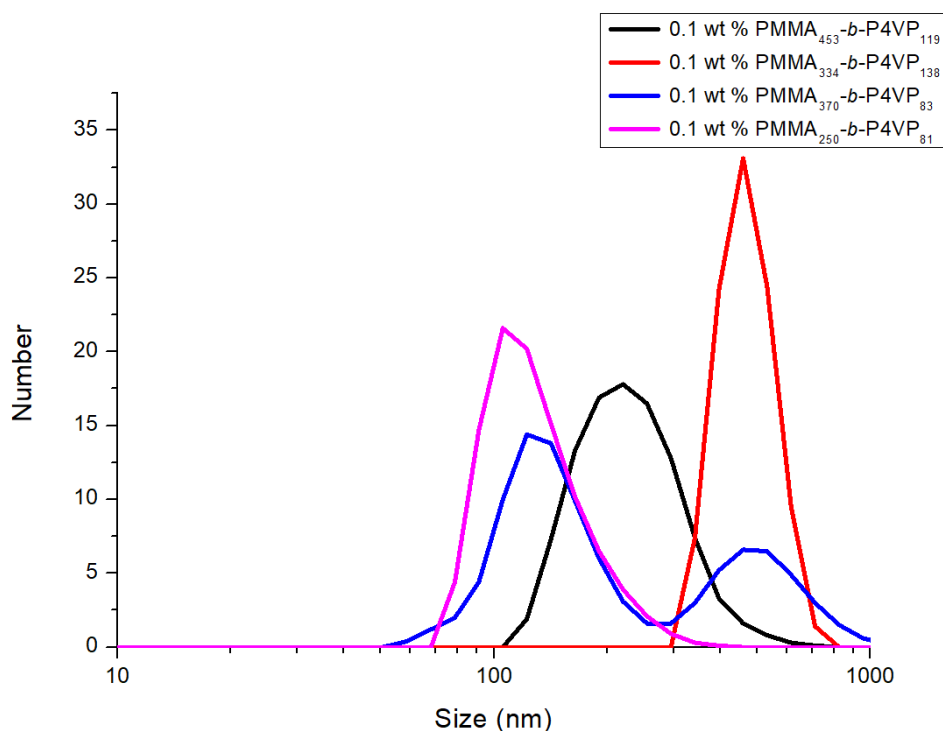


Figure 184 DLS results of self-assembly 0.1wt% in water using 6 mL THF.

The TEM micrographs show that micelles and vesicles to be present. Large structures can be seen in the TEM images as these micelles/ vesicles aggregate together. The individual size range of these micelles are between 20-40 nm. The vesicles which can be seen are much larger and the ones measured were between 194-235nm for all samples. DLS does suggest that there are aggregates present at 100nm and also larger aggregates 200nm. This supports TEM and the aggregates at 100nm are most likely micellar structures as this is below the maximum micelle size and the aggregates above are most likely vesicular structures. DLS does also suggest in the case of PMMA₃₃₄-*b*-P4VP₁₃₈ that there are bigger structures present at 500nm. These are likely to be bigger vesicles or DLS is picking up on aggregation of the vesicular structures.

The case of PMMA₃₇₀-*b*-P4VP₈₃ is very interesting with the solid spheres. They are the biggest structures seen yet from the self-assembly and could be bicontinuous nanospheres. Bicontinuous nanospheres have been recorded up to 500 nm and the spheres seen with PMMA₃₇₀-*b*-P4VP₈₃ are defiantly not spherical micelles or vesicles.

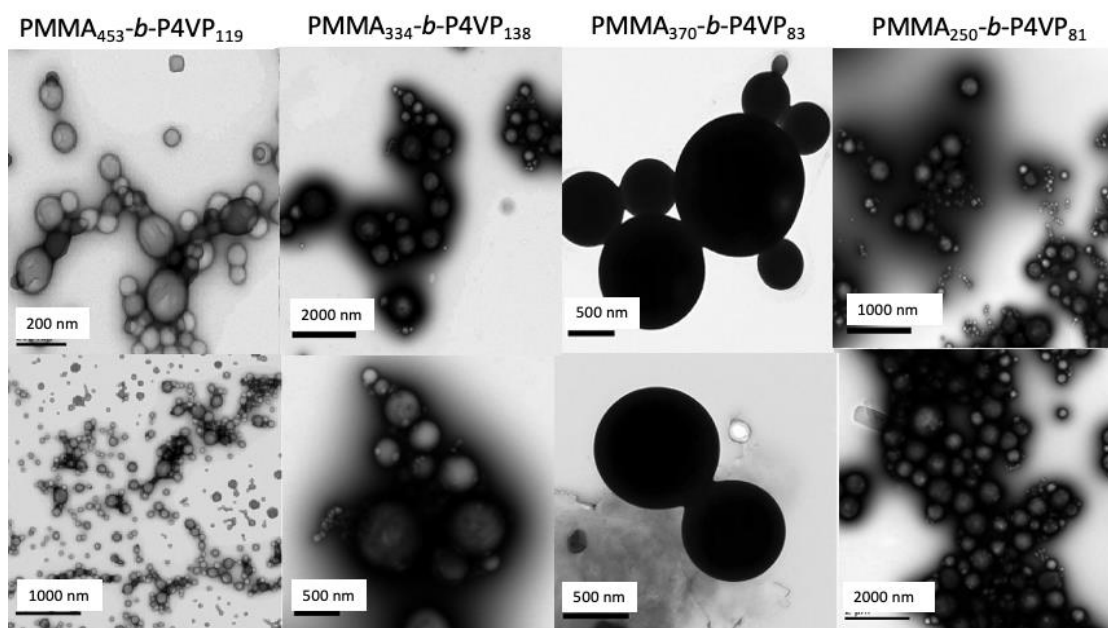


Figure 185 TEM images of self-assembly 1.0wt% in water using 6 mL THF.

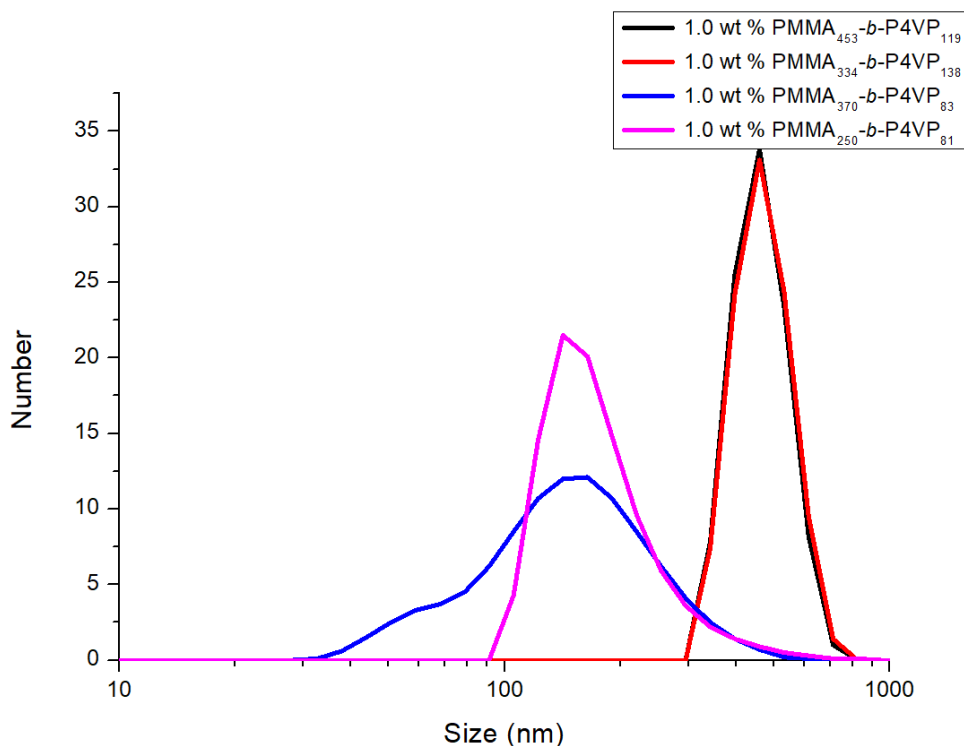


Figure 186 DLS results of self-assembly 1.0 wt% in water using 6 mL THF.

The TEM micrographs in most cases show vesicles which are around 167nm. These are most likely to be vesicles as many of the structures appear to be hollow inside. The maximum micelle was worked out to be between 114-118nm for the samples shown above. As the structures are much larger than this range, they are most likely not spherical micelles. The sample of PMMA₃₃₄-*b*-P4VP₁₃₈ and PMMA₄₅₃-*b*-P4VP₁₁₉ shows much larger samples which are greater than 500nm from DLS. TEM disagrees with this and shows structures much smaller in size. For PMMA₃₇₀-*b*-P4VP₈₃ It is difficult to tell what they are as the structures are so dark but it is interesting that they very different to the microspheres that the University of Nottingham had previously seen. DLS also shows

that most structures are above 100nm indicating that these aggregates are most likely not micelles. The slight exception was PMMA₃₃₄-*b*-P4VP₈₃ which seemed to have smaller structures present at 50 nm.

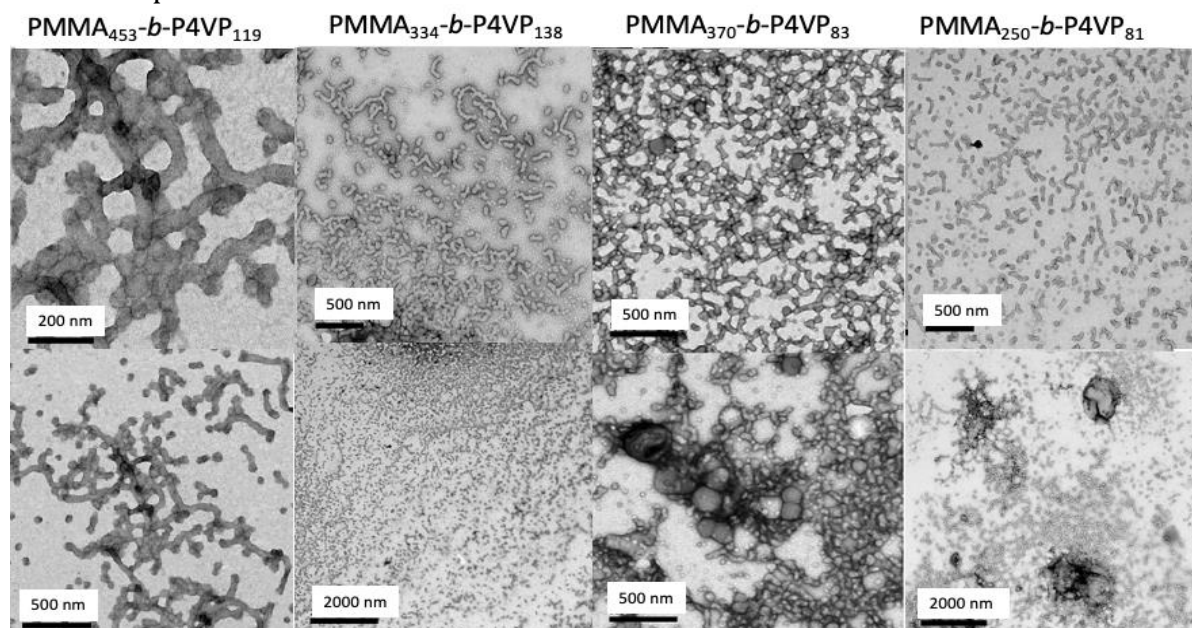


Figure 187 TEM images of self-assembly 0.1 wt% in ethanol using 6 mL THF.

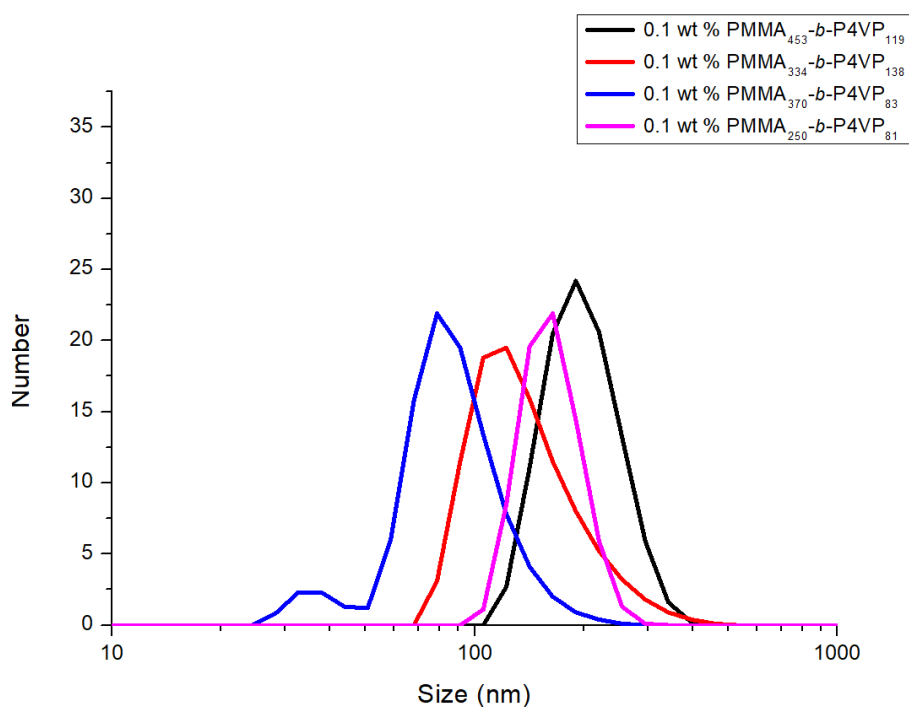


Figure 188 DLS results of self-assembly 0.1wt% in ethanol using 6 mL THF.

The TEM images show spherical micelles along with cylindrical micelles. Looking at the size of these micelles, they are very small (20-30 nm) but the cylindrical micelles are much bigger. The TEM images show aggregation where particles are coming together to form larger structures. Dynamic light scattering (DLS) does support the TEM images and reports in most cases that bigger particles of 100 nm are being observed. This difference is due to the aggregation of micelles/ cylindrical structures which has allowed the DLS to measure particles that are bigger than what actually is in solution.

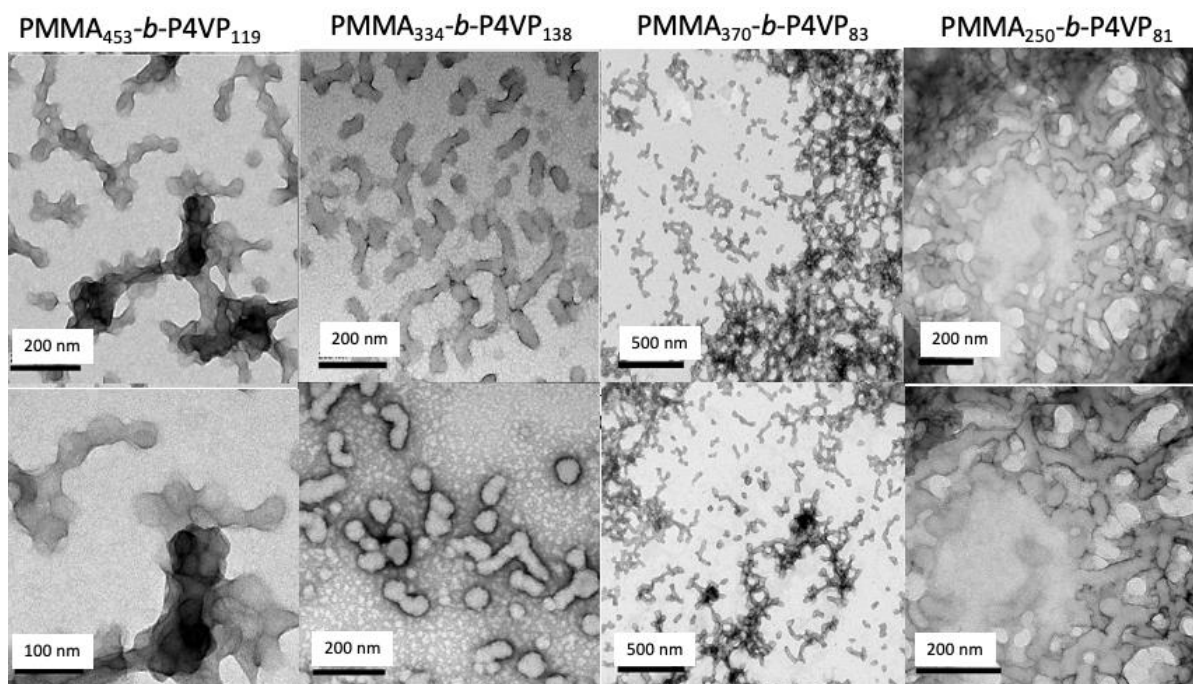


Figure 189 TEM images of self-assembly 1.0 wt% in ethanol using 6 mL THF.

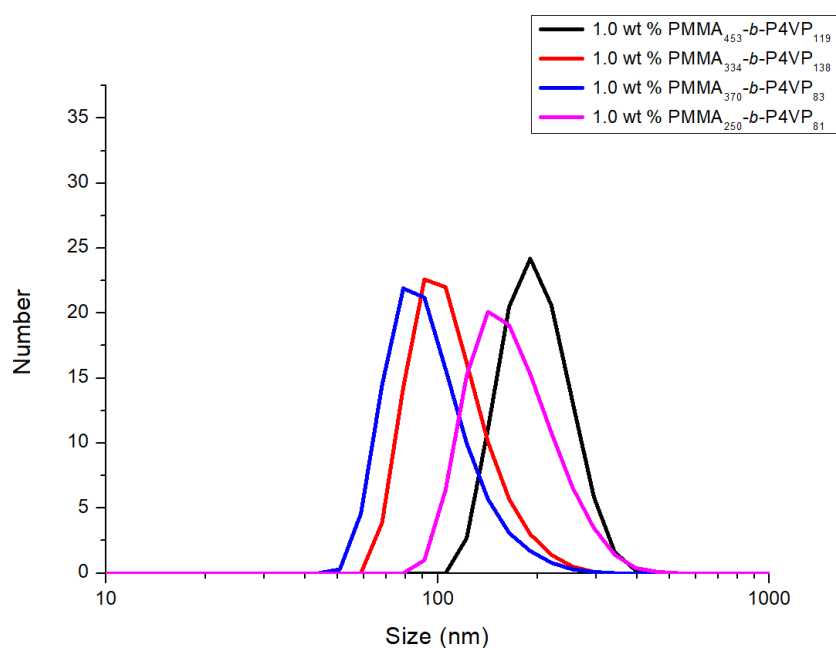


Figure 190 DLS results of self-assembly 1.0 wt% in ethanol using 6 mL THF.

The TEM images show spherical micelles along with cylindrical micelles. Looking at the size of these micelles, they are very small (20-30 nm) but the cylindrical micelles are much bigger. The TEM images show aggregation where particles are coming together to form larger structures. Dynamic light scattering (DLS) does support the TEM images in the cases of PMMA₄₅₃-b-P4VP₁₁₉ & PMMA₂₅₀-b-P4VP₈₁ and reports that bigger particles of 100 nm are being observed. The other samples suggest smaller particles which we can see from TEM are most likely spherical and cylindrical micelles. This difference is due to the aggregation of micelles/ cylindrical structures which has allowed the DLS to measure particles that are bigger than what actually is in solution.

4.3.6 Self-assembly of PEO₄₄-*b*-PODMA₂₆ in Ethanol

In an earlier chapter, PEO₄₄-*b*-PODMA₂₆ was successfully made by ATRP and was self-assembled in water to form complex aggregate species such as bicontinuous nanospheres. The aim here was to self-assemble this block copolymer in ethanol to see which aggregate species would result. If more complex aggregates such as bicontinuous or lamella did form then this could be an alternative polymer for The University of Nottingham to try in their research.

PEO₄₄-*b*-PODMA₂₆ was self-assembled in ethanol where 1 litre of ethanol was used and the ethanol was changed 4 times.

Sample Preparation

The exact quantities of polymer and ethanol used in each case are given in Table 44 below.

Table 44 Quantities used to make a 0.1 and 1.0 wt% sample.

Self-assembled Concentration wt %	Mass of polymer used (g)	THF Volume (mL)	Ethanol Volume (mL)	Total Volume (mL)
0.1	0.01	6.0	4.0	10
1.0	0.1	6.0	4.0	10

Ethanol was added dropwise (at 5.15 mL h⁻¹) at 60.0 °C to avoid precipitation.

PEO₄₄-*b*-PODMA₂₆ 0.1 wt% (Ethanol)

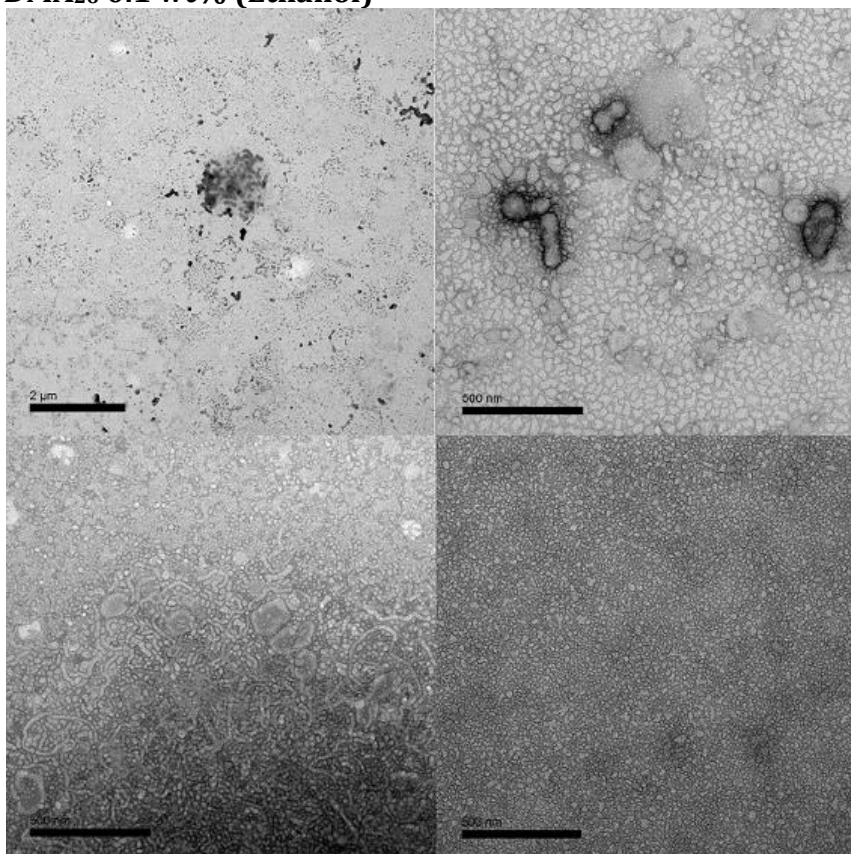


Figure 191 TEM images of self-assembly 0.1 wt% in ethanol using 6 mL THF.

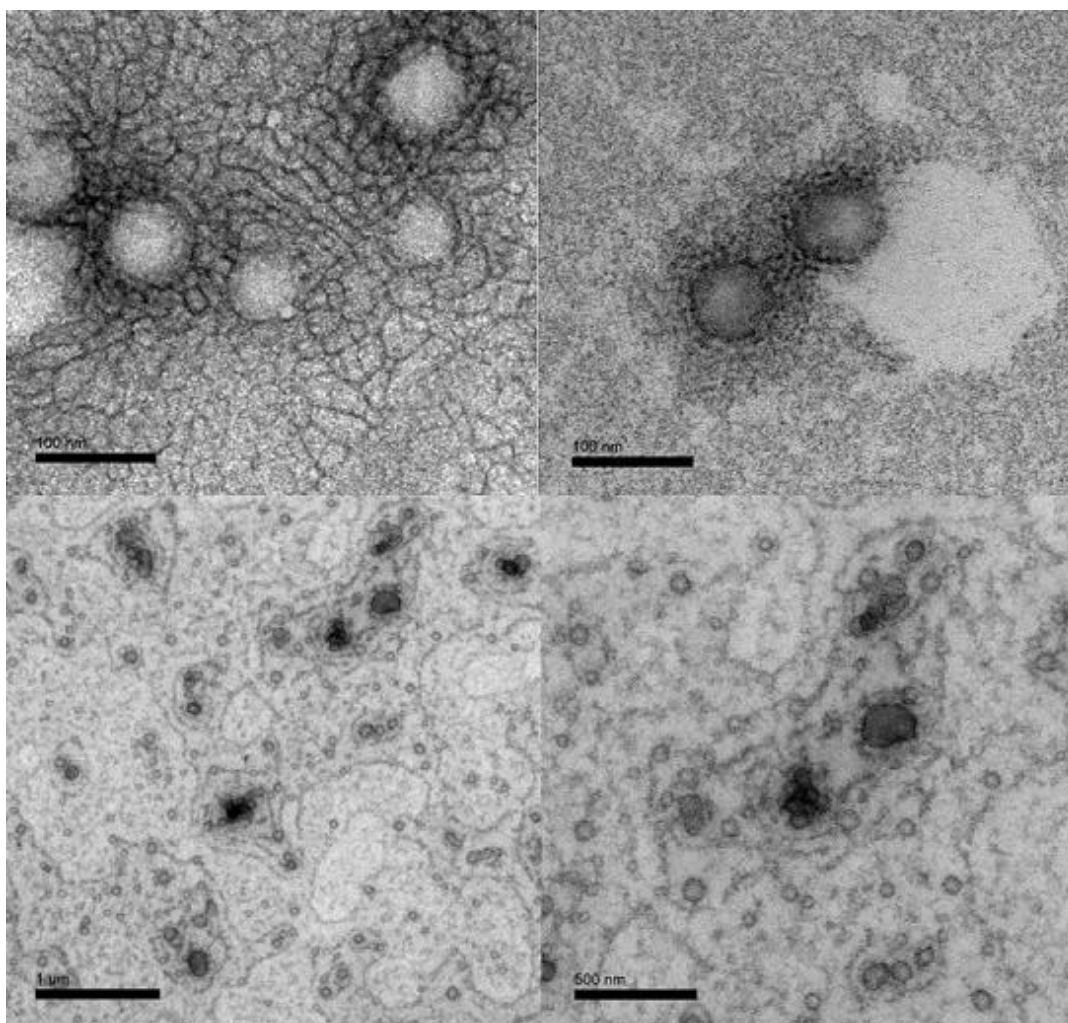


Figure 192 TEM images of self-assembly 1.0 wt% in ethanol using 6 mL THF.

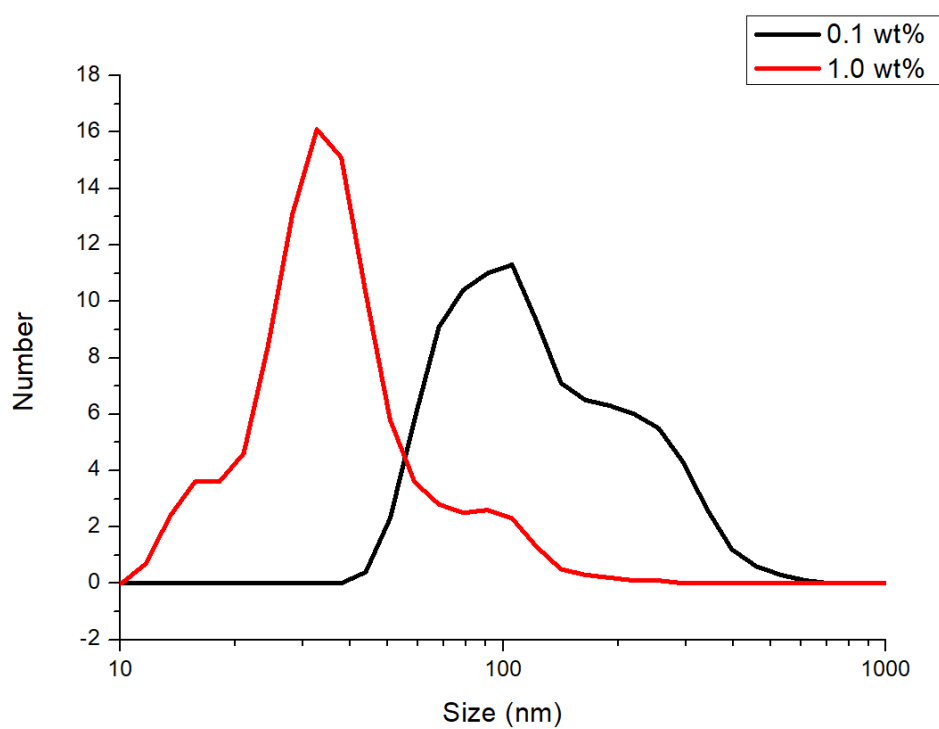


Figure 19375 DLS results of self-assembly PEO₄₄-b-PODMA₂₆ 0.1 & 1.0 wt% in ethanol using 6 mL THF.

When PEO₄₄-b-PODMA₂₆ is self-assembled in ethanol, only simple aggregate species such as spherical micelles and cylindrical micelles can be seen. This is very different to the complex aggregate structures previously seen in earlier chapters of this thesis. A complex aggregate species is desired for this project as something like a bicontinuous or lamella structure would allow high surface area as well as being easily tuneable. It was deemed at this point that PEO₄₄-b-PODMA₂₆ would not be a good alternative to use as the species formed in ethanol was no different to the structures that PMMA-*b*-P4VP formed.

4.3.7 Attempted synthesis of P4VP-*b*-PODMA

The final thing tried for this project was to see whether a block copolymer of P4VP-*b*-PODMA would form complex aggregate species in both water and ethanol. This was to be made by RAFT Polymerisation but the first thing to do was to assess how PODMA performed in scCO₂. This testing was performed at the University of Nottingham.

Polymerisation in scCO₂

After reacting the monomer for 24 hours in the presence of 1 wt% AIBN radical initiator and 5 wt% PDMS-MA polymeric stabiliser, the product was obtained as a white crystalline solid. The product was shown to be highly pure PODMA product with no sign of monomer impurities in the ¹H NMR.

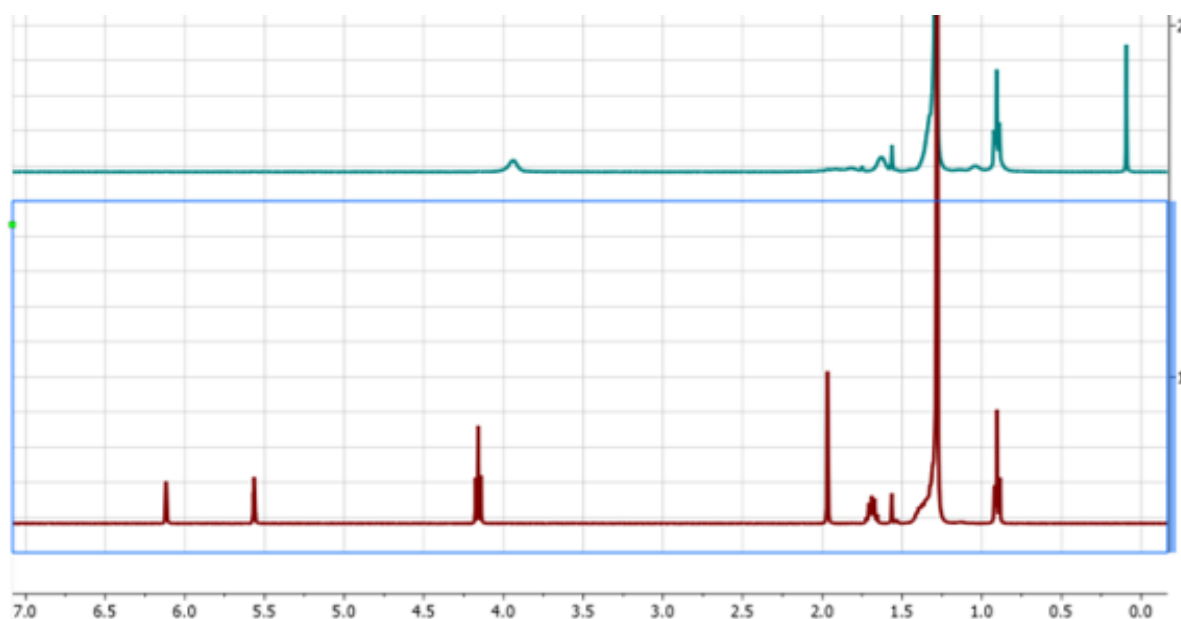


Figure 194 ¹H NMR of stearyl methacrylate starting material (bottom red spectra) and PODMA free-radical product (top blue spectra) made by RAFTS in scCO₂.

The GPC analysis indicates the product is a low molecular weight product with very high dispersity (typical for free-radical polymerisation). GPC trace can be seen in Figure 195. For the RAFT controlled reaction, enough DDMAT RAFT agent was added to target a molecular weight of 50 kDa. The molecular weight values were calculated as follows:

Free radical: 29.5 kDa (dispersity = 3.978)
RAFT controlled: 39.6 kDa (dispersity = 1.838)

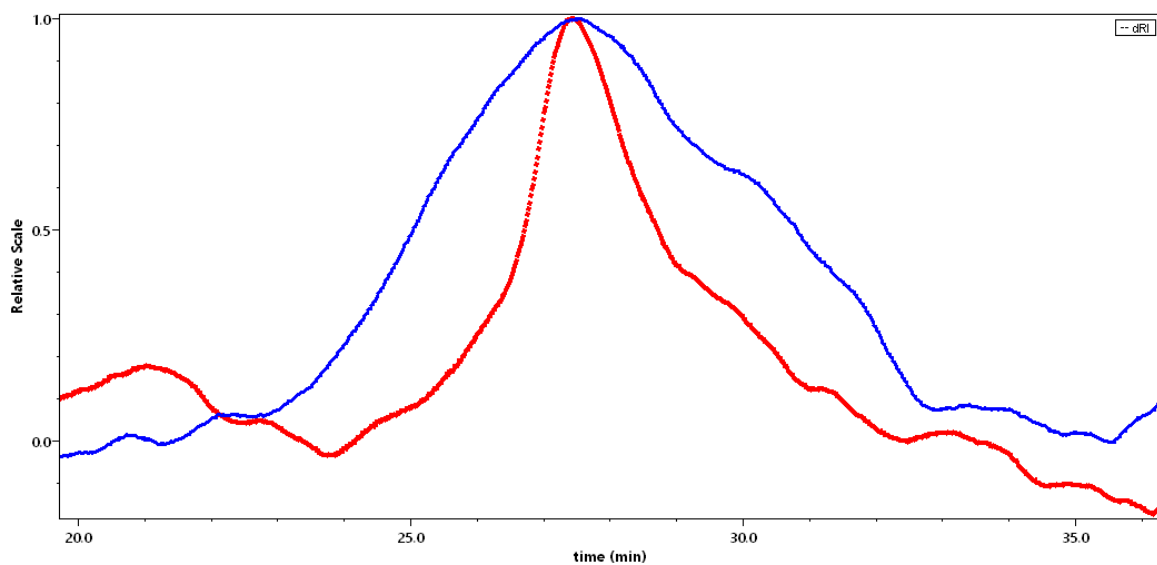


Figure 195 GPC traces for PODMA via free-radical polymerisation (blue) and RAFT controlled polymerisation (red).

SEM image of the free-radical product can be seen in Figure 196. For a dispersion polymerisation we would expect to see a microparticle structure in the polymer, however for the PODMA product no such morphology is observed.

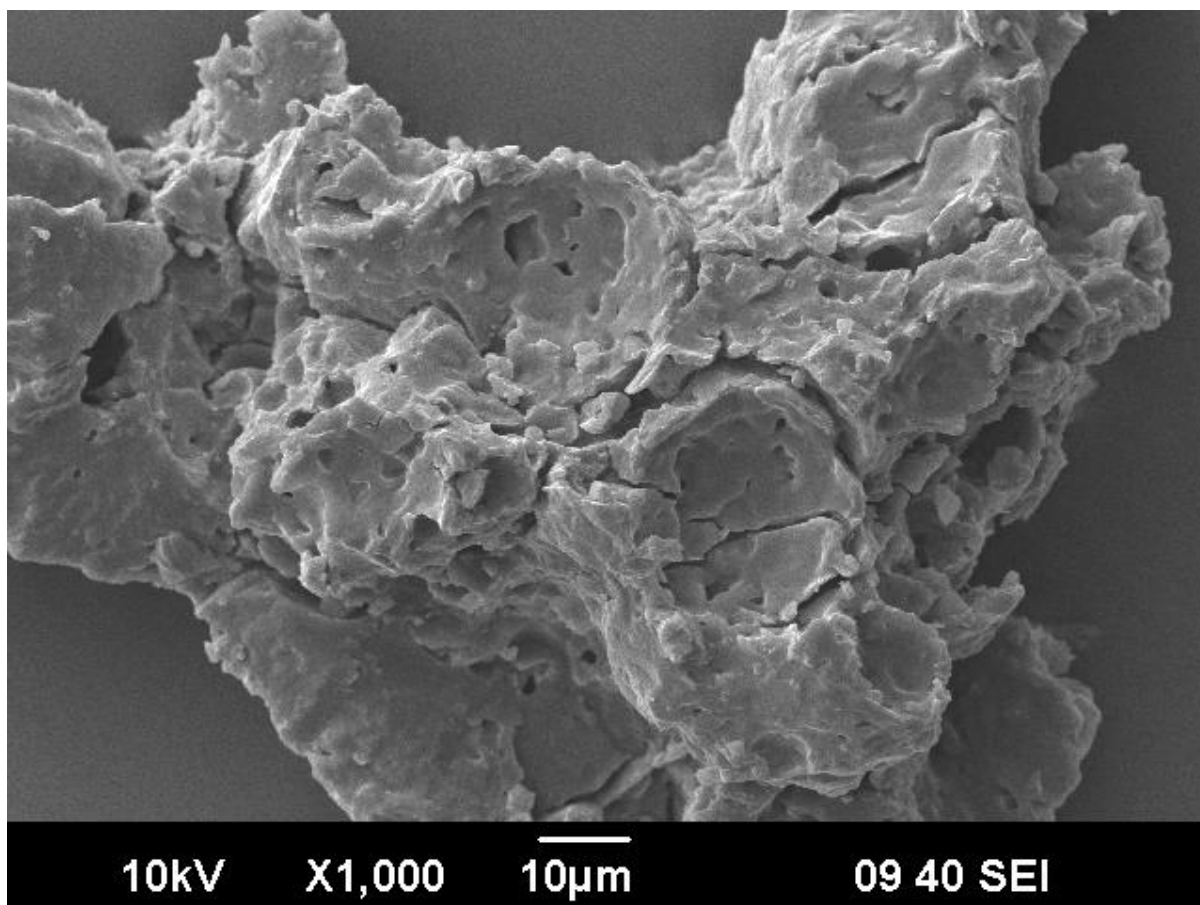


Figure 196 SEM image of the free-radical product shows a disordered material structure with no defining features.

The combination of data indicates that the PODMA is precipitating out of the scCO₂ solvent once a particular molecular weight is obtained, rather than being stabilised in microparticle form by the polymeric stabiliser (PDMS-MA). Under the conditions used, polymerisation may occur to form PODMA but the reaction terminates upon precipitation from the scCO₂ solvent. This prevents any significant control of the molecular weight.

Conclusion

This chapter successfully self-assembled PMMA-*b*-P4VP to form different aggregate structures. The main structures seen in water and ethanol consisted of spherical micelles, cylindrical micelles and vesicles. In the case of PMMA₃₇₀-*b*-P4VP₈₃ large dark spheres were seen which could be of the bicontinuous nature. All these different aggregate species were very different to what was seen previously by The University of Nottingham.

ATRP was attempted to make PMMA-*b*-P4VP but all reactions failed to add the 4VP block onto PMMA-Cl or PMMA-Br initiators. This can be clear from the H-NMR taken of the reaction mixture. It seems the easiest way to make PMMA-*b*-P4VP is by RAFT polymerisation but it is difficult to make block copolymers with a molecular weight less than 33,500 KDa.

PEO-*b*-PODMA which was made in an earlier chapter was suggested as an alternative polymer to try in the hope of producing bicontinuous nanospheres when self-assembled in ethanol. Self-assembly in ethanol seems to produce spherical and cylindrical micelles. This polymer was also made by RAFT polymerisation but showed no defining features when SEM was carried out. It was at this point that it was concluded that it could not be used as alternative polymer for the University of Nottingham.

References

- 1 T. M. Bennett, G. He, R. R. Larder, M. G. Fischer, G. A. Rance, M. W. Fay, A. K. Pearce, C. D. J. Parmenter, U. Steiner and S. M. Howdle, *Nano Lett.*, 2018, **18**, 7560–7569.
- 2 C. M. A. Parlett, K. Wilson and A. F. Lee, *Chem. Soc. Rev.*, 2013, **42**, 3876–3893.
- 3 B. Roose, K. C. Gödel, S. Pathak, A. Sadhanala, J. P. C. Baena, B. D. Wilts, H. J. Snaith, U. Wiesner, M. Grätzel, U. Steiner and A. Abate, *Adv. Energy Mater.*, , DOI:10.1002/aenm.201501868.
- 4 W. Li, J. Liu and D. Zhao, *Nat. Rev. Mater.*, 2016, **1**, 1–17.
- 5 K. E. Shopsowitz, H. Qi, W. Y. Hamad and M. J. MacLachlan, *Nature*, 2010, **468**, 422–426.
- 6 Y.-F. Sun, S.-B. Liu, F.-L. Meng, J.-Y. Liu, Z. Jin, L.-T. Kong and J.-H. Liu, *Sensors*, 2012, **12**, 2610–2631.
- 7 X. Wang, Y. Zhang, W. Luo, A. A. Elzatahry, X. Cheng, A. Alghamdi, A. M. Abdullah, Y. Deng and D. Zhao, *Chem. Mater.*, 2016, **28**, 2356–2362.
- 8 H. Wang, S. Zhuo, Y. Liang, X. Han and B. Zhang, *Angew. Chemie*, 2016, **128**, 9201–9205.
- 9 A. Pan, H. Bin Wu, L. Yu and X. W. D. Lou, *Angew. Chemie*, 2013, **125**, 2282–2286.
- 10 J. Li, S. Xiong, Y. Liu, Z. Ju and Y. Qian, *ACS Appl. Mater. Interfaces*, 2013, **5**, 981–988.
- 11 J. Zhao, Y. Zou, X. Zou, T. Bai, Y. Liu, R. Gao, D. Wang and G. D. Li, *Nanoscale*, 2014, **6**, 7255–7262.
- 12 L. Peng, Y. Zhao, Y. Ding and G. Yu, *Chem. Commun.*, 2014, **50**, 9569–9572.
- 13 Y. Liu, J. Goebel and Y. Yin, *Chem. Soc. Rev.*, 2013, **42**, 2610–2653.
- 14 Y. Deng, J. Wei, Z. Sun and D. Zhao, *Chem. Soc. Rev.*, 2013, **42**, 4054–4070.
- 15 S. Xu, C. M. Hessel, H. Ren, R. Yu, Q. Jin, M. Yang, H. Zhao and D. Wang, *Energy Environ. Sci.*, 2014, **7**, 632–637.
- 16 M. G. Fischer, X. Hua, B. D. Wilts, I. Gunkel, T. M. Bennett and U. Steiner, *ACS Appl. Mater. Interfaces*, 2017, **9**, 22388–22397.
- 17 Y. Boyjoo, M. Wang, V. K. Pareek, J. Liu and M. Jaroniec, *Chem. Soc. Rev.*, 2016, **45**, 6013–6047.
- 18 J. Jennings, M. Beija, A. P. Richez, S. D. Cooper, P. E. Mignot, K. J. Thurecht, K. S. Jack and S. M. Howdle, *J. Am. Chem. Soc.*, 2012, **134**, 4772–4781.
- 19 S. Choudhury, M. Agrawal, P. Formanek, D. Jehnichen, D. Fischer, B. Krause, V. Albrecht, M. Stamm and L. Ionov, *ACS Nano*, 2015, **9**, 6147–6157.
- 20 D. Fattakhova-Rohlfing, A. Zaleska and T. Bein, *Chem. Rev.*, 2014, **114**, 9487–9558.
- 21 G. He, T. M. Bennett, M. Alauhdin, M. W. Fay, X. Liu, S. T. Schwab, C. G. Sun and S. M. Howdle, *Polym. Chem.*, 2018, **9**, 3808–3819.
- 22 Y.-N. Zhou, Z.-C. Chen, C. Wei and Z.-H. Luo, *Macromol. Chem. Phys.*, 2015, **216**, 329–333.
- 23 J. Xia, X. Zhang and K. Matyjaszewski, *Macromolecules*, 1999, **32**, 3531–3533.
- 24 M. Alauhdin, T. M. Bennett, G. He, S. P. Bassett, G. Portale, W. Bras, D. Hermida-Merino and S. M. Howdle, *Polym. Chem.*, 2019, **10**, 860–871.
- 25 S. Horstmann, M. C. Leimenstoll and H. Menzel, in *Progress in Colloid and Polymer Science*, Springer, Berlin, Heidelberg, 2004, vol. 129, pp. 50–61.
- 26 P. Guo, W. Guan, L. Liang and P. Yao, *J. Colloid Interface Sci.*, 2008, **323**, 229–234.
- 27 J. G. Kennemur, *Macromolecules*, 2019, **52**, 1354–1370.
- 28 J. Burke, .

Chapter 5. Synthesis and self-assembly of triblock poly(ethylene oxide)-*block*-poly(N-isopropylacrylamide)-*block*- poly(octadecyl methacrylate)

Contents

5.1 Introduction	199
2.0 Experimental	200
2.1 Synthesis of poly(ethylene oxide) macroinitiator	200
2.2 Synthesis of poly(ethylene oxide)-block-poly(butyl methacrylate)	201
3.0 Results and Discussion	202
Low degree of polymerisation PEO initiators.....	202
Low degree of polymerisation PEO- <i>b</i> -PBMA Block copolymers	203
Self-assembly of PEO- <i>b</i> -PBMA (Eindhoven University of Technology collaboration).....	204
Self-assembly via cosolvent method	205
Cryo-TEM characterization	205
Triblock synthesis	211
Initial testing.....	211
Low DP PEO initiators	213
Low DP Block copolymers of PEO- <i>b</i> -PNIPAM-Cl.....	214
4.0 Conclusion	227
5.0 References	228

5.1 Introduction

When block copolymers are self-assembled in aqueous solutions, many different morphologies can form. A few examples being spherical micelles, cylindrical micelles,¹ vesicles.² More complex examples can form with a few examples being disk-like,³ toroidal,⁴ helical structures⁵ and bicontinuous aggregates.⁶ Previously it has been demonstrated that using PEO-poly(octadecyl methacrylate) (PEO-*b*-PODMA)⁷ 18 carbon atoms in side chain and PEO-poly(*n*butyl methacrylate) (PEO-*b*-PBMA)⁶ 4 carbon atoms in side chain can form bicontinuous nanospheres which make these polymers of interest to study.

The University of Manchester⁸ have used molecular dynamic simulations to investigate the self-assembly of PEO-poly(*n*butyl methacrylate)(PEO-*b*-PBMA) in water and THF. With the model used for PEO-*b*-PBMA, they were able to predict what aggregate species would form when the THF:water ratio was varied. This is shown in the phase diagram below (Figure 197).

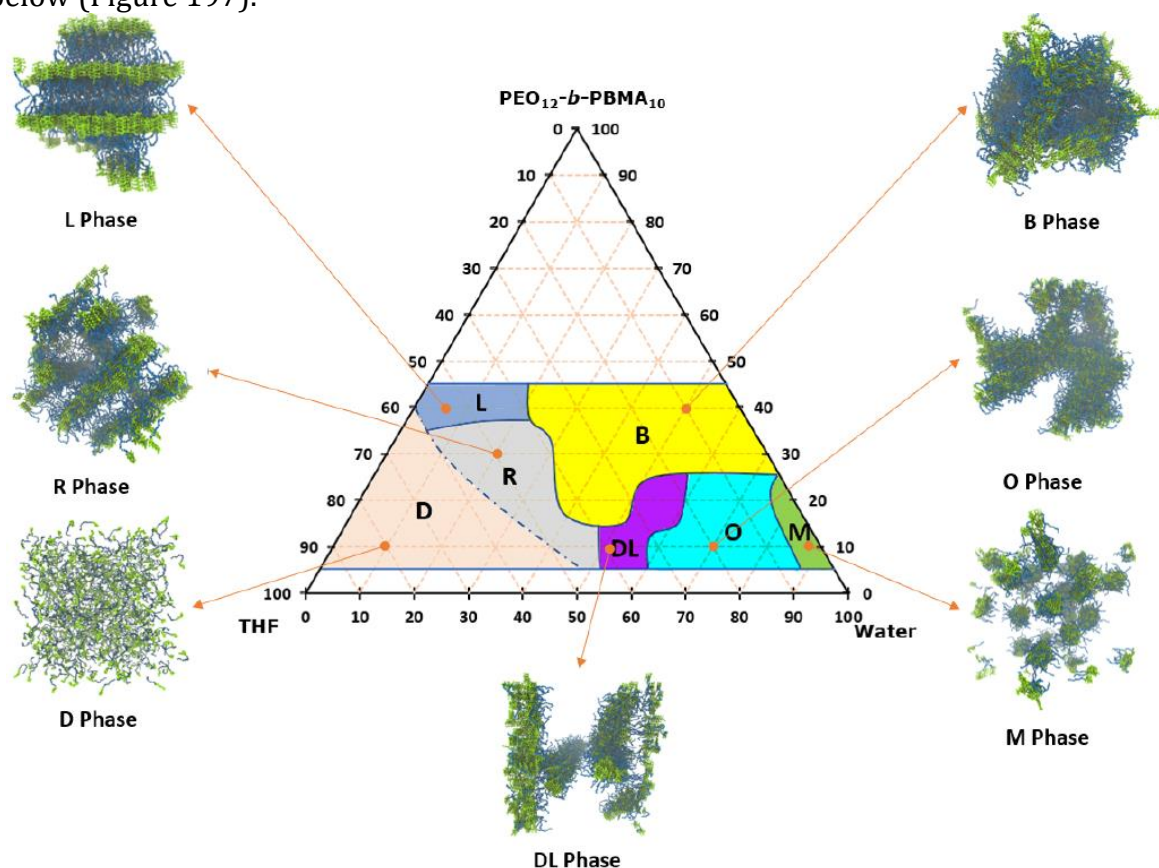


Figure 197 Phase diagram for PEO₁₂-*b*-PBMA₁₀ predicted by MD model.

As the phase diagram shows, there is a region unfilled and this is due to it being very difficult to model in this area. This meant that the aim of this chapter was to work with the Eindhoven University of Technology to make short chain polymers of PEO-*b*-PBMA which they would then self-assemble in different THF:Water concentrations. This would then complete the phase diagram shown in Figure 1. The contact at Eindhoven University was working with the group conducting the molecular dynamic simulations (University of Manchester) and the aim of this collaborative chapter was to assess to see if the

morphologies of the self-assembled aggregates matched those the model predicted for the self-assembly of PEO-*b*-PBMA.

The initial results from the synthesis of PEO-*b*-PBMA with low DP for the PEO and PBMA blocks led to another project where PEO-*b*-PNIPAM-*b*-PODMA was targeted. Polymers which react to external stimuli such as temperature, light and pH have always attracted much attention.⁹ Poly(N-isopropylacrylamide)(PNIPAM) is a very well-known thermoresponsive polymer which is hydrophilic. PNIPAM has been widely used in cosmetics with biomedical applications, wastewater treatment and oil recovery¹⁰ but now it is being considered in applications involving drug delivery. This water soluble polymer exhibits a lower critical solution temperature of 32°C.⁷ When an aqueous solution of PNIPAM is heated above 32°C the polymer chains are dehydrated by the expulsion of water molecules. This causes a coil-to-globule phase transition and chain aggregation. Due to this unique thermoresponsive property, polymers with NIPAM are being used more.¹¹ This second part of this chapter aims to make a triblock PEO-*b*-PNIPAM-*b*-PODMA by ATRP, where it will be self-assembled in aqueous solutions to make bicontinuous nanospheres. A specific molecular weight and DP of each block will be targeted which should lead to thermoresponsive bicontinuous nanospheres like previously witnessed for PEO-*b*-PODMA.

5.2 Experimental

Copper(I) bromide (98%), copper(I) chloride (99%), magnesium sulphate (MgSO₄), N,N,N',N'-pentamethyldiethylenetriamine (PMDETA) (99%), octadecyl methacrylate (ODMA), butyl methacrylate (BMA), dimethylamino pyridine, bromoisobutryl bromide, triethylamine, N-isopropylacrylamide (Nipam) tris[2-(dimethylamino)ethyl]amine (Me₆TREN), tetraethylene glycol monomethyl ether were all purchased from Sigma-Aldrich and used as received. Aluminium oxide for column chromatography was purchased from Acros Organics. Xylene, isopropyl alcohol, tetrahydrofuran (THF), dichloromethane (DCM), butanone, acetonitrile (analytical reagent grade), potassium carbonate, were purchased from Fisher Scientific and used as received. The deuterated chloroform used in ¹H-NMR and ¹³C-NMR was purchased from Cambridge Isotope Laboratories. Xylene was purchased from BDH Lab Supplies.

5.2.1 Synthesis of poly(ethylene oxide) macroinitiator

A literature method⁷ was followed for the synthesis of the PEO-Br macroinitiator. The following method was used to make PEO₃-Br but all methods were similar. 2-bromoisobutryl bromide (1.150g, 5mmol), triethylamine (0.506 g, 5 mmol) and 4-dimethylamino pyridine (0.611 g, 5 mmol) was dissolved in anhydrous dichloromethane and added to a round bottom flask. Tetraethylene glycol monomethyl ether (0.52 g, 2.5 mmol) was dissolved in 10 mL of anhydrous dichloromethane and added dropwise to the reaction mixture at 0°C for 1 hour. The reaction mixture was then left stirring for 18 hours at room temperature. The mixture was then filtered and half the solvent was evaporated off. Dichloromethane was added to bring mixture up to 100 mL. Using a separating funnel, the mixture was washed twice with saturated sodium bicarbonate solution and then twice with hydrochloric acid (10%, 2M). The organic layer was collected and dried over anhydrous magnesium sulphate for 1 hour. The solution was filtered and solvent

evaporated off. Product dried in vacuum oven overnight. The compound was characterised using $^1\text{H-NMR}$, $^{13}\text{C-NMR}$ and GPC.

$^1\text{H-NMR}$ (400 Hz, CDCl_3 , ppm) δ : 1.89 (Singlet, 6H, $(\text{CH}_3)_2\text{C-}$), 3.37 (Singlet, 3H $-\text{OCH}_3$), 3.65 (Broad peak, 4H, $-\text{OCH}_2\text{CH}_2$), 3.73 (triplet, 2H, $(-\text{OCH}_2\text{CH}_2)$), 4.31 (triplet, 2H, $(-\text{OCH}_2\text{CH}_2)$). **$^{13}\text{C-NMR}$ (CDCl_3 , ppm) δ :** 30.8 (Br- $\text{C}(\text{CH}_3)_2$ -), 55.7 (Br-C-), 58.9 ($\text{CH}_3\text{-O-}$), 65.1 ($-\text{COO-CH}_2\text{-CH}_2$), 70.5 ($-\text{COO-CH}_2\text{-CH}_2$), 171.6 (Br- $\text{C}(\text{CH}_3)_2\text{-COO}$).

5.2.2 Synthesis of poly(ethylene oxide)-*block*-poly(butyl methacrylate)

A literature method⁷ was followed for the synthesis of PEO-*b*-PBMA block copolymers. The following method was used to make PEG₃-*b*-PBMA₁₀ but the method to make all three block copolymers were very similar. Cu(I)Br (137 mg, 0.96 mmol) was put into a Schleck tube with a magnetic stirrer. The PEO macroinitiator (0.15 g, 0.48 mmol) was dissolved in xylene:IPA mixture (9:1) (4 mL) and added to Schleck tube. PMDETA (166 mg, 0.96 mmol) and BMA (0.48 g, 3.4 mmol) was added to Schleck tube which was then sealed and degassed (N_2) for 1 hour. The mixture was then stirred at 95°C for 24 hours under nitrogen. After 24 hours, the reaction was run through alumina column to remove the catalyst and ligand, then half of solvent was evaporated off. The polymer was precipitated out into acetonitrile dropwise at 0°C. The block copolymer was characterised by $^1\text{HNMR}$, $^{13}\text{CNMR}$ & GPC.

$^1\text{H-NMR}$ (400 Hz, CDCl_3 , ppm) δ : 0.94 (triplet, 3H, $-(\text{CH}_2)_{17}\text{-CH}_3$), 1.02 (broad peak, 3H, $-\text{CH}_2\text{-C-CH}_3$), 1.38 (broad peak, 14H, $-(\text{CH}_2)_7$ -), 1.58 (broad peak, $\text{CH}_2(\text{CH}_2)_{14}$ -), 3.38 (Singlet, 3H, $\text{CH}_3\text{O-}$), 3.64 (triplet, 4H, $-\text{O-CH}_2\text{CH}_2\text{-O}$), 3.93 (broad peak, 2H, $-\text{COO-CH}_2$ -). **$^{13}\text{C-NMR}$ (CDCl_3 , ppm) δ :** 13.80 ($-\text{CH}_2\text{CH}_2\text{CH}_3$), 19.35 ($-\text{CH}_2\text{CH}_2\text{CH}_3$), 29.38 ($-\text{CH}_2(\text{CH}_2)_7\text{CH}_2$), 30.21 ($-\text{CH}_2(\text{CH}_2)_7\text{CH}_2$), 70.59 ($-\text{CH}_2\text{CH}_2\text{CH}_3$), 71.95 ($-\text{OCH}_2\text{CH}_2\text{O-}$).

5.2.3 Synthesis of poly(ethylene oxide)-*block*-poly(N-isopropylacrylamide) macroinitiator

A literature¹² method was followed and adapted for the PEO-*b*-PNIPAM-Br macroinitiator. PEO-Br (2.3 g 0.885 mmol) was added to a reaction flask. The reaction solvent a mixture of butanone and 2-propanol (1:1) was added. The reaction was degassed under nitrogen for an hour. CuCl (0.0876g, 0.885 mmol) and Me₆TREN (0.204g, 0.885 mmol) was added to reaction and everything was degassed for a further 30 minutes. NIPAM (2.3g 0.02 mol) was added and reaction mixture degassed a further 30 minutes. The polymerisation was left at 60°C for 4 hours. After the polymerisation, THF was added and reaction mixture passed through an alumina column. The product was precipitated from ether three times and product dried in vacuum oven overnight.

$^1\text{H-NMR}$ (400 Hz, CDCl_3 , ppm) δ : 1.20 (broad peak, $\text{NH-CH}(\text{CH}_2)_2$), 1.22 (broad peak, COOCH_3), 1.82 (broad peak, $\text{CH}_2\text{CH}_2\text{-Br}$), 2.18 (broad peak, $\text{CH}_2\text{CH}_2\text{-Br}$), 3.40 (singlet, 3H, $\text{CH}_3\text{O-}$), 3.64 (triplet, 4H, $-\text{O-CH}_2\text{CH}_2\text{-O}$), 4.11 (broad peak, NHCH) 6.60 (broad peak NH) **$^{13}\text{C-NMR}$ (CDCl_3 , ppm) δ :** 23.5, 25.8, 41.0, 41.5, 68.3, 71.2, 174.8

5.2.4 Synthesis of poly(ethylene oxide)-*block*-poly(N-isopropylacrylamide)-*block*-poly(octadecyl methacrylate)

A literature method was followed and adapted for the synthesis of PEO-*b*-PNIPAM-*b*-PODMA block copolymer.⁷ Cu(I)Br (0.012g, 0.084 mmol) was put into a Schlenk tube with a magnetic stirrer. The PEO/PNIPAM macroinitiator (0.215 g, 0.084 mmol) was dissolved in xylene:IPA mixture (9:1) (4 mL) and added to a Schlenk tube. PMDETA (0.0145 g, 0.084 mmol) and ODMA (0.425 g, 1.26 mmol) was added to Schlenk tube which was then sealed and degassed (N₂) for 1 hour. The mixture was then stirred at 95°C for 24 hours under nitrogen. After 24 hours, the reaction was run through alumina column to remove the catalyst and ligand, then half of solvent was evaporated off. The polymer was precipitated out into acetonitrile dropwise at 0°C.

¹H-NMR (400 Hz, CDCl₃, ppm)δ: 0.88 (triplet, 3H, -(CH₂)₁₇-CH₃), 1.00 (broad peak, 3H, -CH₂-C-CH₃), 1.29 (broad peak, 30H, -(CH₂)₁₄-), 1.60 (broad peak, CH₂(CH₂)₁₄-), 3.38 (Singlet, 3H, CH₃O-), 3.65 (triplet, 4H, -O-CH₂CH₂-O), 3.91(broad peak, 2H, -COO-CH₂-). 3.91(broad peak, NH-CH-(CH₂)₂). **¹³C-NMR (CDCl₃, ppm)δ:** 14.22 (-CH₂CH₂CH₃), 22.77 (-CH₂CH₂CH₃), 29.38 (-CH₂(CH₂)₁₆CH₂), 29.80 (-CH₂(CH₂)₁₆CH₂), 31.92 (-CH₂CH₂CH₃), 70.59 (-OCH₂CH₂O-).

5.3 Results and Discussion

5.3.1 Synthesis of PEO initiators

Three PEO initiators were made which were PEO₃-Br, PEO₁₂-Br and PEO₁₆-Br. Proton and carbon NMR were performed on each sample, all giving similar traces. SEC was not performed as the molecular weights of these initiators fell outside the range of the SEC.

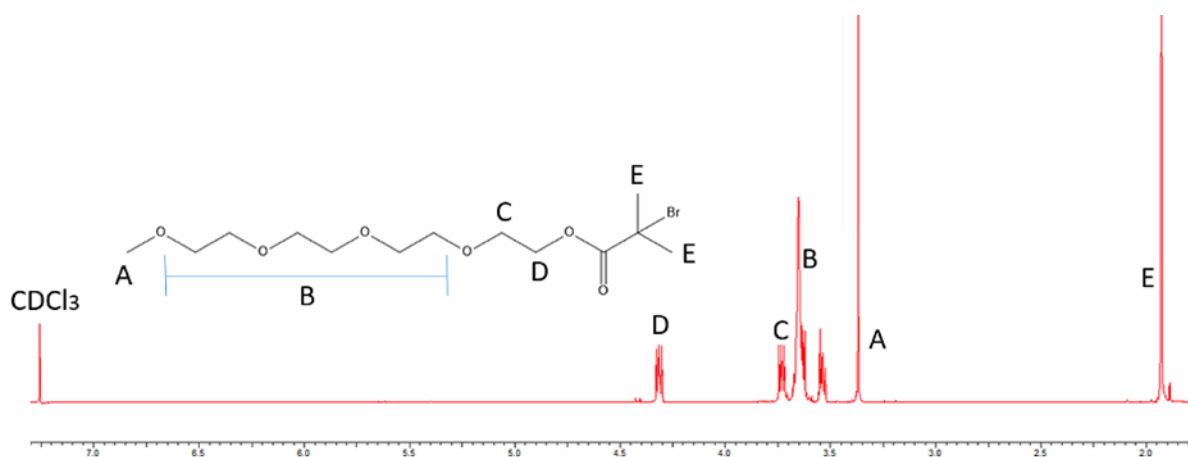


Figure 198 ¹H NMR of PEO initiators made by ATRP.

The ¹H NMR clearly shows the clear and distinct peaks of the macroinitiator. The degree of polymerisation was discussed before in an earlier chapter and was calculated from NMR through comparison of the integrals of the terminal CH₃O group (peak A, Figure 198) and the CH₃ groups (peak E, Figure 198).

5.3.2 Low degree of polymerisation PEO-*b*-PBMA Block copolymers

After the three PEO initiators were made, they were reacted with butyl methacrylate to make the block copolymers by ATRP. After the polymerisation with butyl methacrylate, the structures were confirmed by NMR (Figure 199) and this time the molecular weight of each polymer was larger enough to be observed between the calibration range of the SEC. (Figure 200). The molecular weight parameters are given in Table 45. Three polymers were made to give the University of Manchester and Eindhoven more samples to test and model.

Table 45 Molecular weight parameters recorded by GPC and NMR.

Structure	DP _{PEO}	DP _{PBMA}	M _n NMR	M _n SEC	M _w / M _n
PEO ₃ - <i>b</i> -PBMA ₁₀	3	10	1700	1900	1.60
PEO ₁₂ - <i>b</i> -PBMA ₁₀	12	10	2100	2300	1.50
PEO ₁₆ - <i>b</i> -PBMA ₁₀	16	10	2800	2600	1.63

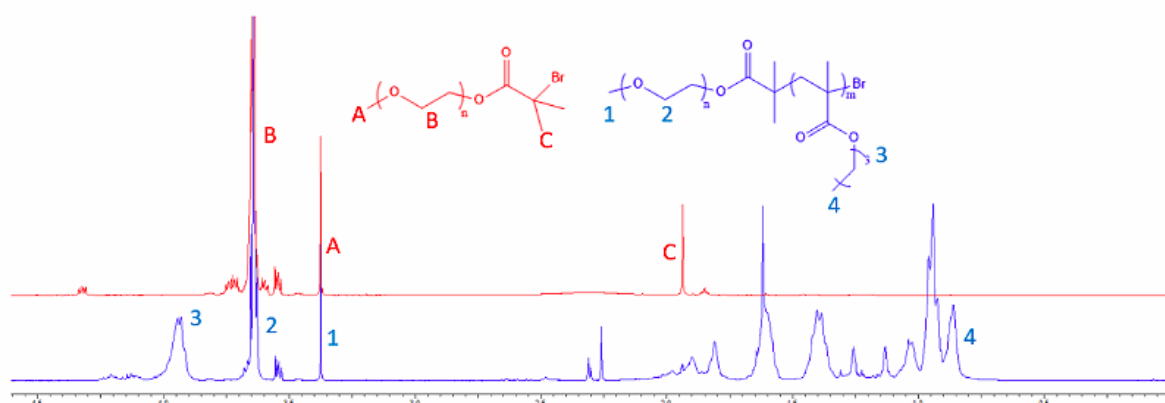


Figure 199 ¹H-NMR of PEO-*b*-PBMA overlaid with PEO initiator showing the polymerisation occurred.

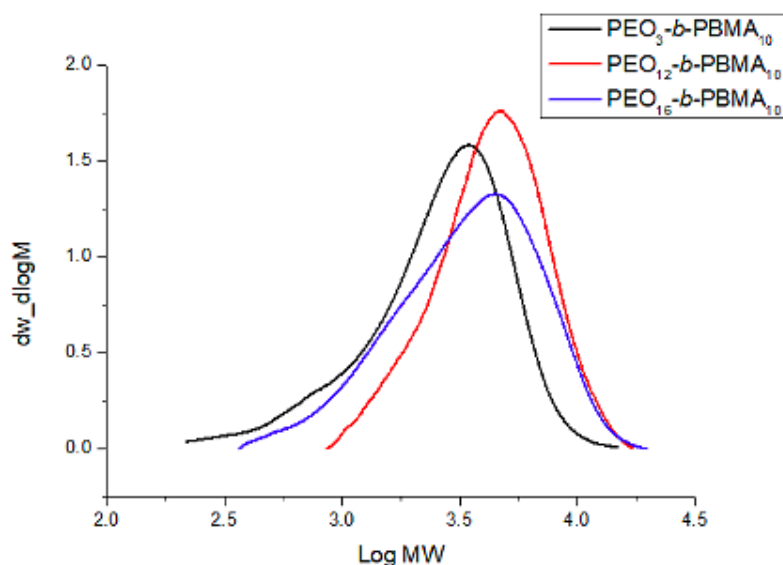


Figure 200 GPC results of the three block copolymers made by ATRP.

5.3.3 Self-assembly of PEO-*b*-PBMA (Eindhoven University of Technology collaboration)

The three samples of PEO-*b*-PBMA were sent to Holland to be self-assembled by a PhD Student called Paula Vena part of the Sommerdijk group. The samples were self-assembled and Cryo-TEM were performed. The main purpose for synthesising and self-assembling these compounds was to support a chemistry model proposed by the University of Manchester which the Sommerdijk group was collaborating with. If the experiments matched the model, then the model could be used for a range of different compositions of PEO-*b*-PBMA with a degree of certainty associated with the model's predictions. The PEO-*b*-PBMA was also needed to be self-assembled in the region which is blank to complete the phase diagram.

The model seemed to have some difficulty predicting the aggregate structures for low THF to high water percentages. This is shown in Figure 201, where the top half of the triangle is left incomplete. The aim of the self-assembly in Holland was to finish off this phase triangle as well as confirm the predictions made by the model

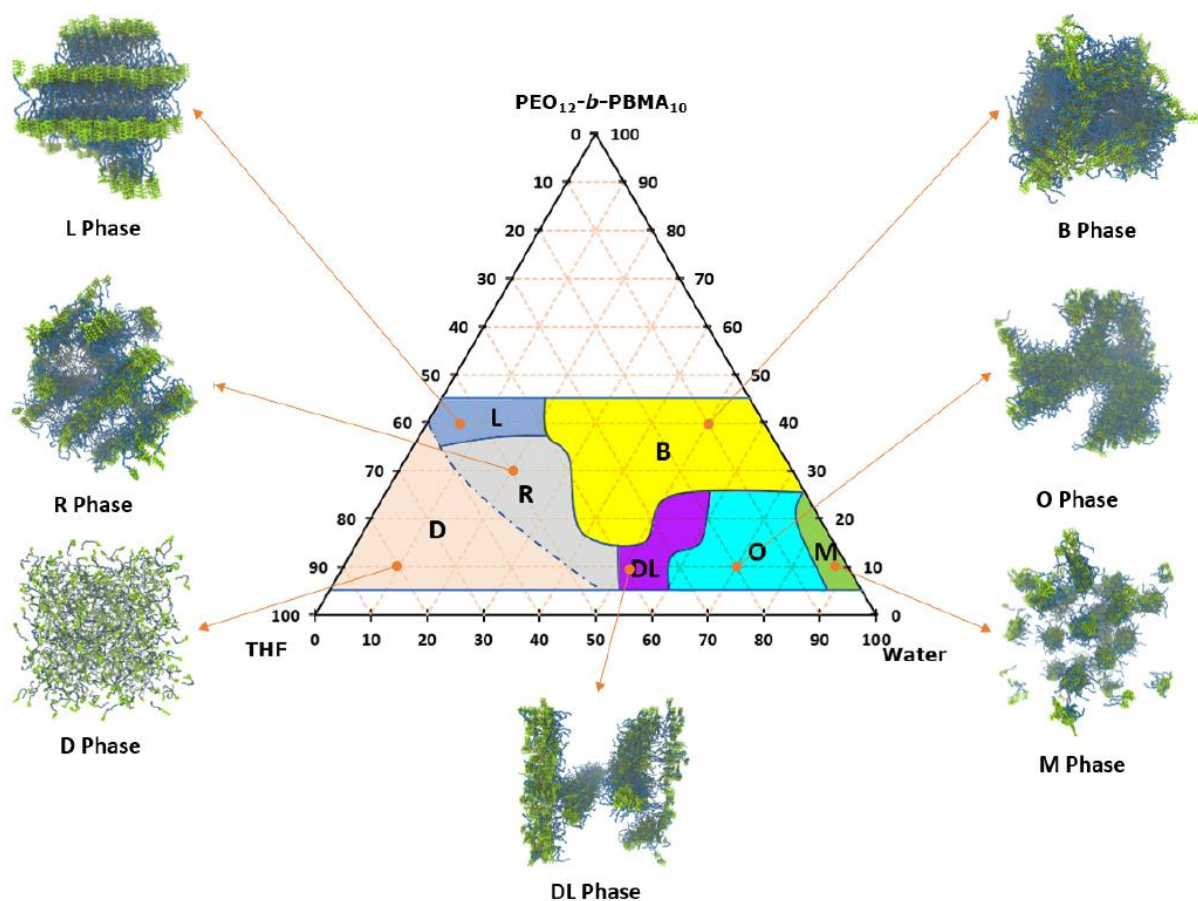


Figure 201 Phase diagram for PEO₁₂-*b*-PBMA₁₀ predicted by MD model

10 wt% of PEO₁₂-*b*-PBMA₁₀ was added to water ascertain the block copolymers solubility. The polymer remained undissolved. The solution with 10wt% of PEO₁₂-*b*-PBMA₁₀ was then heated to 80°C to encourage the polymer to dissolve with no effect. A co-solvent approach to self-assembly was then adopted.

Self-assembly via cosolvent method

10 wt% solutions of the polymers (Table 46) were prepared in THF and aliquots were diluted with THF according to table 2. Milli Q water was added dropwise with a syringe pump (rate 1 mL/h) to each sample until reaching a final volume of 1 mL. The solvent switch was carried on under vigorous stirring at 35°C in an oil bath.

Table 46 Quantities used for the self-assembly of block copolymers at 1% in Holland.

THF:H ₂ O	50:50	40:60	30:70	20:80	10:90
Final Polymer	1%	1%	1%	1%	1%
Vol 10% wt	0.1mL	0.1 mL	0.1 mL	0.1 mL	0.1 mL
Vol THF	0.4 mL	0.2 mL	0.2 mL	0.1 mL	0.0 mL
Vol H₂O	0.5 mL	0.6 mL	0.7 mL	0.8 mL	0.9 mL

Cloudy self-assembled samples suggest bigger structures on the micron scale whereas clear solutions suggest structures on the nano scale. Each sample made is shown in Figure 202.



Figure 202 Polymer dispersions in THF: Water (Left)- PEO₁₆-b-PBMA₁₀ and (Right)- PEO₁₂-b-PBMA₁₀

The samples of H₂O:THF 80:20 & 90:10 for PEO₁₆-b-PBMA₁₀ were identified as cloudy and for PEO₁₂-b-PBMA₁₀ 60:40, 70:30, 80:20 and 90:10 all gave cloudy solutions. This seemed to give a slight trend that self-assembling at 90:10 and 80:10 solutions is likely to give submicron structures whereas when there is more THF used at the start, the solutions are more likely to be nanoscale.

Cryo-TEM characterization

The samples were prepared on 200 mesh Cu TEM grids containing a R2/2 Quantifoil carbon support film (Quantifoil Micro Tools GmbH, Jena, Germany). The carbon support film was hydrophilized by surface plasma treatment in a Cressington 208 carbon coater directly prior to use.

3 μ L of the block copolymer dispersion in THF:H₂O was applied to the TEM grid, blotted and vitrified in an automated vitrification robot (FEI Vitrobot™ Mark III) by plunging into liquid ethane. This was performed with the environmental chamber of the Vitrobot at 35°C under a THF and water atmosphere.

10% PEO₁₂-b-PBMA₁₀ in THF:H₂O 10:90

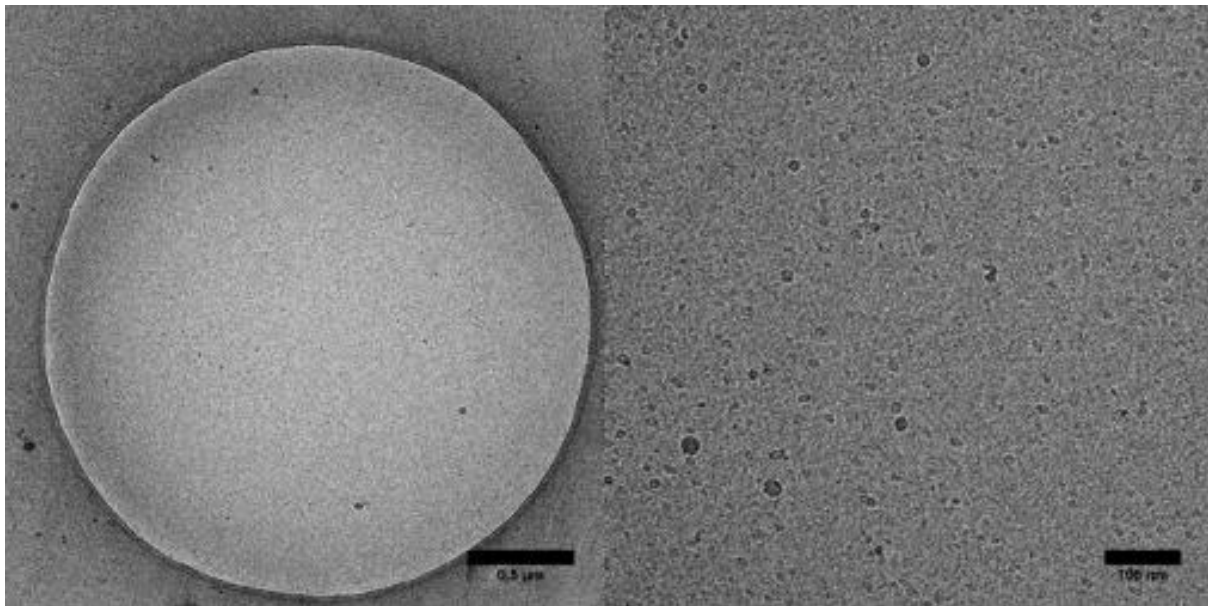


Figure 203 Cryo-TEM image of PEO₁₂-b-PBMA₁₀ in THF:H₂O 10:90

10% PEO₁₂-b-PBMA₁₀ in THF:H₂O 20:80

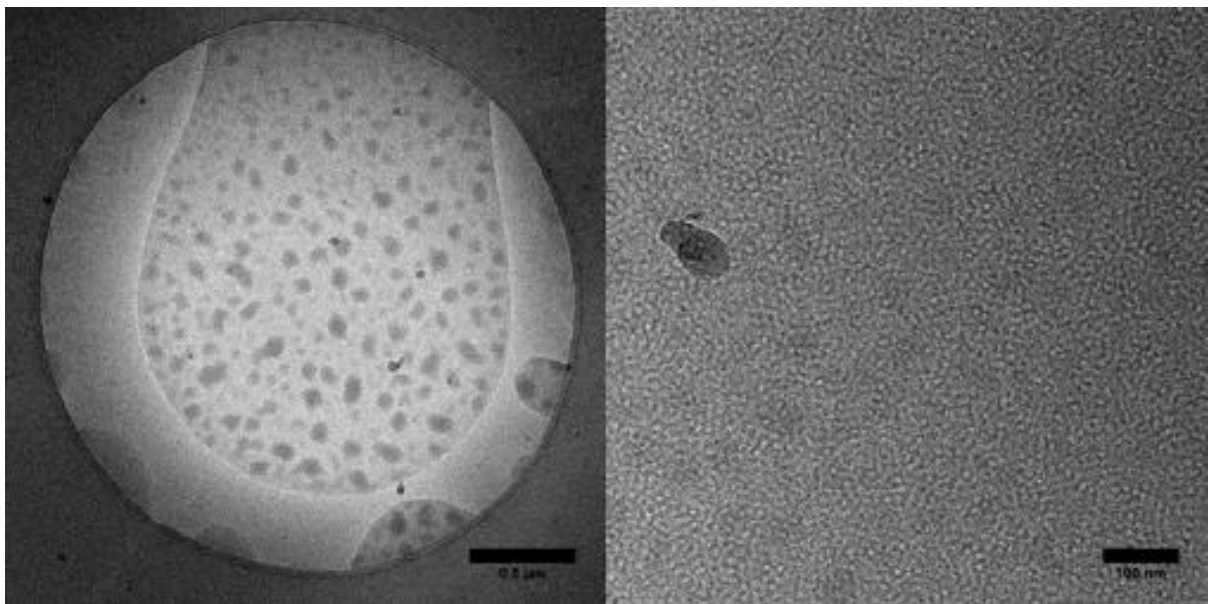


Figure 204 Cryo-TEM image of PEO₁₂-b-PBMA₁₀ in THF:H₂O 20:80

10% PEO₁₂-b-PBMA₁₀ in THF:H₂O 30:70

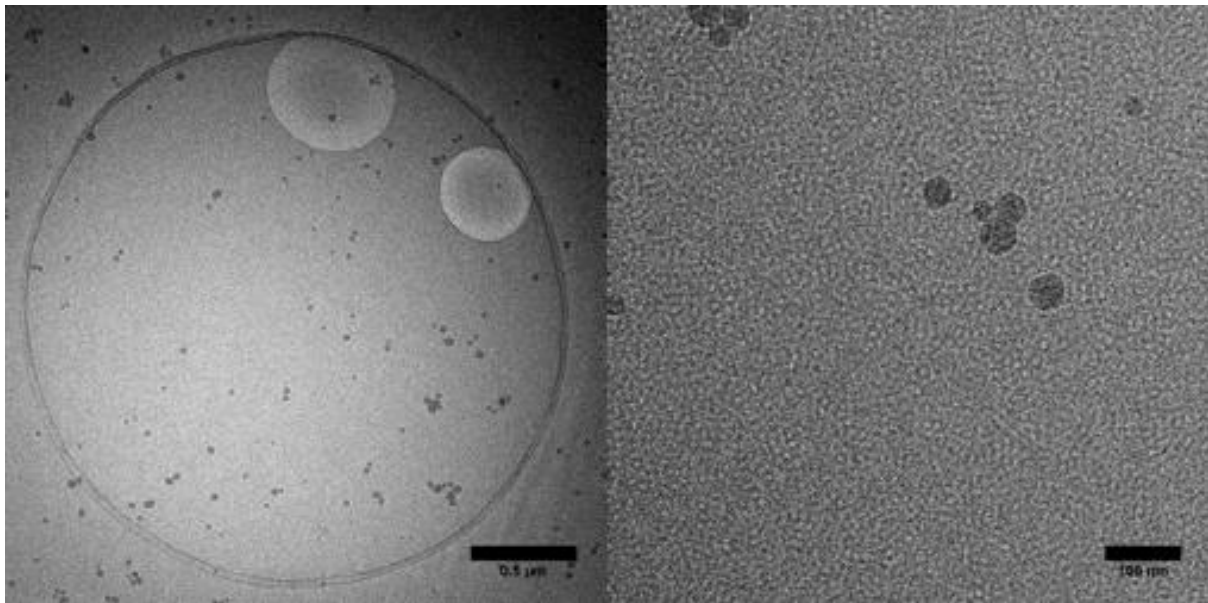


Figure 205 Cryo-TEM image of PEO₁₂-b-PBMA₁₀ in THF:H₂O 30:70

10% PEO₁₂-b-PBMA₁₀ in THF:H₂O 40:60

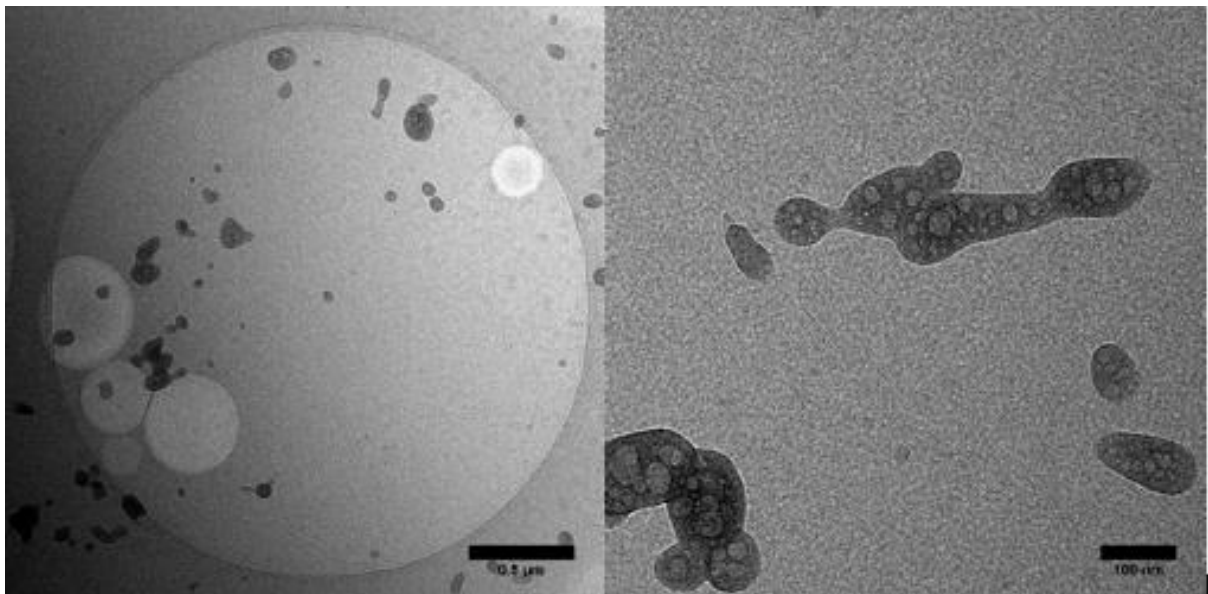


Figure 206 Cryo-TEM image of PEO₁₂-b-PBMA₁₀ in THF:H₂O 40:60

10% PEO₁₂-b-PBMA₁₀ in THF:H₂O 50:50

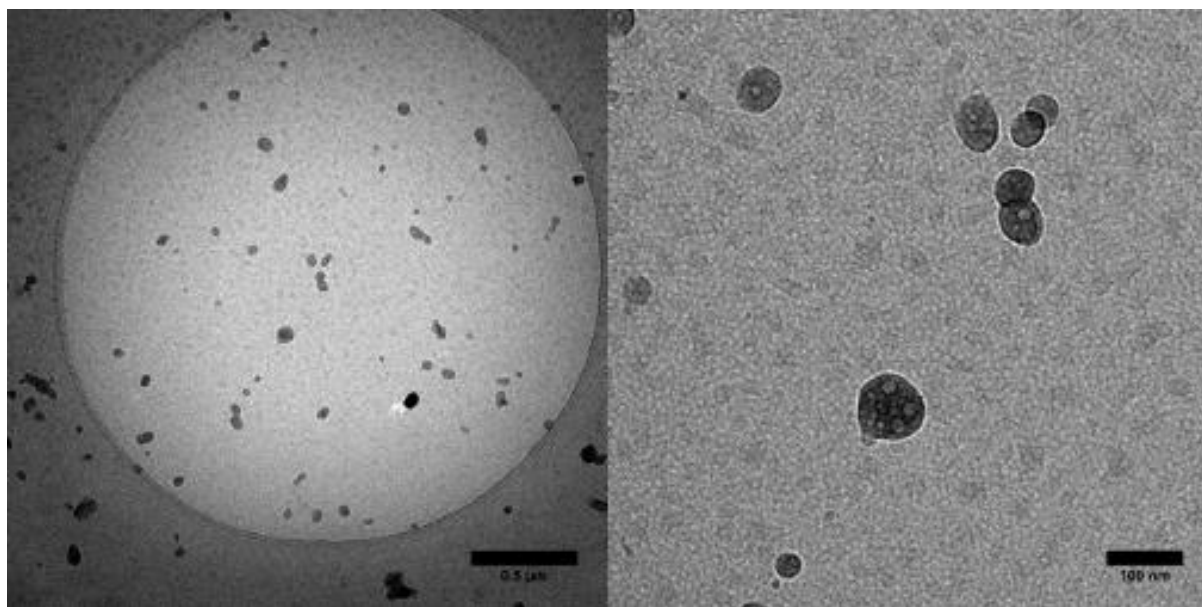


Figure 207 Cryo-TEM image of PEO₁₂-b-PBMA₁₀ in THF:H₂O 50:50

The Cryo-TEM images from the self-assembly of PEO₁₂-b-PBMA₁₀ suggest that in all cases that micelles are present. The self-assembly at 90:10 H₂O: THF seem to give tiny spherical micelles which are very small. However, when you add more THF (80:20), bigger micelles are seen which are around 100nm. Figure 205 also suggests micelles at 70:30 which are similar size to the ones seen using 80:20 H₂O: THF. The most interesting case is Figure 206 where micelles present are not simple micelles. They are much larger and seem to have internal structure associated with them. Figure 207 is also similar to Figure 206 where the micelles present are not simple. This suggests that as the amount of THF is increased, bigger structures are seen under cryo-TEM and more complex micellar structures are being seen.

10% PEO₁₆-b-PBMA₁₀ in THF:H₂O 10:90

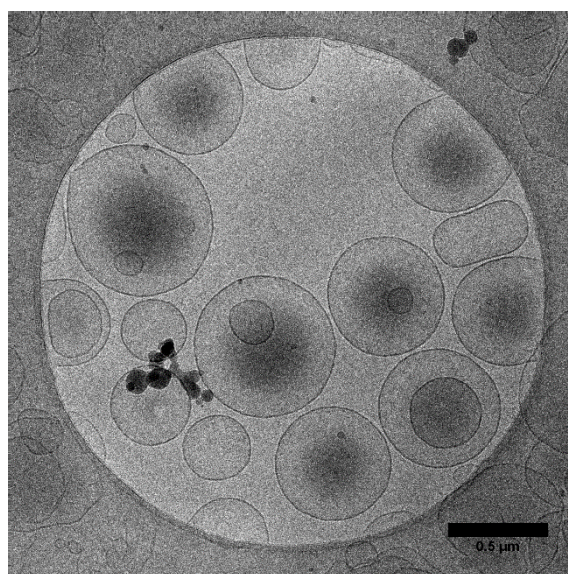


Figure 208 Cryo-TEM image of PEO₁₆-b-PBMA₁₀ in THF:H₂O 10:90

10% PEO₁₆-b-PBMA₁₀ in THF:H₂O 20:80

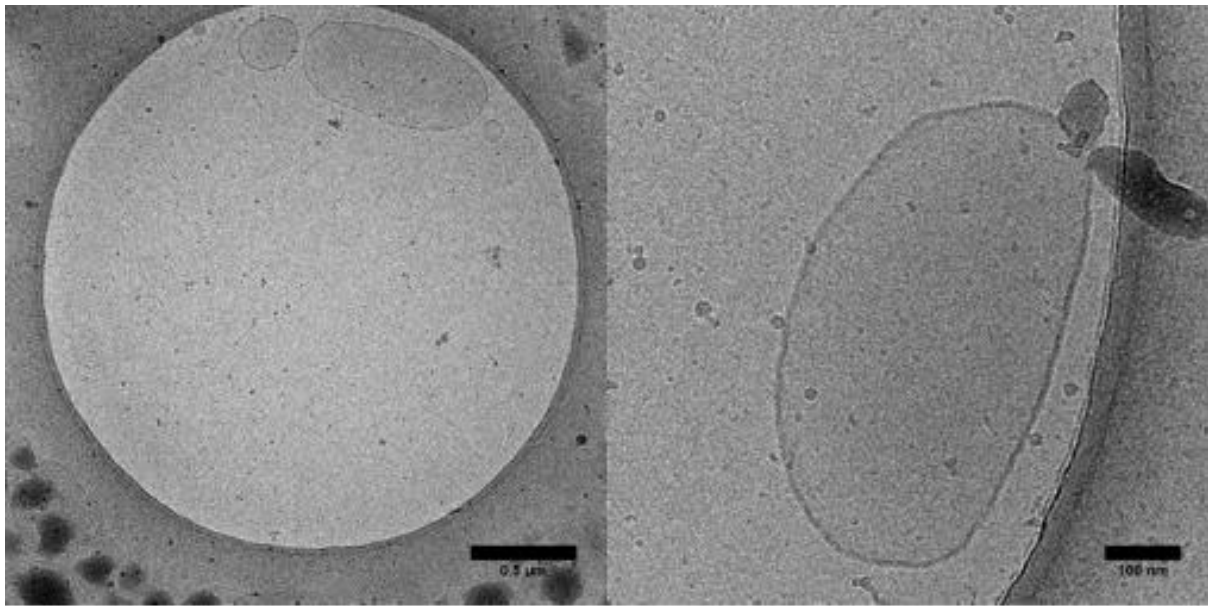


Figure 209 Cryo-TEM image of PEO₁₆-b-PBMA₁₀ in THF:H₂O 20:80

10% PEO₁₆-b-PBMA₁₀ in THF:H₂O 30:70

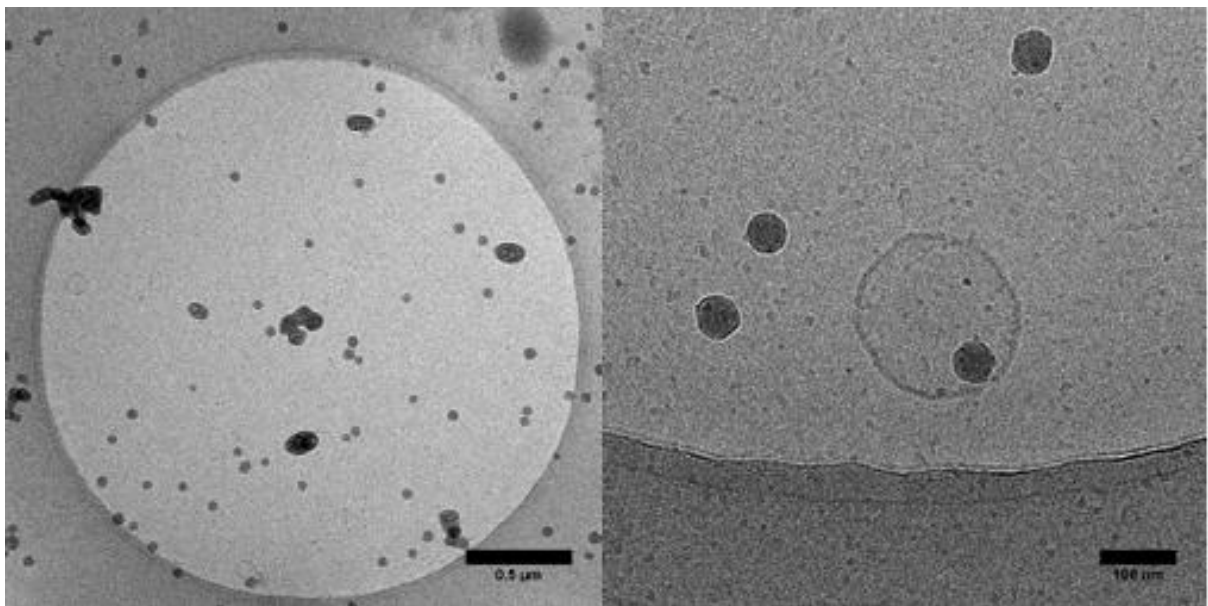


Figure 210 Cryo-TEM image of PEO₁₆-b-PBMA₁₀ in THF:H₂O 30:70

10% PEO₁₆-b-PBMA₁₀ in THF:H₂O 40:60

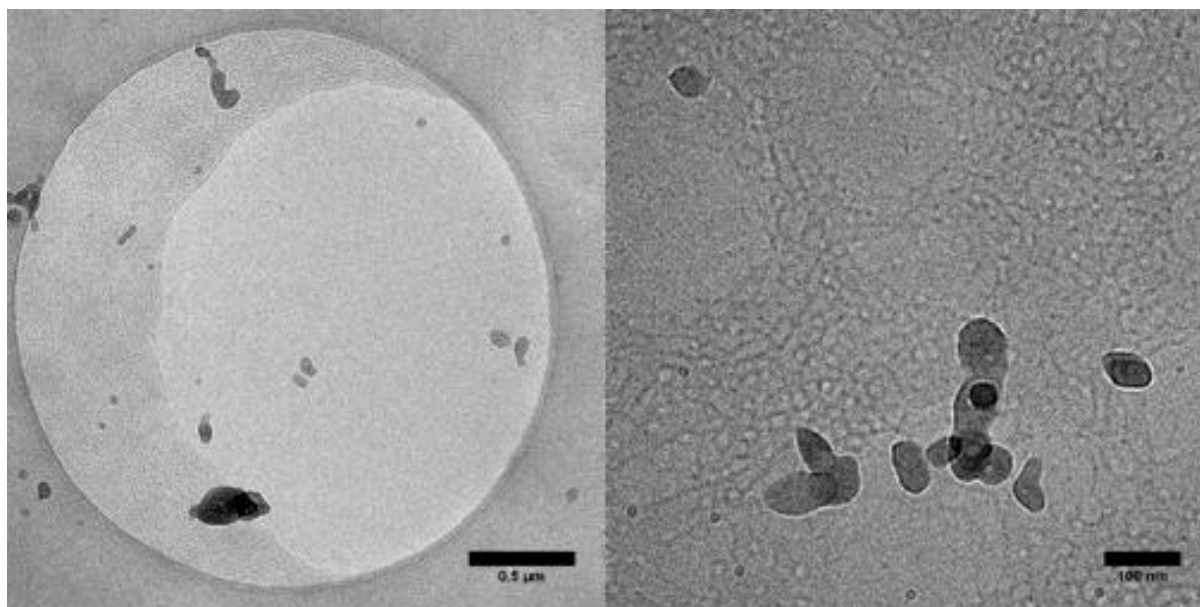


Figure 211 Cryo-TEM image of PEO₁₆-b-PBMA₁₀ in THF:H₂O 40:60

10% PEO₁₆-b-PBMA₁₀ in THF:H₂O 50:50

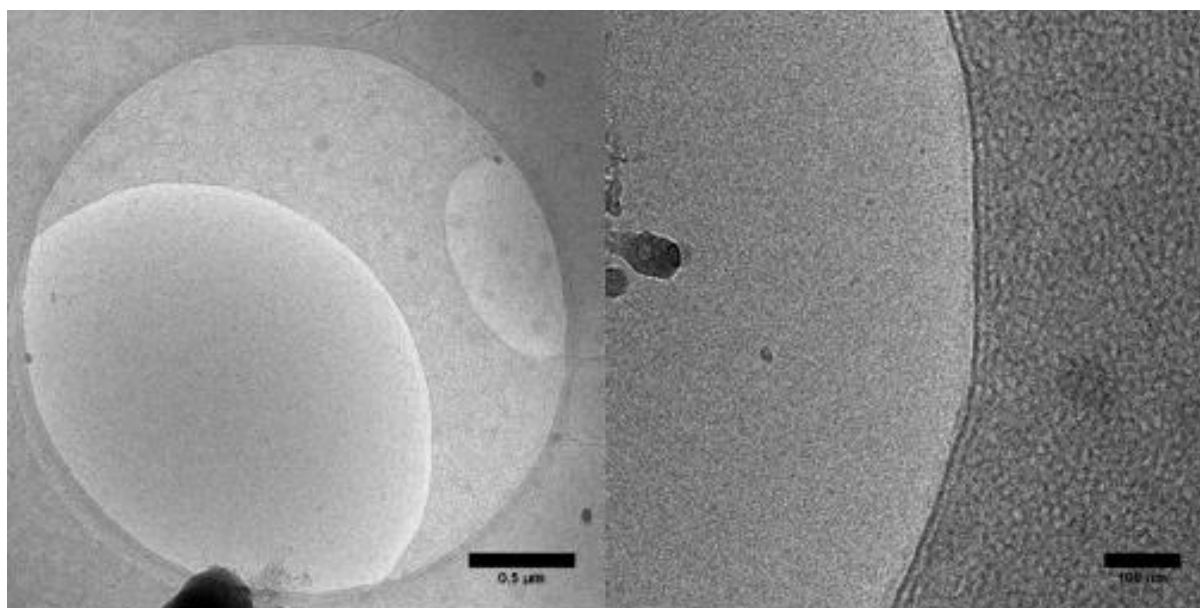


Figure 76 Cryo-TEM image of PEO₁₆-b-PBMA₁₀ in THF:H₂O 50:50

The Cryo-TEM images from the self-assembly of PEO₁₆-b-PBMA₁₀ suggest that micelles and vesicles are present which is different to what was seen with PEO₁₂-b-PBMA₁₀. Figure 208 shows lots of vesicles with some micelles. Figure 209 shows much fewer vesicles with tiny spherical micelles. Figure 210 shows much larger micelles and these are starting not to be simple but rather more complex with some evidence of an internal structure. Figures 211 and 212 show much more complex micellar structures which is similar to what was seen with PEO₁₂-b-PBMA₁₀. A similar trend can be seen which is that the size of the micelles increase as more THF is used. The aggregate structures also seem to become much more complex as the amount of THF is increased.

5.3.4 Triblock synthesis

As it was proven that low degree of polymerisation of PEO initiators could be made from the beginning of this chapter with the work involving the University of Eindhoven, it led allowed for a second project which involved a triblock copolymer. Further testing was carried out with a triblock polymer which was to be self-assembled to see if bicontinuous nanospheres would form. The reason for this is that the nipam block has a LCST of 32°C which would allow drugs to be encapsulated and released at temperatures above and below this temperature.

From earlier chapters and previous work, block copolymers of PEO-*b*-PODMA forms bicontinuous aggregates depending on the molecular weight and PEO weight fraction. Another hydrophilic polymer heavily studied is PNIPAM and many block copolymers have been made from this polymer. This chapter assesses if a triblock of PEO-*b*-PNIPAM-*b*-PODMA can be made and self-assembled to form bicontinuous aggregates. For this to be successful, the degree of polymerisation of the PEO and NIPAM would have to be low.

Phase 1 testing

The PEO₄₄-Br initiator which was synthesised and characterised in Chapter 2, was used as a macroinitiator in the ATRP of NIPAM in this chapter. A sample of PEO₄₄-Br was taken and reacted with NIPAM in a Schlenk tube under nitrogen. ATRP was performed and a second block of NIPAM was added to the macroinitiator.

A DP for the PNIPAM of 16 was targeted. The reason why a small amount of NIPAM was targeted as due to the overall molecular weight of the block copolymer. For bicontinuous nanospheres to form the molecular weight should be below 25,000 KDa. The ATRP reaction was performed and PEO₄₄-*b*-PNIPAM₁₆-Cl looked to be made as a white solid.

PMDETA was used initially used in the ATRP but no polymerisation occurred. Me₆TREN was used instead and this allowed the NIPAM to be added as a second block. The use of Me₆TREN as a ligand was important for this reaction to proceed and the involvement of this ligand is backed by literature.¹²

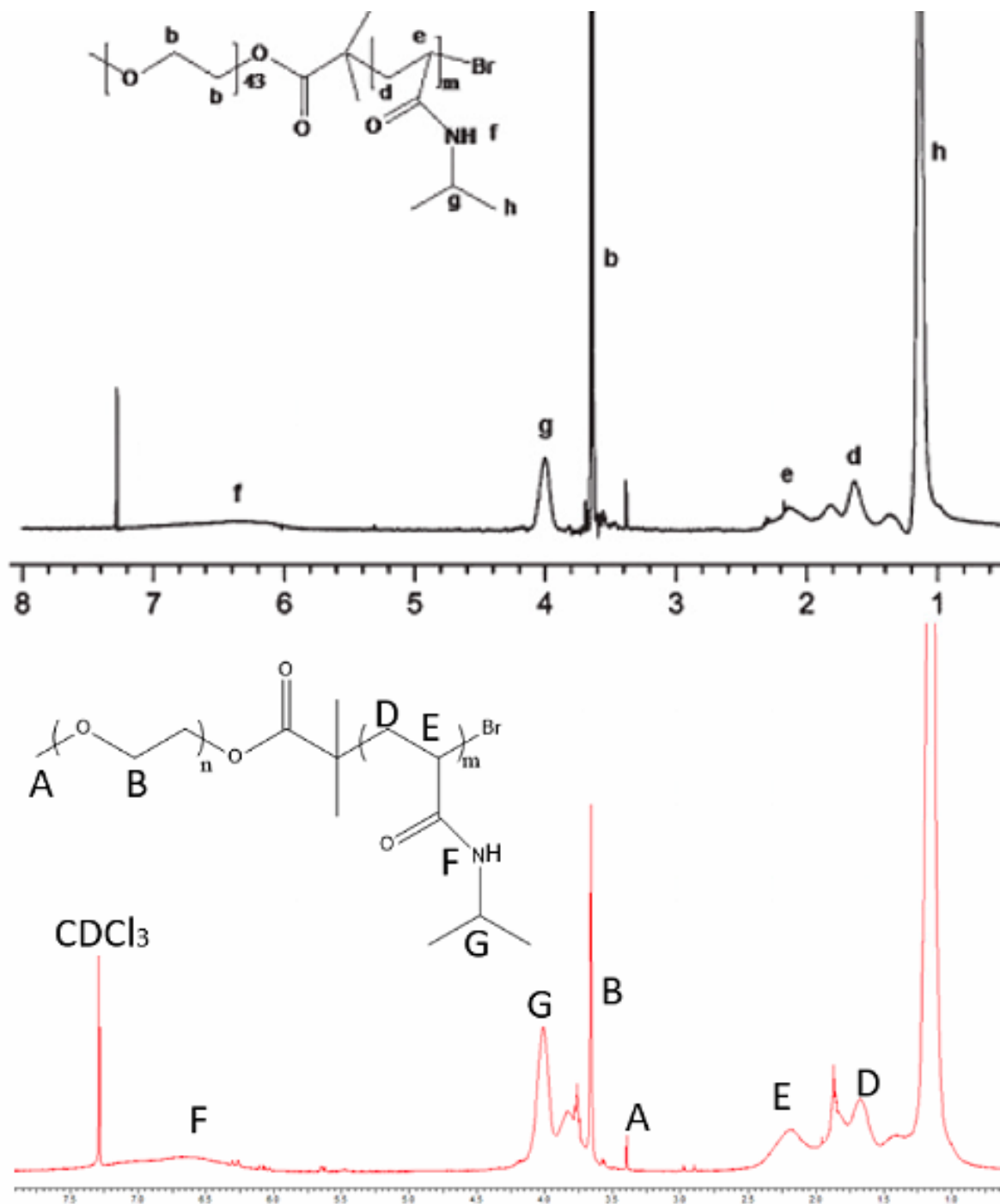


Figure 213 ^1H NMR of PEO-b-PNIPAM-Cl initiator overlaid with NMR spectra from literature¹² to demonstrate that the ATRP reaction had worked.

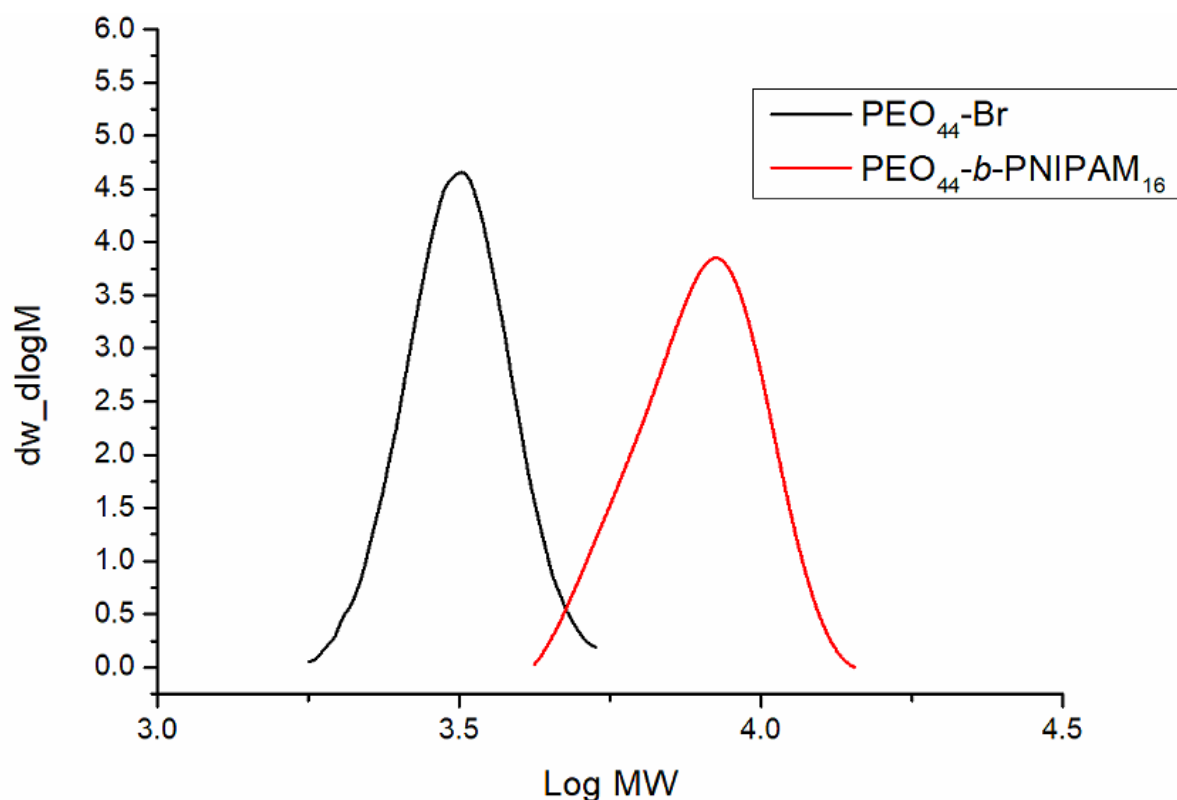


Figure 214 SEC traces of starting material and product showing that the molecular weight has increased.

Table 47 SEC and NMR data for PEO initiator and PEO-*b*-PNIPAM block copolymer.

Structure	M _n NMR	M _n GPC	M _w / M _n
PEO ₄₄ -Br	2200	3100	1.03
PEO ₄₄ - <i>b</i> -PNIPAM ₁₆ -Cl	4000	7700	1.05

The SEC and NMR results show that nipam can be added to a PEO initiator so the same method was repeated for the PEO₁₂-Cl and PEO₁₆-Cl.

Low DP PEO initiators

Table 48 NMR and SEC data for low DP PEO initiators.

Structure	DP _{PEO}	M _n NMR	M _n GPC	M _w / M _n
PEO ₁₂ -Cl	12	600	1200	1.07
PEO ₁₆ -Cl	16	800	1300	1.06

SEC suggested values twice those calculated from H-NMR. This could be due to the fact that the values were recorded outside the SEC calibration range. The H-NMR spectra of PEO₁₂-Cl, PEO₁₂-Cl, PEO₄₄-Cl were identical for all macroinitiators used for this project with the only difference being a different integral for the DP of PEO.

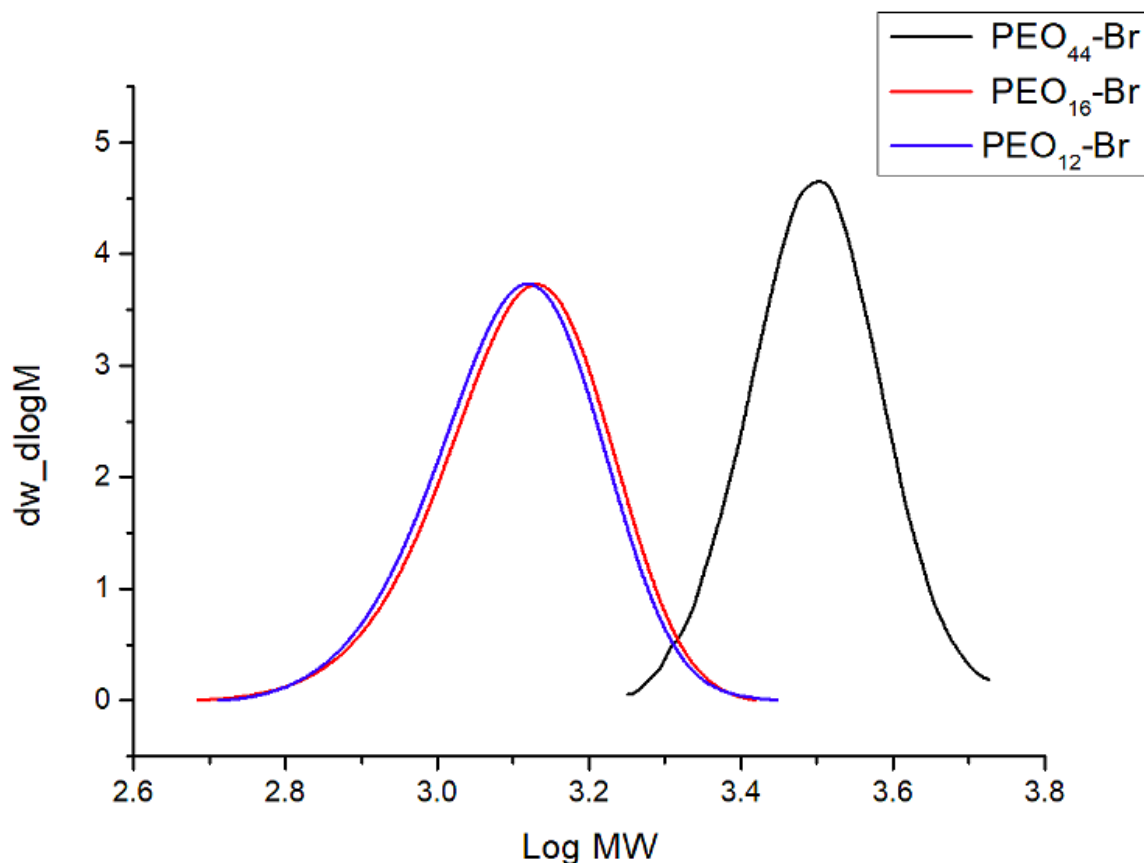


Figure 215 GPC traces of PEO initiators overlaid.

Low DP Block copolymers of PEO-b-PNIPAM-Cl

After large amounts of PEO₁₂-Br and PEO₁₆-Br were made the next ATRP reaction was to add nipam as a second block. A series of ATRP reactions were carried out using the two initiators with nipam. A DP of 16 was targeted in all situations for the nipam block. All reactions were stopped once the integrals peaks of the PNIPAM stopped changing in ¹HNMR.

At first only two ATRP reactions were carried out where it appeared from the H-NMR that only 50% of the nipam had reacted. When the integrals of the proton signals stopped changing, the reactions were taken off and worked up. The DP of the nipam block was calculated to be 8 chains. This led to two additional reactions which were put on with double the quantity of nipam needed for a DP 16. In these situations, again only 50% nipam polymerised but it allowed block copolymers to be made containing a nipam block with DP of 16.

Table 49 NMR and GPC data recorded for the PEO initiators and PEO-PNIPAM block copolymers.

Structure	DP _{PEO}	DP _{PNIPAM}	M _n NMR	M _n SEC	M _w / M _n
PEO ₁₂ -Cl	12	-	600	1200	1.07
PEO ₁₂ - <i>b</i> -PNIPAM ₈	12	8	1500	2200	1.44
PEO ₁₂ - <i>b</i> -PNIPAM ₁₆	12	16	2600	3300	1.59
PEO ₁₆ -Cl	16	-	800	1300	1.06
PEO ₁₆ - <i>b</i> -PNIPAM ₈	16	8	1600	2100	1.30
PEO ₁₆ - <i>b</i> -PNIPAM ₁₆	16	16	2600	2800	1.20

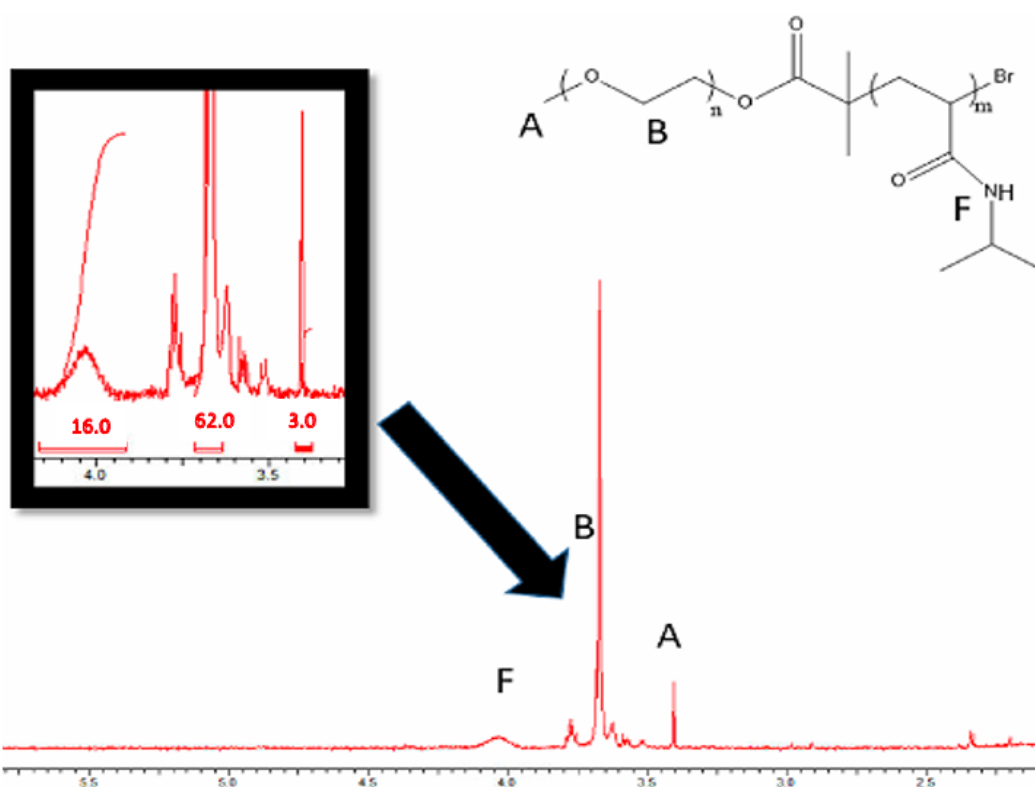


Figure 216 ¹H NMR of PEO₁₆-*b*-PNIPAM₁₆-Cl clearly showing which peaks were used to calculate the DP of the two blocks.

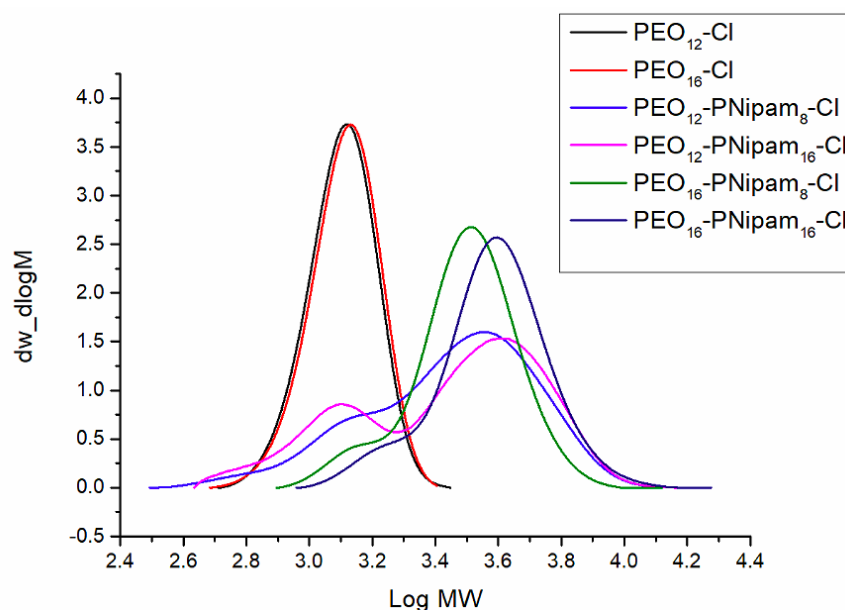


Figure 217 GPC traces of all PEO-PNIPAM-Cl block copolymers made by ATRP.

After just one work up there seemed to be a lot of starting material left over in each PEO-*b*-PNIPAM block copolymer. This suggests that a lot of nipam has not polymerised and been added to the PEO macroinitiator. The block copolymers that contained a PNIPAM block of DP 16 were selected and purified further. The main reason for this was that the yields for some of the ATRP reactions were very low and it was the polymers of PEO₁₆-*b*-PNIPAM₁₆ and PEO₁₂-*b*-PNIPAM₁₆ which were present in the highest amount.

It is also important to note that PEO₄₄-*b*-NIPAM₁₆-Cl produced a polymer which was white in colour. Every polymer sample made with short degree of polymerisations, produced samples that were green. This suggested that copper was still present and had not been completely removed from the alumina column.

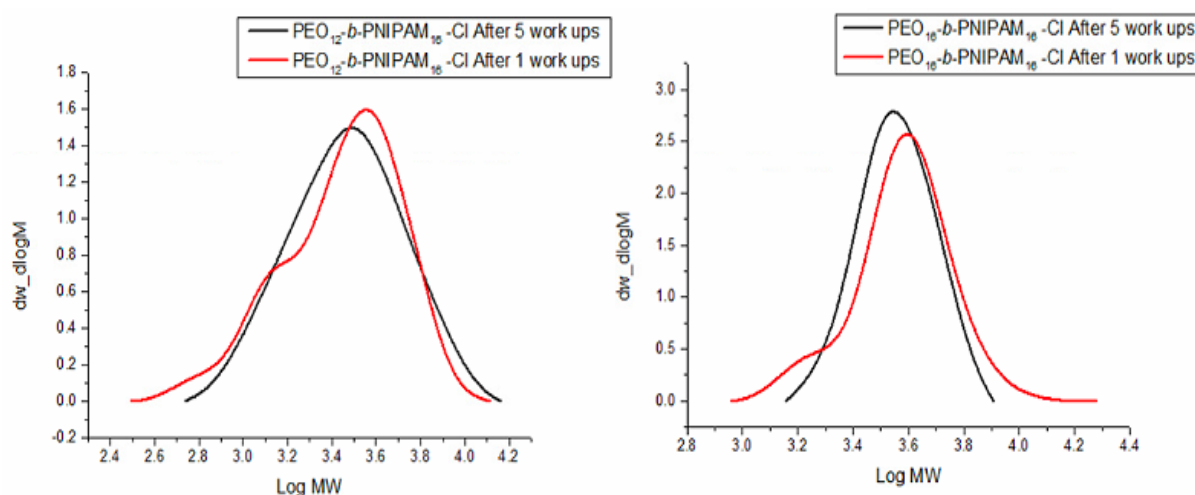


Figure 218 SEC traces of the first work up overlaid with the 5th workup to demonstrate that the second curve had been removed.

After precipitating 5 times in cold diethyl ether from THF, a green solid was collected which showed one peak on the SEC trace. The polydispersity also narrowed suggested that starting material had been successfully removed.

Different reaction solvents

The standard method to make PEO-*b*-PNIPAM-Cl used a mixture of butanone:IPA 1:1. This led to percentage yield of 16% with a NMR conversion of 60.4%. Different reaction solvents were tried to see if this improved the NMR conversion and whether more of the desired product could be collected.

Table 50 Different reaction solvents used for the ATRP reaction of PEO-*b*-PNIPAM-Cl.

Reaction Solvent	NMR Conversion (%) (PNIPAM)	Percentage Yield (%)
Butanone:IPA 1:1	60.4	16.0
DMF	58.7	15.4
DMF:IPA (9:1)	58.3	15.7
H ₂ O	50.2	14.6

The reaction solvents involving DMF & water came from other literature methods. It appeared that in all situations that the NMR conversion and percentage yields were very similar and still low.

Low DP Block copolymers of PEO-*b*-PNIPAM-*b*-PODMA

The main issue from the synthesis of PEO-*b*-NIPAM-Cl was that the product was green. This suggested that copper was still very much in the product despite being run a numerous of times down an alumina column. At this point samples of PEO₁₂-*b*-PNIPAM₁₆ and PEO₁₆-*b*-PNIPAM₁₆ were taken and reacted in an ATRP reaction with ODMA where a DP of 50 was targeted for the ODMA block.

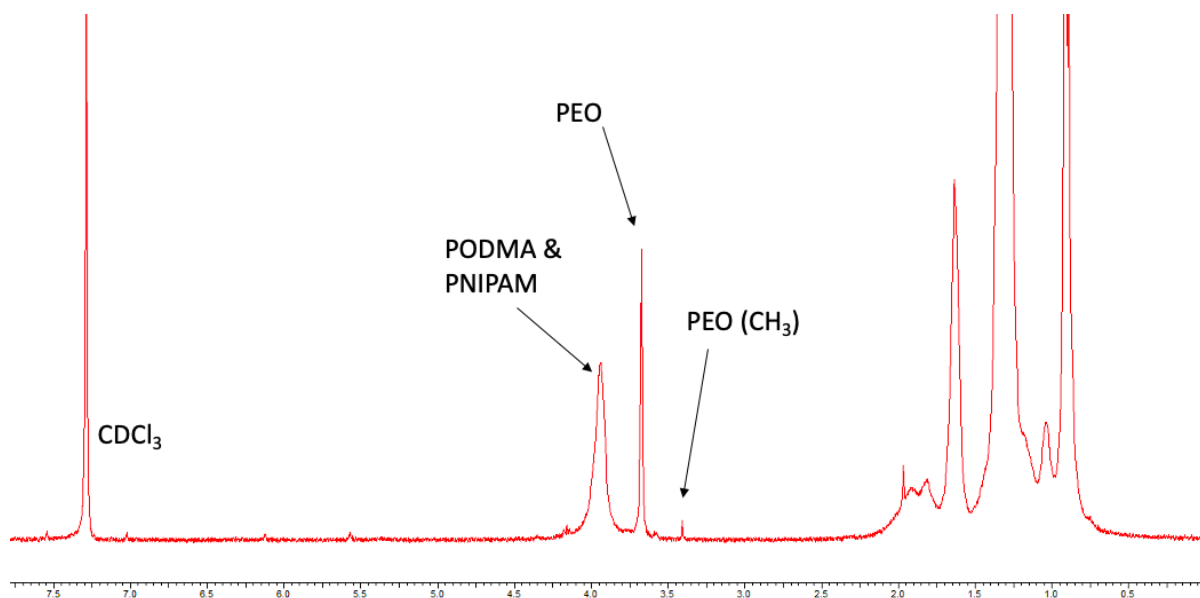


Figure 219 ¹H NMR of PEO-*b*-PNIPAM-*b*-PODMA

The slight issue that arose when studying the ¹H NMR of PEO-*b*-PNIPAM-*b*-PODMA was that the PODMA peak overlaid with the PNIPAM. To calculate the DP of the PODMA block the integral of the peak had to be first taken, then the number of PNIPAM chains had to be subtracted and then that value had to be divided by 2.

Table 51 NMR and GPC data for PEO-*b*-PNIPAM-*b*-PODMA

Structure	DP _{PEO}	DP _{PNIPAM}	DP _{PODMA}	M _n NMR	M _n GPC	M _w / M _n
PEO ₁₂ - <i>b</i> -PNIPAM ₁₆ - <i>b</i> -PODMA ₉₇	12	16	97	35,400	56,000	2.03
PEO ₁₆ - <i>b</i> -PNIPAM ₁₆ - <i>b</i> -PODMA ₁₁₄	16	16	114	41,400	58,500	1.44

Despite that a DP of 50 was targeted, in both cases the DP of the PODMA block went much higher (Approximately 50 additional units for both polymers). Due to the inability to completely remove the catalyst from PEO-*b*-PNIPAM-Cl, this initiator is probably not fully initiating causing the DP to vary a lot.

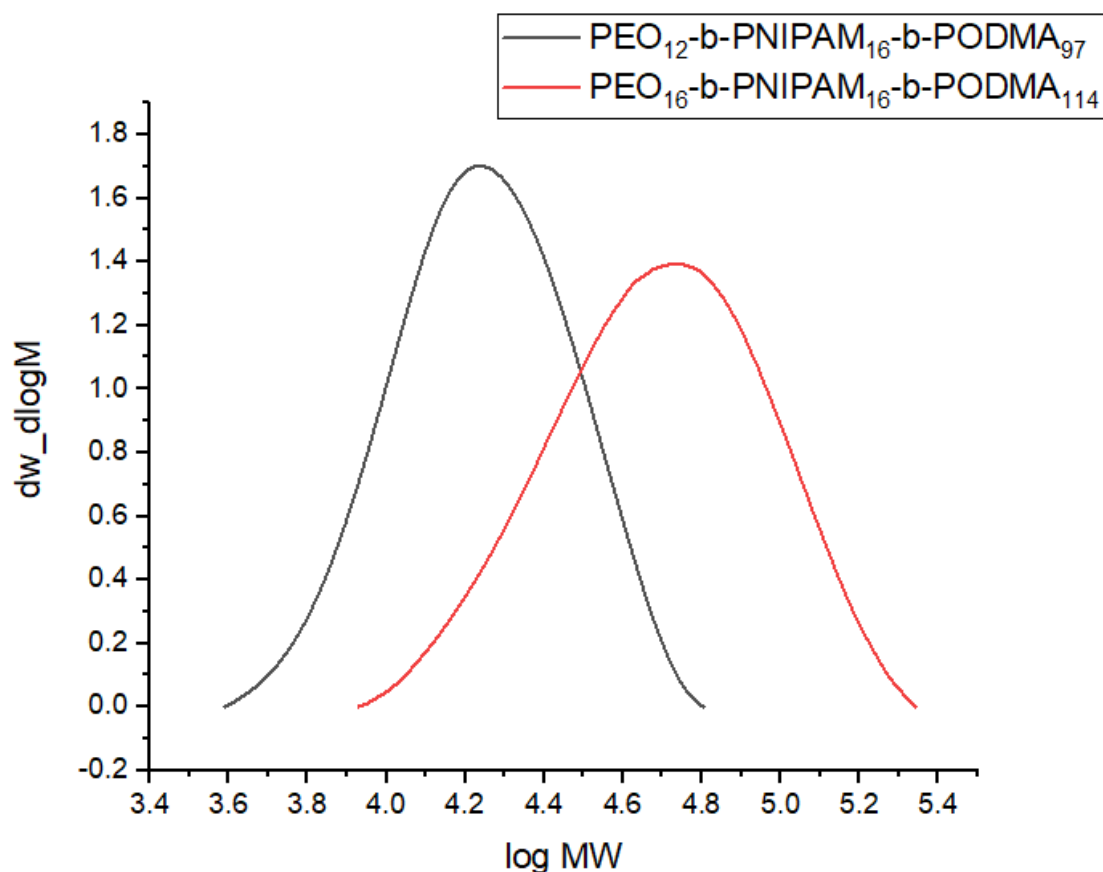


Figure 220 GPC traces of the two triblock polymers made by ATRP.

After the two polymers of PEO-*b*-PNIPAM-*b*-PODMA were made, they were self-assembled at 0.1 and 1.0wt % solutions. TEM and DLS were then carried out on each sample.

PEO₁₂-b-PNIPAM₁₆-b-PODMA₉₇

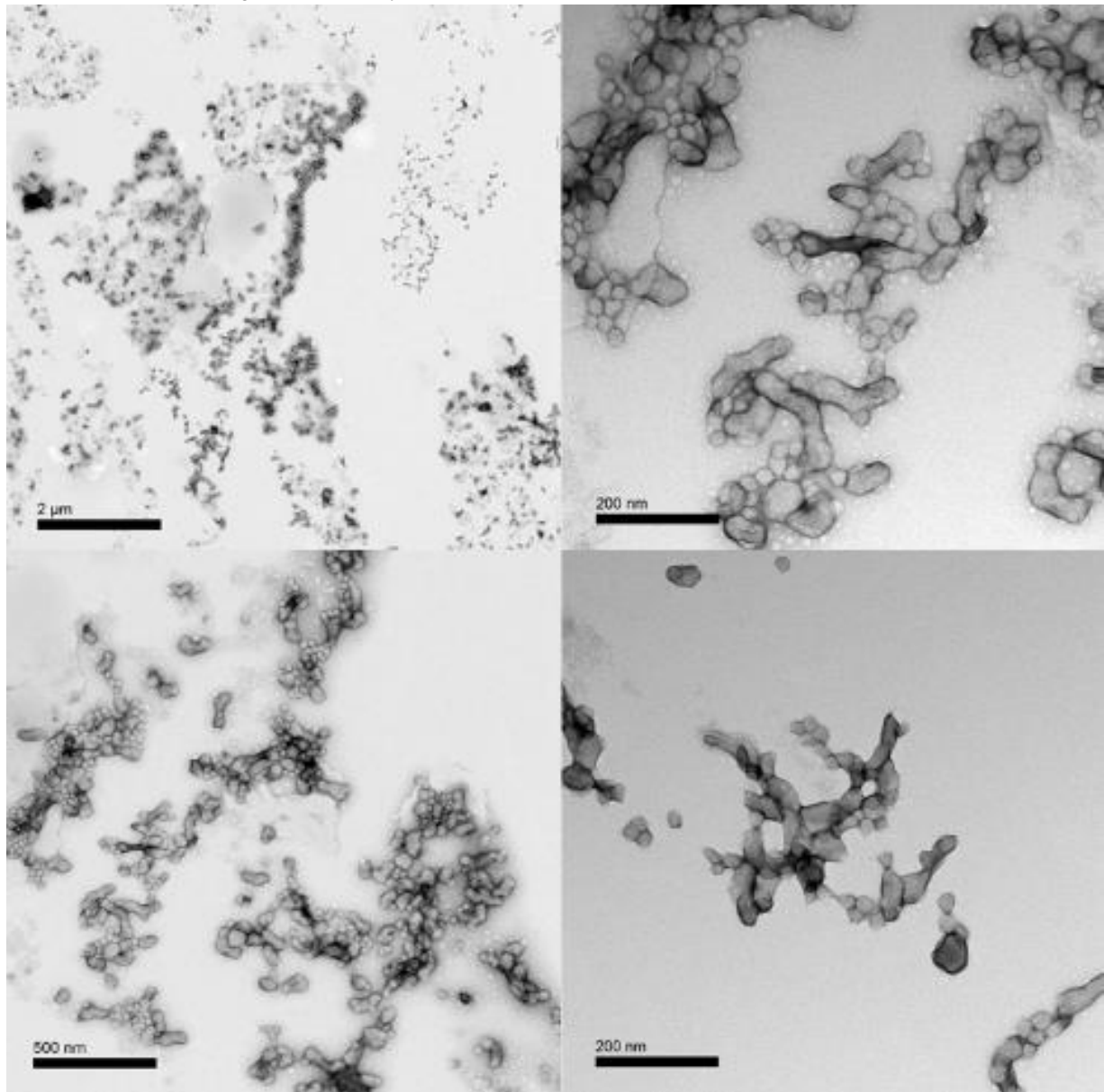


Figure 221 0.1 wt% PEO₁₂-b-PNIPAM₁₆-PODMA₉₇ self-assembled in water. Spherical and cylindrical micelles are present.

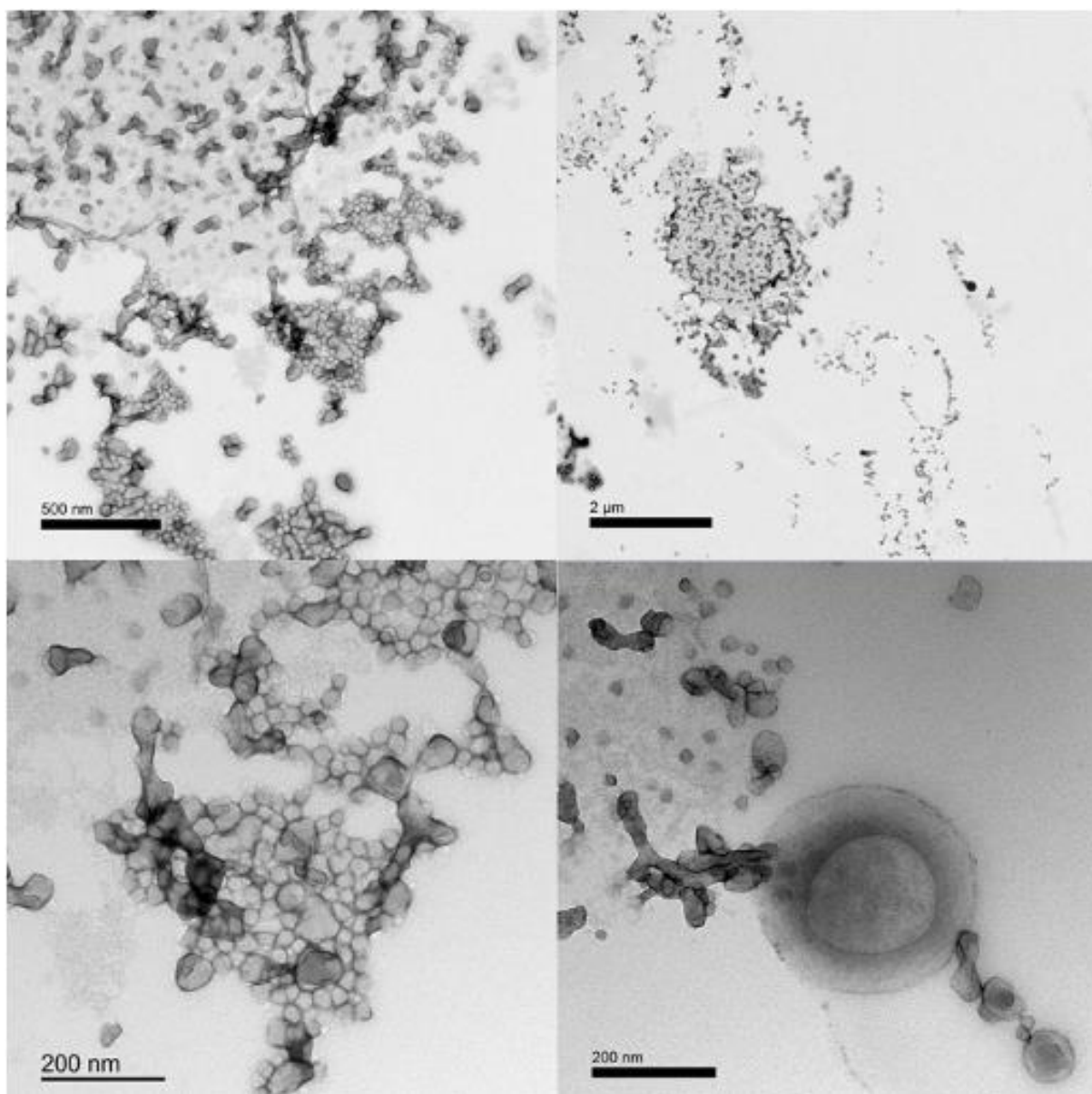


Figure 222 Figure 77 1.0 wt% PEO₁₂-b-PNIPAM₁₆-PODMA₉₇ self-assembled in water. Spherical and cylindrical micelles are present.

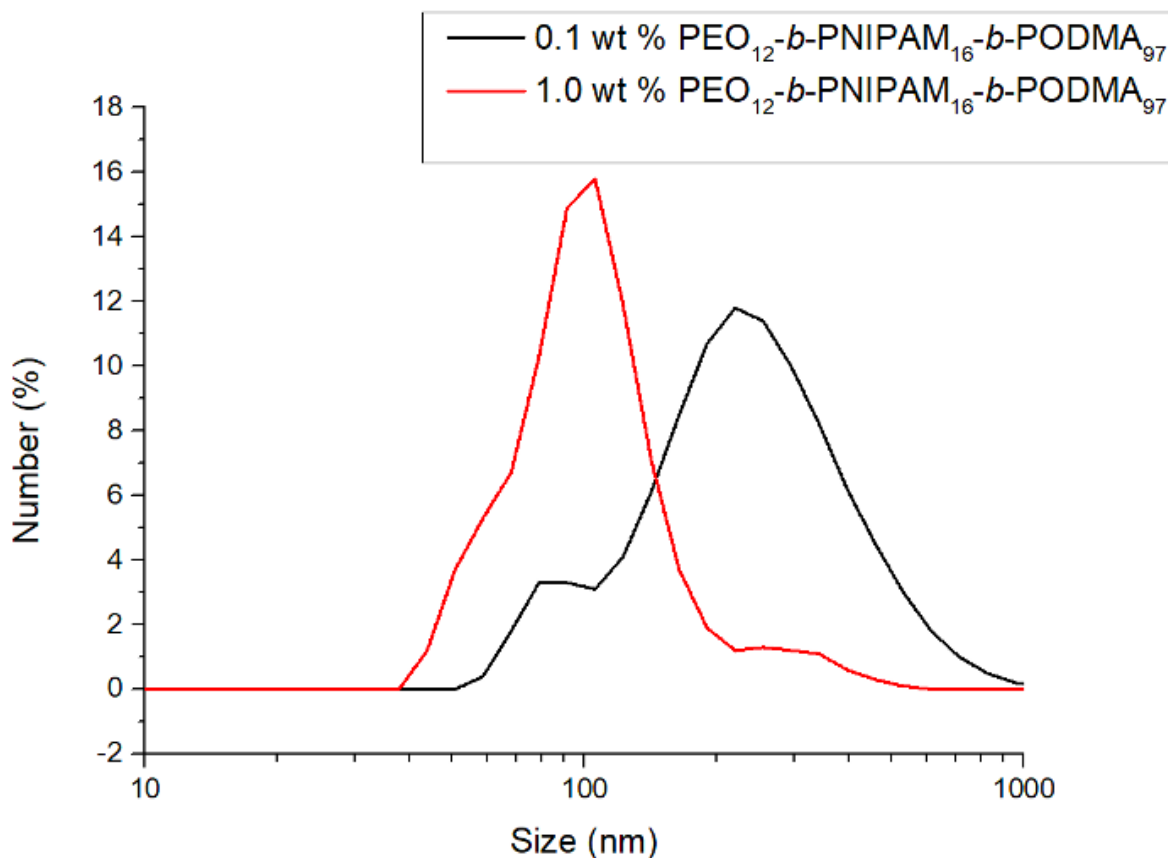
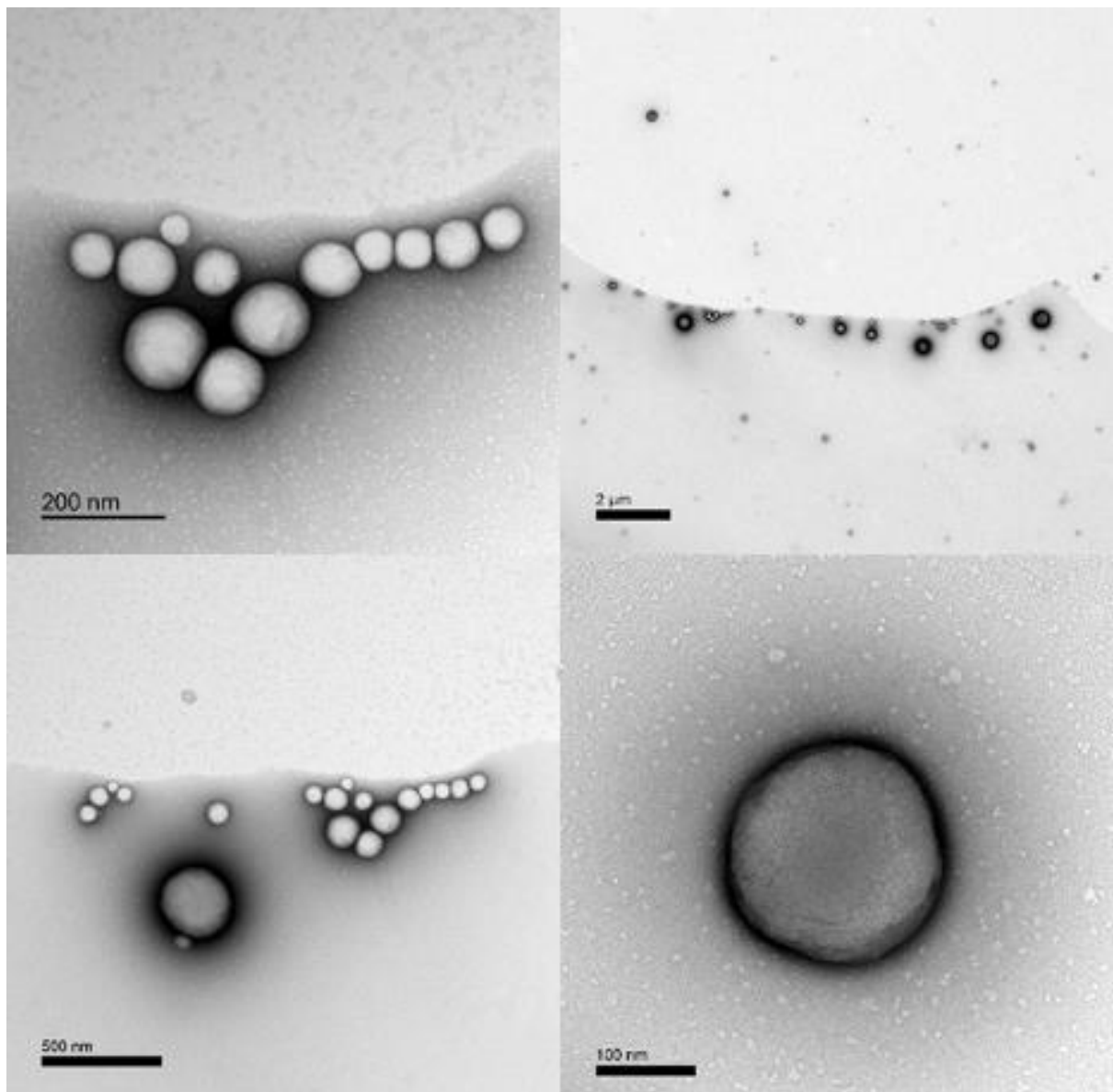


Figure 223 DLS results for 0.1 & 1.0 wt% solution.

From the TEM images there are spherical and cylindrical micelles at 0.1 and 1.0 wt% when PEO₁₂-b-PNIPAM₁₆-b-PODMA₉₇ is self-assembled in water. TEM in both cases suggest that these particles are around 80nm which agrees with the DLS at 1.0 wt% but disagrees for the 0.1 wt%. The 0.1 wt% DLS results suggest that there are particles present at just under 100nm which supports TEM but DLS also suggests something larger in solution. The larger results could be caused by aggregation or it could be picking up the cylindrical micelles which are much longer in diameter than the spherical micelles.

PEO₁₆-*b*-PNIPAM₁₆-*b*-PODMA₁₁₄



*Figure 224 0.1 wt% PEO₁₆-*b*-PNIPAM₁₆-PODMA₁₁₄ self-assembled in water. Spherical and cylindrical micelles are present.*

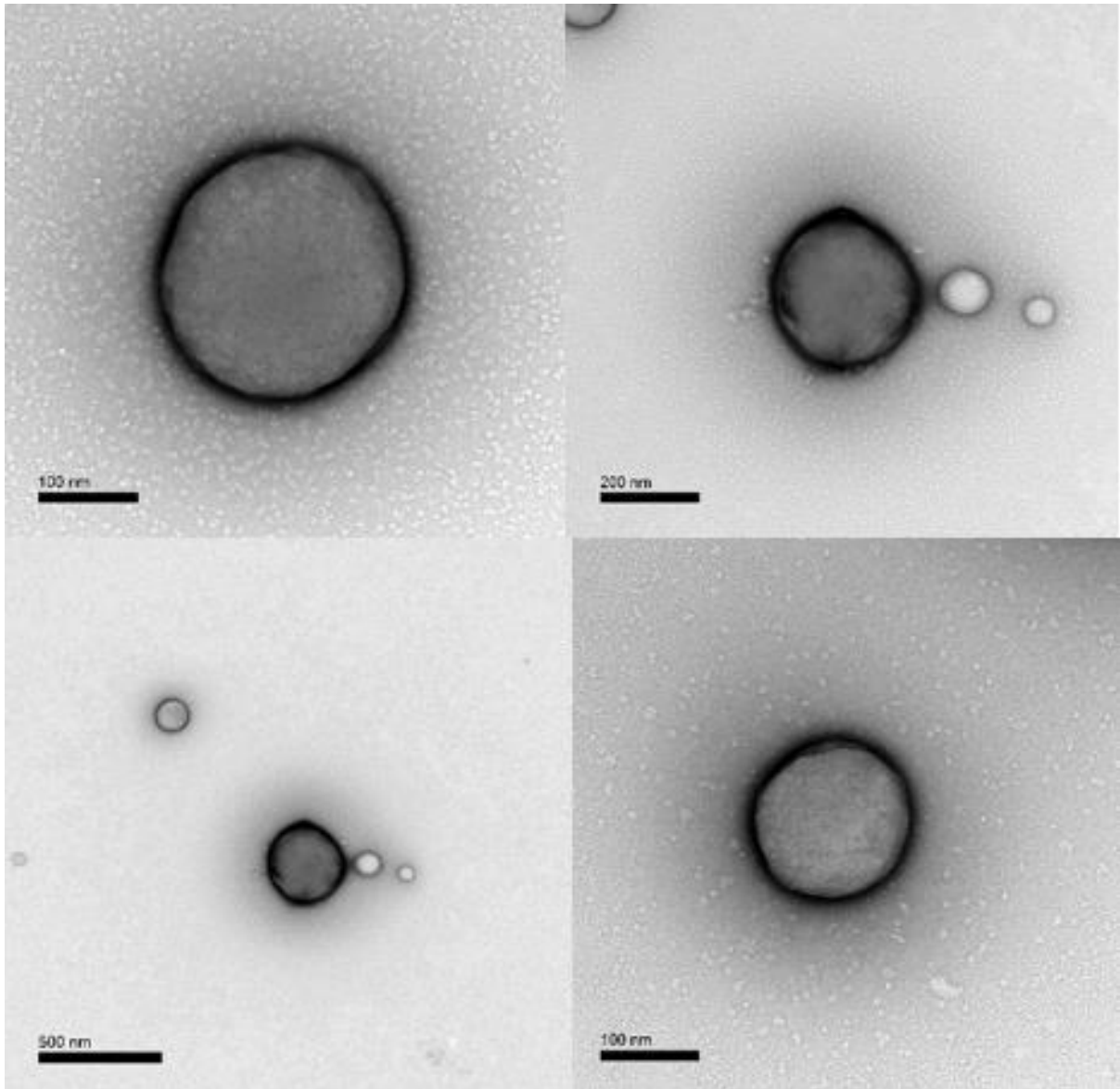


Figure 78 1.0 wt% PEO_{16} - b - $PNIPAM_{16}$ - $PODMA_{114}$ self-assembled in water. Spherical and cylindrical micelles are present.

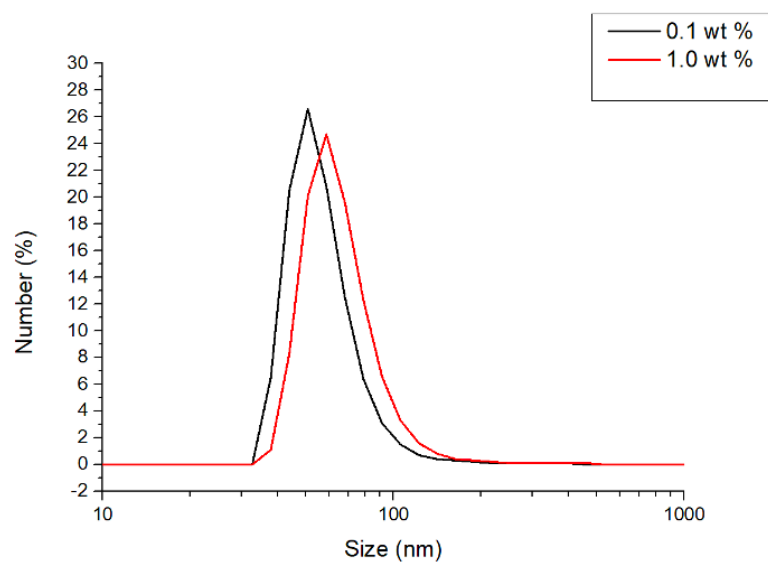


Figure 79 DLS Results for PEO_{16} - b - $PNIPAM_{16}$ - $PODMA_{114}$ self-assembled in water.

TEM suggest that for 0.1wt % that micelles are present at 106nm and for 1.0wt% that micelles are present at 122 nm. TEM seems to disagree with DLS as DLS suggest that there are much smaller particles in solution.

PEO-*b*-PNIPAM-*b*-PODMA (PODMA Block at 50 DP)

From the ¹H-NMR of the previous two triblock polymers, it suggested that some of the PEO-*b*-PNIPAM-Cl was not initiating in the ATRP reaction causing DP to be must higher than expected. The same reaction was repeated but less ODMA was used to try and target a DP of around 50. This would mean that the molecular weight would be lower and when this new triblock polymer was self-assembled in water then bicontinuous nanospheres may result.

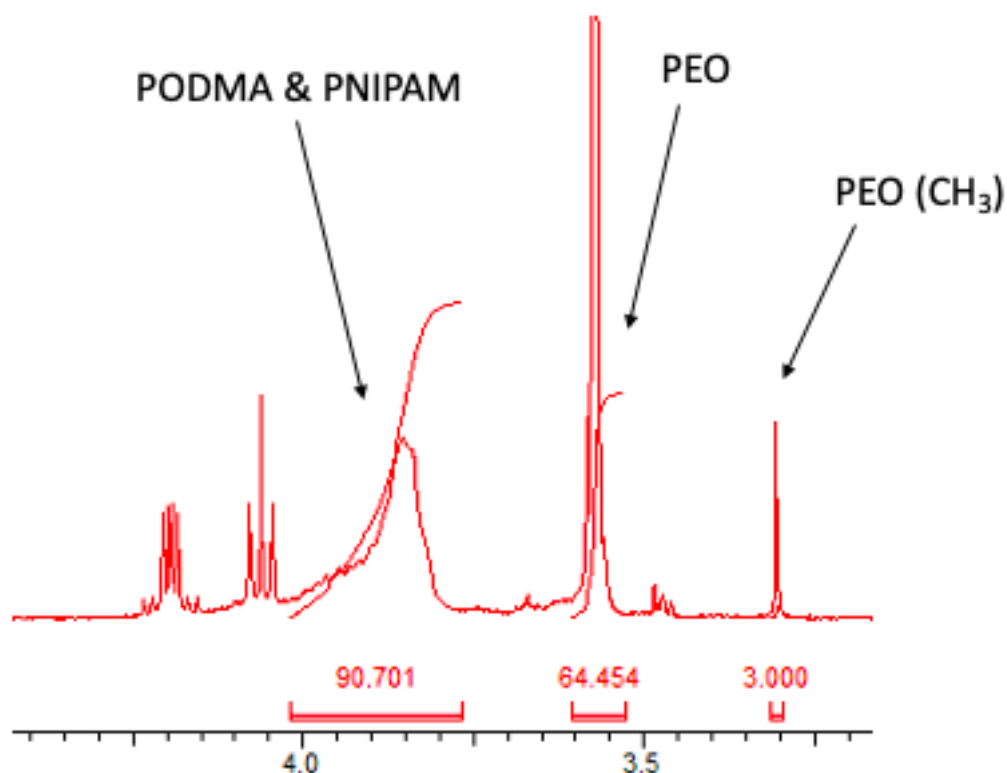


Figure 80 ¹H-NMR of the new triblock made by ATRP

The DP of each block was calculated and this was added in Table 52. The DP of PEO and PNIPAM blocks were known previously from the ATRP reaction of PEO-*b*-PNIPAM-Cl.

Table 52 NMR and GPC data of PEO-*b*-PNIPAM-PODMA triblock.

Structure	DP _{PEO}	DP _{PNIPAM}	DP _{PODMA}	M _n NMR	M _n GPC	M _w / M _n
PEO ₁₆ - <i>b</i> -PNIPAM ₁₆ - <i>b</i> -PODMA ₃₈	16	16	38	19100	24000	1.26

After NMR and GPC had been performed, the triblock was self-assembled in water to see what aggregates would form.

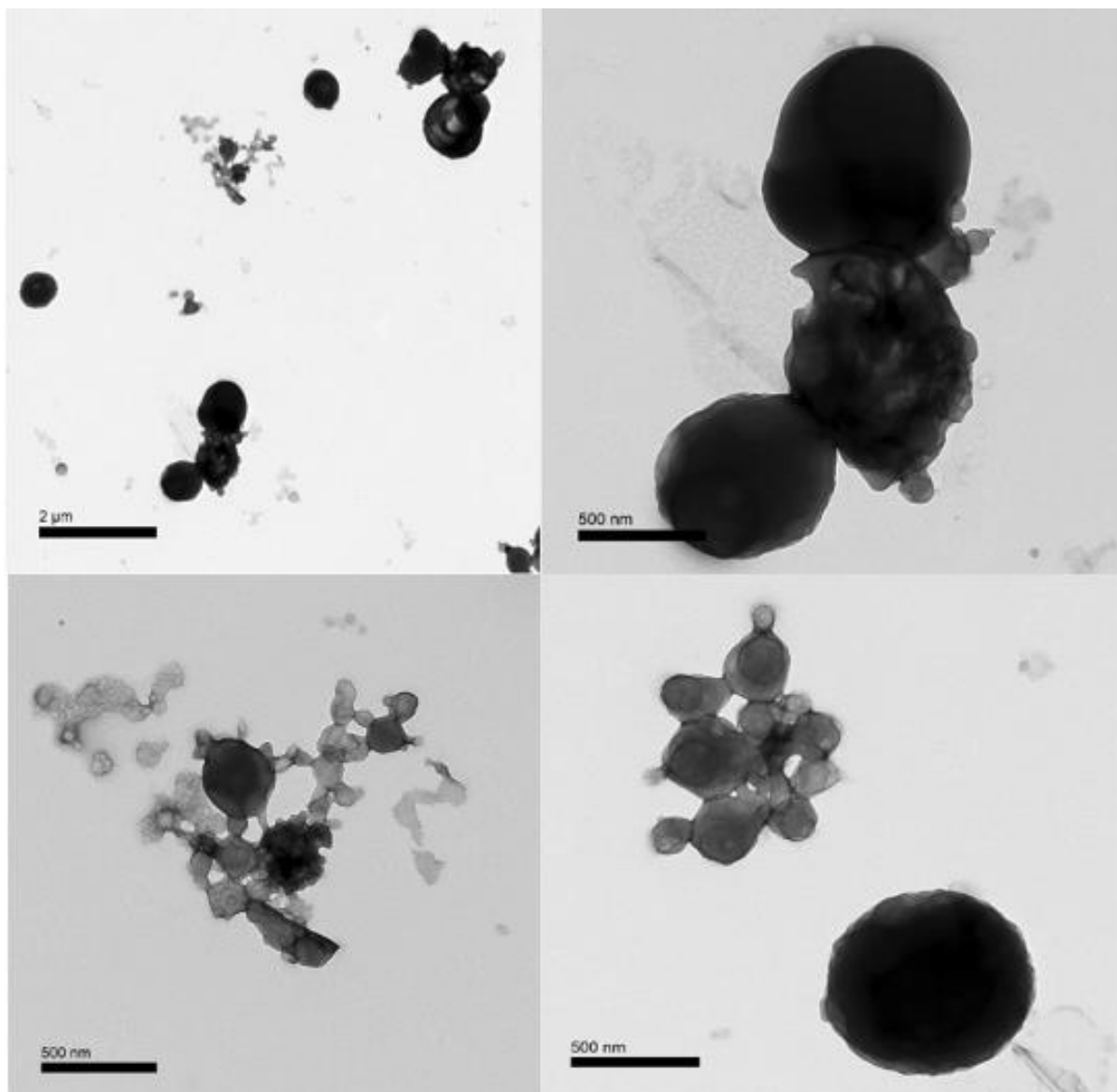


Figure 81 0.1 wt% PEO₁₆-b-PNIPAM₁₆-PODMA₃₈ in water.

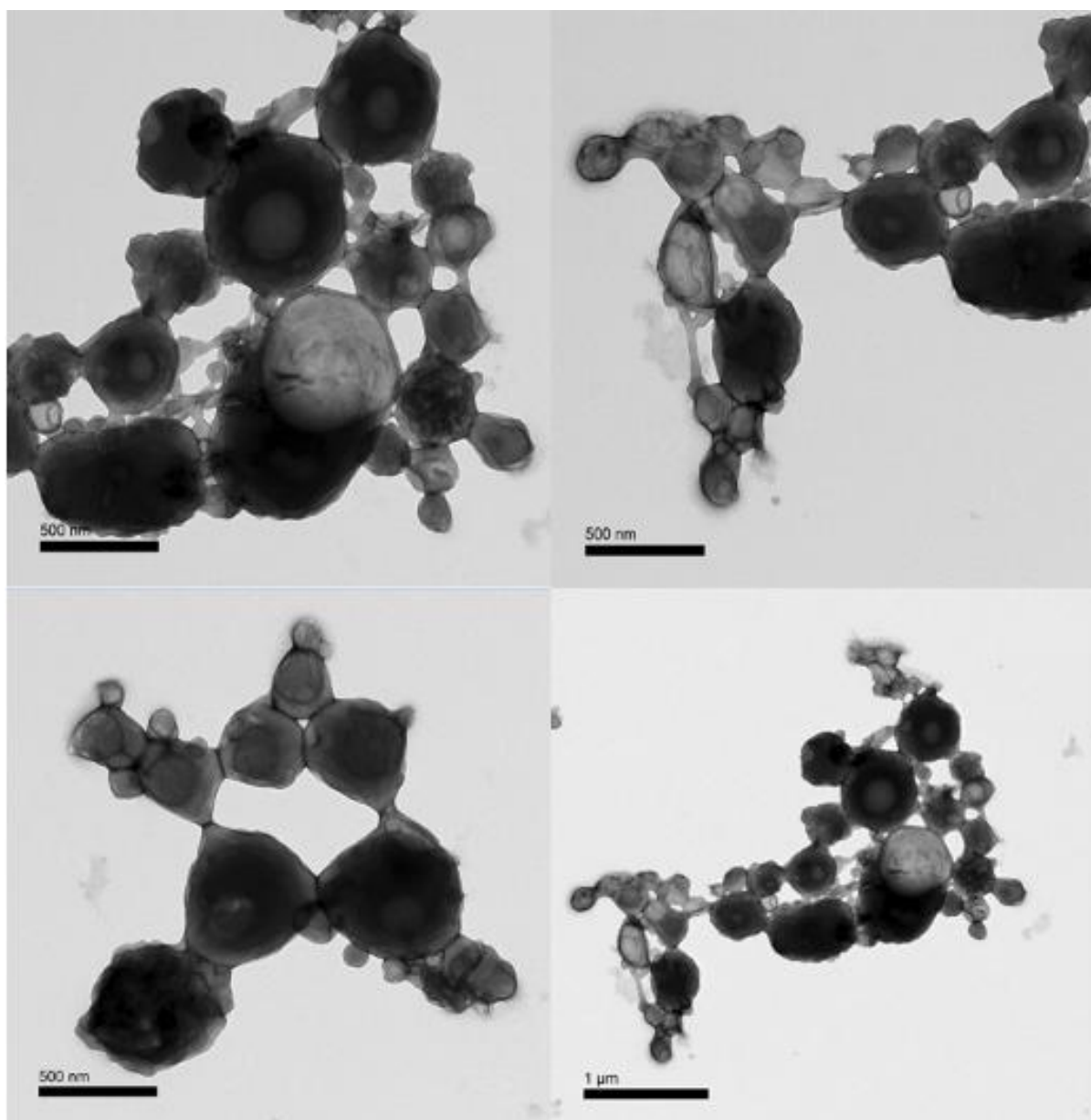


Figure 82 1.0 wt% PEO₁₆-b-PNIPAM₁₆-PODMA₃₈ in water.

Unlike the previous triblock polymers, PEO₁₆-b-PNIPAM₁₆-PODMA₃₈ formed much bigger aggregate structures around 356 nm. Some of these structures were as big as 500nm. There seems to be a mixture of different aggregate species present. The first being spherical micelles and the second being vesicles. Some of the dark spheres could be bicontinuous aggregates present which makes these TEM very interesting for both 0.1 and 1.0 wt% solutions. This means that this triblock polymer is behaving differently to the block copolymers previously seen in the early chapters of this thesis.

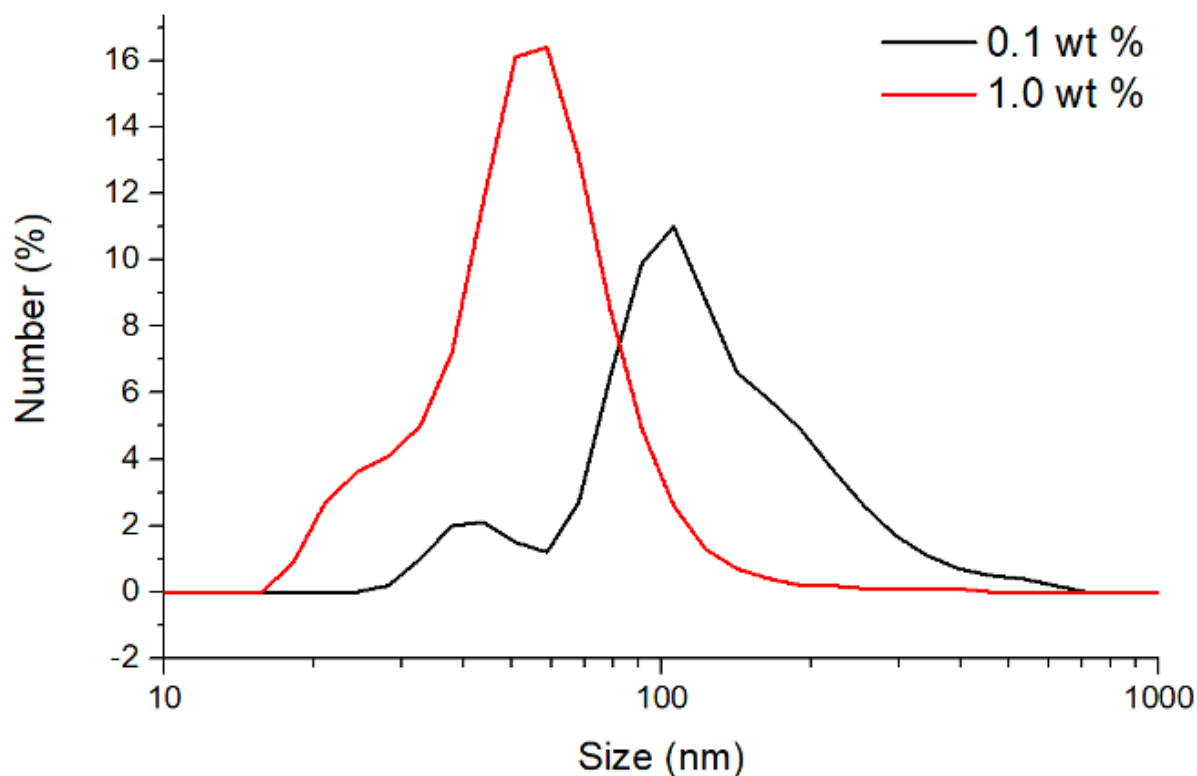


Figure 83 DLS Results for 0.1 & 1.0 wt% solutions of triblock polymer self-assembled in water.

The DLS results for 0.1 wt% solution agrees with the TEM results suggesting small particles present at 50nm and larger particles present at 300 nm. However, DLS disagrees with the TEM for the 1.0wt% solutions as it suggests that particles present are smaller than 100nm. The TEM images for 1.0 wt% clearly show bigger structures which are not being picked up by the DLS.

5.4 Conclusion

A triblock of PEO-*b*-PNIPAM-*b*-PODMA was successfully made by ATRP with low DP for the PEO & PNIPAM blocks at 0.15 hydrophilic fraction. It was successfully self-assembled but vesicles were seen instead of bicontinuous aggregates which were previously seen when a block copolymer of PEO-*b*-PODMA was self-assembled at 0.18 PEO fraction.

This work has paved the way for future work to study the effect of the nipam block. The aim was to be able to make a triblock that could release a drug effective once the temperature was taken past the LCST of the nipam block. Future work could include self-assembling a drug within the centre of the triblock and monitor the amount of drug released over time.

5.5 References

- 1 A. Blanz, S. P. Armes and A. J. Ryan, *Macromol. Rapid Commun.*, 2009, **30**, 267–277.
- 2 J. A. Opsteen, J. J. L. M. Cornelissen and J. C. M. Van Hest, in *Pure and Applied Chemistry*, Walter de Gruyter GmbH, 2004, vol. 76, pp. 1309–1319.
- 3 Z. Li, Z. Chen, H. Cui, K. Hales, K. Qi, K. L. Wooley and D. J. Pochan, *Langmuir*, 2005, **21**, 7533–7539.
- 4 Y. L. Liu, Y. H. Chang and W. H. Chen, *Macromolecules*, 2008, **41**, 7857–7862.
- 5 J. J. L. M. Cornelissen, M. Fischer, N. A. J. M. Sommerdijk and R. J. M. Nolte, *Science (80-.)*, 1998, **280**, 1427–1430.
- 6 B. E. McKenzie, J. F. De Visser, H. Friedrich, M. J. M. Wirix, P. H. H. Bomans, G. De With, S. J. Holder and N. A. J. M. Sommerdijk, *Macromolecules*, 2013, **46**, 9845–9848.
- 7 B. E. McKenzie, F. Nudelman, P. H. H. Bomans, S. J. Holder and N. A. J. M. Sommerdijk, *J. AM. CHEM. SOC.*, 2010, **132**, 10256–10259.
- 8 G. Campos-Villalobos, F. R. Siperstein, A. Charles and A. Patti, *J. Colloid Interface Sci.*, 2020, **572**, 133–140.
- 9 C. De las Heras Alarcón, S. Pennadam and C. Alexander, *Chem. Soc. Rev.*, 2005, **34**, 276–285.
- 10 D. A. Z. Wever, F. Picchioni and A. A. Broekhuis, *Prog. Polym. Sci.*, 2011, **36**, 1558–1628.
- 11 K.-I. Seno, I. Tsujimoto, S. Kanaoka and S. Aoshima, *J. Polym. Sci. Part A Polym. Chem.*, 2008, **46**, 6444–6454.
- 12 J. Chen, M. Liu, H. Gong, Y. Huang and C. Chen, *J. Phys. Chem. B*, 2011, **115**, 14947–14955.